

Binding Energies in Large Ionic Clusters
from Kinetic Energy Release Measurements

ELEONORA BRUZZI, MChem

Thesis Submitted to The University of Nottingham
for the Degree of Doctor of Philosophy

JUNE 2014

Abstract

The determination of binding energy is a very important piece of information that an experiment can provide. We have devised a new experimental procedure to measure binding energies for unimolecular (metastable) decay of multiply charged metal-ligand cluster ions in gas phase.

The new technique consists in preparing clusters by supersonic expansion, and in generating metal-ligand clusters by pick-up technique. A high resolution double-focusing mass spectrometer having reversed sector geometry is used to obtain mass-analysed ion kinetic energy spectra. The evaporative ensemble statistical model by C. E. Klots is used to analyse the kinetic energy releases and to obtain the corresponding binding energies. Our new experimental method has been applied to measure the binding energy for the loss of one neutral molecule in a unimolecular (metastable) dissociation in $\text{H}^+(\text{H}_2\text{O})_n$, $\text{H}^+(\text{H}_2\text{O})_n$, and $\text{H}^+(\text{CH}_3\text{OH})_n$ for $n \leq 30$. The main results were:

- (i) for $n > 6$ each fragmentation corresponds to breaking one hydrogen bond
- (ii) no magic numbers were observed.

This experimental procedure was used to measure the binding energy for the loss of one neutral molecule in the unimolecular (metastable) decay of $[\text{M}(\text{L})_n]^{2+}$ for $n \leq 20$, where $\text{M} = \text{Mg}, \text{Ca}, \text{Sr}$ and $\text{L} = \text{H}_2\text{O}, \text{NH}_3, \text{CH}_3\text{OH}$. This investigation determined that:

- (i) the coordination number is six for all the metal-solvent cluster ions, except for $[\text{Mg}(\text{NH}_3)_n]^{2+}$ having coordination number equal to four;
- (ii) the double charge affects the binding interactions on the solvation shells up to $n = 20$ with the exception of $[\text{Sr}(\text{H}_2\text{O})_n]^{2+}$, for which $n = 14$;
- (iii) binding energies correspond to breaking one hydrogen bond;
- (iv) no magic numbers were detected.

Acknowledgements

First, and foremost, I express my gratitude to Professor Anthony J. Stace, also known as Tony; he gave me the privilege to work in his research group and guided me in the discovery of the beauty of experimental work. I thank Tony for his support, illuminating discussions, understanding, and help throughout these years.

During my doctoral studies, I appreciated that experimental work continuously gives opportunities to extend our knowledge, but can present unexpected challenges when a complex instrumentation has problems. All the technical staff deserve credit for the in-house support and for what I learnt from them: a great thank to the physical chemistry research technician Neil Barnes, the workshop technicians Kevin Hind and John Whalley, and the electronics technicians David Litchfield and James Warren.

I will remember with joy the long days spent in the laboratory and the company of the colleagues in Tony's group: Joseph Koka, Xiaojing Chen, Gerardo Raggi, Christopher Harris, Lifu Ma, Adrian Boatwright, Stuart Hamish, and Hisham Al-Zubaidi.

Thanks to Emilio...he knows why.

Finally, I thank my mother, Elena, and my sister, Daniela, for their encouragement. A loving thought goes to my father, Benedetto.

Contents

1	Introduction	17
1.1	Measurements of the Binding Energy of Clusters	17
1.2	Related Experimental Techniques	20
1.3	Advantages of Stace's Technique	24
2	Experimental Apparatus	33
2.1	Schematic Diagram of the Experimental Apparatus	33
2.2	Cluster Chamber	34
2.2.1	Free Jet: an Overview	36
2.3	Solvent Reservoir	38
2.4	Cluster Formation in Supersonic Beams	40
2.5	Pick-Up Chamber	41
2.5.1	Knudsen Effusion Cell	43
2.6	Ion Source Chamber	45
2.7	Mass Spectrometer	46
2.7.1	Magnetic Sector: Magnet Analyser Tube	46
2.7.2	Electric Sector: Energy Analyser Tube	47
2.8	Detection System	48
2.9	Sources of Uncertainty	49
3	From Kinetic Energy Release Measurements to Binding Energies	53
3.1	Overview	53
3.2	Cluster Ions Preparation and Detection	54
3.3	MIKE Spectrometry	56
3.3.1	Artefact Peaks	57
3.4	Time of Flight	59
3.5	Data Analysis: Binding Energy Determined from KER Measurements	59
3.6	Example of MIKE scan analysis	67

4	Binding Energy of $H^+(NH_3)_n$, $H^+(CH_3OH)_n$, and $H^+(H_2O)_n$	73
4.1	Experimental details	73
4.2	Plot of Binding Energies as a Function of the Number of Molecules in Each Cluster as a Calibration Graph	74
4.3	Binding Energies of Protonated Molecular Cluster Ions $H^+(H_2O)_n$, $H^+(NH_3)_n$, and $H^+(CH_3OH)_n$ from Metastable Kinetic Energy Release Measurements	77
4.4	Related Experimental Work	83
4.5	Related Theoretical Work	89
4.6	KER Data: Comparison with the Literature	93
5	Binding Energies of $[Mg(CH_3OH)_n]^{2+}$, $[Ca(CH_3OH)_n]^{2+}$, and $[Sr(CH_3OH)_n]^{2+}$	103
5.1	Experimental Details	103
5.2	Binding Energies from Metastable KER Measurements	105
5.3	A Note on Coordination Numbers	115
5.4	Related Theoretical Work	116
5.5	Solvation of Monovalent Mg, Ca, and Sr ions in Methanol	118
6	Binding Energy of $[Mg(NH_3)_n]^{2+}$, $[Ca(NH_3)_n]^{2+}$, and $[Sr(NH_3)_n]^{2+}$	125
6.1	Experimental Details	125
6.2	Binding Energies from Metastable KER Measurements	127
6.3	A Note on Coordination Numbers	135
6.4	Related Work on Monovalent Mg, Ca, and Sr	137
7	Binding Energy of $[Mg(H_2O)_n]^{2+}$, $[Ca(H_2O)_n]^{2+}$, and $[Sr(H_2O)_n]^{2+}$	145
7.1	Experimental Details	145
7.2	Binding Energies of KER Measurements	149
7.3	Related Experimental Work	158
7.4	Related Theoretical Work	162
7.5	A Note on Coordination Numbers	168
7.6	Hydration of Monovalent Mg, Ca, and Sr Ions	173
8	Conclusion	185
9	Supporting Information	193
9.1	$H^+(H_2O)_n$	193
9.2	$H^+(NH_3)_n$	197
9.3	$H^+(CH_3OH)_n$	201

9.4	$[\text{Mg}(\text{NH}_3)_n]^{2+}$	205
9.5	$[\text{Ca}(\text{NH}_3)_n]^{2+}$	209
9.6	$[\text{Sr}(\text{NH}_3)_n]^{2+}$	212
9.7	$[\text{Mg}(\text{CH}_3\text{OH})_n]^{2+}$	215
9.8	$[\text{Ca}(\text{CH}_3\text{OH})_n]^{2+}$	220
9.9	$[\text{Sr}(\text{CH}_3\text{OH})_n]^{2+}$	222
9.10	$[\text{Mg}(\text{H}_2\text{O})_n]^{2+}$	225
9.11	$[\text{Ca}(\text{H}_2\text{O})_n]^{2+}$	226
9.12	$[\text{Sr}(\text{H}_2\text{O})_n]^{2+}$	230
9.13	Conversion Units	234
9.14	Atomic Weights and Isotopic Compositions of Elements	235
9.15	Some Physical Parameters of the Atoms and Molecules Under Examination	235
10	Experimental Details	237
10.1	Details on the Reagents	237
10.2	Experimental Metal Vaporization or Sublimation Temperature	238
10.3	Experimental Extracting Potential At The Ion Source	238
10.4	Energy of Bombarding Electrons	238
10.5	Experimental Pressure	238
10.6	Reference to Digitizing Software Employed to Derive the Data from Images Found in the Literature	239

List of Figures

2.1.1	Schematic view of the apparatus from the top [2]	33
2.2.1	Schematic diagram of the cluster chamber (adapted from [3]) . . .	34
2.2.2	Schematic diagram of the stagnation vessel (adapted from [3]) . .	35
2.2.3	Structure of free jet expansion [5, Ch. 2, pp. 15, Fig. 2.1 by D. R. Miller.]	37
2.2.4	Schematic representations of free jet expansion and molecular speed distribution (adapted from [6])	38
2.3.1	Schematic diagram of the solvent reservoir (adapted from [3]) . .	39
2.5.1	Schematic representation of pick-up process followed by electron impact (EI) ionisation (adapted from [3])	42
2.5.2	Photo of the Pick-Up Chamber [19]	43
2.5.3	Schematic diagram of the Knudsen effusion cell (adapted from [3])	44
2.8.1	Physical layout of ion detector tube (Fig. 1, page 265 from [21]) .	48
3.2.1	Example of metastable peaks recorded for the fragmentation of $H^+(H_2O)_{21}$, $H^+(CH_3OH)_7$, and $[Mg(CH_3OH)_{20}]^{2+}$	55
3.3.1	Examples of artefact in MIKE spectrum of metastable methanol, ammonia, and water protonated cluster ions	58
3.6.1	Example of metastable peaks recorded for the unimolecular frag- mentation of $[Mg(NH_3)_7]^{2+}$ cluster ions	68
4.1.1	Examples of MIKE scan for $H^+(NH_3)_6$, $H^+(CH_3OH)_7$, and $H^+(H_2O)_{21}$	74
4.2.1	Parameter $\ell = 1.0, 1.5, 2.0$ for the definition of the transition state temperature in the water, methanol, and ammonia protonated clus- ter ions	76
4.3.1	Summary of measurements of binding energies for large cluster ions from the literature	77
4.3.2	Plot of binding energies extracted from kinetic energy release measurements on water, ammonia and methanol cluster ions . . .	82

5.1.1	Examples of MIKE scan for for $[\text{Mg}(\text{CH}_3\text{OH})_n]^{2+}$, $[\text{Ca}(\text{CH}_3\text{OH})_n]^{2+}$ and $[\text{Sr}(\text{CH}_3\text{OH})_n]^{2+}$	104
5.2.1	Plot of binding energies from kinetic energy release measurements on $[\text{Mg}(\text{CH}_3\text{OH})_n]^{2+}$, $[\text{Ca}(\text{CH}_3\text{OH})_n]^{2+}$, and $[\text{Sr}(\text{CH}_3\text{OH})_n]^{2+}$ cluster ions	107
5.2.2	Binding energies extracted from kinetic energy release measurements on $[\text{Mg}(\text{CH}_3\text{OH})_n]^{2+}$, $[\text{Ca}(\text{CH}_3\text{OH})_n]^{2+}$, $[\text{Sr}(\text{CH}_3\text{OH})_n]^{2+}$.	111
6.1.1	Examples of MIKE scans for $[\text{Mg}(\text{NH}_3)_n]^{2+}$, $[\text{Ca}(\text{NH}_3)_n]^{2+}$, and $[\text{Sr}(\text{NH}_3)_n]^{2+}$	126
6.2.1	Plot of binding energies from kinetic energy release measurements on $[\text{Mg}(\text{NH}_3)_n]^{2+}$, and $[\text{Ca}(\text{NH}_3)_n]^{2+}$, $[\text{Sr}(\text{NH}_3)_n]^{2+}$ cluster ions	129
6.2.2	Binding energies (kJ mol^{-1}) extracted from kinetic energy release measurements on $[\text{Mg}(\text{NH}_3)_n]^{2+}$, $[\text{Ca}(\text{NH}_3)_n]^{2+}$, $[\text{Sr}(\text{NH}_3)_n]^{2+}$, which are compared with $\text{H}^+(\text{NH}_3)_n$ as a function of n, the number of ammonia molecules in each cluster	134
7.1.1	Examples of MIKE scans for $[\text{Mg}(\text{H}_2\text{O})_n]^{2+}$	147
7.1.2	Examples of MIKE scan for $[\text{Sr}(\text{H}_2\text{O})_n]^{2+}$	148
7.2.1	Plot of binding energies from kinetic energy release measurements on $[\text{Mg}(\text{H}_2\text{O})_n]^{2+}$, $[\text{Ca}(\text{H}_2\text{O})_n]^{2+}$, and $[\text{Sr}(\text{H}_2\text{O})_n]^{2+}$ cluster ions	152
7.2.2	Plot of binding energies from kinetic energy release measurements on $[\text{Ca}(\text{H}_2\text{O})_n]^{2+}$, $[\text{Sr}(\text{H}_2\text{O})_n]^{2+}$, and $\text{H}^+(\text{H}_2\text{O})_n$ cluster ions	155

List of Tables

3.6.1	Numerical data for the experimental metastable peaks in Figure 3.6.1	67
4.3.1	Experimental measurements of the average kinetic energy release, $\langle \varepsilon_\tau \rangle$, associated with the unimolecular (metastable) decay of cluster ions. Each value is the average of at least four separate measurements and the error, $\pm \Delta \langle \varepsilon_\tau \rangle$, reflects the spread in uncertainty in the measurements	78
4.3.2	Binding energies determined from the kinetic energy release data presented in Table 4.3.1	79
4.4.1	Comparison between binding energies determined in these experiments for small $\text{H}^+(\text{CH}_3\text{OH})_n$ clusters ($n \leq 10$) and those available from other experimental sources	84
4.4.2	Comparison between binding energies determined in these experiments for small $\text{H}^+(\text{NH}_3)_n$ clusters ($n \leq 10$) and those available from other experimental sources	85
4.4.3	Comparison between binding energies determined in these experiments for small $\text{H}^+(\text{H}_2\text{O})_n$ clusters ($n \leq 10$) and those available from other experimental sources	86
4.4.4	Comparison between binding energies determined in these experiments for $\text{H}^+(\text{CH}_3\text{OH})_n$ clusters ($11 \leq n \leq 20$) and those available from other experimental sources	87
4.4.5	Comparison between binding energies determined in these experiments for $\text{H}^+(\text{NH}_3)_n$ clusters ($11 \leq n \leq 22$) and those available from other experimental sources	87
4.4.6	Comparison between binding energies determined in these experiments for $\text{H}^+(\text{H}_2\text{O})_n$ clusters ($2 \leq n \leq 28$) and those available from other experimental sources	88
4.4.7	Comparison between binding energies determined in these experiments for $\text{H}^+(\text{H}_2\text{O})_n$ clusters ($3 \leq n \leq 4$) and those available from other experimental sources from [37] calculated at 0 K	88

4.5.1	Comparison between binding energies determined in these experiments for $\text{H}^+ (\text{H}_2\text{O})_n$ clusters ($1 \leq n \leq 28$) and those available from theoretical sources	91
4.5.2	Comparison between binding energies determined in these experiments for $\text{H}^+ (\text{NH}_3)_n$ clusters ($2 \leq n \leq 17$) and those available from theoretical sources. (The superscript indicates the temperature)	92
4.5.3	Comparison between binding energies determined in these experiments for $\text{H}^+ (\text{CH}_3\text{OH})_n$ clusters ($2 \leq n \leq 4$) and those from theoretical sources. (The superscript indicates the temperature)	93
4.6.1	Comparison between kinetic energy releases determined in these experiments for $\text{H}^+ (\text{CH}_3\text{OH})_n$ clusters ($2 \leq n \leq 15$) and those available from other experimental sources ($\langle \text{KER} \rangle$)	94
4.6.2	Comparison between kinetic energy releases determined in these experiments for $\text{H}^+ (\text{NH}_3)_n$ clusters ($2 \leq n \leq 17$) and those available from other experimental sources ($\langle \text{KER} \rangle$)	95
5.2.1	Experimental measurements of the average kinetic energy release, $\langle \varepsilon_\tau \rangle$, associated with the unimolecular (metastable) decay of cluster ions	105
5.2.2	Binding energies determined from the kinetic energy release data presented in Table 5.2.1	106
5.2.3	Some physical parameters of the alkaline earth metal ions under examination from reference [6]	109
5.3.1	Coordination numbers are from published inorganic chemistry books [5, 6]	115
5.3.2	Relative fragment ion intensity distribution for $2 \leq n \leq 20$ from mass spectroscopic measurements following unimolecular metastable loss of CH_3OH [13]	115
5.3.3	<i>Ab initio</i> Car-Parrinello molecular dynamics [26]; Monte-Carlo simulations of statistical perturbation theory [27]	116
5.4.1	Comparison between binding energies determined in these experiments for $[\text{Mg}(\text{CH}_3\text{OH})_n]^{2+}$ clusters ($4 \leq n \leq 6$) and those available from theoretical sources ($1 \leq n \leq 6$)	117
5.4.2	Comparison between binding energies determined in these experiments for $[\text{Ca}(\text{CH}_3\text{OH})_n]^{2+}$ clusters ($4 \leq n \leq 7$) and those available from theoretical sources	117

5.5.1	Comparing binding energies determined in these experiments for $[\text{Mg}(\text{CH}_3\text{OH})_n]^{2+} \rightarrow [\text{Mg}(\text{CH}_3\text{OH})_{n-1}]^{2+} + \text{CH}_3\text{OH}$ and published theoretical ones for $[\text{Mg}(\text{CH}_3\text{OH})_n]^+ \rightarrow [\text{Mg}(\text{CH}_3\text{OH})_{n-1}]^+ + \text{CH}_3\text{OH}$	119
6.2.1	Experimental measurements of the average kinetic energy release	127
6.2.2	Binding energies determined from the kinetic energy release data of Table 6.2.1	128
6.3.1	Comparing coordination numbers of Mg^{2+} , Ca^{2+} , and Sr^{2+} mono-atomic ions available from literature	136
6.3.2	Comparing coordination numbers for $[\text{Mg}(\text{NH}_3)_n]^{2+}$, $[\text{Ca}(\text{NH}_3)_n]^{2+}$, and $[\text{Sr}(\text{NH}_3)_n]^{2+}$ in these experiments with other experimental studies	137
6.3.3	Comparing coordination numbers for $[\text{Mg}(\text{NH}_3)_n]^{2+}$, $[\text{Ca}(\text{NH}_3)_n]^{2+}$, and $[\text{Sr}(\text{NH}_3)_n]^{2+}$ of these experiments with other theoretical studies	137
6.4.1	Comparing binding energies in these experiments for $[\text{Mg}(\text{NH}_3)_n]^{2+} \rightarrow [\text{Mg}(\text{NH}_3)_{n-1}]^{2+} + \text{NH}_3$ and those available in [25]	138
6.4.2	Comparing binding energies in these experiments for $[\text{Mg}(\text{NH}_3)_n]^{2+} \rightarrow [\text{Mg}(\text{NH}_3)_{n-1}]^{2+} + \text{NH}_3$ and those available in the literature for $[\text{Mg}(\text{NH}_3)_n]^+ \rightarrow [\text{Mg}(\text{NH}_3)_{n-1}]^+ + \text{NH}_3$	138
7.2.1	Experimental measurements of $\langle \varepsilon_\tau \rangle$ (average kinetic energy re- lease) associated with the unimolecular (metastable) decay of clus- ter ions	149
7.2.2	Binding energies determined from the kinetic energy release data presented in Table 7.2.1	150
7.2.3	Critical size (n_c) of $[\text{Mg}(\text{H}_2\text{O})_n]^{2+}$, $[\text{Ca}(\text{H}_2\text{O})_n]^{2+}$, and $[\text{Sr}(\text{H}_2\text{O})_n]^{2+}$ from selected literature determined experimentally	156
7.3.1	Binding energies in these experiments for $[\text{Mg}(\text{H}_2\text{O})_n]^{2+}$ clusters and those experimental ones from literature ($1 \leq n \leq 14$)	160
7.3.2	Binding energies in these experiments for $[\text{Ca}(\text{H}_2\text{O})_n]^{2+}$ clusters and those experimental ones from literature ($1 \leq n \leq 14$)	161
7.3.3	Binding energies in these experiments for $[\text{Sr}(\text{H}_2\text{O})_n]^{2+}$ clusters and those experimental ones from literature ($1 \leq n \leq 13$)	162
7.4.1	Binding energies in this experiment for $[\text{Sr}(\text{H}_2\text{O})_n]^{2+}$ clusters and theoretical ones from the literature ($1 \leq n \leq 6$)	164

7.4.2	Binding energies in these experiments for $[\text{Ca}(\text{H}_2\text{O})_n]^{2+}$ clusters and those theoretical ones from literature ($1 \leq n \leq 9$)	165
7.4.3	Binding energies in these experiments for $[\text{Ca}(\text{H}_2\text{O})_n]^{2+}$ clusters and those theoretical ones from literature ($1 \leq n \leq 18$)	166
7.4.4	Binding energies in these experiments for $[\text{Ca}(\text{H}_2\text{O})_n]^{2+}$ clusters and those theoretical ones from literature ($1 \leq n \leq 18$)	167
7.4.5	Binding energies in these experiments for $[\text{Mg}(\text{H}_2\text{O})_n]^{2+}$ clusters and theoretical ones from literature ($1 \leq n \leq 18$)	168
7.5.1	Examples of coordination numbers for $[\text{Mg}(\text{H}_2\text{O})_n]^{2+}$, $[\text{Ca}(\text{H}_2\text{O})_n]^{2+}$, and $[\text{Sr}(\text{H}_2\text{O})_n]^{2+}$ from theoretical literature	169
7.5.2	Examples of coordination numbers for $[\text{Mg}(\text{H}_2\text{O})_n]^{2+}$, $[\text{Ca}(\text{H}_2\text{O})_n]^{2+}$, and $[\text{Sr}(\text{H}_2\text{O})_n]^{2+}$ from experimental literature	169
7.5.3	Examples of coordination numbers for Mg^{2+} , Ca^{2+} , and Sr^{2+} from literature on crystal structure from aqueous solution measurements with spectroscopic methods	169
7.5.4	Examples of coordination numbers for Mg^{2+} , Ca^{2+} , and Sr^{2+} from literature on simulations of condensed phase metal ions solvated in water	170
7.5.5	Highest number of entries on CSD and PDB for structures containing	173
7.6.1	Comparison between determined experimentally binding energies for $[\text{Sr}(\text{H}_2\text{O})_n]^{2+} \rightarrow [\text{Sr}(\text{H}_2\text{O})_{n-1}]^{2+} + \text{H}_2\text{O}$ and those available from the literature for $[\text{Sr}(\text{H}_2\text{O})_n]^+ \rightarrow [\text{Sr}(\text{H}_2\text{O})_{n-1}]^+ + \text{H}_2\text{O}$	174
9.15.1	Enthalpy of vaporization at boiling temperature and at 25° C of H_2O , CH_3OH , and NH_3	235
9.15.2	Ionisation potential of atoms and molecules in gas phase investigated in this work	236
9.15.3	Ionisation enthalpies and ionic radii of the Mg, Ca, and Sr atoms (Z is the atomic number, and CN is the coordination number)	236
10.2.1	Temperature of vaporization of the metals in these experiments	238
10.3.1	Accelerating voltage on the Ion Source for each cluster ion in these experiments	239

Chapter 1

Introduction

1.1 Measurements of the Binding Energy of Clusters

The importance of clusters has been remarked by Robert Boyle in his book “The Sceptical Chymist” in 1661 [1]; Boyle has written

- “Proposition I. It seems not absurd to conceive that at the first production of mixt bodies, the universal matter whereof they among other parts of the universe consisted, was actually divided into little particles of several sizes and shapes variously moved.”
- “Proposition II. Neither is it impossible that of these minute particles divers of the smallest and neighbouring ones were here and there associated into minute masses or clusters, and did by their coalitions constitute great store of such little primary concretions or masses as were not easily dissipable into such particles as composed them.”
- “Proposition III. I shall not peremptorily deny, that from most of such mixt bodies as partake either of animal or vegetable nature, there may by the help of the fire be actually obtained a determinate number (whether three, four, or five, or fewer or more) of substances, worthy of differing denominations.”
- “Proposition IV. It may likewise be granted, that those distinct substances, which concretes generally either afford or are made up of, may without very much inconvenience be called the elements or principles of them.”

In other words, Boyle was attributing the formation of the various substances to minute particles of a primordial matter, in particular he proposed that differences in size, shape, interactions, and motions of these particles of matter would

give rise to the different materials; although he was using the words clusters, principles, elements, and particles, it is probable that he was not defining the chemical elements as described in the Periodic Table, in fact, it is asserted in [2] that he doubted the existence of the atoms.

A cluster is formed by a finite number of constituents, either atoms or molecules; big clusters have up to 10^7 constituents; clusters can be classified as [3] small clusters, that is clusters containing less than 100 atoms, medium-sized clusters, that is clusters containing between 100 and 10000 atoms, and large clusters, that is clusters with more than 10000 atoms. The studies on clusters offer the opportunity to identify and characterize the unique properties of the finite-sized particles [4], which are phenomena that do not appear in macroscopic systems. Moreover, the research on gas-phase clusters can shed light on how the properties of a system evolve during the aggregation process of either atoms or molecules from the gas phase to the condensed phase [4]. For example the changes in the properties when forming a cluster by adding one molecule at time may be monitored and investigated. Beyond the importance that clusters have in chemistry; their study is paramount for the understanding of processes in biological systems [5] or in the atmosphere [6, 7, 8].

One of the main drawbacks in the study of clusters has been the technical difficulties of the experimental procedures to investigate multiply charged ions in gas phase, in particular metal-ligand ions [4]. Gas phase studies of the chemical and physical properties of metal ions have concentrated on singly charged species since they form easily [4, 9]. In contrast, the most frequent charge state of condensed phase metal ion chemistry is $2+$. Difficulties with studying metal dication chemistry arise in the gas phase because of the very high probability of charge transfer, a situation that is easy to appreciate when the second ionization energy of a metal is typically ≥ 15 eV, whilst the first ionization energy of an attached molecule or ligand is ≤ 10 eV. Despite these difficulties, significant progress has been made on the development of techniques for both generating and studying the thermochemistry, chemistry, spectroscopy, and spectrometry of solvated metal dications [4]. One aspect of metal dication chemistry where quantitative data is of particular significance concerns ion solvation and the determination of individual metal-molecule binding energies. Such information not only contributes towards a better understanding of the behaviour of metal ions in bulk solvents, but it can also provide a benchmark against which quantum mechanical and molecular mechanics calculations can be judged. Indeed, the aim of measuring binding energies with experimental techniques is to study the process of solvation at a molecular level. In particular, the studies of small molecules aggregates and metal ion-molecules complexes in gas phase provide

a mean to relate clusters properties with condensed phase behaviour [4]. An approach to the investigation of clusters is to measure the binding energy of unimolecular metastable decay for the loss of a single molecule (either a neutral or ionic fragment) from a cluster. This work continues the research on developing reliable experimental techniques to generate and study wide varieties of multiply charged and large clusters. In particular, the aim is to extend the range of available binding energy measurements for clusters containing up to 30 molecules.

The studies of Kebarle and co-workers on the thermodynamic equilibrium on small clusters [10, 11, 12] have been complemented by experiments designed to obtain binding energy data for large water clusters, $H^+ (H_2O)_n$ for $n > 6$, that focused on monitoring either the relative intensities of ions as observed in a mass spectrum [13], or the intensities of their fragmentation products [7, 14]. Engelking [15, 16] proposed an alternative approach whereby kinetic models are used together with kinetic energy release (KER) data recorded following the unimolecular (metastable) decay of a cluster ion. In these calculations Engelking used quasi-equilibrium theory/Rice-Ramsperger-Kassel (QET/RRK) kinetic model to determine the binding energy of single molecules to carbon dioxide and single atoms to argon cluster ions [13, 14]. Stace and Shukla measured the kinetic energy release of cluster ions using calculations based on the finite heat bath theory of Klots [17, 18, 19, 20, 21], where a low resolution, single focusing (magnetic field only) mass spectrometer was used to study the decay of carbon dioxide cluster ions [22]. Fragmentation of small CO_2 complexes generated by ion-molecule reactions have been also investigated by Bowers and co-workers [23, 24]. Such studies were followed by measurements of Stace and co-authors on argon cluster ions, in which the data range were extended by using a double focusing sector field instrument; in those studies, the link between excess energy present in the ions with statistical energy partitioning was established through computer simulation [25, 26, 27]. A correlation between kinetic energy release and the appearance of magic numbers (*i.e.* particularly stable cluster sizes [3, 28]) following the metastable decay of small protonated ammonia and methanol clusters has been established by Lifshitz et al. [29, 30]. The approach of Castleman et al. in [31] was to apply Engelking's model to a determination of the binding energy of ammonia cluster ions; in later work those researchers used finite heat bath theory to extract binding energy for ammonia and xenon cluster ions [32, 33]. Further to this analysis, Lifshitz et al. suggested that the average kinetic energy with which a monomer leaves a cluster is a measure of the temperature of a transition state of the cluster itself [29]; the quantitative link has been demonstrated in a series of experiments where kinetic energy releases

were measured following the single photon infrared excitation of cluster ions [34, 35, 36]. Initial applications of those investigations are the determination of binding energy for fullerene cluster ions [37]. Furthermore, Märk et al. have measured kinetic energy releases and hence binding energies for rare gas cluster ions [38, 39] and oxygen cluster ions [40] by applying finite heath bath theory to kinetic energy release data.

1.2 Related Experimental Techniques

The outstanding experimental techniques that are in use to prepare and study cluster ions in the gas phase have been designed and developed by the research groups of Peter B. Armentrout, A. Welford Castleman Jr., Paul Kebarle, Evan R. Williams, and by the research group of Anthony J. Stace. We now summarise those techniques.

The experimental procedure and thermochemical analysis used in the group of Armentrout consists in measuring the cross sections for the threshold collision induced dissociation (TCID) using a guided ion beam tandem mass spectrometer (GIBMS) [41, 42, 43, 44], and to calculate the binding energies by using unimolecular reaction rate Rice-Ramsperger-Kassel-Marcus (RRKM) theory. The complexes are produced by electrospray ionisation (ESI) of aqueous metal solutions (the ESI source consists of an electrospray emitter, heated capillary, ion funnel, and radio-frequency-only hexapole ion guide). Another method of Armentrout's group to generate clusters is to use a direct current discharge flow tube ion (DC/FT) source [42]. The production of small complexes (usually $n \leq 6$) requires the additional step of in-source fragmentation technique since such complexes are not directly formed with sufficient intensities. This procedure allows the preparation of a reactant ion beam containing only the lowest energy conformer for each cluster ion, which is thermalised to room temperature, and those internal energies can be described by a Maxwell-Boltzmann distribution at 300 K. The ion beam is next extracted from the source and mass selected using a magnetic momentum analyser; then the beam is decelerated to well-defined kinetic energies and focused into a radio frequency octopole ion guide where collision induced dissociation (CID) occurs by using xenon as the collision gas. The ions resulting from the dissociation are selected according to their mass using a quadrupole mass filter and detected by a scintillation ion detector. Finally, the ion intensities are converted into absolute cross sections. The timescale of an experiment is $\sim 10^{-4}$ s. The kinetic-energy-dependent cross sections are modelled to derive the dissociation energy of a CID by using the empirical threshold model. The model takes into account multiple collisions in

order to ensure rigorous single collision conditions; moreover, the model considers energy distribution effects and lifetime effects. In addition, this model requires vibrational frequencies and rotational constants that are obtained via quantum mechanical calculations. The reaction threshold energy calculated with this thermochemical analysis represents the binding energy at 0 K, and it assumes that the transition state of the heterolytic bond cleavage, such as the loss of one neutral water molecule, has no reverse activation barrier. The technique of Armentrout's group also enables the study of various dissociation products such as those resulting from the fragmentation in competing reactions.

The experimental technique developed in Kebarle's group permits the performing of equilibrium experiments, therefore the thermodynamic change in enthalpy for the loss of one molecule at a particular temperature can be determined [45]. More precisely, the experimental procedure in Kebarle's group consists in producing a solution from the salt of the species of interest and then to introduce the ions by ESI into a fore-chamber containing nitrogen gas at a known pressure. Next, the ions drift into the reaction chamber where nitrogen gas (at the same pressure as the one in the fore-chamber) and solvent vapour (at a known partial pressure) are present. After a period of time, the components in the chamber are at thermodynamic equilibrium, then a sample of the gaseous mixture is allowed to enter an evacuated chamber of a triple quadrupole mass spectrometer. In this way, it is possible to measure the intensity ratio of reactant ions and product ions at a precise solvent partial pressure (under the assumption that the ratio in the evacuated chamber and in the reaction chamber coincide). Also, the measurements are made at a known temperature. The plot of intensity ratio versus solvent partial pressure allows one to determine the equilibrium constant of the reaction at the temperature of the experiment from the slope of the straight line. Then the van't Hoff plot (logarithm of the equilibrium constant versus the respective reciprocal temperature) permits the derivation of the enthalpy change for the reaction (from the slope of the straight line).

The group of Castleman has adopted two different experimental techniques to measure the binding energy of cluster ions. The group's oldest investigations are on the thermodynamic properties of cluster ions by performing equilibrium experiments [46, 47, 48]. An appositely constructed high pressure reaction cell is used to allow the preparation of the sample. More precisely, a gaseous reactant at known concentration is introduced into the cell by using a carrier gas; metal ions are obtained by heating a filament (the filament was prepared by fusing the solid metal onto a platinum wire). The reaction temperature inside the chamber is measured as soon as chemical and thermal equilibrium is obtained. A sample is allowed to leak inside the vacuum of a quadrupole mass spectrome-

ter to measure the relative intensities of the reactants and product ions by using pulse counting techniques. The enthalpy and entropy for a cluster reaction are derived from van't Hoff plots. The second technique of Castleman's group uses an apparatus that permits the investigation of dissociation processes [49, 50, 51]; also the apparatus permitted to measure decay fractions and average kinetic energy releases (KER) of metastable ions. These measurements are used to derive binding energies by either applying Klot's evaporative ensemble model for decay fractions [14, 50, 51] or for kinetic energy releases [50], or by using classical unimolecular reaction rate theory of Rice-Ramsperger-Kassel (RRK) combined with phase space theory from the work of Engelking [31, 49, 50]. The experimental technique produces a beam of neutral clusters in a supersonic expansion, and then multiphoton ionisation of the beam occurs with the output of a Nd:YAG pumped dye laser. The ions are accelerated by a time-of-flight mass spectrometer (TOF) so that they can travel through two field-free regions of 210 cm total length at a pressure of $\sim 6 \times 10^{-7}$ mbar. The use of reflecting electric field (permits) to separate parent and daughter ions and to obtain a TOF spectrum of those ions. Such spectrum provides data to derive decay fractions and kinetic energy releases to be determined. Decay fractions are obtained by integrating the intensity of the peaks as a function of a cluster size. KER values are obtained by the analysis of the peak shapes [51]. The determination of KER with the theory of Klots requires that (a) the peaks have a Gaussian shape, (b) the signal-to-noise ratio is good, and (c) there is small channel width in the ion peak. Moreover, it requires choosing the heat capacity for each cluster as well as a value for the Gspann parameter; this parameter is dimensionless and connects "the highest microcanonical temperature in the ensemble to the activation energy" [52] of a unimolecular (metastable) decay. The use of the Engelking theory requires the determination of the KER and unimolecular dissociation rate from the analysis of experimental spectrum, and to choose several parameters [50, 51]. As observed in [50], the inaccuracy in the measurements of a TOF spectrum derives from the signal distortion in the ion detector, the correction of the ion trajectory in the reflective field (since accurate measurements require parent and daughter ions to follow the same path), and the overlap of peaks that may be present in the spectrum.

The techniques designed to study cluster ions in Williams' group are two. The first method is designed to study infrared multiple photon dissociation (IRMPD) action spectra [53, 54] and to obtain information on structure, coordination number, and bonding interactions. The second method allows performing equilibrium experiments with the objective of deriving binding energies from blackbody infrared radiative dissociation (BIRD) measurements [55, 56, 57, 58].

In particular, the experimental procedure consists of an ESI source Fourier-transform ion cyclotron resonance (FT-ICR) mass spectrometer. The BIRD experiments are accomplished using a cylindrical ion cell that is surrounded by a thermal jacket which permits a chosen temperature to be maintained. The dissociation occurs by absorption of blackbody photons generated by the heated chamber at a pressure below 10^{-8} mbar [55, 56, 57, 58]. Unimolecular dissociation rate constants are measured as a function of temperature. The threshold dissociation energy equals the enthalpy if the reverse activation barrier for dissociation is negligible. The threshold dissociation energy is derived by a master equation calculation to fit the experimental dissociation rate constants and Arrhenius parameters. The necessary parameters for the master equation are obtained by theoretical calculation. In particular, the microcanonical dissociation rate constants are calculated using unimolecular reaction rate RRKM theory.

The experimental procedure designed in Stace's group consists in using a supersonic expansion source to generate a neutral beam, which contains mixed clusters each formed by carrier gas and molecular solvent, where the carrier gas is an inert gas. The pick-up process, which is a technique developed in Stace's group [59, 60, 61, 62, 63, 64, 65, 66, 67], is used to prepare the metal-solvent neutral beam. In particular, the collision in the pick-up process between the metal atom and the cluster beam made of neutral carrier gas and molecular solvent allows the metal to be embedded into the molecular solvent. Moreover, the collision in the pick-up process causes the evaporation of the carrier gas, so that the complex can dissipate energy by using the carrier gas as an energy sink [59]. The cluster beam reaches a high resolution mass spectrometer having reverse geometry, where the clusters are

- i. ionised by electron impact,
- ii. extracted from the ion source and accelerated to a known kinetic energy,
- iii. mass selected at a magnetic sector, and
- iv. analysed at an electric sector with mass-analysed ion kinetic energy (MIKE) spectrometry.

The MIKE technique is used to measure the KER [68, 69] of a selected unimolecular metastable decay, and specifically in this work neutral loss. Accurate measurements have been performed by collecting a large amount of data for each MIKE spectrometry scan. Moreover, in order to minimise the effects of a kinetic energy spread in precursor ions, the laboratory frame full width half maximum (FWHM) peak widths of the precursor ions are (almost) all at

least ~ 2 eV (*cf.* Chapter 9). For the purpose of analysing MIKE spectra it has been assumed that both the peak shapes of fragment and precursor ions are Gaussian (it is required that the goodness of peak shape measured by the correlation coefficient is as close as possible to the maximum value, which is 1). The experiments are performed at a pressure $< 1 \times 10^{-7}$ mbar that ensures minimal interference from collision induced fragmentation [26]. The analysis of the data consists in transforming KER values to binding energies; this transformation is achieved using the evaporative ensemble statistical model by Klots [17, 18, 19, 20, 21] (also known as finite heat bath theory by Klots). The employment of Klots theory implies assigning a value to the Gspann parameter and the heat capacity C (at constant volume); the former is set at 23.5 ± 1.5 (which appears to be the most frequently used value in calculations of the type discussed in these studies [68]) and for the latter we set $C = 6(n - 1)$ in units of Boltzmann constant minus one [70] where n is the number of molecules in the cluster. This expression of C assumes that none of the intramolecular vibrations in any of the molecules are active and that overall rotation and translation of a cluster do not contribute to the heat capacity.

1.3 Advantages of Stace's Technique

The experimental studies presented in this work provide binding energies for the unimolecular metastable detachment of a neutral molecule for $[M(\text{H}_2\text{O})_n]^{2+}$, $[M(\text{NH}_3)_n]^{2+}$, and $[M(\text{CH}_3\text{OH})_n]^{2+}$ with $4 \leq n \leq 20$ where M is magnesium, calcium, or strontium; and for $\text{H}^+(\text{H}_2\text{O})_n$, $\text{H}^+(\text{NH}_3)_n$, and $\text{H}^+(\text{CH}_3\text{OH})_n$ with $3 \leq n \leq 30$.

The experimental procedure to measure accurate binding energies has been developed in this laboratory using the study on the binding energy measurements on $\text{H}^+(\text{H}_2\text{O})_n$, $\text{H}^+(\text{NH}_3)_n$, and $\text{H}^+(\text{CH}_3\text{OH})_n$ for $3 \leq n \leq 30$ as a calibration method [71]. Also, our results on $\text{H}^+(\text{H}_2\text{O})_n$, $\text{H}^+(\text{NH}_3)_n$, and $\text{H}^+(\text{CH}_3\text{OH})_n$ molecular clusters have been compared with several studies, in particular with those of Kebarle's group [10, 11, 72, 73, 74, 75], Castleman's group [14, 31, 32, 48, 49, 76, 77, 78], and of Armentrout's group [79, 80].

Experimental investigations on doubly charged clusters in gas phase for the loss of a single neutral molecule and binding energy measurements have also been performed

- by Armentrout's group on $[\text{Mg}(\text{H}_2\text{O})_n]^{2+}$ for $2 \leq n \leq 10$, on $[\text{Ca}(\text{H}_2\text{O})_n]^{2+}$ for $2 \leq n \leq 8$ [44, 41], on $[\text{Sr}(\text{H}_2\text{O})_n]^{2+}$ for $1 \leq n \leq 6$ [42];
- by Kebarle's group on $[\text{Mg}(\text{H}_2\text{O})_n]^{2+}$ for $n = 2$ and $6 \leq n \leq 14$ [81, 45,

82], on $[\text{Ca}(\text{H}_2\text{O})_n]^{2+}$ for $n = 2$ and $6 \leq n \leq 14$ [81, 45, 82], and on $[\text{Sr}(\text{H}_2\text{O})_n]^{2+}$ for $6 \leq n \leq 14$ [81, 45];

- and by the group of Williams on $[\text{Mg}(\text{H}_2\text{O})_n]^{2+}$ for $5 \leq n \leq 10$ [55, 56, 57], on $[\text{Ca}(\text{H}_2\text{O})_n]^{2+}$ for $5 \leq n \leq 10$ [55, 56, 57, 58], and on $[\text{Sr}(\text{H}_2\text{O})_n]^{2+}$ for $5 \leq n \leq 7$ [55, 56].

In addition, experimental investigations on singly charged clusters in gas phase for the loss of a single neutral molecule and binding energy measurements have been performed

- by the group of Armentrout on $[\text{Mg}(\text{H}_2\text{O})_n]^+$ for $1 \leq n \leq 4$ [83], on $[\text{Mg}(\text{NH}_3)_n]^+$ for $1 \leq n \leq 5$ [84]; and on $[\text{Mg}(\text{CH}_3\text{OH})_n]^+$ for $1 \leq n \leq 3$ [84];
- by Castleman's group on $[\text{Sr}(\text{H}_2\text{O})_n]^+$ for $1 \leq n \leq 9$ [85].

The experimental methodology designed by Stace coupled with the evaporative ensemble statistical model developed by Klots has given the possibility to measure accurate KER and to derive binding energies for doubly charged metal ions solvated in water, methanol, and ammonia.

The principal result of the first applications of this method revealed the importance of the doubly positive charge of the metal in the binding interactions. More precisely, the double charge of the metal is involved in the solvation of the clustering solvent molecules even after the first solvation shell is completed. This behaviour has been observed for Mg^{2+} , Ca^{2+} , and Sr^{2+} in ammonia, methanol, and water up to twenty solvent molecules. The other important results that can be determined with these experiments are coordination number and binding energies. In contrast, the experiments of other groups for those metals only investigated the solvation in water for small number of molecules.

The experimental procedure developed by Stace's group detects unimolecular metastable decay from experiments that are not at equilibrium. Similarly, Armentrout's experimental procedure is not performed at equilibrium; conversely, the studies of Castleman and Williams are measurements of gas phase clustering equilibria. Also, the latter studies enable quantitative measurements of the enthalpy of solvation over a temperature and pressure range.

Bibliography

- [1] R. Boyle, in *The Sceptical Chymist, 1st edn.*, 1661, Everyman's Library, J. M. Dent & Sons Ltd., London, 1st published in this edn. 1911.
- [2] L. Principe, *Nature* 469 (2011) 30.
- [3] R.L. Johnston, in *Atomic and Molecular Clusters*, Taylor & Francis, London and New York, 2002, pp. 7.
- [4] A.J. Stace, *The Journal of Physical Chemistry* 106 (2002) 7993.
- [5] H. Lodish, A. Berk, P. Matsudaira, C.A. Kaiser, M. Krieger, M.P. Scott, S.L. Zipursky, *Molecular Cell Biology*, W. H. Freeman and Company, New York, 2004.
- [6] J.Q. Searcy, J.B. Fenn, *Journal of Chemical Physics* 61 (1974) 5282.
- [7] T.F. Magnera, D.E. David, J. Michl, *Chemical Physical Letters* 182 (1991) 363.
- [8] T. Schindler, C. Berg, G. Niedner-Schatteburg, V.E. Bondybey, *Chemical Physical Letters* 250 (1996) 301.
- [9] R.G. Keesee, A.W. Castleman, Jr., *Journal of Physical and Chemical Reference Data* 15 (1986) 1011.
- [10] P. Kebarle, S.K. Searles, A. Zolla, J. Scarborough, M. Arshadi, *Journal of the American Chemical Society* 89 (1967) 6393.
- [11] A.J. Cunningham, J.D. Payzant, P. Kebarle, *Journal of the American Chemical Society* 94 (1972) 7627.
- [12] Y.K. Lau, S. Ikuta, P. Kebarle, *Journal of the American Chemical Society* 104 (1982) 1462.
- [13] K. Hansen, P.U. Andersson, E. Uggerud, *Journal of Chemical Physics* 131 (2009) 124303.

- [14] Z. Shi, J.V. Ford, S. Wei, A.W. Castleman Jr., *Journal of Chemical Physics* 99 (1993) 8009.
- [15] P. C. Engelking, *The Journal of Chemical Physics* 85 (1986) 3103.
- [16] P. C. Engelking, *The Journal of Chemical Physics* 87 (1987) 936.
- [17] C.E. Klots, *Journal of Chemical Physics* 83 (1985) 5854.
- [18] C.E. Klots, *Nature* 327 (1987) 222.
- [19] C.E. Klots, *Journal of Physical Chemistry* 92 (1988) 5864.
- [20] C.E. Klots, *Accounts of Chemical Research* 21 (1988) 16.
- [21] C.E. Klots, *Journal of Chemical Physics* 90 (1989) 4470.
- [22] A.J. Stace, A.K. Shukla, *Chemical Physics Letters* 85 (1982) 157.
- [23] A.J. Illies, M.F. Jarrold, M.T. Bowers, *International Journal of Mass Spectrometry* 47 (1983) 93.
- [24] A.J. Illies, M.F. Jarrold, L.M. Bass, M.T. Bowers, *Journal of the American Chemical Society* 105 (1983) 5775.
- [25] A.J. Stace, *Journal of Chemical Physics* 85 (1986) 5774.
- [26] C.A. Woodward, A.J. Stace, *Journal of Chemical Physics* 94 (1991) 4234.
- [27] A.J. Stace, P.G. Lethbridge, J.E. Upham, C.A. Woodward, *Journal of the Chemical Society, Faraday Transactions* 86 (1990) 2405.
- [28] A.W. Castleman Jr., R.G. Keesee, *Chemical Reviews* 86 (1986) 589.
- [29] C. Lifshitz, F. Louage, *International Journal of Mass Spectrometry and Ion Processes* 101 (1990) 101.
- [30] M. Iraqi, C. Lifshitz, *International Journal of Mass Spectrometry and Ion Processes* 88 (1989) 45.
- [31] S. Wei, W.B. Tzeng, A.W. Castleman Jr., *Journal of Chemical Physics* 92 (1990) 332.
- [32] S. Wei, K. Kilgore, W.B. Tseng, A.W. Castleman Jr., *Journal of Physical Chemistry* 95 (1990) 8306.

- [33] S. Wei, Z. Shi, A.W. Castleman Jr., *Journal of Chemical Physics* 94 (1991) 8604.
- [34] S. Atrill, A.J. Stace, *International Journal of Mass Spectrometry* 180 (1998) 253.
- [35] S. Atrill, A. Mouhandes, J.F. Winkel, A. Goren, A.J. Stace, *Faraday Discussions* 102 (1995) 339.
- [36] S. Atrill, A.J. Stace, *Journal of Chemical Physics* 108 (1998) 1924.
- [37] S. Matt, M. Sonderegger, R. David, O. Echt, P. Scheier, J. Laskin, C. Lifshitz, T.D. Märk, *Chemical Physics Letters* 303 (1999) 379.
- [38] R. Parajuli, S. Matt, O. Echt, A. Stamatovic, P. Scheier, T.D. Märk, *The European Physical Journal D* 16 (2001) 69.
- [39] R. Parajuli, S. Matt, O. Echt, A. Stamatovic, P. Scheier, T.D. Märk, *Chemical Physics Letters* 352 (2002) 288.
- [40] S. Matt, R. Parajuli, A. Stamatovic, P. Scheier, T.D. Märk, *Journal of Chemical Physics* 116 (2002) 7583.
- [41] D.R. Carl, P.B. Armentrout, *Journal of Physical Chemistry A* 116 (2012) 3802.
- [42] D.R. Carl, B.K. Chatterjee, P.B. Armentrout, *Journal of Chemical Physics* 132 (2010) 044303.
- [43] D.R. Carl, P.B. Armentrout, *ChemPhysChem: A European Journal of Chemical Physics and Physical Chemistry* 14 (2013) 681.
- [44] D.R. Carl, R.M. Moision and P.B. Armentrout, *International Journal of Mass Spectrometry* 265 (2007) 308.
- [45] M. Peschke, A. T. Blades, P. Kebarle. *Journal of Physical Chemistry A* 102 (1998), 9978.
- [46] I.N. Tang, M.S. Lian, A.W. Castleman Jr., *The Journal of Chemical Physics* 65 (1976) 4022.
- [47] I.N. Tang, A.W. Castleman Jr., *The Journal of Chemical Physics* 60 (1974) 3981.
- [48] I.N. Tang, A.W. Castleman Jr., *The Journal of Chemical Physics* 62 (1975) 4576.

- [49] A.W. Castleman Jr., W.B. Tzeng, S. Wei, S. Morgan, *Journal Chem. Soc. Faraday Trans.* 86 (1990) 2417.
- [50] S. Wei, W.B. Tzeng, A.W. Castleman Jr., *The Journal of Chemical Physics* 93 (1990) 2506.
- [51] S. Wei, W.B. Tzeng, A.W. Castleman Jr., *Journal of Physical Chemistry* 95 (1991) 8306.
- [52] K. Hansen, in *Statistical Physics of Nanoparticles in the Gas Phase*, ed. Springer Science+Business Media, Dordrecht, 1st edn., 2013.
- [53] M.F. Bush, J.T. O'Brien, J.S. Prell, C.-C. Wu, R.J. Saykally, E.R. Williams, *Journal of the American Chemical Society* 131 (2009) 13270.
- [54] M.F. Bush, R.J. Saykally, E.R. Williams, *Journal of the American Chemical Society* 130 (2008) 15842.
- [55] S.E. Rodriguez-Cruz, R.A. Jockusch, E.R. Williams, *Journal of the American Chemical Society* 121 (1999) 1986.
- [56] S.E. Rodriguez-Cruz, R.A. Jockusch, E.R. Williams, *Journal of the American Chemical Society* 121 (1999) 8898.
- [57] R.L. Wong, K. Paech, E.R. Williams, *International Journal of Mass Spectrometry* 232 (2004) 59.
- [58] S.E. Rodriguez-Cruz, R.A. Jockusch, E.R. Williams, *Journal of the American Chemical Society* 120 (1998) 5842.
- [59] G. Del Mistro, A.J. Stace, *Chemical Physical Letters* 196 (1992) 67.
- [60] T.E. Gough, M. Mengel, P.A. Rowntree, G. Scoles, *Journal of Chemical Physics* 83 (1985) 4958.
- [61] D.J. Levandier S. Goyal, J. McCombie, B. Pate, G. Stoles, *Journal of the Chemical Society, Faraday Transactions* 86 (1990) 2361.
- [62] X.J. Gu, D.J. Levandier, B. Zhang, G. Scoles, D. Zhuang, *Journal of Chemical Physics* 93 (1990) 4898.
- [63] M.P. Dobson, A.J. Stace, *Chemical Communications* 13 (1996) 1533.
- [64] C.A. Woodward, M.P. Dobson, A.J. Stace, *Journal of Physical Chemistry* 100 (1996) 5605.

- [65] J.F. Winkel, A.B. Jones, C.A. Woodward, D. A. Kirkwood, A. J. Stace, *Journal of Chemical Physics* 101 (1994) 9436.
- [66] A.B. Jones, R. Lopez-Martens, A.J. Stace, *Journal of Physical Chemistry* 99 (1995) 6333.
- [67] N. Walker, M.P. Dobson, R.R. Wright, P.E. Barran, J.N. Murrell, A.J. Stace, *Journal of the American Chemical Society* 122 (2000) 11138.
- [68] C. Lifshitz, C.-Y. Ng, T. Baer, I. Powis (Eds.), in *Cluster Ions*, Wiley, Chichester, 1st edn., 1993, ch. 2, pp. 121-164.
- [69] R.G. Cooks, J.H. Beynon, R.M. Caprioli, G.R. Lester, in *Metastable Ions*, ed. Elsevier Scientific Pub. Co., Amsterdam, New York, 1st edn., 1973.
- [70] A.E.K. Sundén, K. Støchkel, S. Panja, U. Kadhane, P. Hvelplund, S. Brønsted Nielsen, H. Zettergren, B. Dynefors, K. Hansen, *Journal of Chemical Physics* 130 (2009) 224308.
- [71] E. Bruzzie (E. Bruzzi), R. Parajuli, A.J. Stace, *International Journal of Mass Spectrometry* 345 (2013) 160.
- [72] J.D. Payzant, A.J. Cunningham, P. Kebarle, *International Canadian Journal of Chemistry* 51 (1973) 3242.
- [73] S.K. Searles, P. Kebarle, *Journal of Physical Chemistry* 72 (1968) 742.
- [74] A.M. Hogg, R.N. Haynes, P. Kebarle, *Journal of American Chemical Society* 88 (1966) 28.
- [75] Y.K. Lau, S. Ikuta, P. Kebarle, *Journal of the American Chemical Society* 104 (1982) 1462.
- [76] K. Stephan, J.H. Futrell, K.I. Peterson, A.W. Castleman, Jr., H.E. Wagner, N. Djuric, T.D. Mark, *International Journal of Mass Spectrometry and Ion Physics* 44 (1982) 167.
- [77] S. Wei, Z. Shi, A.W. Castleman Jr., *Journal of Chemical Physics* 94 (1991) 3268.
- [78] P.M. Holland, A.W. Castleman, Jr., *Journal of Chemical Physics* 72 (1980) 5.
- [79] K. Honma, L.S. Sunderlin, P.B. Armentrout, *Journal of Chemical Physics* 99 (1993) 1623.

- [80] N.F. Dalleska, K. Honma, P.B. Armentrout, *Journal of the American Chemical Society* 115 (1993) 12125.
- [81] A.T. Blades, P. Jayaweera, M.G. Ikononou, P.Kebarle, *Journal of Chemical Physics* 92 (1990) 5900.
- [82] M. Peschke, A.T. Blades, P. Kebarle, *International Journal of Mass Spectrometry* 185/186/187 (1999) 685.
- [83] N.F. Dalleska, B.L. Tjelta, P.B. Armentrout, *Journal of Physical Chemistry* 98 (1994) 4191.
- [84] A. Andersen, F. Muntean, D. Walter, C. Rue, P.B. Armentrout, *Journal of Physical Chemistry A* 104 (2000) 692.
- [85] I.N. Tang, M.S. Lian, A.W. Castleman, *Journal of Chemical Physics* 65 (1976) 4022.

Chapter 2

Experimental Apparatus

2.1 Schematic Diagram of the Experimental Apparatus

The experimental apparatus [1, 2] for the generation, selection, and detection of gas phase charged clusters is shown in the schematic diagram of Figure 2.1.1. The main components of the instrumentation are a supersonic nozzle, an effusion cell, and a Nier-Jordan high resolution double-focusing mass spectrometer having reversed sector geometry.

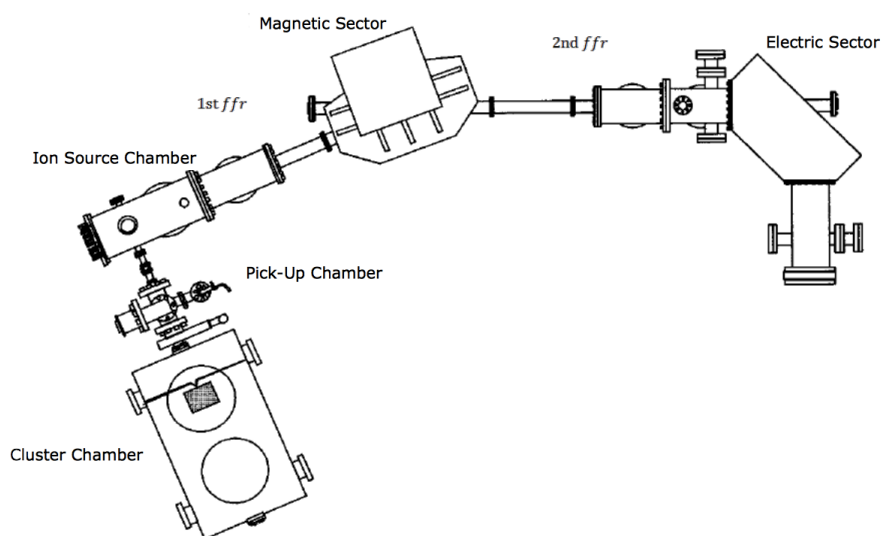


Figure 2.1.1: Schematic view of the apparatus from the top [2]

2.2 Cluster Chamber

The cluster chamber contains the apparatus for formation and growth of a molecular beam of clusters. The cluster chamber is made of stainless steel and it has a cylindrical shape. As illustrated in Figure 2.2.1, the cluster chamber is divided into two parts by a 20 mm thick bulkhead: the expansion and the collimation sections, which have approximate volumes of 0.18 m^3 and 0.02 m^3 , respectively. The cluster chamber is kept at high vacuum through the use of vacuum pumps.

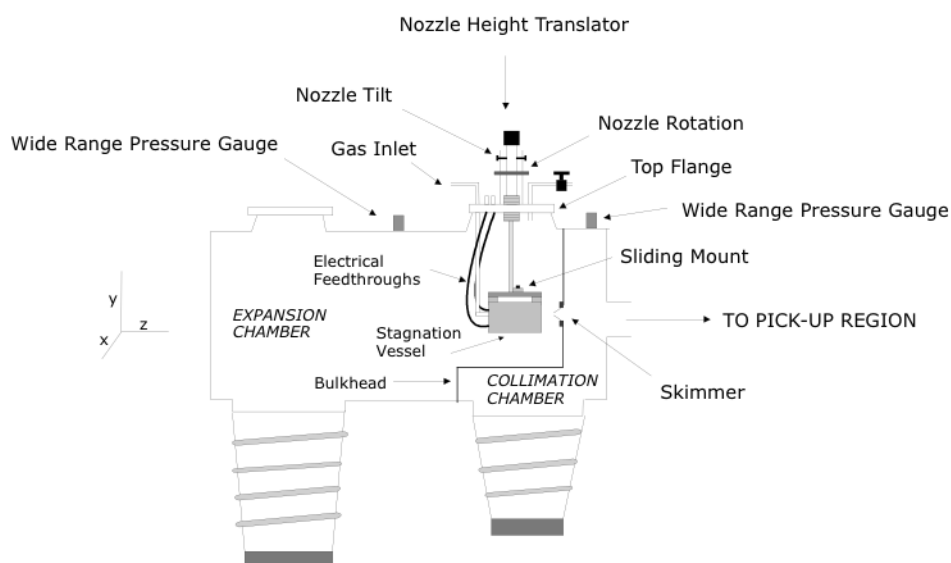


Figure 2.2.1: Schematic diagram of the cluster chamber (adapted from [3])

The pumping system controller is placed at the console; it is a device that was designed and manufactured in our laboratory in 1989 [4]. When the nozzle is not in use, the expansion section has a pressure of 10^{-7} mbar, which is maintained by using an 8000 L s^{-1} diffusion pump backed by a two stage rotary vane pump (Edwards E2M40). When the nozzle is operating, the pressure within the range of $10^{-5} - 10^{-6}$ mbar is maintained by the additional support of a mechanical booster pump (Edwards EH250). The collimation region is pumped by a 2000 L s^{-1} diffusion pump (Edwards Diffstak) backed with a two stage rotary vane pump (Edwards E2M40). As a result, the collimation section is kept at a pressure of 10^{-7} mbar if the nozzle is not utilized and at a pressure of 10^{-6} mbar if the nozzle is functioning.

As shown in Figure 2.2.1, the stagnation vessel (also known as nozzle chamber) hangs from the top flange of the expansion section by a stainless steel rod. The nozzle chamber is made of aluminium and it has a volume of approximately

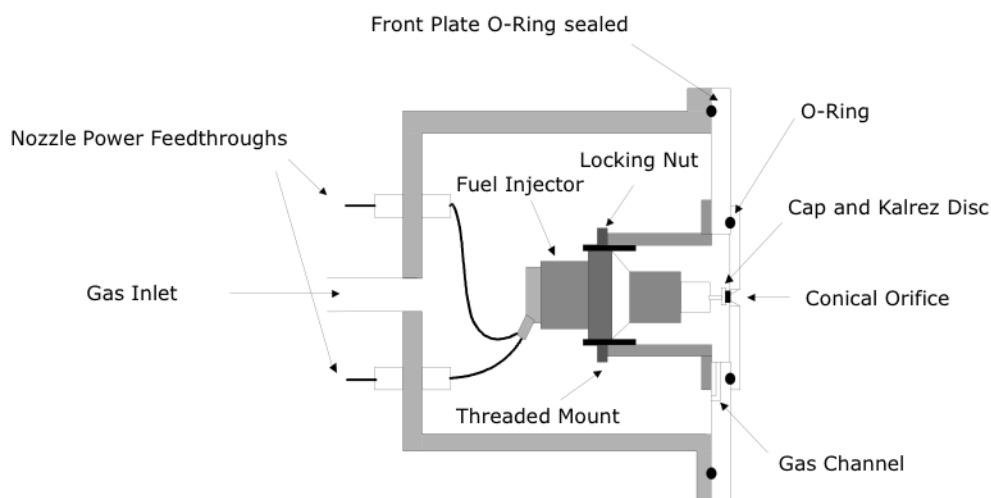


Figure 2.2.2: Schematic diagram of the stagnation vessel (adapted from [3])

0.8 L. It can be seen from the Figure 2.2.2 that the front plate of the nozzle chamber is O-ring sealed and the pulsed nozzle orifice is placed in its centre. The nozzle has a conical shape with a $200\ \mu\text{m}$ diameter hole, 30° opening cone angle, and a channel length of 5 mm. Furthermore, as shown in Figure 2.2.1, the skimmer (made of nickel) is mounted on the bulkhead and it is O-ring sealed with a brass locking ring. The skimmer is 25 mm long and has a conical shape with an internal cone of 25° , an external angle of 30° , and a 1 mm diameter. The nozzle orifice and the skimmer are aligned by a three adjustable connectors placed on the external surface of the expansion chamber. The adjusters allow the nozzle to move in the x,y,z directions; more precisely 360° rotation in the horizontal plane, 25 mm translation vertically, and tilt control. The fuel injector valve (Bosch, Serial No. 028 150 045) is placed inside the stagnation vessel and is mounted on the front plate. The fuel injector is driven by an electrical signal of $0\ \text{V} - 12\ \text{V}$ square wave pulse at a frequency between 10 Hz and 20 Hz. The plunger is mounted onto the fuel injector needle; it consists of a 3 mm diameter stainless steel cap covered in a disc of Kalrez (Du Pont U.K. Ltd.) rubber piece. The pulse generator (Digital Delay/Pulse Generator Stanford Research Systems, Inc. Model DG535) has an external trigger; the pulse generator allows control of the pulse frequency, pulse width, and delay of the pulse. The maximum pressure and the maximum frequency supported by the nozzle are 180 psi and 40 Hz

respectively.

A pulsed nozzle was chosen for these experiments; it enabled to easily obtain higher source stagnation pressure than the one provided by a continuous nozzles at the same backing pressure [5].

2.2.1 Free Jet: an Overview

A free jet source is designed to produce a free jet molecular beam, also known as supersonic beam, through the evolution of a continuum flow to a free jet expansion from a high pressure region into the vacuum. The characteristic of a free jet expansion is to cool the internal degrees of freedom of the gas by narrowing the distribution of speeds and the internal energy distribution. Moreover, an inert gas may be used as carrier of the gaseous sample and its presence may lead to a further cooling of the internal degrees of freedom of the gas and to enhance cluster formation. In particular, nucleation and growth of clusters are observed in expanding gas flows.

The main components of a free jet source are a mechanical device to inject the gas, a nozzle, a skimmer, and a pumping system. The free jet source is maintained at low pressure by the use of high vacuum pumps. Typically, a pulsed beam source is used in order to keep a constant high stagnation pressure inside the chamber in which the mechanical device is placed. In fact, the vacuum pumps system may restore the initial pressure after each pulse. It is necessary that the gas initially has its mean free path λ smaller than the diameter D of the orifice of the nozzle; this condition is achieved by placing the gas in a sufficiently high pressure region and/or by increasing the size of the hole of the nozzle. As described by the Knudsen number

$$K_n = \frac{\lambda}{D}$$

a supersonic expansion is achieved when $K_n \ll 1$, namely when $\lambda \ll D$, since $\lambda \propto \frac{1}{\text{pressure}}$. In contrast, an effusive beam is originated if $\lambda \gg D$, and the distribution of speed of the molecules would be the same as the velocity in the stagnation chamber. The free jet expansion can be viewed as an adiabatic and isentropic process [5], that is as a process performed at constant energy and entropy. The gas expands into the vacuum from the pressurised reservoir (*i.e.* the gas is at stagnation pressure initially), and the collisions between the particles during expansion cool the translational, rotational and vibrational degrees of freedom. Furthermore, the collisions of the gas molecules with the inert gas molecules contribute to convert the rotational and vibrational energies into translational energy. As a consequence, the gas obtains a supersonic jet distri-

bution of speed. As shown in Figure 2.2.3, the gas reaches the speed of sound at the nozzle exit in the zone of silent, where the Mach number equals 1. The Mach number (hereafter denoted by M) is a measure of the average speed of the gas molecules in the expanding gas with respect to the local speed of sound. As the jet flows away from the nozzle, i.e. $M \gg 1$, the expansion of the gas becomes isentropic [5], and the molecular beam is formed. The high pressure gas that exits from the high pressure zone to the low pressure chamber expands and compresses the gas in front of it producing shock fronts, Mach Disk and Barrel Shock. In particular, the Mach disc shock is a wave that forms downstream at the point in which the collision with background gas becomes predominant. The shockwave is not an isentropic region and it has high density, pressure, temperature, and velocity gradients [5]. The supersonic jet keeps expanding until $M < 1$, where the beam adjusts to the boundary conditions imposed by the background pressure. These relations are due to the difference in energies between

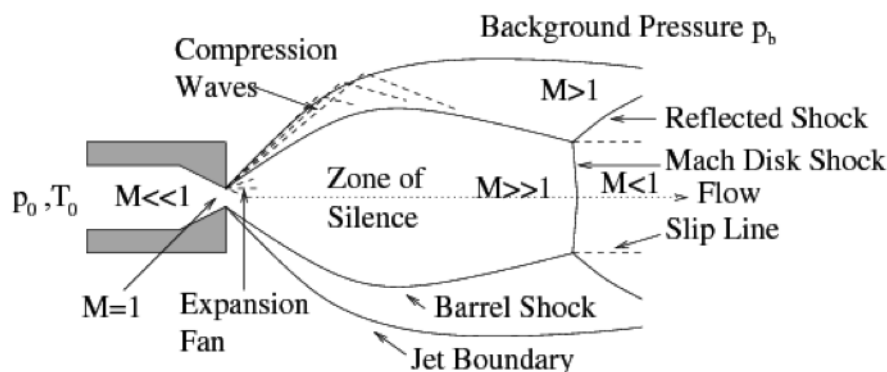


Figure 2.2.3: Structure of free jet expansion [5, Ch. 2, pp. 15, Fig. 2.1 by D. R. Miller.]

adjacent quantum states that determine the cooling efficiency.

The supersonic expansion does not lead to equilibrium between the internal degrees of freedom of any molecules present in the jet. In fact, the collisions in the expanding gas relax rotational degrees of freedom more readily than vibrational degrees of freedom since not enough collisions are available in order to reach the equilibrium. The final spread of velocity becomes narrower than before the expansion through mainly translational and rotational velocity distribution narrowing, so that the initial molecules temperature is much higher than the final rotational and translational temperatures:

$$T_{\text{initial}} \geq T_{\text{vibrational}} \geq T_{\text{rotational}} \equiv T_{\text{translational}}$$

In order to extract the jet beam for experimental purposes, a skimmer is used. The skimmer is placed in the core of the supersonic expansion, namely in the zone of silence. (Nevertheless, our experiment is designed to avoid the formation of the shockwave which would degrade the jet.) Collision rates, excessive condensation, background scattering, and skimmer losses are the factors that mostly affect the supersonic expansion.

The speed distribution of a molecular beam seeded in a carrier gas is narrower than the one of a net molecular beam (*i.e.* without carrier gas). Moreover, the narrowing of the molecular speed distributions corresponds to increasing the Mach number; consequently $M = 1$ for a Maxwell-Boltzmann speed distribution and $M = \infty$ for an infinitely narrow speed distribution.

Figure 2.2.4 compares the Maxwell-Boltzmann speed distribution in the stagnation chamber, with the speed distribution in the supersonic beam.

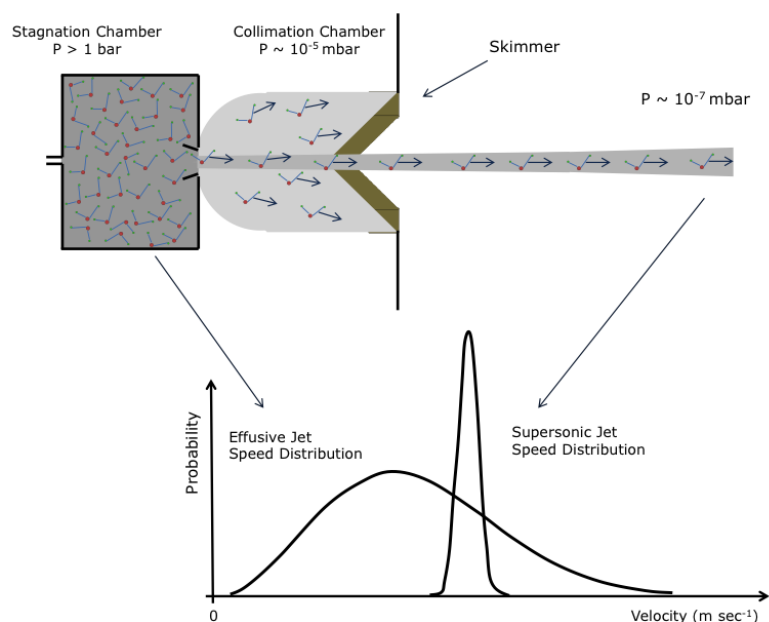


Figure 2.2.4: Schematic representations of free jet expansion and molecular speed distribution (adapted from [6])

2.3 Solvent Reservoir

In these experiments, molecular beams of clusters are produced by pulsed supersonic free jet expansion of a mixture formed by a gaseous solvent and an inert gas. The function of the inert gas is to carry molecules of solvent and to enhance aggregation. The solvent may be either in the gaseous phase or in the liquid phase at room temperature and room pressure. If the solvent is liquid, the substance is placed in a stainless steel reservoir, and the inert gas is passed

through the liquid. The reservoir is placed in the gas line between the carrier gas cylinder and the supersonic nozzle chamber. This reservoir is filled with approximately 20 mL of liquid; furthermore, it may be placed in an ice bath to decrease the vapour pressure of the solvent. As shown in Figure 2.3.1, the carrier gas expands inside the reservoir through the carrier gas inlet, and vapour solvent molecules are seeded into the inert carrier gas, so that a gas-vapour mixture forms and flows outside the reservoir through the output.

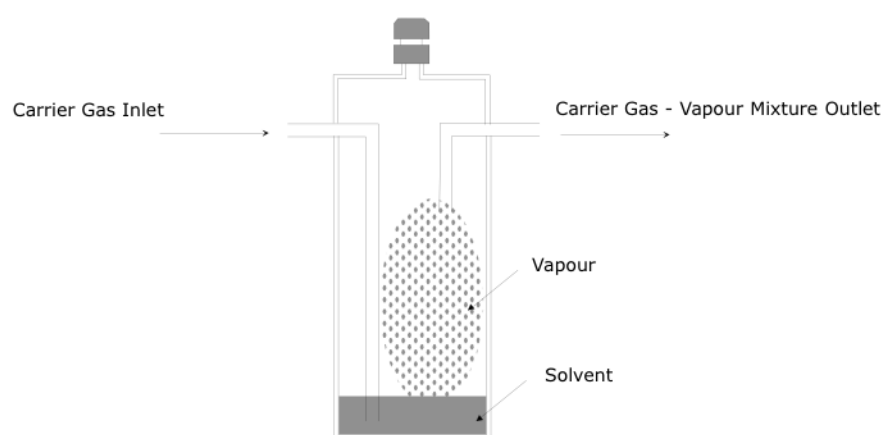


Figure 2.3.1: Schematic diagram of the solvent reservoir (adapted from [3])

In order to obtain generation of gas phase clusters, it is required that the vapour pressure of the solvent is adequate to the experimental requirements. In particular, the intensity of the signal of a beam of clusters can be improved by regulating the ratio of carrier gas and solvent. This is obtained by adjusting the pressure of the carrier gas and by reducing the vapour pressure of the solvent in the reservoir, whilst keeping the pressure of the nozzle chamber lower than 4×10^{-5} mbar and the pressure in the pick-up chamber lower than 2×10^{-5} mbar. Moreover, the use of an ice bath contributes to improve the conditions for the production of high intensity beam signals by reducing the vapour pressure of the liquid.

The addition of an inert gas (carrier gas) to a monomer supersonic expansion enhances the formation of clusters [5]. In fact, the collisions with the carrier gas facilitate the removal of condensation energy. In order to achieve maximum cluster sizes or high cluster abundances, the partial pressure of the inert gas can be increased. Another effect is the production of clusters containing one or more atoms of inert gas. It has been observed that the nature of the inert gas (heavy

or light molecular mass) may have an effect on both the degree of solvation and the cooling process [5].

If the solvent is gaseous, it can be made available with a carrier gas as a gaseous mixture in a premixed cylinder; therefore the mixture is connected from the cylinder to the nozzle chamber via a gas line.

2.4 Cluster Formation in Supersonic Beams

Between 1961 and 1965, mass spectrometry provided the first evidence of cluster formation in a supersonic beam [5]. The main techniques available to prepare cluster beams are [5]

- Knudsen effusion, flow aggregation (Schulze, Sattler, Andres, Martin, Wexler)
- continuous supersonic expansion (free jet, seeded free jet, constrained expansion, electrospray, ion clustering), and
- pulsed supersonic expansion (standard, rotating slit in high-temperature over, MPD/MPI on metal carbonyls, laser vaporisation).

The flux of generated clusters is the highest with supersonic expansion method and the lowest with Knudsen effusion technique.

The extent of cluster content and average cluster size in a free jet depends on various factors. More precisely, on stagnation pressure, initial gas temperature, and aperture cross section of nozzle geometry [5].

Theoretical models for the description of cluster nucleation in a supersonic beam are [5]:

- (1) macroscopic classical nucleation rate theory and time-dependent macroscopic classical nucleation rate theory,
- (2) molecular dynamics (MD) and Monte-Carlo (MC) simulations,
- (3) phenomenological-microscopic approach.

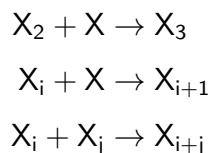
Two-body collisions cool a gas in a supersonic expansion, whereas three-body collisions in a supersonic jet cause the formation of van der Waals complexes and, therefore, of clusters. In a three-body (termolecular) collision, two bodies form a new species and the third body participates to stabilise the new species before leaving [7]. Nucleation of clusters through two-body (bimolecular) collision is possible [7], if the new species has an enough long lifetime to

allow collision with another body (in a two-body collision) in order to form a stable species.

There are three steps in the formation of clusters in a molecular beam: cluster nucleation, cluster growth, and cluster cooling [8]. The former step is a collision of three monomers; more precisely, this collision leads to the formation of a dimer, and the third atom removes the excess energy as kinetic energy to allow the dimer to stabilise



The second step, cluster growth, occurs by collision and subsequent coalescence of two species:



The final step, cluster cooling, lowers the internal energy (temperature) of the cluster; the cooling of clusters can proceed by two mechanisms. Collisional cooling allows the cluster to lose kinetic energy by a two-body collision with a monomer or with a carrier gas atom. Evaporative cooling is a unimolecular dissociation, in which the excess energy remains on the departing atom. For evaporation to occur, the energy must be channeled in the correct vibrational mode to overcome the kinetic energy barrier and allow bond breaking. If there are no conditions for collisional cooling to occur, then evaporative cooling is the only alternative mechanism observed.

Radiative cooling in the infrared radiation (IR) region can be disregarded owing to the lifetimes of clusters in a typical experiment.

2.5 Pick-Up Chamber

The pick-up process [9, 10, 11] happens in the pick-up chamber, which contains the Knudsen effusion cell. The pick-up technique was developed in this laboratory in 1996 [12, 13] to produce metal complexes in the gas phase by embedding the metal in a solvent environment before ionisation [12]; and to contribute to studying the properties of metals in the presence of solvent molecules. More precisely, as shown in Figure 2.5.1, the pick-up technique [14] allows the metal vapour (the metal atoms constituting the metal vapour are formed in the Knudsen effusion cell) and the cluster supersonic free jet to perpendicularly cross and

collide; consequently, a metal atom becomes embedded into the surface of the neutral carrier gas and solvent cluster, and is then solvated while the inert carrier gas molecules (or molecule) detach from the surface of the metal solvent cluster. It is unknown the stage of the process at which the metal atom becomes solvated. The electron impact ionisation (E.I.) process will cause definitive evaporation of any carrier gas atoms that remain adsorbed on the cluster surface. Therefore the presence of the carrier gas in the neutral clusters is essential; it can be defined as an energy sink since it participates in achieving the conditions for both the attachment of the metal atom and the stabilization of the ionic species after ionisation [15, 16]. In fact, it was shown [14] with a molecular dynamics simulation that in the simple case of colliding Ar_{20} with a single acetonitrile molecule, the cluster first melts and the molecule then moves below the surface within 40 ps of the collision; the mixed cluster then achieves stabilisation through the evaporation of argon. Moreover, experiments have proved that the energy of the collision in each of the two collisional processes is dispersed by ejecting carrier gas atoms [17].

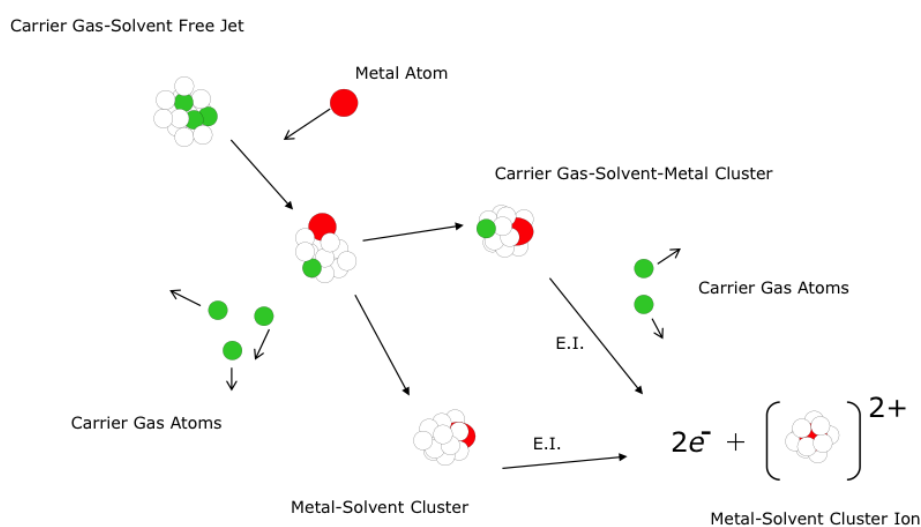


Figure 2.5.1: Schematic representation of pick-up process followed by electron impact (EI) ionisation (adapted from [3])

The pressure in the pick-up section is $\sim 7 \times 10^{-7}$ mbar when the apparatus is not in use, while it can reach a maximum of 2×10^{-5} mbar during experiments. These low pressures are achieved by the performance of two turbomolecular pumps with a pumping speed of 150 L s^{-1} (Oerlikon Leybold Vacuum TURBOVAC SL300), and by two backing two stage rotary vane pump (Edwards E2M18). The pick-up chamber incorporates the Knudsen effusion cell, and a crucible is placed inside the Knudsen effusion cell. The material of

the crucible is Pyrolytic Boron Nitride (PBN crucible BN, CVT GmbH & Co. KG) for these experiments. Pyrolytic Boron Nitride is an inert and non porous compound. The heating element in the effusion cell is a tungsten filament. A power supply provides the voltage to the filament heater, while a thermocouple connected to a temperature controller measures the temperature inside the effusion cell.

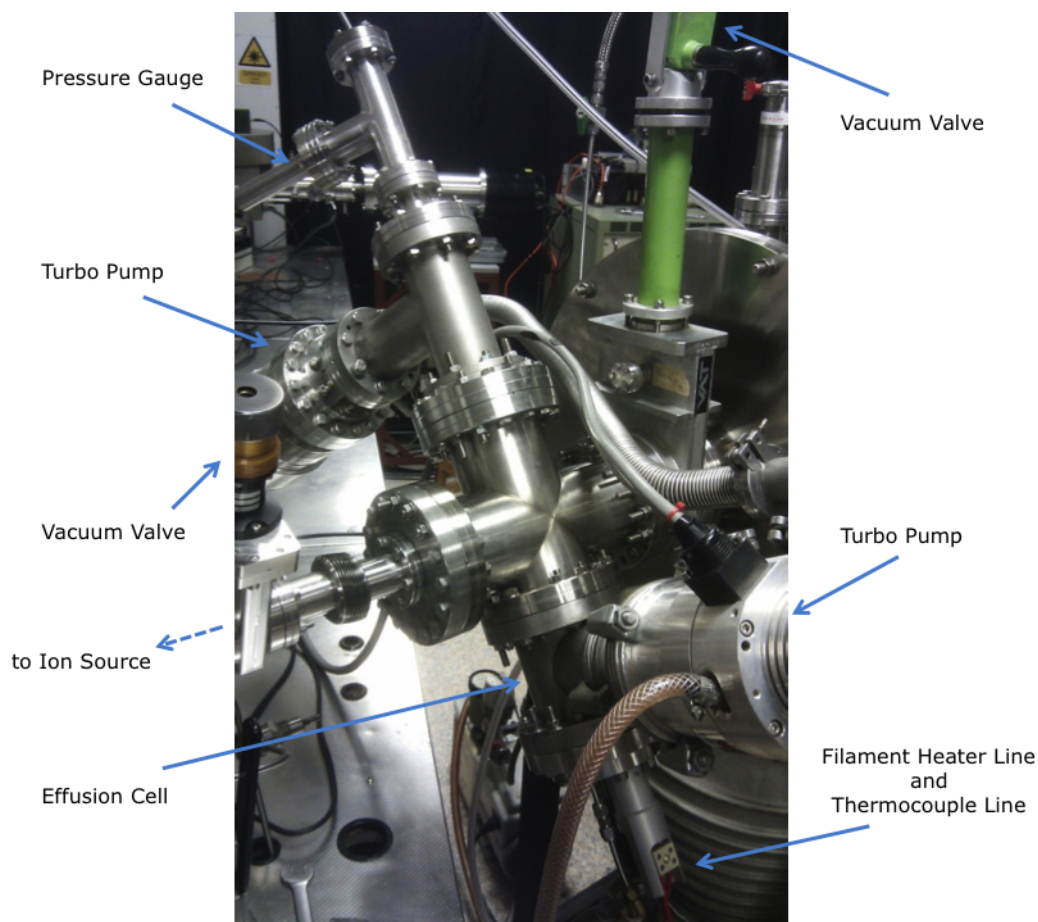


Figure 2.5.2: Photo of the Pick-Up Chamber [19]

2.5.1 Knudsen Effusion Cell

A Knudsen effusion cell (DCA Instruments, EC-40-63-21) is assembled inside the pick-up chamber within the vacuum system. It is connected to a power supply through a thermocouple line and a filament heater power line. The thermocouple junction inside the Knudsen effusion cell is linked to a temperature controller through a thermocouple line.

As Figure 2.5.3 shows, the Knudsen cell comprises crucible, flange, water cooling system, and heating filament. The effusion cell used in this work was a 2000° C high temperature cell provided with a thick foil tantalum filament. No shutter at the exit of the effusion cell has been used during these experiments.

The effusion cell is tightened through its pair flange to the chamber (DN100 CF Flange - Kurt J. Lesker Company) to provide high vacuum seal. The effusion cell is placed at an angle of 45° to the xy plane to the cluster chamber, approximately 500 mm from both the cluster chamber and the ion source.

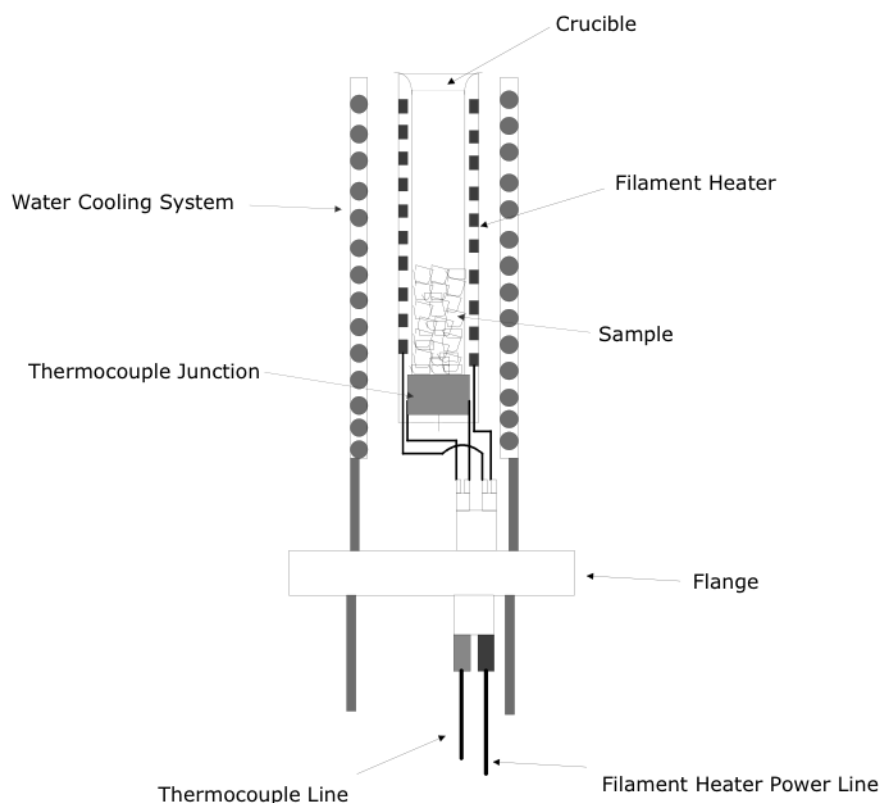


Figure 2.5.3: Schematic diagram of the Knudsen effusion cell (adapted from [3])

The cell has a furnace of cylindrical shape with an aperture much smaller than the total internal cavity area. The non volatile sample is placed inside a crucible, which in turn is inserted into the furnace. Crucibles are manufactured in a variety of materials and sizes to be suitable to different experimental conditions; therefore a crucible is chosen according to the size of the furnace, the sample chemical composition and the reactivity, and the temperature of evaporation or sublimation. The crucible is half filled with the sample and introduced into the furnace. The sample is evacuated and then heated by a filament heater into vapour phase (when new, the crucible is conditioned at high temperature).

Knudsen effusion cell is a type of cluster beam source, which allows to perform high-temperature mass spectrometry experiments. The sample material is typically in the solid state under ambient pressure and temperature conditions, and it is heated to vapour state. The resulting cluster beam is an effusive (sub-

sonic) molecular beam¹, in which the flux of clusters is very low compared with other cluster beam sources. In fact, it is mainly formed by monomers but also some clusters in thermal equilibrium, owing to few collisions between effusing species. The resulting effusive beam has a broad velocity distribution and it is highly divergent.

2.6 Ion Source Chamber

The cluster beam generation system is connected to the mass spectrometer via an edge welded metal bellows. The ion source chamber is located after the pick-up chamber (*cf.* Figure 2.1.1). The electron impact ion source is placed inside the ion source chamber. It generates a beam of energetic electrons in order to bombard neutral gaseous species and to produce ions. Ionic species are generated by electron impact ionisation [18]; namely ionisation occurs if the bombarding electron energy exceeds the ionisation energy of the neutral species. The probability of formation of a particular ion would mainly depend on the energy of the electrons and on the composition and geometry of the neutral species. In fact, the collision may trigger several reaction pathways.

The type of ion source used in these experiments may be operated at a potential difference in the range 15 – 125 eV and at an accelerating voltage in the range 3 – 10 kV. The cluster beam exits the pick-up chamber to enter the ion source through a 5 mm² diameter hole and perpendicular with respect to the flight tube of the mass spectrometer and to the electron beam produced in the ionisation chamber. The ionisation chamber is the region inside the ion source in which the ions are produced owing to the presence of the bombarding electrons. A filament (an electrode) produces the electrons; in addition, the trap (an electrode) allows regulation of the filament current. In these experiments the filament material was tungsten. Once the ion beam is generated and it has left the ionisation chamber, owing to the influence of a small magnetic field of the repeller electrode (which provides the ion of ~ 1 eV kinetic energy), it is accelerated by the voltage present inside the ion source by the ion accelerator. In particular, the ions in the beam will all have the same kinetic energy as a result of the electric field, because the focusing plates placed in the ion accelerator region avoid the penetration of the strong electric field inside the ionisation chamber. The beam is then focused, and directed to the first field-free region (*1st ffr* in Figure 2.1.1) towards the mass analyzer by a series of extraction optics. The background pressure in the ion source chamber is lower than 10^{-7} mbar if

¹The mean free path of the gas is larger than the orifice, and the aperture area is much smaller than the evaporating surface.

experiments are not performed, whereas it is approximately 10^{-6} mbar during ionisation processes. The vacuum pump system consists of one 700 L s^{-1} diffusion pump (Edwards Diffstak) and one backing two stage rotary vane pump (Edwards E2M8).

2.7 Mass Spectrometer

A Nier-Jordan high resolution double-focusing mass spectrometer having reversed sector geometry (VG Analytica LTD ZAB-E) is used. This is an high resolution instrument that permits measuring with high accuracy and precision because of high mass resolving power, sensitivity of detection, and high resolution. The magnetic sector field has an angle of 35° and radius of 66 cm; the electric sector field has an angle of 81° and radius of 38 cm. The sum of the length of the field-free flight regions is ~ 2.4 m. This instrumentation has a focusing action on mono-energetic beam of ions of the same mass to charge ratio; namely, the magnetic analyser produces focusing action as momentum selector whilst the energy analyser accomplishes focusing action as energy selector. The magnetic and electric sectors of this double-focusing instrument operate only in a direction perpendicular to the field known as the y direction. In fact, the ion beam travels along the x -direction and it is focused in the y -direction. The flight tube consists of two separate parts: the First Field-Free Region (*1st ffr*) of ~ 107 cm and the Second Field-Free Region (*2nd ffr*) of ~ 136 cm. The background pressure during the course of these experiments remained below 10^{-7} mbar in the *2nd ffr*. The reason for keeping high vacuum is to ensure minimal interference from collision induced fragmentation [20] that could be caused by collisions of background molecules. A pump system is therefore designed to suit the aim, which comprise five 700 L s^{-1} diffusion pumps (Edwards Diffstak) and each with two backing dual stage rotary vane pumps (Edwards E2M8).

2.7.1 Magnetic Sector: Magnet Analyser Tube

The mono-energetic ions of interest can be selected at the magnetic sector according to the value of their mass-to-charge ratio by varying the applied magnetic field during their passage along the curvature of the magnetic sector. The ions are focused depending on their momentum [18]. In fact, the kinetic energy of a mono-energetic beam of ions which leave the ion source chamber having mass m and charge z is equal to the accelerating voltage V

$$\frac{1}{2}mv^2 = zV \quad (2.1)$$

where v is the velocity of the ion. The magnet only has focusing action in the direction perpendicular to the direction of motion of the ion beam.

As it enters the magnetic sector, the ion experiences a magnetic field B and travels along a curvature of radius r depending on its momentum

$$r = \frac{mv}{zB} \quad (2.2)$$

By equations (2.1) and (2.2), we obtain

$$\frac{m}{z} = \frac{1}{2V} r^2 B^2$$

relating the mass to charge ratio value ($\frac{m}{z}$) to the distance travelled in a magnetic field with a constant potential.

2.7.2 Electric Sector: Energy Analyser Tube

The ions of interest can be selected at the electric sector depending on their kinetic energy, provided that the accelerating voltage and the magnetic field are kept constant [18]. In fact, an ion of mass m and charge z accelerated by a potential V experiences an electric field E through its passage along the curvature d of the electric sector. Hence, the ion travels with a centrifugal force to balance the electrostatic force

$$\frac{1}{d} mv^2 = zE \quad (2.3)$$

where v is the velocity of the ion.

This electric field is produced by a voltage difference between two curved parallel metal plates; it has focusing action only in the direction perpendicular to the direction of motion of the ion beam. By substituting Equation (2.1) in Equation (2.3) we obtain

$$\frac{2V}{E} = d$$

That is, all the ions accelerated through a potential V , which are experiencing an electric field E , are focused by travelling across a path of radius d , regardless of their mass to charge ratio.

A mono-energetic beam of ions can be selected by tuning the electric field according to the equations above.

2.8 Detection System

The detection system consists of a fast photomultiplier (EMI 9324), a Daly scintillation type ion detector [21], and a lock-in amplifier (Stanford Research Systems, Inc., SR850-100 kHz DSP lock-in amplifier).

The Daly detector consists of an aluminium dynode with a very high polished surface that is raised to a certain potential. As it can be seen in Figure 2.8.1, the ions of interest, after passing through the ESA, are drawn toward the dynode of the Daly detector through a collector defining slit. The dynode is a conver-

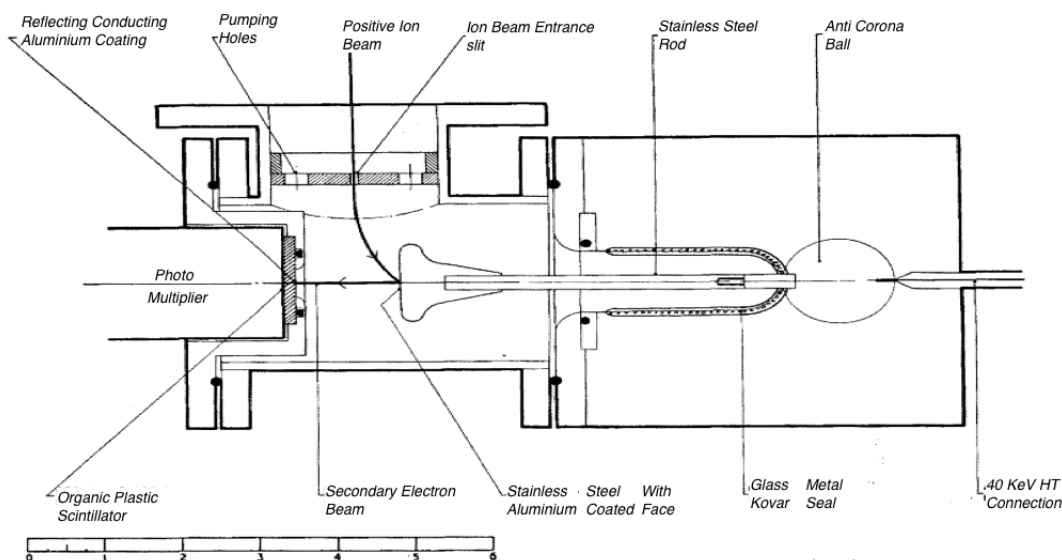


Figure 2.8.1: Physical layout of ion detector tube (Fig. 1, page 265 from [21])

sion electrode, which releases secondary electrons in proportion to the number of ions that impact onto its surface. These electrons are accelerated onto an organic scintillator and, as a result of the impact onto the surface of the scintillator, photons are emitted. These photons are collected by a photomultiplier tube, which is placed opposite to the Daly detector. The photomultiplier is an electron multiplier which detects photons; in fact, it allows one to enhance the photon signal by producing an electron current signal proportional to the photon flux. More precisely, the photomultiplier detects the photons at a cathode, which emits electrons. These electrons are accelerated and focused to a first dynode of an electron multiplier, which in turn emits electrons. Then these latter electrons are accelerated and focused onto a second dynode, and next onto several other dynodes, where the previously described process is repeated. The ratio of emitted electrons to incident electrons at each dynode couple depends on the energy of the colliding electrons, moreover, the ratio can be controlled by varying the interpotential between dynodes. The Daly detector and the photomultiplier

are placed perpendicular to the ion beam, in order to separate the incoming ion beam from the electron beam produced at the dynode. The signal from the photomultiplier tube is linked to the lock-in amplifier. The lock-in amplifier is used to detect and amplify the AC (alternating current) signal from the photomultiplier; moreover, it uses the signal from the pulse generator as reference signal, in order to provide phase sensitive detection synchronised with the nozzle pulse. Therefore, the lock-in amplifier filters the signals from the photomultiplier so as to yield only those in phase with the reference signal.

The scintillation type ion detector developed for mass spectrometer by N.R. Daly [21] and shown in Figure 2.8.1 provides a few advantages. In fact, the Daly detector allows us to improve the efficiency of the photomultiplier, to restrict the contamination of the photomultiplier detecting surface, and to easily replace the photomultiplier (if more performing ones are available or in case of faults) because it is placed external to the vacuum system of the apparatus.

2.9 Sources of Uncertainty

The uncertainty in the measurements in these experiments has three primary causes. The first is the inaccuracy of the electronic components. The effects are multiple: spread of the signal due to imperfection in focusing, inaccuracy in selecting, detecting, and recording data. The second cause of uncertainty is the width of the slits which are placed in front of the magnetic and electric sectors. In fact, the spread of the signal increases as the degree of the slits widens. In order to obtain well resolved peaks, the slit width should be as narrow as possible, which in turn allows the resolution to be improved to the maximum. In fact, the ideal condition is an infinitely narrow slit width, but the effect of limiting the slit width is diminished sensitivity. The third source of uncertainty is the degree of signal-to-noise ratio, which influences the accuracy of the experiments.

Bibliography

- [1] P.G. Lethbridge, A.J. Stace, *Journal of Chemical Physics* 89 (1988) 4062.
- [2] A.J. Stace, *Physical Chemistry Chemical Physics* 3 (2001) 1935.
- [3] X. Chen, *Unimolecular Dissociation of Cluster ions*, D. Phil. Thesis, The University of Nottingham (2011).
- [4] P.G. Lethbridge, *Structures and Fragmentation Patterns of Ionic Clusters*, D. Phil. Thesis, The University Of Sussex (1989).
- [5] G. Scoles (Ed.), in *Atomic and Molecular Beam Methods*, ed. Oxford University Press, vol. 1, 1988.
- [6] S.Y.T. van de Meerakker, H.L. Bethlem, G. Meijer, *Nature Physics* 4 (2008) 595.
- [7] O. F. Hagen, *Surface Science* 106 (1981) 101.
- [8] R.L. Johnston, in *Atomic and Molecular Clusters*, Taylor & Francis, London and New York, 2002.
- [9] T.E. Gough, M. Mengel, P.A. Rowntree, G. Scoles, *Journal of Chemical Physics* 83 (1985) 4958.
- [10] D.J. Levandier S. Goyal, J. McCombie, B. Pate, G. Scoles, *Journal of the Chemical Society, Faraday Transactions* 86 (1990) 2361.
- [11] X.J. Gu, D.J. Levandier, B. Zhang, G. Scoles, D. Zhuang, *Journal of Chemical Physics* 93 (1990) 4898.
- [12] M.P. Dobson, A.J. Stace, *Chemical Communications* 13 (1996) 1533.
- [13] C.A. Woodward, M.P. Dobson, A.J. Stace, *Journal of Physical Chemistry* 100 (1996) 5605.
- [14] G. Del Mistro, A.J. Stace, *Chemical Physics Letters* 196 (1992) 67.

- [15] J.F. Winkel, A.B. Jones, C.A. Woodward, D. A. Kirkwood, A. J. Stace, *Journal of Chemical Physics* 101 (1994) 9436.
- [16] A.B. Jones, R. Lopez-Martens, A.J. Stace, *Journal of Physical Chemistry* 99 (1995) 6333.
- [17] N. Walker, M.P. Dobson, R.R. Wright, P.E. Barran, J.N. Murrell, A.J. Stace, *Journal of the American Chemical Society* 122 (2000) 11138.
- [18] R.G. Cooks, J.H. Beynon, R.M. Caprioli, G.R. Lester, in *Metastable Ions*, ed. Elsevier Scientific Pub. Co., Amsterdam, New York, 1st edn. , 1973.
- [19] Courtesy of Christopher Harris.
- [20] C.A. Woodward, A.J. Stace, *Journal of Chemical Physics* 94 (1991) 4234.
- [21] N.R. Daly, *Review of Scientific Instruments* 31 (1960) 264.

Chapter 3

From Kinetic Energy Release Measurements to Binding Energies

3.1 Overview

The principal objective of this study is to develop a reliable technique for measuring binding energies in large clusters in a gas phase experiment. The resulting approach is applied to analyse charged metal-ligand complexes. Large molecular cluster ions are generated in these experiments. The process of neutral loss of one single molecule by unimolecular metastable decay is the subject of our observations.

In these experiments, a metastable ion is a molecular ion sufficiently stable to leave the ionisation chamber, but that decomposes into an ion and a neutral fragment in the second field-free region (*2nd ffr*). In contrast, a stable ion has enough energy to travel from the ionisation chamber to the collector without decomposition, whereas an unstable ion fragments before leaving the ionisation chamber.

A series of accurate measurements are made of peak profiles resulting from the unimolecular decay, which are coupled with data analysis using finite heat bath theory as developed by Cornelius E. Klots [1, 2, 3, 4, 5].

Under these experimental conditions, the excitation energy of the molecular ion is converted into translational energy during the dissociation. In other words, if the precursor cluster ion attains the necessary internal energy and acquires the critical configuration through energy distribution amongst the available degree of freedom, it may undergo unimolecular decomposition.

The purpose of mass-analysed ion kinetic energy (MIKE) spectrometry [6, 7] is to analyse metastable ion fragmentation occurring in the *2nd ffr* of a high resolution reversed geometry double-focusing mass spectrometer. Hence, the

peak shape of any fragment ion that is detected will be broader than the precursor ion. The diffuse and broad peak shape of the fragment with respect to the precursor is an effect due to the energy released in the dissociation and detected by the instrument, as well as a measure of the amount of internal energy of the molecular ion that has been converted into kinetic energy of the fragments.

The effects of the kinetic energy spread of the precursor ion are minimized to the highest possible degree, when the most favourable conditions are achieved: the slits are adjusted for the optimal sensitivity and resolution, and the energy resolving capabilities are excellent.

3.2 Cluster Ions Preparation and Detection

Neutral clusters were generated in a free jet. Clusters under investigation in this work were proton bound, and formed either by one single species of molecules or by a metal atom incorporated into the solvent cluster via the pick-up technique. Neutral clusters in the beam were ionized by electron impact ionisation; the resulting ion beam was extracted from the ion source chamber and accelerated through a potential drop into the flight tube of the mass spectrometer.

Once the ion beam had passed the first field-free region (*1st ffr*), the positively charged ions of interest (mono- or doubly-charged) were selected at the magnetic sector according to their mass to charge ratio value. Then the signal intensity of the molecular cluster ions was improved as much as possible.

As the beam reached the electrostatic analyser, the MIKE technique was used to study metastable unimolecular decomposition occurring in the *2nd ffr* of the flight tube placed between the magnetic and the electric sector. Consequently, a MIKE scan was recorded for both the reactant precursor ion and the product molecular ion; the former having a narrower laboratory frame full width half maximum (laboratory frame FWHM) peak width than the latter. The measurement consisted of pairs of MIKE scans, one for the reactant precursor ion (parent ion) and one for the product molecular ion (daughter ion); each member of the pair had the same number of collected data, each of which was recorded in the same amount of time for all the experiments.

In order to minimize the kinetic energy spread in precursor ions, it is necessary that the laboratory frame FWHM of those ions is as narrow as possible (ideally ~ 1 eV) and has a good signal-to-noise ratio. Therefore, the resolving capabilities of the mass spectrometer were improved to obtain laboratory frame FWHM peak widths of the precursor ions < 3 eV (generally they were ~ 2 eV) for almost all the experiments. Such value of laboratory frame FWHM is to be compared with the value > 5 eV, for a typical fragment ion laboratory frame

FWHM energy width.

Examples of MIKE spectrometry scans are shown in Figure 3.2.1.

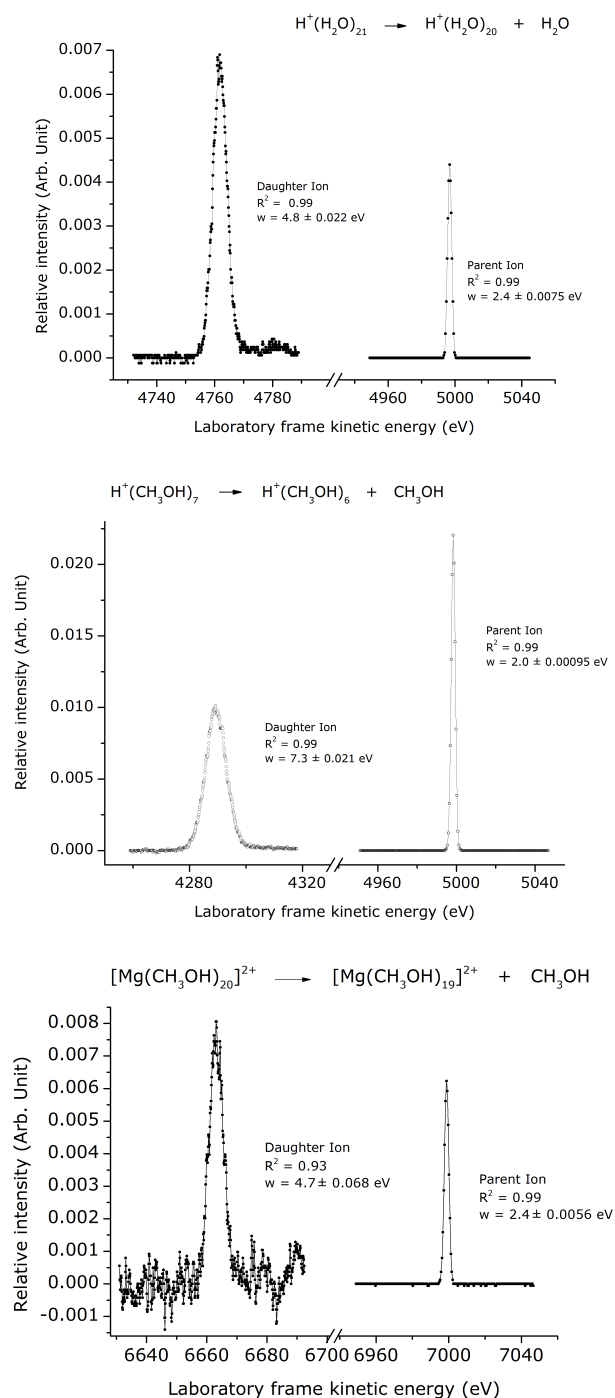


Figure 3.2.1: Example of metastable peaks recorded for the fragmentation of $H^+(H_2O)_{21}$, $H^+(CH_3OH)_7$, and $[Mg(CH_3OH)_{20}]^{2+}$. Each peak is plotted as a function of laboratory frame kinetic energy, where R^2 measures the goodness of the fit to a Gaussian profile and $\frac{w}{2}$ is the standard deviation

The MIKE spectra were assumed to have a Gaussian distribution. For almost all the experiments, the measurements of peak widths were only accepted when the goodness of fit to a Gaussian profile was > 0.9 , where 1.0 is a perfect fit.

During the course of these experiments, the background pressure in the second field-free region remained $< 10^{-7}$ mbar, which ensured minimal interference from collision induced fragmentation [8].

3.3 MIKE Spectrometry

Unimolecular decomposition [9] is an elementary reaction in the gas phase of a single reactant going through a transition state and then dissociating, as described by the following chemical reaction



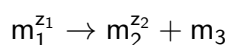
where $L_n^{z_1}$ is an ion, z_1 is the charge, and n is the number of atoms or molecules. Metastable decay describes a unimolecular dissociation that occurs in the field-free region of magnetic sector instruments.

In these experiments, the reactant (parent ion) undergoes metastable fragmentation into an ion (daughter ion) and a neutral species (neutral fragment); in other words, the reactant loses one neutral molecule. These investigated dissociations are defined as metastable neutral loss for

- i. protonated cluster ion: $H^+L_n \rightarrow H^+L_{n-1} + L$
- ii. metal ligand complex: $ML_n^{z_1} \rightarrow ML_{n-1}^{z_1} + L$

where H is a hydrogen atom, M^{z_1} is a multiply charged metal, and L is a neutral molecule.

Let the transition under investigation be represented as follows



An ion beam containing molecule of mass m_1 and charge z_1 is accelerated through a potential V at the ion source; hence it acquires translational energy, E_1 , equal to this accelerating voltage supplied outside the ionisation chamber. Thus, fragment ions are identified from the magnitude of the electric sector voltage necessary to transmit them

$$\frac{m_1}{z_1} E_1 = \frac{m_2}{z_2} E_2$$

where the kinetic energy after fragmentation, E_2 , of the fragment ion with mass m_2 and charge z_2 is correlated to the kinetic energy, E_1 , of the parent ion of mass m_1 and charge z_1 .

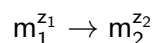
As a consequence, decomposition in the second field-free region can be detected at the electric sector, owing to the identification of the daughter ions, as shown in the relationship below

$$E_2 = \frac{m_2 z_1}{m_1 z_2} \times E_1$$

More precisely, performing a MIKE spectrometry scan of a daughter ion (charge z_2 and mass m_2) amounts to selecting a particular cluster ion (charge z_1 and mass m_1) using the magnet and to scanning the electric sector field voltage while the accelerating voltage and magnetic field remain constant.

3.3.1 Artefact Peaks

In these studies a double focusing mass spectrometer configured in a reverse geometry was used to study fragmentation in the *2nd ffr* by scanning the electric sector as kinetic energy analyser. This procedure has given rise to the observation of ion peaks which were not associated with the fragmentation process under consideration. These peaks are referred to as apparent ions or artefact peaks [10, 11, 12, 13]. During a MIKE experiment, a large number of ions with different masses form at the ion source. If we consider a MIKE scan for the following reaction taking place in the *2nd ffr*:



where $m_1^{z_1}$ is a parent ion and $m_2^{z_2}$ is a daughter ion, then an artefact peak will be recorded in the scan if the corresponding artefact ion has a mass m^* (also known as apparent mass) as described by the following relationship:

$$m^* = \frac{m_2^2}{m_1}$$

Moreover, since the artefact ion has been produced either in the ion source or in the *1st ffr*, it will be transmitted to the electrostatic sector with a translational kinetic energy which is lower than the acceleration voltage applied at the ion source.

The artefact peak appears in the spectrum owing to poor focusing resolution of the magnet sector. It is possible to enhance the resolution of the single focusing to eliminate the artefacts at low masses, but only to the point at which the decrease in sensitivity does not affect the detection of ion clusters with low intensities. Also, as the mass of a parent ion increases, the ratio $\frac{m_2^2}{m_1}$ converges towards the apparent mass of a smaller ion cluster. Hence, it is not possible to

improve the single focusing resolution indefinitely.

Examples of artefacts detected in the MIKE scans in these experiments are presented in Figure 3.3.1.

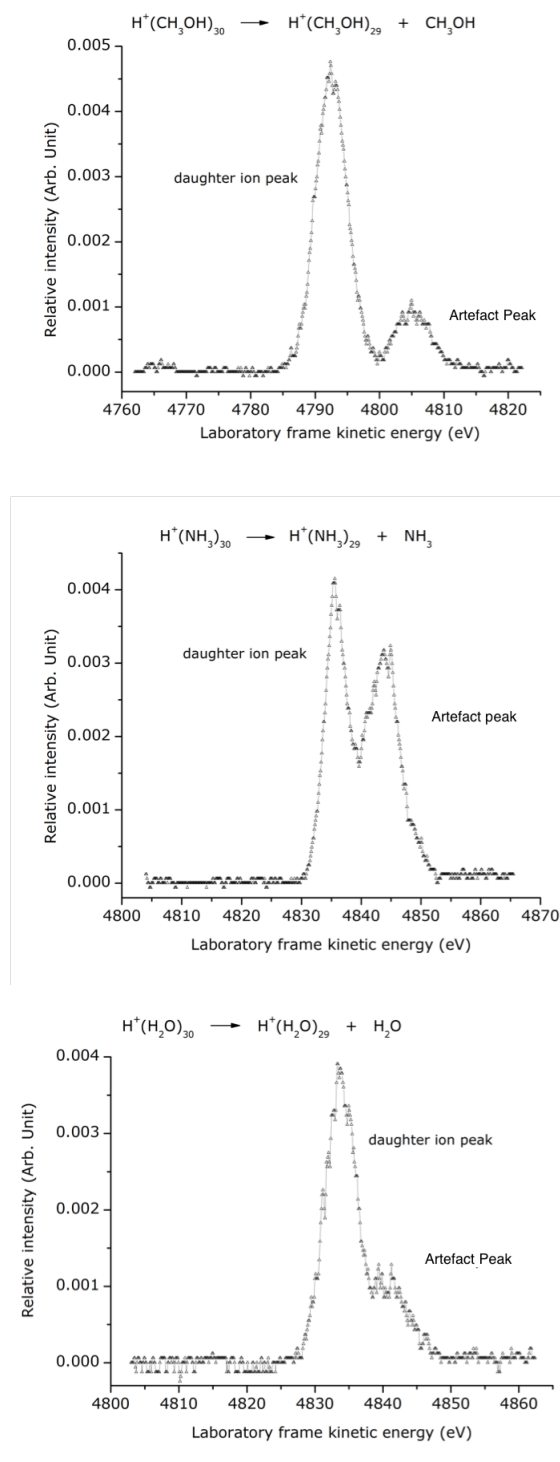


Figure 3.3.1: Examples of artefact in MIKE spectrum of metastable methanol, ammonia, and water protonated cluster ions

Artefact peaks were present for some of the large cluster ions scans and, where the overlap with the peak of interest was significant, their contribution

to the overall peak shape was deconvoluted by fitting both profiles separately. Nevertheless, in many cases the tuning of the signal allowed complete removal of the artefact in the scan at the electric sector.

3.4 Time of Flight

The approximate timescale of an experiment for a stable cluster ion includes the time the ion spends inside the ion source chamber, $\sim 10^{-6}$ s (which includes ionisation process of $\sim 10^{-16}$ s [7]), then the time to reach the mass sector, $\sim 10^{-4}$ s, and finally the time to fly to the detector at the electrostatic analyser, $\sim 10^{-4}$ s.

The time of flight through the *1st ffr* and the *2nd ffr* can be calculated for each cluster ion. A cluster ion of mass m and charge z is accelerated through a potential V at the ion source; hence it acquires translational energy, E_1 , equal to the accelerating voltage, eV , supplied by the ion source

$$eV = E_1 = \frac{1}{2} \frac{m}{z} \frac{1}{N_A} v^2$$

where v is the velocity of the ion and N_A the Avogadro constant. The time of flight Δt is calculated by knowing that the velocity is

$$v = \frac{\Delta l}{\Delta t}$$

where Δl is the length travelled by the ion.

3.5 Data Analysis: Binding Energy Determined from KER Measurements

The data collected and recorded by the lock-in amplifier for a MIKE scan is analysed using Origin 7.0 [14]. This software uses the experimental data to fit a normalized Gaussian distribution; Origin 7.0 provides the values of w and R^2 . More precisely, $\frac{w}{2}$ is the standard deviation of the fitting and R^2 – called the correlation coefficient – is a measure of the goodness of fit to the Gaussian profile, where 1.0 is a perfect fit. Each measurement consisted of pairs of MIKE scans for parent and daughter ions; the number of data in each scan is the same for all parent ions and have all been recorded in the same amount of time (similarly, for the number of data and the recording time of daughter ions, although the number of collected data and the recording time of parent ions differ from the number of collected data and recording time of daughter ions).

The peak in a MIKE scan is produced by detecting a mono-energetic beam of ions flowing out of a slit and entering a field-free region; the products of a metastable decomposition may have a MIKE scan with either a similar or a wider peak than the precursor ion. The conversion of internal energy (excitation energy) into external energy (kinetic energy) of separation of the fragments is the cause of the diffuse nature of the peaks, owing to the range of speeds and directions acquired by the daughter ions. It is possible to relate the width of the peak of a MIKE scan to the energy release using the laws of conservation energy and conservation of momentum. In fact, the initial kinetic energy of the precursor ion is equal to the total kinetic energy of the fragments. This kinetic energy is shared between the fragments in the ratio of their masses. More precisely, the direction of the velocity of a fragment ion is calculated with respect to a coordinate system moving with the centre of mass system, *i.e.* the centre of mass of the parent ion.

The centre of mass FWHM of the parent ion (ΔE_1), and the centre of mass FWHM of the daughter ion (ΔE_2) are calculated using the standard deviation $\frac{w}{2}$ of a Gaussian profile (where w is the laboratory frame FWHM), *viz.*

$$\text{FWHM}_i = \Delta E_i = w_i \sqrt{2 \ln(2)}$$

Adjusting the slits of the double-focusing mass spectrometer allows one to optimize the energy resolving capability, in order to take into account the effects of a kinetic energy spread in precursor ions.

Furthermore, a mass-weighted correction to the kinetic energy spread of the fragment ion was made by using the relationship [15, 16, 17, 18]

$$\Delta E^2 = \Delta E_2^2 - \Delta E_1^{*2} \quad (3.1)$$

where ΔE_1^* is the parent correction defined as

$$\Delta E_1^* = \frac{m_2 z_1}{m_1 z_1} \Delta E_1 \quad (3.2)$$

therefore, by substituting (3.2) in (3.1), the deconvoluted width ΔE is derived:

$$\Delta E = \sqrt{\Delta E_2^2 - \left(\frac{m_2 z_1}{m_1 z_1} \Delta E_1\right)^2}$$

The relation between the laboratory frame kinetic energy spread and the average centre of mass kinetic energy release for a MIKE scan with Gaussian profile corresponds to the average kinetic energy release ($\langle \varepsilon_\tau \rangle$), which is calculated

according to the following relation (cf. [7, 17, 18, 19]).

$$\langle \varepsilon_\tau \rangle = 2.16 \frac{z_2^2 m_1^2 (\Delta E)^2 e V}{16 z_1 m_2 m_3 (E_1)^2}$$

where $e V$ is the kinetic energy of an ion of mass m_1 and charge e accelerated through potential drop V outside the ionisation chamber and E_1 concurs with the reference voltage at the electric sector.

In these experiments E_1 is equal to the initial parent ion kinetic energy $e V$. Moreover, the decomposition processes investigated in this work have $z_1 = z_2$. It follows

$$\langle \varepsilon_\tau \rangle = 2.16 \frac{z_1 m_1^2 (\Delta E)^2}{16 m_2 m_3 e V}$$

An error for the average width, $\Delta \Delta E$, is estimated on the h measurements with respect to the biggest value of ΔE , $\max \Delta E_{j=1, \dots, h}$, amongst the h measurements as determined from the following relationship

$$\Delta \Delta E = \max_{j=1, \dots, h} (\Delta E)_j - \frac{1}{h} \sum_{j=1}^h (\Delta E)_j \quad (3.3)$$

The uncertainty $\pm \Delta \langle \varepsilon_\tau \rangle$ for each measurement j reflects the magnitude of $\Delta \Delta E$ in terms of a quoted accuracy for each kinetic energy release from h experimental kinetic energy release measurements.

Unimolecular reaction theory [9] aims to quantitatively define the rate constant for the decay process of the precursor species to the product species. The decay process in a unimolecular reaction is not instantaneous. There is a delay between the excitation of a reactant (parent) system and its subsequent dissociation into a product (daughter) system, because the internal energy of the system is statistically distributed. This process is known as complete statistical mixing [20]. The consequence is that the decay is independent of the experimental method used to impart the excitation energy into the reactant. (In fact, the preparation method causes a wide distribution of internal energy of the reactant system.) Therefore, the unimolecular dissociation rate constant determined with statistical theory depends on the internal energy and number of active modes before the excitation process, because the particle conserves the energy and angular momentum between two unimolecular decays in an ensemble of freely evaporating particles.

The evaporative ensemble is a statistical approach to understand unimolecular (metastable) reactions; this theory was developed by Cornelius E. Klots [1, 2, 3, 4, 5, 21, 20]; it is also known as finite heat bath theory (FHBT) or as theory of evaporation from small particles. The evaporative ensemble describes the loss

of energy and mass of the reactant system by evaporation in vacuum. In the case of evaporation in vacuum, the system cannot be described as a microcanonical system because the particles cannot reach an equilibrium with external sources of energy; therefore, evaporative ensemble theory is necessary for the study of this system.

The FHBT by C. E. Klots [1, 2, 3, 4, 5, 21, 20] has been developed to quantitatively and theoretically interpret the kinetic energy release of unimolecular (metastable) decomposition. Such theory is called evaporation from small particles because there is a minimum energy needed for the evaporation of one molecule from the surface of a cooling cluster, which corresponds with the heat of evaporation at absolute zero. C. E. Klots has studied evaporative cooling processes and he has conjectured that the average kinetic energy for a monomeric unit leaving an aggregate is a measure of the temperature of the respective transition state, so that it becomes possible to determine the binding energy of the evaporative process from the temperature of the transition state. In particular, he stated that it is possible to relate the experimentally measured kinetic energy release $\langle \varepsilon_{\tau} \rangle$ into evaporative energy (or binding energy) of the unimolecular (metastable) decay, where $\langle \varepsilon_{\tau} \rangle$ is defined as the conversion of internal energy of the parent into translational energy of the fragments.

We give a brief summary of the theory by Klots

- (I) All particles have undergone at least one decay before experimental measurement [21]; in particular, at least one evaporative cooling event should occur after production and before mass selection at the magnetic sector. Collision or radiative energy decay losses are absent.

In these experiments there is no collisional cooling owing to the experimental pressure being $< 1 \times 10^{-7}$ mbar in the field-free regions, in fact, the pressure in the *2nd ffr* is too low for the former mechanism to be responsible for initiating unimolecular (metastable) decay in these experiments. Also, radiative cooling is absent because of the time scale of the experiment ($\sim 10^{-4}$ s). Electron impact ionisation can result in extensive excitation and the ions have been formed by $> 10^{-4}$ s when they are observed to undergo unimolecular (metastable) decay; consequently, molecular evaporation is most probably the only effective energy loss mechanism, as required by the Klots evaporative ensemble theory.

This requirement creates the condition that the evaporative ensemble is formed by a distribution of ions, which does not contain cold particles. In fact, it is not possible to have any information about the fraction of cold particles within the beam [20]. The observation of the fragment ion

is possible if an excess of energy is provided to the particles during the preparation process. In these experiments, neutral clusters are prepared by supersonic free jet expansion and therefore they are at temperatures within a few degrees of absolute zero. Successively, the preparation of cluster ions is achieved by electron impact, where a nearly monoenergetic beam of electrons collide and excite the free jet beam. As a result, the cluster ions possess an excess energy and their internal energy is unknown. The minimum amount of this excess energy is the sum of the activation energy required for the fragmentation and the kinetic shift (*i.e.* the energy necessary to ensure that the lifetime of the particles is long enough to reach the region of the instrumentation where the fragment can be detected). In particular, after the acceleration at the magnetic sector, unimolecular (metastable) decay of ions may occur at any point in space during the flight through the *2nd ffr*.

- (II) The temperature $T^\#$ of the transition state is defined [21] as the average kinetic energy $\langle \varepsilon_\tau \rangle$ on passing through the transition state of a monomeric unit leaving the surface of an aggregate

$$\langle \varepsilon_\tau \rangle = \ell k_B T^\# \quad (3.4)$$

where k_B is Boltzmann constant and $0 \leq \ell \leq 2$ is a dimensionless parameter [21] that gives a measure of the number of degrees of freedom at the transition state.

This assumption is plausible if there is no reverse activation energy on the potential energy profile of the investigated ensemble [7, 21]. It is expected that simple bond cleavage have zero or a very small reverse activation energy so to be negligible [7, 21]. Moreover, the kinetic shift can be neglected, even though fragments may contain a finite amount of thermal excitation energy [21]. As a result, all the excess energy of the activated complex will be statistically partitioned amongst the available degrees of freedom of the products and the translational (kinetic energy) of their separation [20].

This assumption is experimentally satisfied by the experimental laboratory frame kinetic energy profile of both the parent and the daughter ions; in fact, the peak shape of the two ions has to be the shape of a Gaussian distribution. This requirement is justified by the central limit theorem [21, 22], indeed if sufficiently many numbers sampled from the same distribution are averaged, the probability distribution is a Gaussian (or

normal) distribution for the average. Such averaging provides a Gaussian distribution of error even when the experimental data measured do not themselves follow that distribution. Hence, the actual distribution is immaterial [21, 22].

The use of a Gaussian distribution implies that only random errors are possible (absence or negligible presence of systematic errors); the measurements are around the true value, and – between a lower and an upper limit – the smaller the laboratory frame FWHM of the curve the closer the measurements are to the true value and the smaller is the standard deviation [23].

- (III) The amount of energy corresponding to an evaporative cooling event concurs with the activation energy because of the requirement (II). The temperature of the activated state is higher than the temperature T^\ddagger of the transition state [21]. Therefore, the evaporative cooling is an endothermic process which cools an isolated system.
- (IV) The definition of isokinetic temperature T_b is given in [20] as follows:

“ T_b is an equivalent temperature as the temperature T^\ddagger which gives the same rate constant in a canonical ensemble as the microcanonical rate constant at the excitation energy”.

In other words, T_b is defined in [21] as the

“isokinetic temperature to which a heat bath must be set to yield a thermal rate constant equal to the microcanonical rate coefficient”.

A unimolecular (metastable) decay experiment is linked with the timescale of the experiment, *i.e.* the time of flight of the metastable ions through the field-free regions. In other words, only a decay occurring in metastable time window is detectable. Consequently, the rate constant of a decay event determines if the metastable fragmentation is observable.

In a microcanonical ensemble, the partition function provides the number of states of a system at thermal equilibrium; through a link between macroscopic and microscopic properties of a system [20]. Each of the replica of the ensemble has specified three macroscopic constants: volume, energy, and number of constituents (molecules or atoms), so to determine a link between the microscopic and the macroscopic properties of the system at thermal equilibrium. Specifically, relating the volume to

the size of a vacuum chamber shows how the properties of the free particles are not affected by the volume once the constituents are in thermal equilibrium with respect to their translational degrees of freedom [20].

The FHBT by Klots defines T_b as

$$T_b = T^\# \frac{\exp^{\frac{\gamma}{C}} - 1}{\gamma} C \quad (3.5)$$

where γ is the dimensionless Gspann parameter and C is the heat capacity in units of k_B minus 1. The Gspann parameter – after J. Gspann who claimed that clusters have a highest temperature in molecular beams without providing any experimental basis [24, 20] – connects

“the highest microcanonical temperature in the ensemble to the activation energy” [20].

The Gspann parameter γ was taken as $\gamma = 23.5 \pm 1.5$, which appears to be the most frequently used value in calculations of the type discussed here [21].

C. E. Klots proposed calculations and several lines of experimental evidence [3] for which the Gspann parameter results to be generally independent of the cluster size and content. Furthermore, Klots wrote in [25] that a strict analysis of experimental data would reveal a dependence of the Gspann parameter on the rate constant, which would require different values of γ for different cluster compositions. However, for a rate constant of 10^5 s^{-1} for thermal evaporation $\gamma = 23.5 \pm 1.5$ is acceptable for various materials, owing to the imprecision associated with the experimental measurements in evaluating γ . In fact, this value is assumed to be a universal parameter applicable to all materials and to all sizes [26]. The value of the Gspann parameter can be defined by using the Arrhenius equation [16] as follows:

$$\gamma = \ln(A) - \ln(k)$$

where A is the pre-exponential factor for reactions with no reverse activation energy (expected to have a loose transition state [27]) and k is the most probable rate constant for a particular time of flight. Klots proposes $\gamma = 23.5 \pm 1.5$ if $A = 1.6 \times 10^{15} \text{ s}^{-1}$ and $k = 10^5 \text{ s}^{-1}$ as the most probable rate constant for a flight time of $10 \mu\text{s}$ [27]. It is worth noting that γ depends also on the characteristic flight time through the field-free region of an experiment.

The choice of $\gamma \sim 25$ has been considered in [26] for the analysis of the kinetic energy release from the metastable decay of clusters of protonated ammonia: if the pre-exponential factor of $A = 10^{16} \text{ s}^{-1}$ and the rate constant is $k = 10^5 \text{ s}^{-1}$, then $\gamma = 25.3$ [26]. In addition, a pre-exponential factor in the range $3.5 \times 10^{15} - 1.3 \times 10^{16} \text{ s}^{-1}$ at 100 K has been obtained by using Rice-Ramsperger-Kassel-Marcus/Quasi Equilibrium Theory (RRKM/QET).

It is clear that the uncertainty in the Gspann parameter value leads to uncertainty in the calculated T_b and, therefore, in the binding energy determined with the finite heat bath theory. An example is provided by the observation of unimolecular (metastable) fragmentation of fullerene ions. The analysis of metastable fractions (MFs) of fullerene provided $\gamma = 31$ [28], whereas a value of $\gamma = 33$ was obtained from RRKM modelling of MFs and the breakdown curves [29]. Recently, in [30] it has been performed an analysis of some of the data used by Klots to determine the value of the Gspann parameter; the results showed a higher value than the Gspann value derived by Klots.

Each cluster has been assigned the value $C = 6(n - 1)$, where n is the number of molecules in a cluster. (As a consequence, the hydrogen in a protonated cluster is not included in the total number molecules, but considered in the calculation of the molecular weight of a cluster.) In other words, the heat capacity of each replica in the ensemble is expressed as a function of the degrees of freedom of a cluster. This expression assumes that none of the intramolecular vibrations in any of the molecules are active and that overall cluster rotation and translation do not contribute to the heat capacity; that is, only the intermolecular vibrations are active.

These assumptions are in agreement with the conclusions reached by Sundén et al. [31] following a detailed analysis of the heat capacities of water clusters $\text{H}^+(\text{H}_2\text{O})_n$ in the size range $n = 5 - 300$. The report has determined size dependent heat capacity and showed that the heat capacity increases with $6k_B - 8k_B$ per added molecule, indicating that

- for each water molecule there are six external degrees of freedom added, and that
- the intramolecular vibrations, rotational, and translational degrees of freedom are frozen.

There are no analogous data available for ammonia or methanol clusters. This expression for the heat capacity gives values for C that are slightly

higher than those determined by Hock et al. [32] following observations on the melting of water clusters larger in size ($n = 48$ and $n = 118$) than those studied here. In [26], the heat capacity was chosen as $C \sim 5n$ in units of k_B .

According to the requirements of the FHBT, the heat capacity is determined at constant volume.

- (V) The evaporation energy (or binding energy as it will be called in the following chapters) E_b of a neutral fragment leaving a cluster in a unimolecular (metastable) decay can then be calculated from the expression defined by Klots:

$$E_b = \gamma k_B T_b$$

The uncertainty $\pm \Delta E_b$ is calculated as per the formula (3.3) (*cf.* page 61) where evaporation energies are substituted for ΔE .

3.6 Example of MIKE scan analysis

An example of MIKE scan for a metastable process and the preliminary values that can be extracted by these fittings can be seen in Figure 3.6.1. Each peak is plotted as a function of laboratory frame kinetic energy, where the maximum of each curve is respectively E_1 for the parent ion and E_2 for the daughter ion. Moreover, R^2 , w , and FWHM parameters for the parent ion and the daughter ion are reported in Table 3.6.1. Laboratory frame kinetic energy is the kinetic energy

Ion	w (eV)	R^2	$\Delta E_i = (\text{FWHM})_i$ (eV)
Parent Ion	1.885	0.99	2.220
Daughter Ion	5.637	0.99	6.638

Table 3.6.1: Numerical data for the experimental metastable peaks in Figure 3.6.1

determined in an experiment with respect to the laboratory frame of reference, whereas centre of mass kinetic energy is the kinetic energy determined with respect to the centre of mass frame of reference (*cf.* Section 3.5).

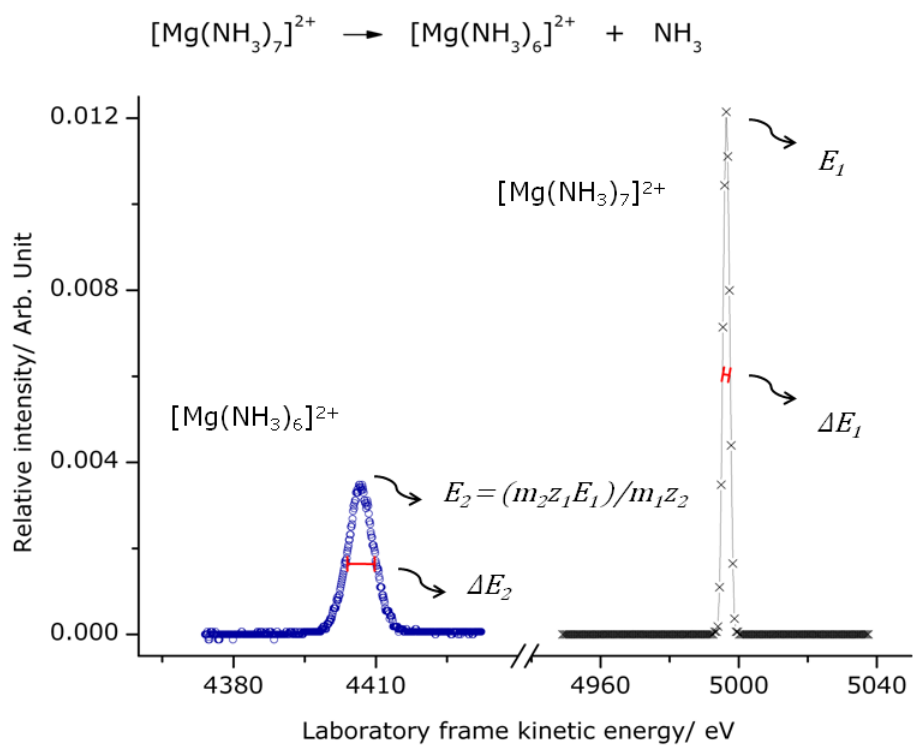


Figure 3.6.1: Example of metastable peaks recorded for the unimolecular fragmentation of $[\text{Mg}(\text{NH}_3)_7]^{2+}$ cluster ions

Bibliography

- [1] C.E. Klots, *Journal of Chemical Physics* 83 (1985) 5854.
- [2] C.E. Klots, *Nature* 327 (1987) 222.
- [3] C.E. Klots, *Journal of Physical Chemistry* 92 (1988) 5864.
- [4] C.E. Klots, *Accounts of Chemical Research* 21 (1988) 16.
- [5] C.E. Klots, *Journal of Chemical Physics* 90 (1989) 4470.
- [6] J.H. Beynon, *Analytical Chemistry* 42 (1970) 97A.
- [7] R.G. Cooks, J.H. Beynon, R.M. Caprioli, G.R. Lester, in *Metastable Ions*, ed. Elsevier Scientific Pub. Co., Amsterdam, New York, 1st edn. , 1973.
- [8] C.A. Woodward, A.J. Stace, *Journal of Chemical Physics* 94 (1991) 4234.
- [9] W. Forst, in *Unimolecular Reactions: a Concise Introduction*, Cambridge University Press, Cambridge, 1st edn., 2003.
- [10] P.G. Lethbridge, A.J. Stace, *Journal of Chemical Physics* 89 (1988) 4062.
- [11] J.N. Bilton, N. Kyriakidis, E.S. Waight, *Organic Mass Spectrometry* 13 (1978) 489.
- [12] R.P. Morgan, C.J. Porter, J.H. Beynon, *Organic Mass Spectrometry* 12 (1977) 735.
- [13] J.A. Hipple, E.U. Condon, *Physical Review* 68 (1945) 54.
- [14] Origin (OriginLab, Northampton, MA).
- [15] M.A. Baldwin, P.J. Derrick, R.P. Morgan, *Organic Mass Spectrometry* 11 (1976) 440.

- [16] J. Laskin, C. Lifshitz, *Journal of Mass Spectrometry and Ion Processes* 36 (2001) 459.
- [17] R. Parajuli, B. J. Duncombe, A. J. Stace, *International Journal of Mass Spectrometry* 296 (2010) 10.
- [18] J. L. Homes, J. K. Terlouw, *Organic Mass Spectrometry* 15 (1980) 383.
- [19] J. L. Homes, A. D. Osborne, *Organic Mass Spectrometry* 23 (1977) 189.
- [20] K. Hansen, in *Statistical Physics of Nanoparticles in the Gas Phase*, ed. Springer Science+Business Media, Dordrecht, 1st edn., 2013.
- [21] C. Lifshitz, C.-Y. Ng, T. Baer, I. Powis (Eds.), in *Cluster Ions*, Wiley, Chichester, 1st edn., 1993, ch. 2, pp. 121-164.
- [22] P. G. Francis, in *Mathematics for Chemists*, ed. Chapman and Hall Ltd., Bristol, 1st edn., 1984.
- [23] J. R. Taylor, in *Introduzione all'analisi degli errori. Lo studio delle incertezze nelle misure fisiche*, ed. Zanichelli, Bologna, 2nd Italian edn., 2000.
- [24] J. Gspann, in *Physics of Electronic and Atomic Collisions*, ed. In S. Datz, North Holland, Amsterdam, 1982.
- [25] C.E. Klots, *International Journal of Mass Spectrometry* 100 (1988) 457.
- [26] C. Lifshitz, F. Louage, *International Journal of Mass Spectrometry and Ion Processes* 101 (1990) 101.
- [27] B.G. Reuben, M. Iraqi, C. Lifshitz, *Journal of Physical Chemistry* 95 (1991) 9713.
- [28] K. Hansen, E. E. B. Campbell, *Journal of Chemical Physics* 104 (1996) 5012.
- [29] J. Laskin, B. Hadas, T. D. Märk, C. Lifshitz, *International Journal of Mass Spectrometry and Ion Processes* 177 (1998) L9.
- [30] K. Hansen, E. E. B. Campbell, *Journal of Chemical Physics* 233 (2004) 215.
- [31] A.E.K. Sundén, K. Støchkel, S. Panja, U. Kadhane, P. Hvelplund, S. Brønsted Nielsen, H. Zettergren, B. Dynefors, K. Hansen, *Journal of Chemical Physics* 130 (2009) 224308.

- [32] C. Hock, M. Schmidt, R. Kuhnen, C. Bartels, L. Ma, H. Haberland, B.V. Issendorff, *Physical Review Letters* 103 (2009) 073401.

Chapter 4

Binding Energy of $\text{H}^+(\text{NH}_3)_n$, $\text{H}^+(\text{CH}_3\text{OH})_n$, and $\text{H}^+(\text{H}_2\text{O})_n$

In this chapter we discuss the results of the experimental investigation of unimolecular (metastable) decay (neutral loss, in these experiments) of single solvent molecule for cluster ions $\text{H}^+(\text{NH}_3)_n$, $\text{H}^+(\text{CH}_3\text{OH})_n$, and $\text{H}^+(\text{H}_2\text{O})_n$ for $3 \leq n \leq 30$.

4.1 Experimental details

Artefact peaks have been registered from $n \geq 23$ for $\text{H}^+(\text{H}_2\text{O})_n$, from $n \geq 26$ for $\text{H}^+(\text{CH}_3\text{OH})_n$, and from $n \geq 24$ for $\text{H}^+(\text{NH}_3)_n$. The experiments were performed at the pressure of 10^{-7} mbar. The value of laboratory frame FWHM peak widths of each precursor ion was $2.3 \text{ eV} < w < 2.5 \text{ eV}$ for $\text{H}^+(\text{H}_2\text{O})_n$, $1.8 \text{ eV} < w < 2.4 \text{ eV}$ for $\text{H}^+(\text{CH}_3\text{OH})_n$, and $1.4 \text{ eV} < w < 2.0 \text{ eV}$ at $4 \leq n \leq 30$ and $w \sim 2.5 \text{ eV}$ at $n = 3$ for $\text{H}^+(\text{NH}_3)_n$. The goodness of fit to a Gaussian profile was $R^2 > 0.9$ for all the experimental measurements on both precursor ions and daughter ions. We refer the reader to Chapter 9 for the experimental values of w and R^2 and to Chapter 10 for more details on the experimental settings. At least four measurements have been used to determine the kinetic energy release for the metastable neutral loss for each cluster size.

Figure 4.1.1 yields examples of MIKE scan profiles for a precursor ion and the respective daughter ion for $\text{H}^+(\text{H}_2\text{O})_n$, $\text{H}^+(\text{CH}_3\text{OH})_n$, and $\text{H}^+(\text{NH}_3)_n$ clusters.

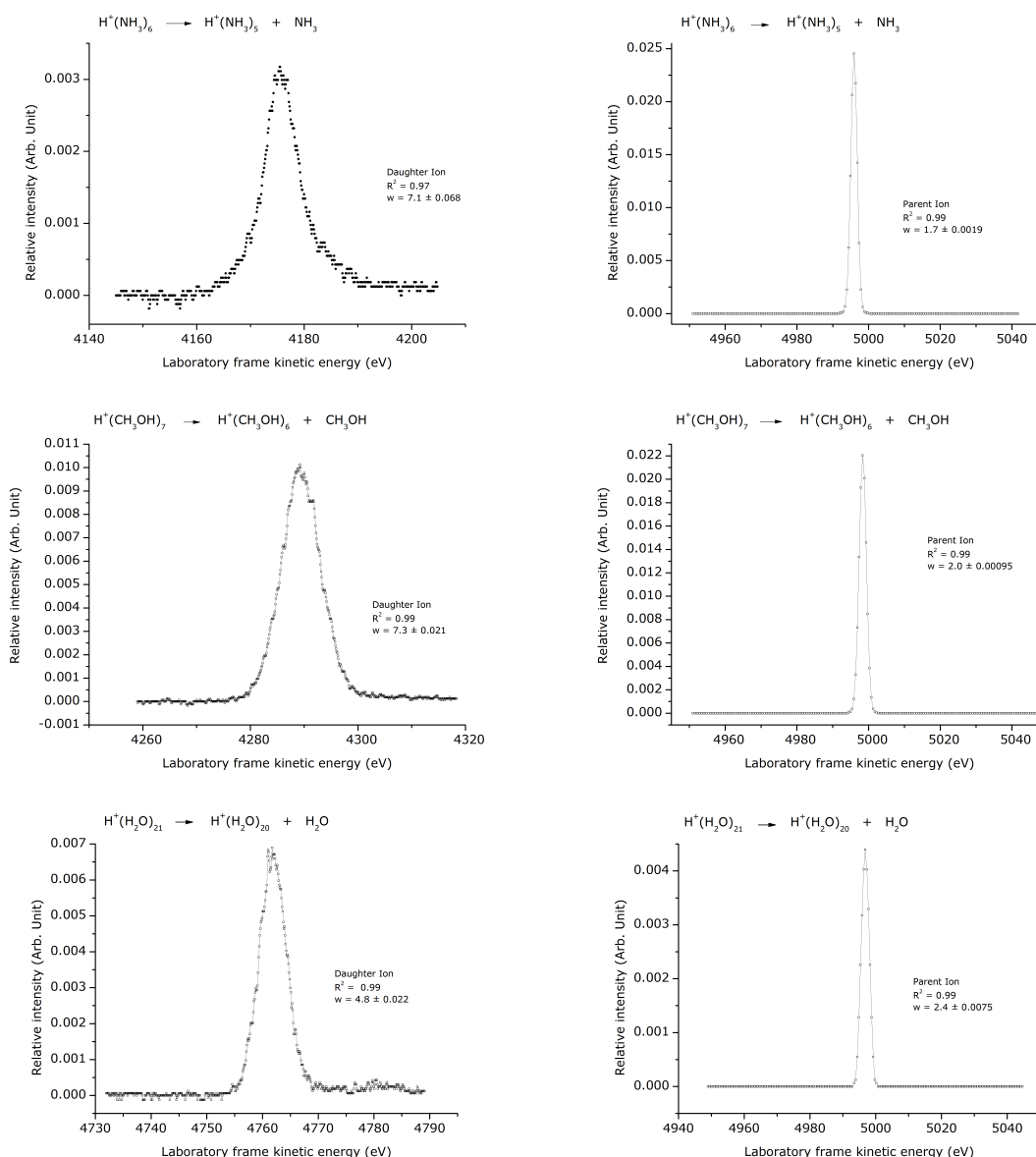


Figure 4.1.1: Examples of MIKE scan for $\text{H}^+(\text{NH}_3)_6$, $\text{H}^+(\text{CH}_3\text{OH})_7$, and $\text{H}^+(\text{H}_2\text{O})_{21}$: daughter ions (left column) with $R^2 = 0.97, 0.99, 0.99$ and respective parent ions (right column) with $R^2 = 0.99$ and $w = 1.7 \text{ eV}, 2.0 \text{ eV}, 2.4 \text{ eV}$

4.2 Plot of Binding Energies as a Function of the Number of Molecules in Each Cluster as a Calibration Graph

We now illustrate how the calibration of the techniques developed in this research (*cf.* Chapter 3) has been conducted. More precisely, we show that our technique is capable of yielding binding energies in large cluster ions containing up to 30 molecules. From the results presented here it would appear that accurate measurements of kinetic energy release coupled with their analysis us-

ing the theory due to Klots can yield quantitative results. This approach may be applied to the determination of binding energy for protonated molecular cluster ions and multiply charged metal-ligand complexes (*cf.* Chapters 5, 6, and 7) undergoing unimolecular metastable decay.

Stepwise binding energies have been established from experimental measurements of the protonated molecular cluster ions $\text{H}^+(\text{H}_2\text{O})_n$, $\text{H}^+(\text{CH}_3\text{OH})_n$, and $\text{H}^+(\text{NH}_3)_n$ for $3 \leq n \leq 30$. The investigation has been repeated multiple times for each n , and only the scans fitting a Gaussian distribution function have been examined. More precisely, experimental measurements of peak widths were only accepted when the goodness of fit to a Gaussian profile R^2 was > 0.9 . Furthermore, in order to minimize the effects of kinetic energy spread in precursor ions, the energy resolving capability has been optimized. The front slit of the mass analyser has been closed as much as possible. (This slit is placed between the mass analyser and the flight tube of the *Ist ffr*; closing the slit means narrowing the width of the slit aperture, and therefore decreasing the number of ions passing through the slit.) In this way, we obtained a high resolution at the minor cost of sensitivity. Remarkably, the limit to which the slit can be closed has to be determined, for each cluster, according to the detectability of the fragment's signal. The position of the slit for the protonated cluster ions experiment has resulted in laboratory frame FWHM peak widths of the precursor ions < 3 eV which has to be compared with a typical fragment ion laboratory frame energy width > 5 eV. The iteration of measurements has allowed us to estimate an average value of the binding energy and its respective error. The binding energy has been determined by applying the evaporative ensemble statistical model by Klots [1, 2, 3, 4, 5], after that the kinetic energy release had been extracted from the experimental MIKE scans [6]. Two parameters γ (called the Gspann parameter) and ℓ are employed in the Equations (3.4) and (3.5). We have adopted the most frequently used value of the Gspann parameter $\gamma = 25 \pm 1.5$ [7]; such a value provides reliable results from these experiments. We set parameter ℓ to 1.5; such value appeared to be the most appropriate for these experimental data analysis. Indeed, we have ascertained the most reliable numerical value for ℓ by calculating the binding energy of each cluster for $\ell = 1$, $\ell = 1.5$, and $\ell = 2$. Then the resulting binding energy values paired with their respective errors have been plotted as function of n to obtain a calibration curve for each molecular protonated cluster.

Figure 4.2.1 shows that, as n approaches to 30, the binding energy values calculated by using $\ell = 1.5$ approaches the value of the standard enthalpy of vapourisation determined at the transition temperature, the latter being 44 kJ mol^{-1} for water [8, 9, 10, 11, 13], 37 kJ mol^{-1} for methanol [9, 10, 11, 12, 13, 14], and

23 kJ mol⁻¹ for ammonia [9, 10, 11, 13].

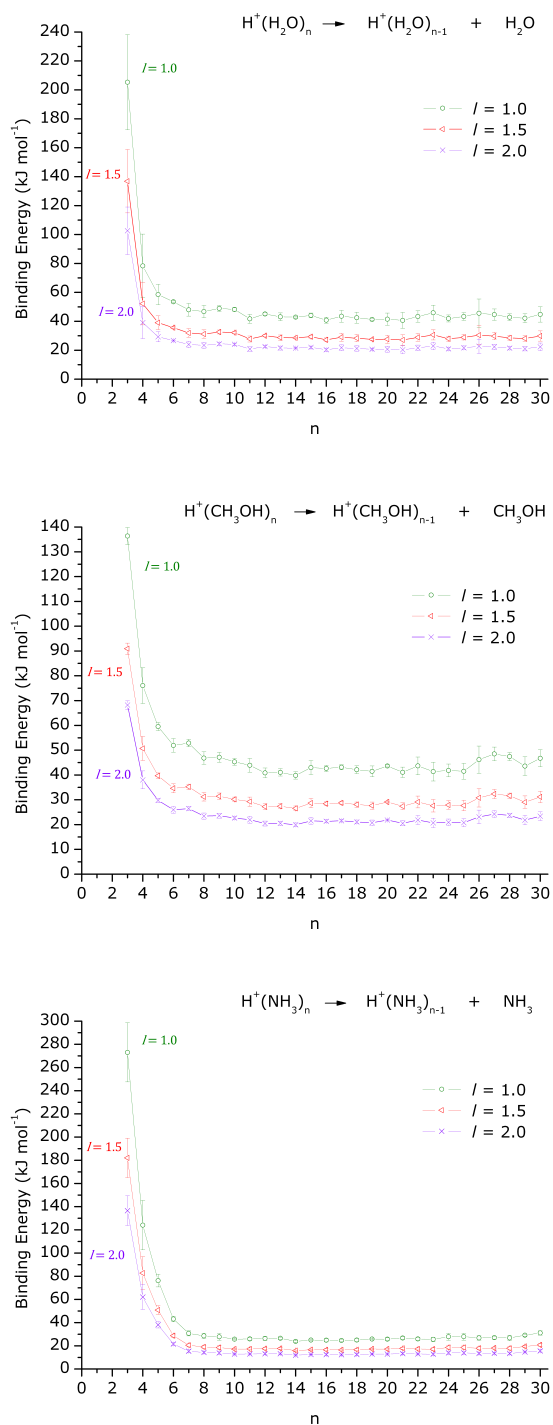


Figure 4.2.1: Parameter $\ell = 1.0, 1.5, 2.0$ for the definition of the transition state temperature in the water, methanol, and ammonia protonated cluster ions

In order to verify the correctness and reproducibility of this experimental procedure and the suitability of the chosen theory and its parameters for data analysis, the resulting derived binding energies have been compared against the available sources as reported in Section 4.3 below.

4.3 Binding Energies of Protonated Molecular Cluster Ions $\text{H}^+(\text{H}_2\text{O})_n$, $\text{H}^+(\text{NH}_3)_n$, and $\text{H}^+(\text{CH}_3\text{OH})_n$ from Metastable Kinetic Energy Release Measurements

Our results (published in [15]) lead to the conclusion that, for all three molecular systems, $\text{H}^+(\text{H}_2\text{O})_n$, $\text{H}^+(\text{NH}_3)_n$, and $\text{H}^+(\text{CH}_3\text{OH})_n$, the larger cluster ions decay – for n bigger than six – via the breaking of a single hydrogen bond.

The magnitude of the binding energy depends quite critically on the environment of the molecule that is being lost from a cluster. For hydrogen bonded systems, there are most probably two options, with either one or two hydrogen bonds being broken. Taking water as an example, a molecule held in position by a single hydrogen bond should have a binding energy of approximately 22 kJ mol^{-1} , whereas, the enthalpy of vaporization of water at approximately 44 kJ mol^{-1} would equate with the breaking of two hydrogen bonds.

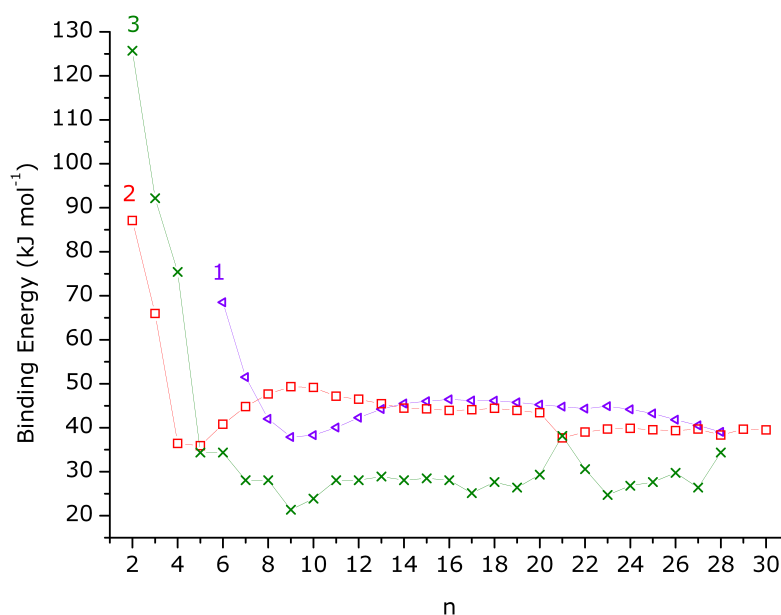


Figure 4.3.1: Summary of measurements of binding energies for large cluster ions from the literature. The binding energies are given in kJ mol^{-1} and are plotted as a function of n , the number of water molecule in each cluster. The set of data 1, 2, and 3 were taken respectively from [16], [17], and [14]. (These data and this work results are in Table 4.4.6)

Figure 4.3.1 summarizes the existing binding energy data for the neutral loss process described by the following reaction



The data are taken from three separate experimental studies on the fragmentation of large water clusters [14, 16, 17]. Broadly speaking, energies determined from the relative intensities of ions and/or their fragments fall into two categories; they are either $\sim 25 \text{ kJ mol}^{-1}$ (breaking a single hydrogen bond) or $\sim 45 \text{ kJ mol}^{-1}$ (breaking two hydrogen bonds).

n	$\text{H}^+(\text{NH}_3)_n$		$\text{H}^+(\text{CH}_3\text{OH})_n$		$\text{H}^+(\text{H}_2\text{O})_n$	
	$\langle \varepsilon_T \rangle$ (meV)	$\pm \Delta \langle \varepsilon_T \rangle$ (meV)	$\langle \varepsilon_T \rangle$ (meV)	$\pm \Delta \langle \varepsilon_T \rangle$ (meV)	$\langle \varepsilon_T \rangle$ (meV)	$\pm \Delta \langle \varepsilon_T \rangle$ (meV)
3	35	3.3	17	0.42	26	4.1
4	26	4.4	15	1.4	16	4.5
5	19	1.4	15	0.41	14	1.7
6	12	0.65	14	0.77	15	0.18
7	9.6	0.68	16	0.46	14	1.3
8	9.4	0.70	15	0.82	15	1.4
9	9.5	0.98	16	0.66	16	0.70
10	9.1	0.18	15	0.47	16	0.40
11	9.4	0.46	15	0.98	15	1.1
12	9.7	0.60	14	0.72	16	0.44
13	9.9	0.37	15	0.54	16	1.0
14	9.0	0.24	15	0.55	16	0.22
15	9.6	0.18	16	1.0	16	0.62
16	9.6	0.56	16	0.48	15	0.78
17	9.6	0.42	16	0.38	16	1.5
18	9.8	0.56	16	0.61	16	1.4
19	10	0.11	16	0.86	16	0.36
20	10	0.45	17	0.17	16	1.6
21	10	0.49	16	0.83	16	2.1
22	10	0.54	17	1.4	17	1.5
23	10	0.75	16	1.5	18	2.1
24	11	1.2	16	1.0	16	0.97
25	11	1.2	16	1.2	17	1.0
26	10	0.80	18	2.2	18	4.0
27	11	0.52	19	1.1	18	1.5
28	11	0.89	19	0.65	17	0.93
29	12	0.34	17	1.5	17	1.2
30	12	0.76	19	1.4	18	2.1

Table 4.3.1: Experimental measurements of the average kinetic energy release, $\langle \varepsilon_T \rangle$, associated with the unimolecular (metastable) decay of cluster ions. Each value is the average of at least four separate measurements and the error, $\pm \Delta \langle \varepsilon_T \rangle$, reflects the spread in uncertainty in the measurements

Table 4.3.1 and Table 4.3.2 (below) report values of kinetic energy release and binding energy for the systems $\text{H}^+(\text{H}_2\text{O})_n$, $\text{H}^+(\text{NH}_3)_n$, and $\text{H}^+(\text{CH}_3\text{OH})_n$ losing one neutral molecule in a unimolecular (metastable) decay as calculated from the analysis given in Chapter 3. The data obtained in these experiments were truncated after the second significant digit only once all the calculations

n	$\text{H}^+(\text{NH}_3)_n$		$\text{H}^+(\text{CH}_3\text{OH})_n$		$\text{H}^+(\text{H}_2\text{O})_n$	
	E_b	$\pm\Delta E_b$	E_b	$\pm\Delta E_b$	E_b	$\pm\Delta E_b$
	(kJ mol ⁻¹)	(kJ mol ⁻¹)	(kJ mol ⁻¹)	(kJ mol ⁻¹)	(kJ mol ⁻¹)	(kJ mol ⁻¹)
3	189	17	90	2.2	138	22
4	85	14	50	4.7	52	14
5	52	3.7	39	1.0	39	4.7
6	29	1.5	34	1.8	35	0.43
7	20	1.4	35	1.0	32	2.9
8	19	1.4	31	1.6	31	2.8
9	18	1.9	31	1.3	32	1.3
10	17	0.35	30	0.91	32	0.77
11	17	0.85	29	1.8	27	2.0
12	17	1.0	27	1.3	30	0.80
13	17	0.67	27	0.98	28	1.7
14	16	0.43	26	0.97	28	0.40
15	16	0.32	28	1.8	29	1.1
16	16	0.97	28	0.84	27	1.3
17	16	0.73	28	0.66	29	2.7
18	16	0.96	28	1.0	28	2.5
19	17	0.19	27	1.4	27	0.61
20	17	0.76	29	0.29	27	2.8
21	17	0.81	27	1.4	27	3.6
22	17	0.90	29	2.4	28	2.6
23	17	1.2	27	2.5	30	3.4
24	18	1.9	27	1.7	28	1.6
25	18	1.9	27	2.1	28	1.7
26	17	1.3	30	3.6	30	6.5
27	18	0.85	32	1.8	29	2.6
28	17	1.4	31	1.0	28	1.5
29	19	0.55	29	2.5	28	2.0
30	20	1.2	31	2.2	29	3.5

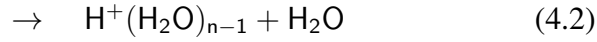
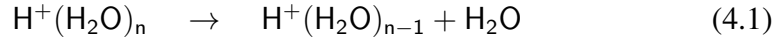
Table 4.3.2: Binding energies determined from the kinetic energy release data presented in Table 4.3.1

had been processed.

The data show a rapid variation when n is small, but drop to a more or less fixed value when $n > 6$. This value is approximately 26 kJ mol⁻¹ for water, 16 kJ mol⁻¹ for ammonia, and 27 kJ mol⁻¹ for methanol. Remarkably, the values obtained in our study are very close to the single hydrogen bond strengths, despite the approximations present in the theory used to derive them. Moreover, the consistency of the results for $6 \leq n \leq 30$ underpins the accuracy of the measurements that have been made on the larger clusters. For $n < 6$, the error bars on some of the data points are significantly larger than those seen when $n > 6$; this is due to the reduced probability smaller ions have of fragmenting in the *2nd ffr*, which means that signal strengths are low and the peak profiles are less

reproducible. In contrast, the large cluster ions benefit from the appearance of reproducible profiles with excellent signal-to-noise ratios.

Given that the molecules on the periphery of a cluster could be held in place by either one or two hydrogen bonds, it is necessary (and appropriate) to consider what the implications of this difference are in terms of the measurements discussed here. Consider two fragmentation channels:



where molecule (4.1) is held in place by one hydrogen bond and molecule (4.2) by two hydrogen bonds, which means that the activation energies are approximately 22 kJ mol^{-1} and 44 kJ mol^{-1} , respectively. The intensity of a metastable peak for process (4.1) can be calculated from the expression [18, 19]:

$$m_a^* = \alpha \int_{\varepsilon_a}^{E_{\max}} f(E) \frac{k_a(E)}{k_{a,b}} \{e^{-k_{a,b}t_1} - e^{-k_{a,b}t_2}\} dE \quad (4.3)$$

where α is a normalization constant, $f(E)$ is an internal energy distribution for $\text{H}^+(\text{H}_2\text{O})_n$, $k_a(E)$ and $k_b(E)$ respectively are rate constants for steps (4.1) and (4.2) at energy E , $k_{a,b} = k_a(E) + k_b(E)$, and t_1 and t_2 respectively are the instants when the *2nd ffr* is entered and left. Although $t_1 < t_2$, both values depend on the geometry of the particular mass spectrometer being used. The flight paths on the ZAB-E are long (approximately 2 m to the *2nd ffr*) and so both numbers are of the order of 10^{-4} s. For the present analysis knowledge of the exact shape of $f(E)$ is not necessary. If step (4.1) is to yield a metastable peak then $k_a(E) \approx \frac{1}{t_1}$; therefore, since $t_1 < t_2$ and $k_a(E) \gg k_b(E)$ (as the latter step has a much higher activation energy) an estimate of the metastable peak intensity at a given energy can be obtained from the expression [20]:

$$m_a(E)dE \approx \alpha f(E)dE \quad (4.4)$$

If the same analysis is repeated for step (4.2) assuming $k_b(E) \approx \frac{1}{t_1}$, then the equation equivalent to (4.4) gives:

$$m_b^*(E)dE \approx \alpha f(E) \frac{k_b(E)}{k_a(E) + k_b(E)} e^{-(k_a(E)t_1)} dE$$

However, at an energy where step (4.2) could be observed in the form of a metastable peak (*i.e.* when $k_b(E) \approx \frac{1}{t_1}$), we have that $k_a(E)$ is still very much larger than $k_b(E)$ and therefore, $m_b^*(E)dE \approx 0$ over the appropriate energy range (see Figure 3 of [20] for a graphical analysis). This ability that the lowest en-

ergy step has to influence the intensities of competing reactions is referred to as the competitive shift [19, 21]. In the analysis of cluster ion fragmentation patterns, detailed kinetic modelling of competing unimolecular reactions shows that competitive shifts can be influenced by a difference of just about 5 kJ mol^{-1} in binding energy [20, 22]. Because of the competitive shift, we will only record a metastable peak, and hence a binding energy, for the most weakly bound molecule present in a given cluster. In these experiments the binding energy for large values of n should equate with the energy of a single hydrogen bond. The loss of a molecule could entail the breaking of two hydrogen bonds, but this would need to be a two-step process, with the final step being responsible for the observation of a fragment. It should be noted that this analysis only applies to clusters that undergo unimolecular (metastable) decay. Ions that have been subject to collisional activation can behave very differently because the time window available for fragmentation is not defined so precisely [14]. In particular, the lower time limit t_1 in Equation (4.3) no longer applies as ions may be free to undergo very rapid fragmentation following collisional activation.

Figure 4.3.2 shows a graphical summary of binding energies as a function of n of Table 4.3.1. A clear difference emerges between the binding energy determined for ammonia clusters and those for the other two molecular systems. This distinction obviously reflects a difference in hydrogen bond strength, but also the strong similarity shown between the data recorded for water and methanol matches the fact that these two molecules have very similar hydrogen bond strengths.

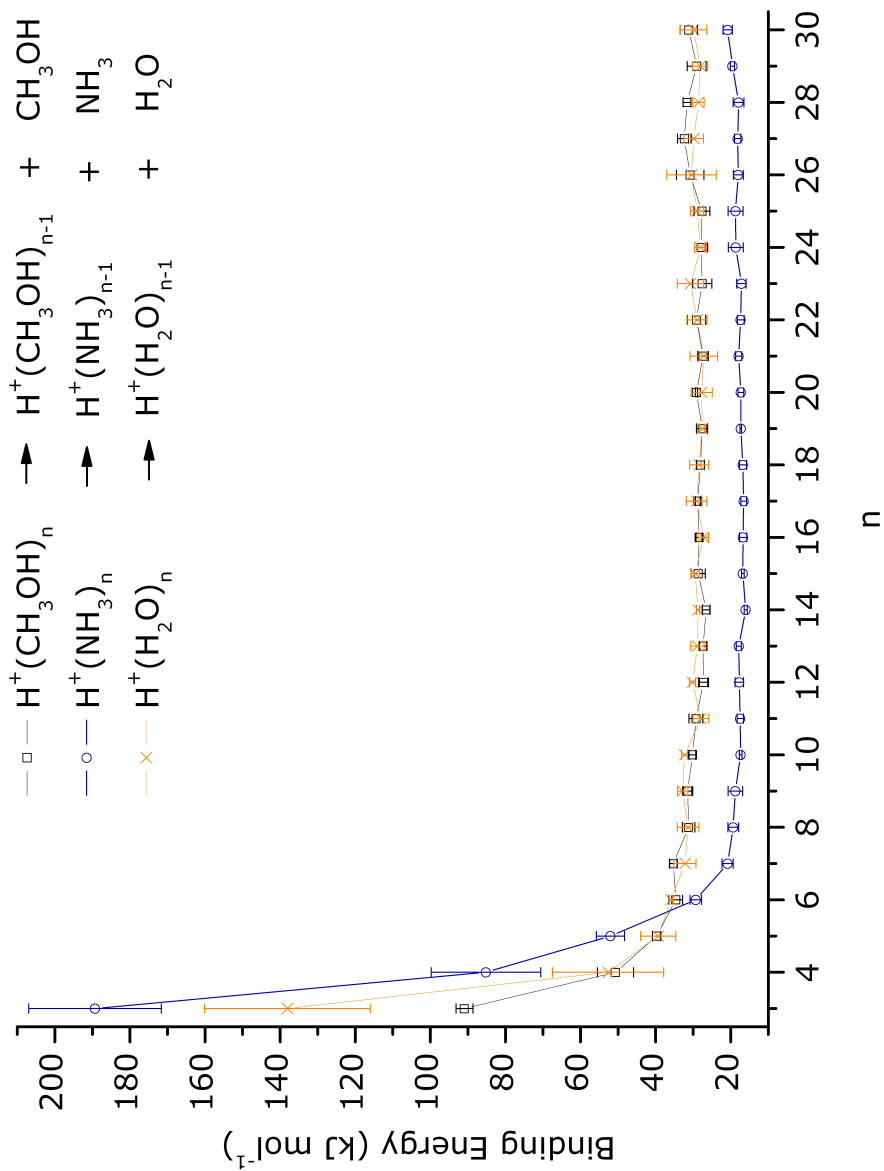


Figure 4.3.2: Plot of binding energies extracted from kinetic energy release measurements on water, ammonia and methanol cluster ions. The binding energies are given in kJ mol^{-1} and are plotted as a function of n , the number of molecules in each cluster.

4.4 Related Experimental Work

A number of experiments have focused on the significance of $\text{H}^+(\text{H}_2\text{O})_{21}$ and classification of the ion as a “magic” number [16, 23, 25]. Here, we need to provide a definition of magic number. In [24], a magic number is defined as a particularly stable cluster size; more precisely, the cluster size of a product ion from a unimolecular (metastable) decay that shows to have a higher metastable ion fraction than the other cluster sizes [7]. Where metastable ion fraction as a function of cluster size is the metastable peak intensity (product ion peak) with respect to the corresponding parent ion peak intensity. Metastable ion fractions can be calculated by using the evaporative ensemble statistical model by C. E. Klots. Magic numbers have been observed in kinetic energy release experiments also [7]. Quantitative theoretical interpretation for the latter is provided by both the evaporative ensemble statistical model by Klots and the microcanonical statistical Rice-Ramsperger-Kassel-Marcus/quasi equilibrium theory.

Although some experiments also show evidence for the presence of particularly stable structures, *i.e.* the dodecahedron $\text{H}^+(\text{H}_2\text{O})_{21}$ [14, 16, 23, 26, 25, 27, 28, 29, 30, 31, 32, 33], which does not appear to be the case from the binding energies presented here. Nevertheless, it is not obvious that the entire ensemble of any cluster of a given size will be composed solely of dodecahedral structures or of a similar stable form. The latter case occurs for experiments where low temperature ions are generated via supersonic expansion [28]; however, in experiments where ions are generated by high energy electron impact or by the bombardment of ice, a wide range of structures are expected to be formed at each value of n . Whilst a cornerstone of the evaporative ensemble model is that evaporation prior to the point of observation establishes a temperature for an ion, this does not necessarily equate to forming the most stable structure. A mixture of structures would account for the fact that some fraction of the $\text{H}^+(\text{H}_2\text{O})_n$ ions where $n > 21$, will preferentially decay to form the stable $\text{H}^+(\text{H}_2\text{O})_{21}$ structure [25]; those ions do not then decay, but instead live long enough to reach the end of the apparatus where they contribute to an ion signal with a higher than expected intensity. However, fragmentation of the same fraction of ions would not be expected to have a significant impact on the peak width for metastable decay when averaged over contributions from all the ions present.

Although the main purpose of this work was to focus on large clusters where data is difficult to obtain by conventional equilibrium thermodynamic methods, results have been obtained for a number of small clusters ($n \leq 10$) and these are summarized in Tables 4.4.1-4.4.3 where they are compared with a range of data from other sources. In addition, Tables 4.4.4-4.4.6 outline results for clusters

with $n > 10$. Although some of the measurements from equilibrium experiments are labelled as enthalpy changes, for the purposes of this comparison, the data are taken as binding energies. The largest discrepancies appear to be for the very small clusters, where the kinetic energy release measurements give an overestimate of the binding energy, particularly for $\text{H}^+(\text{NH}_3)_3$, $\text{H}^+(\text{NH}_3)_4$, and $\text{H}^+(\text{H}_2\text{O})_3$. As already noted, this lack of agreement could be due to poor peak profiles resulting from weak fragment ion signals. Beyond these sizes there is, within experimental error, *i.e.* $\pm\Delta\langle\varepsilon_\tau\rangle$ and $\pm\Delta E_b$, agreement with at least one other result. For $\text{H}^+(\text{CH}_3\text{OH})_n$ clusters the agreement with existing data is good for all values of n .

$\text{H}^+(\text{CH}_3\text{OH})_n \rightarrow \text{H}^+(\text{CH}_3\text{OH})_{n-1} + \text{CH}_3\text{OH}$						
n	$E_b(\text{kJ mol}^{-1})$	$E(\text{kJ mol}^{-1})$				
	This work	[34]	[35]	[36]	[37]	[38]
2		134	138	132		117
3	90 ± 2.2	87.2	89.2	88.8	95.5, 90.5	82.1
4	50 ± 4.7	66.6	67.4	58.6		67.1
5	39 ± 1.0	55.7	56.5	47.3		60.0
6	34 ± 1.8	52.0	52.3	42.7		54.4
7	35 ± 1.0	49.8	49.8	38.9		50.9
8	31 ± 1.6		50.2	37.7		48.6
9	31 ± 1.3			39.3		47.0
10	30 ± 0.9			38.1		46.0

Table 4.4.1: Comparison between binding energies determined in these experiments for small $\text{H}^+(\text{CH}_3\text{OH})_n$ clusters ($n \leq 10$) and those available from other experimental sources

$H^+(NH_3)_n \rightarrow H^+(NH_3)_{n-1} + NH_3$													
n	E_b												
	E												
	(kJ mol ⁻¹) (kJ mol ⁻¹)												
	This work	[39]	[40]	[41]	[42, 43]								
2		57.8	57.8	103	113	106	90.0						
3	189 ± 17	26.8	43.5	65.7	71.2	72.4	70.8	67.8					
4	85 ± 14		57.8	69.1	74.5	59.4	63.2	55.3	56.5				
5	52 ± 3.7		52.3	60.7	66.6	49.4	56.5	44.4	49.0	54.0			
6	29 ± 1.5			31.4			40.2		29.3				
7	20 ± 1.4								27.2				
8	19 ± 1.4									24.2	24.6	24.6	
9	18 ± 1.9									22.5	23.3	19.6	23.4
10	17 ± 0.3									19.6	20.9	16.4	21.2
										18.2	19.9	14.9	19.8

Table 4.4.2: Comparison between binding energies determined in these experiments for small $H^+(NH_3)_n$ clusters ($n \leq 10$) and those available from other experimental sources

$\text{H}^+(\text{H}_2\text{O})_n \rightarrow \text{H}^+(\text{H}_2\text{O})_{n-1} + \text{H}_2\text{O}$		E																
n	E_b (kJ mol ⁻¹)	[14]	[16]	[17]	[34]	[44]	[45]	[46]	[47]	[48]	[49]	[50, 51]	[52]	[53]	[54]	[55]	[56]	[57]
	This work	[14]	[16]	[17]	[34]	[44]	[45]	[46]	[47]	[48]	[49]	[50, 51]	[52]	[53]	[54]	[55]	[56]	[57]
2		125			132	133	132	150		132	29.3	68.2, 69.1	138		135, 126	156		146
3	138 ± 22	92.1		85.4	78.8	79.6	81.7	93.4		83	54.4	62.0	87.9		85.8, 62.4	93.0	83	84
4	52 ± 14	75.4		62.2	73.2	73.7	73.3	71.2	75.0	77	70.3	73.7	67.0	72.0	69.9, 38.1	75.0	67.8	
5	39 ± 4.7	34.3		31.8	47.0	48.1		64.1	53.2	54	54.0			50.6	53.2, 18.0		62.0	
6	35 ± 0.4	34.3	68.5	30.9	45.2	46.5		54.4	48.6	49	35.6			43.9	51.1, 18.8			
7	32 ± 2.9	28.0	51.4	36.2	43.3			49.0	44.8	44				39.3				
8	31 ± 2.8	28.0	42.0	40.7	41.5			43.1						39.8				
9	32 ± 1.3	21.3	37.8	43.4														
10	32 ± 0.7	23.8	38.2	45.2														

Table 4.4.3: Comparison between binding energies determined in these experiments for small $\text{H}^+(\text{H}_2\text{O})_n$ clusters ($n \leq 10$) and those available from other experimental sources

$\text{H}^+(\text{CH}_3\text{OH})_n \rightarrow \text{H}^+(\text{CH}_3\text{OH})_{n-1} + \text{CH}_3\text{OH}$				
n	$E_b(\text{kJ mol}^{-1})$	$E(\text{kJ mol}^{-1})$		
	This work	[35]	[36]	[38]
11	29 ± 1.8	36.4	44.8	44
12	27 ± 1.3	36.0	43.8	43
13	27 ± 0.98	35.6	42.8	42
14	26 ± 0.97	36.0	42.2	42
15	28 ± 1.8		41.9	41
16	28 ± 0.84		41.6	41
17	28 ± 0.66		40.9	41
18	28 ± 1.0		41.0	41
19	27 ± 1.4		40.6	40
20	29 ± 0.29		40.3	40

Table 4.4.4: Comparison between binding energies determined in these experiments for $\text{H}^+(\text{CH}_3\text{OH})_n$ clusters ($11 \leq n \leq 20$) and those available from other experimental sources

$\text{H}^+(\text{NH}_3)_n \rightarrow \text{H}^+(\text{NH}_3)_{n-1} + \text{NH}_3$					
n	$E_b(\text{kJ mol}^{-1})$	$E(\text{kJ mol}^{-1})$			
	This work	[40]	[41]	[42, 43]	
11	17 ± 0.85	15.7	18.0	13.8	18.0
12	17 ± 1.0	19.1	21.3	13.4	21.6
13	17 ± 0.67	15.7	17.9	13.7	18.2
14	16 ± 0.43	17.7	20.1	14.5	20.3
15	16 ± 0.32	15.7	17.9	15.0	18.3
16	16 ± 0.97	15.0	17.4	15.7	17.5
17	16 ± 0.73	14.0	16.2	16.3	16.5
18	16 ± 0.96			16.8	
19	17 ± 0.19			17.4	
20	17 ± 0.76			18.3	
21	17 ± 0.81			19.4	
22	17 ± 0.90			20.3	

Table 4.4.5: Comparison between binding energies determined in these experiments for $\text{H}^+(\text{NH}_3)_n$ clusters ($11 \leq n \leq 22$) and those available from other experimental sources

The data from [37] in Tables 4.4.7 and 4.4.1 are bond energies calculated at 0 K from literature experimental enthalpies. These values do not differ consistently from the other experimental results which were obtained at various temperatures and from $\text{H}^+(\text{CH}_3\text{OH})_3$ of this work; in contrast the agreement with $\text{H}^+(\text{H}_2\text{O})_3$ and $\text{H}^+(\text{H}_2\text{O})_4$ is poor. (It is worth stressing that the temperature at which the unimolecular metastable decay of a cluster has been recorded in these experiments is unknown.)

$\text{H}^+(\text{H}_2\text{O})_n \rightarrow \text{H}^+(\text{H}_2\text{O})_{n-1} + \text{H}_2\text{O}$				
n	$E_b(\text{kJ mol}^{-1})$	$E(\text{kJ mol}^{-1})$		
	This work	[14]	[16]	[17]
2		125		
3	138 ± 22	92		87
4	52 ± 14	75		65
5	39 ± 4.7	34		36
6	35 ± 0.43	34	68.50	35
7	32 ± 2.9	28	51.49	40
8	31 ± 2.8	28	42.02	44
9	32 ± 1.3	21	37.87	47
10	32 ± 0.77	23	38.29	49
11	27 ± 2.0	28	40.05	49
12	30 ± 0.80	28	42.27	47
13	28 ± 1.7	28	44.24	46
14	28 ± 0.40	28	45.50	45
15	29 ± 1.1	28	46.00	44
16	27 ± 1.3	28	46.42	44
17	29 ± 2.7	25	46.17	43
18	28 ± 2.5	27	46.13	44
19	27 ± 0.61	26	45.75	44
20	27 ± 2.8	29	45.25	43
21	27 ± 3.6	38	44.79	43
22	28 ± 2.6	30	44.33	37
23	30 ± 3.4	24	44.87	39
24	28 ± 1.6	26	44.16	39
25	28 ± 1.7	27	43.24	39
26	30 ± 6.5	29	41.81	39
27	29 ± 2.6	26	40.51	39
28	28 ± 1.5	34	39.05	39

Table 4.4.6: Comparison between binding energies determined in these experiments for $\text{H}^+(\text{H}_2\text{O})_n$ clusters ($2 \leq n \leq 28$) and those available from other experimental sources

$\text{H}^+(\text{H}_2\text{O})_n \rightarrow \text{H}^+(\text{H}_2\text{O})_{n-1} + \text{H}_2\text{O}$								
n	E_b	E						
	(kJ mol^{-1})	(kJ mol ⁻¹)						
	This work	[37]						
3	138 ± 22	80.4, 77.9	82.5, 80.0	82.9	91.7	88.8, 86.3	84.2	85.0
4	52 ± 14	73.7, 72.9	72.4	69.1	73.3	67.4, 66.2	68.2	75.0

Table 4.4.7: Comparison between binding energies determined in these experiments for $\text{H}^+(\text{H}_2\text{O})_n$ clusters ($3 \leq n \leq 4$) and those available from other experimental sources from [37] calculated at 0 K

4.5 Related Theoretical Work

Here, we use the term “bond energy” (BE) to indicate the energy corresponding to a dissociation process evaluated by theoretical calculations; whereas we use the term “binding energy” to designate the energy corresponding to a dissociation reaction determined by experimental analysis (E_b for the data of this work, and E for the data from experimental sources in the literature). This differentiation stresses that theoretical calculations and experimental results from the literature can be compared with the data determined in this work, provided that we consider the details of the computational procedure (*e.g.* level of theory, basis set) used in the theoretical calculations, and the experimental procedure with the corresponding data analysis. For instance, a theoretical investigation will calculate the binding energy of a complex at a precisely defined temperature; in addition, the geometry of the complex will be known and generally it will correspond to the lowest energy geometry optimised. Theoretical calculations may provide bond energies corresponding to breaking either one or two hydrogen bonds. In contrast, the temperature of complexes in the experiments reported here is unknown. As a matter of fact, a ion peak signal detected at the mass analyser and at the energy analyser may contain different isomers of the same cluster ion. The analysis of the kinetic energy release cannot provide a mean to distinguish amongst different structures for the same precursor (metastable) ion in these experiments; unimolecular (metastable) decay is dominated by those pathways with the lowest activation energy, because of competitive shift (*cf.* Section 4.3). Nonetheless, it is known from these experiments that it is the most weakly bound molecule in the outer solvation shell to undergo unimolecular (metastable) reaction, owing to the competitive shift. Consequently, the binding energy has been measured for a decay channel corresponding to the cluster structure having the lowest activation energy.

In addition to the available experimental data, large ($n > 6$) water [38, 58, 59], ammonia [59] and methanol [38] clusters have been the subject of theoretical attention. For the most part, these calculations have searched for minimum energy structures where molecules are invariably held in place by two hydrogen bonds. As such, many of the bond energies calculated for water clusters are going to be of the order of approximately 44 kJ mol^{-1} . Likewise, the bond energies determined for large ammonia clusters are higher than the values given here, but not necessarily by a factor of two.

The available theoretical bond energies (BE) are reported in Tables 4.5.2, 4.5.3, and 4.5.1, where the results are given at 0 K for [38, 60], at 298 K for some of the data in [59], and at 300 K for [58]. Note that those tables pro-

vide only the number n of the total number of molecules composing the cluster without any details on the geometry corresponding to the particular value of n . Furthermore, the tables show calculation details (level of theory and basis set level) for each corresponding referenced investigations. In particular, the method used by [38] is Austin Model 1 (AM1), a parametric quantum mechanical molecular model (*i.e.* self consistent field molecular orbital Austin Model 1, AM1 SCF-MO method), [58] uses Monte-Carlo (MC) method with Matsuoka-Clementi-Yoshimine (MCY) configuration interaction potential, [60] Hartree-Fock level of theory, and [59] Becke-3-parameter-Lee-Yang-Parr exchange-correlation functional (B3LYP) level of theory.

$\text{H}^+(\text{H}_2\text{O})_n \rightarrow \text{H}^+(\text{H}_2\text{O})_{n-1} + \text{H}_2\text{O}$			
n	$E_b(\text{kJ mol}^{-1})$	$\text{BE}(\text{kJ mol}^{-1})$	
	This work	[58] ^{300 K}	[60] ^{0 K}
		MC MCY	HF 4 – 31G
2			155
3	138 ± 22	97	108
4	52 ± 14	77	92
5	39 ± 4.7	58	67
6	35 ± 0.43	55	62
7	32 ± 2.9	54	
8	31 ± 2.8	49	
9	32 ± 1.3	47	
10	32 ± 0.77	36	
11	27 ± 2.0	35	
12	30 ± 0.80	37	
13	28 ± 1.7	32	
14	28 ± 0.40	34	
15	29 ± 1.1	33	
16	27 ± 1.3	32	
17	29 ± 2.7	28	
18	28 ± 2.5	31	
19	27 ± 0.61	32	
20	27 ± 2.8	32	
21	27 ± 3.6	34	
22	28 ± 2.6	37	
23	30 ± 3.4	30	
24	28 ± 1.6	33	
25	28 ± 1.7	35	
26	30 ± 6.5	32	
27	29 ± 2.6	27	
28	28 ± 1.5	39	
29	28 ± 2.0	28	

Table 4.5.1: Comparison between binding energies determined in these experiments for $\text{H}^+(\text{H}_2\text{O})_n$ clusters ($1 \leq n \leq 28$) and those available from theoretical sources. (The superscript indicates the temperature)

$H^+(NH_3)_n \rightarrow H^+(NH_3)_{n-1} + NH_3$												
n	E_b (kJ mol ⁻¹)	BE (kJ mol ⁻¹)										
This work		[59]					[59] ^{298 K}					
		HF	B3LYP	HF	HF	HF	HF	HF	HF	HF	HF	B3LYP
		D95V	cc-pVDZ	STO-3G	3-21G	D95V	3-21G*	3-21G**	6-31G**	cc-pVDZ		
2		106	129	176	155.5	134	109.8					
3	189 ± 17	85.8	104	134	111.4	103.2	86.39		98.29			124.4
4	85 ± 14	70.3	85	96.7	90.33	85.35			77.72			103.2
5	52 ± 3.7	57.8	70	73.7	72.0				62.17			73.82
6	29 ± 1.5	30	43						49.94			63.47
7	20 ± 1.4	29	42									
8	19 ± 1.4	28	41									
9	18 ± 1.9	28	40									
10	17 ± 0.3	18	28									
11	17 ± 0.85	17	28									
12	17 ± 1.0	17	27									
13	17 ± 0.67	17	27									
14	16 ± 0.43	8.7	17									
15	16 ± 0.32	8.7	17									
16	16 ± 0.97	8.7	17									
17	16 ± 0.73	8.7	16									

Table 4.5.2: Comparison between binding energies determined in these experiments for $H^+(NH_3)_n$ clusters ($2 \leq n \leq 17$) and those available from theoretical sources. (The superscript indicates the temperature)

$H^+(CH_3OH)_n \rightarrow H^+(CH_3OH)_{n-1} + CH_3OH$		
n	$E_b(kJ mol^{-1})$	$BE(kJ mol^{-1})$
	This work	[38] ^{0 K} AM1SCF – MO
2		124
3	189 ± 17	95
4	85 ± 14	76
5	52 ± 3.7	66

Table 4.5.3: Comparison between binding energies determined in these experiments for $H^+(CH_3OH)_n$ clusters ($2 \leq n \leq 4$) and those from theoretical sources. (The superscript indicates the temperature)

4.6 KER Data: Comparison with the Literature

The comparison among experimental kinetic energy release measurements for protonated ammonia and methanol clusters for $2 \leq n \leq 17$ in these experiments ($\langle \varepsilon_\tau \rangle$) and those provided by experimental literature data ($\langle KER \rangle$) can be seen in Tables 4.6.1-4.6.2. The binding energies E^* in the tables are calculated using $\langle KER \rangle$ values from the literature by applying the method used in this work. Measurement of the KER of metastable ions is based on the peak shape analysis; the metastable peak spectra were collected by a high resolution mass spectrometer of reversed geometry [61, 62] (VG ZAB-2F), [63] VG ZAB2-SEQ, and by [42, 43] reflecting electric field placed in the field free region of the TOF mass spectrometer (reflectron TOF mass spectrometer). The peak shapes were analysed by MIKE spectrometry in [61, 62, 63] and by a method proposed by Berry [64] and Franklin et al. [65] in [42, 43]. Overall the comparison amongst the kinetic energy measurements underlies the importance in choosing the experimental method. The diversity in the kinetic energy release results for the methanol ions is conspicuous: the $\langle KER \rangle$ values in [66] are higher than the data of this work, owing to the use of a high-pressure temperature-variable ion source [66]; and, the presence of two hydrogen bonds holding in place one methanol molecule may be reflected in the values of E^* in [63] with respect of the binding energies of this work.

$H^+(CH_3OH)_n \rightarrow H^+(CH_3OH)_{n-1} + CH_3OH$								
n	$\langle \varepsilon_\tau \rangle$ (meV)	$\langle KER \rangle$ (meV)			E_b (kJ mol ⁻¹)	E^* (kJ mol ⁻¹)		
	This work	[63]	[66]		This work	[63]*	[66]*	
2				24				832
3	17 ± 0.42	14.6		35	90 ± 2.2	77		178
4	15 ± 1.4	17.9		50	50 ± 4.7	58		159
5	15 ± 0.41	18.2		54	39 ± 1.0	47		138
6	14 ± 0.77	18.7	21.6	65	34 ± 1.8	43	50	147
7	16 ± 0.46	24.8	20.4	77	35 ± 1.0	53	43	161
8	15 ± 0.82	24.3	24.7	80	31 ± 1.6	49	50	159
9	16 ± 0.66	24.5	25.4		31 ± 1.3	48	49	
10	15 ± 0.47	26.2	25.5		30 ± 0.91	49	48	
11	15 ± 0.98	24.7	25.1		29 ± 1.8	45	46	
12	14 ± 0.72	24.9	24.7		27 ± 1.3	45	44	
13	15 ± 0.54	28.8	25.4		27 ± 0.98	51	45	
14	15 ± 0.55	27.5	25.7		26 ± 0.97	48	45	
15	16 ± 1.0	25.9	25.8		28 ± 1.8	45	45	

Table 4.6.1: Comparison between kinetic energy releases determined in these experiments for $H^+(CH_3OH)_n$ clusters ($2 \leq n \leq 15$) and those available from other experimental sources ($\langle KER \rangle$). Binding energies obtained in this work (E_b) and from other experimental sources (E) are also shown. Data corresponding to references marked with a * have been obtained by applying calculation method used in our work to $\langle KER \rangle$

$H^+(NH_3)_n \rightarrow H^+(NH_3)_{n-1} + NH_3$									
n	$\langle \varepsilon_T \rangle$ (meV)	[42, 43]	$\langle KER \rangle$ (meV)	[61]	[62]	E_b (kJ mol ⁻¹)	E (kJ mol ⁻¹)	E^* (kJ mol ⁻¹)	
	This work	[42, 43]	[61]	[62]		This work	[42, 43]	[42, 43]*	[61]* [62]*
2			1.1						38
3	35 ± 3.3		2.7	4.11	4.54	189 ± 17			13 21 23
4	26 ± 4.4	7.6	6.9	7.6	8.98	85 ± 14	53	24	21 24 29
5	19 ± 1.4	9.3	9.4	9.12	10.84	52 ± 3.7	51	24	23 23 28
6	12 ± 0.65	7.7	7.6	8.12	7.1	29 ± 1.5	28	18	17 18 16
7	9.6 ± 0.68	6.7	8.3		7.2	20 ± 1.4	24	14	17 15
8	9.4 ± 0.70	6.6	10			19 ± 1.4	23	13	19
9	9.5 ± 0.98	6.1				18 ± 1.9	21	12	
10	9.1 ± 0.18	5.8				17 ± 0.3	19	11	
11	9.4 ± 0.46	5.2				17 ± 0.85	18	9.6	
12	9.7 ± 0.60	6.6				17 ± 1.0	21	12	
13	9.9 ± 0.37	5.5				17 ± 0.67	18	9.8	
14	9.0 ± 0.24	6.2				16 ± 0.43	20	11	
15	9.6 ± 0.18	5.6				16 ± 0.32	18	9.8	
16	9.6 ± 0.56	5.4				16 ± 0.97	17	9.4	
17	9.6 ± 0.42	5.1				16 ± 0.73	16	8.8	

Table 4.6.2: Comparison between kinetic energy releases determined in these experiments for H^+ ($(NH_3)_n$ clusters ($2 \leq n \leq 17$)) and those available from other experimental sources ((KER)). Binding energies obtained in this work (E_b) and from other experimental sources (E) are also shown. Data corresponding to references marked with a * have been obtained by applying calculation method used in our work to $\langle KER \rangle$

Bibliography

- [1] C.E. Klots, *Journal of Chemical Physics* 83 (1985) 5854.
- [2] C.E. Klots, *Nature* 327 (1987) 222.
- [3] C.E. Klots, *Journal of Physical Chemistry* 92 (1988) 5864.
- [4] C.E. Klots, *Accounts of Chemical Research* 21 (1988) 16.
- [5] C.E. Klots, *Journal of Chemical Physics* 90 (1989) 4470.
- [6] R.G. Cooks, J.H. Beynon, R.M. Caprioli, G.R. Lester, *Metastable Ions*, Elsevier Scientific Pub. Co., Amsterdam, 1973.
- [7] C. Lifshitz, C.-Y. Ng, T. Baer, I. Powis (Eds.), *Cluster Ions*, Wiley, Chichester, 1st edn., 1993, ch. 2, pp. 121-164.
- [8] I. Wadsö, *Acta Chemica Scandinavica* 20 (1966) 536.
- [9] K.N. Marsh Ed., *Recommended Reference Materials For The Realisation Of Physicochemical Properties*, Blackwell, Oxford, 1987, pp. 3-113.
- [10] P.W. Atkins, *Physical Chemistry*, Oxford University Press, 6th edn., 1999, pp. 921.
- [11] D.R. Lide, *Handbook Of Chemistry And Physics*, CRC Press, 85th edn., (2004-2005), ch.6, pp. 112-113.
- [12] I. Wadsö, *Acta Chemica Scandinavica* 20 (1966) 544.
- [13] David R. Lide, ed., *CRC Handbook of Chemistry and Physics*, Internet Version 2005, <http://www.hbcnetbase.com>, CRC Press, Boca Raton, FL, 2005. If a specific table is cited, use the format: "Physical Constants of Organic Compounds", in *CRC Handbook of Chemistry and Physics*, Internet Version 2005, David R. Lide, ed., <http://www.hbcnetbase.com>, CRC Press, Boca Raton, FL, 2005.

- [14] T.F. Magnera, D.E. David, J. Michl, *Chemical Physics Letters* 182 (1991) 363.
- [15] E. Bruzzie (E. Bruzzi), R. Parajuli, A.J. Stace, *International Journal of Mass Spectrometry*, 345 (2013) 160.
- [16] Z. Shi, J.V. Ford, S. Wei, A.W. Castleman Jr., *Journal of Chemical Physics* 99 (1993) 8009.
- [17] K. Hansen, P.U. Andersson, E. Uggerud, *Journal of Chemical Physics* 131 (2009) 124303.
- [18] A.N. Yeo, D.H. Williams, *Journal of the American Chemical Society* 92 (1970) 3984.
- [19] J.R. Gilbert, A.J. Stace, *International Journal of Mass Spectrometry and Ion Physics* 15 (1974) 311.
- [20] A.J. Stace, A.K. Shukla, *Journal of the American Chemical Society* 104 (1982) 5314.
- [21] C. Lifshitz, F.A. Long, *Journal of Chemical Physics* 41 (1964) 2468.
- [22] A.J. Stace, C. Moore, *Journal of the American Chemical Society* 105 (1983) 1814.
- [23] S.-S. Lin, *Review of Scientific Instruments* 44 (1973) 516.
- [24] A.W. Castleman Jr., R.G. Keesee, *Chemical Reviews* 86 (1986) 589.
- [25] A.J. Stace, C. Moore, *Chemical Physics Letters* 96 (1983) 80.
- [26] J.Q. Searcy, J.B. Fenn, *Journal of Chemical Physics* 61 (1974) 5282.
- [27] S. Wei, Z. Shi, A.W. Castleman Jr., *Journal of Chemical Physics* 94 (1991) 3268.
- [28] J.-W. Shin, N.I. Hammer, E.G. Diken, M.A. Johnson, R.S. Walters, T.D. Jaeger, M.A. Duncan, R.A. Christie, K.D. Jordan, *Science* 304 (2004) 1137.
- [29] R.R. Burke, R.P. Wayne, *International Journal of Mass Spectrometry and Ion Physics* 25 (1977) 199.
- [30] J.L. Kassner, Jr., D.E. Hagen, *Journal of Chemical Physics* 64 (1976) 1860.

- [31] J.Q. Searcy, J.B. Fenn, *Journal of Chemical Physics* 64 (1976) 1861.
- [32] G.M. Lancaster, F. Honda, Y. Fukuda, J.W. Rabalais, *Journal of the American Chemical Society* 101 (1979) 1951.
- [33] P.M. Holland, A.W. Castleman, Jr., *Journal of Chemical Physics* 72 (1980) 5984.
- [34] M. Meot-Ner (Mautner), *Journal of the American Chemical Society* 108 (1986) 6189.
- [35] E.P. Grimsrud, P. Kebarle, *Journal of the American Chemical Society* 95 (1973) 7939.
- [36] M.S. El-Shall, C. Marks, L.W. Sieck, M. Meot-Ner (Mautner), *Journal of Physical Chemistry* 96 (1992) 2045.
- [37] E.R. Lovejoy, R. Bianco, *Journal of Physical Chemistry A* 104 (2000) 10280.
- [38] V.M. Jarvis, M.A. Villanueva, D.E. Bostwick, T.F. Moran, *Organic Mass Spectrometry* 28 (1993) 595. ([38] includes: Y. Xu, V.M. Jarvis, D.E. Bostwick, T.F. Moran, *Organic Mass Spectrometry* 26 (1991) 892).
- [39] R.G. Keesee, A.W. Castleman Jr., *Journal of Physical and Chemical Reference Data* 15 (1986) 1011.
- [40] S. Wei, W.B. Tzeng, A.W. Castleman Jr., *Journal of Chemical Physics* 93 (1990) 2506.
- [41] S. Wei, K. Kilgore, W.B. Tseng, A.W. Castleman Jr., *Journal of Physical Chemistry* 95 (1991) 8306.
- [42] S. Wei, W.B. Tzeng, A.W. Castleman Jr., *Journal of Chemical Physics* 92 (1990) 332.
- [43] A.W. Castleman Jr., W.B. Tzeng, S. Wei, S. Morgan, *Journal of the Chemical Society, Faraday Transactions* 86 (1990) 2417.
- [44] M. Meot-ner (Mautner), C.V. Speller, *Journal of Physical Chemistry* 90 (1986) 6616.
- [45] A.J. Cunningham, J.D. Payzant, P. Kebarle, *Journal of the American Chemical Society* 94 (1972) 7627.

- [46] P. Kebarle, S.K. Searles, A. Zolla, J. Scarborough, M. Arshadi, *Journal of the American Chemical Society* 89 (1967) 6393.
- [47] Y.K. Lau, S. Ikuta, P. Kebarle, *Journal of the American Chemical Society* 104 (1982) 1462.
- [48] P. Kebarle, G.W. Dillow, K. Hiraot and S. Chowdhury, *Faraday Discussion* 85 (1988) 23.
- [49] D.P. Beggs, F.H. Field, *Journal of the American Chemical Society* 93 (1971) 1567.
- [50] D.P. Beggs, F.H. Field, *Journal of the American Chemical Society* 93 (1971) 1576.
- [51] S.L. Bennett, F.H. Field, *Journal of the American Chemical Society* 94 (1972) 5186.
- [52] M. Meot-Ner, F.H. Field, *Journal of the American Chemical Society* 99 (1977) 998.
- [53] Y.-S. Wang, C.-H. Tsai, Y.T. Lee, H.-C. Chang, J.C. Jiang, O. Asvany, S. Schlemmer, D. Gerlich, *Journal of Physical Chemistry A* 107 (2003) 4217.
- [54] N.F. Dalleska, K. Honma, P.B. Armentrout, *Journal of the American Chemical Society* 115 (1993) 12125.
- [55] K. Honma, L.S. Sunderlin, P.B. Armentrout, *Journal of Chemical Physics* 99 (1993) 1623.
- [56] F.H. Field, *Journal of the American Chemical Society* 91 (1969) 2827.
- [57] K. Hiraoka, H. Takimoto, S. Yamabe, *Journal of Physical Chemistry* 90 (1986) 5910.
- [58] R. Kelterbaum, E. Kochanski, *Journal of Physical Chemistry* 99 (1995) 12493.
- [59] H. Nakai, T. Goto, T. Ichikawa, Y. Okada, T. Orii, K. Takeuchi, *Chemical Physics* 262 (2000) 201.
- [60] M.D. Newton, *Journal of Chemical Physics* 67 (1977) 5535.
- [61] C. Lifshitz, F. Louage, *Journal of Physical Chemistry* 93 (1989) 5633.

- [62] C. Lifshitz, F. Louage, *International Journal of Mass Spectrometry and Ion Processes*, 101 (1990) 101.
- [63] A. Gomory, P. Vegh, J. Sztaray, L. Drahos, K. Vekey, *European Journal of Mass Spectrometry* 10 (2004) 213.
- [64] C. E. Berry, *Phys. Rev.* 78, (1950), 597.
- [65] J. L. Franklin, P. M. Hierl, D. A. Whan, *Journal of Chemical Physics* 47 (1976) 3148.
- [66] M. Iraqi, C. Lifshitz, *International Journal of Mass Spectrometry and Ion Processes* 88 (1989) 45.

Chapter 5

Binding Energies of

$[\text{Mg}(\text{CH}_3\text{OH})_n]^{2+}$, $[\text{Ca}(\text{CH}_3\text{OH})_n]^{2+}$,
and $[\text{Sr}(\text{CH}_3\text{OH})_n]^{2+}$

In this chapter we discuss the results of the experimental investigation of unimolecular (metastable) decay (neutral loss, in these experiments) of single methanol molecule for $[\text{Mg}(\text{CH}_3\text{OH})_n]^{2+}$, $[\text{Ca}(\text{CH}_3\text{OH})_n]^{2+}$, and $[\text{Sr}(\text{CH}_3\text{OH})_n]^{2+}$ cluster ions for $4 \leq n \leq 20$.

5.1 Experimental Details

In the recorded scans of $[\text{Mg}(\text{CH}_3\text{OH})_n]^{2+}$ and $[\text{Ca}(\text{CH}_3\text{OH})_n]^{2+}$, no artefact peaks have been observed, while they have been detected for $[\text{Sr}(\text{CH}_3\text{OH})_n]^{2+}$ from $n \geq 18$. The value of laboratory frame FWHM peak widths of the precursor ions were

- $2.1 \text{ eV} < w < 2.4 \text{ eV}$ for $[\text{Mg}(\text{CH}_3\text{OH})_n]^{2+}$,
- $1.9 \text{ eV} < w < 2.3 \text{ eV}$ for $[\text{Ca}(\text{CH}_3\text{OH})_n]^{2+}$, and
- $2.5 \text{ eV} < w < 2.7 \text{ eV}$ at $n = 4$ and $1.7 \text{ eV} < w < 2.1 \text{ eV}$ at $5 \leq n \leq 20$ for $[\text{Sr}(\text{CH}_3\text{OH})_n]^{2+}$.

For the precursor ions of $[\text{Mg}(\text{CH}_3\text{OH})_n]^{2+}$ clusters, the goodness of fit to a Gaussian profile was $R^2 > 0.9$; for the respective daughter ions, the goodness was $0.7 < R^2 < 0.8$ at $4 \leq n \leq 5$ and $R^2 > 0.9$ at $n \geq 6$. For $[\text{Ca}(\text{CH}_3\text{OH})_n]^{2+}$ clusters, the goodness of fit to a Gaussian profile of the precursor ions and the fragment ions was $R^2 > 0.9$ for all the measurements. The goodness of fit to a Gaussian profile for the precursor ions of $[\text{Sr}(\text{CH}_3\text{OH})_n]^{2+}$ clusters was

$R^2 > 0.9$, and for the respective fragment ions was $0.8 < R^2 < 0.9$ at $n \leq 5$ and $R^2 > 0.9$ at $n \geq 6$. MIKE scan for the precursor ion of $[\text{Mg}(\text{CH}_3\text{OH})_3]^{2+}$ was observed, but it was not considered in the analysis because no daughter ion was detected for the neutral loss process under examination. MIKE scan for the precursor ion of $[\text{Ca}(\text{CH}_3\text{OH})_3]^{2+}$ and $[\text{Sr}(\text{CH}_3\text{OH})_3]^{2+}$ were observed, but they were not considered in the analysis because their respective fragment ion had respectively $R^2 < 0.4$ and $R^2 < 0.7$.

Figure 5.1.1 below shows examples of MIKE scan profiles for precursor ion and respective daughter ion for $[\text{Mg}(\text{CH}_3\text{OH})_n]^{2+}$, $[\text{Ca}(\text{CH}_3\text{OH})_n]^{2+}$, and $[\text{Sr}(\text{CH}_3\text{OH})_n]^{2+}$ clusters.

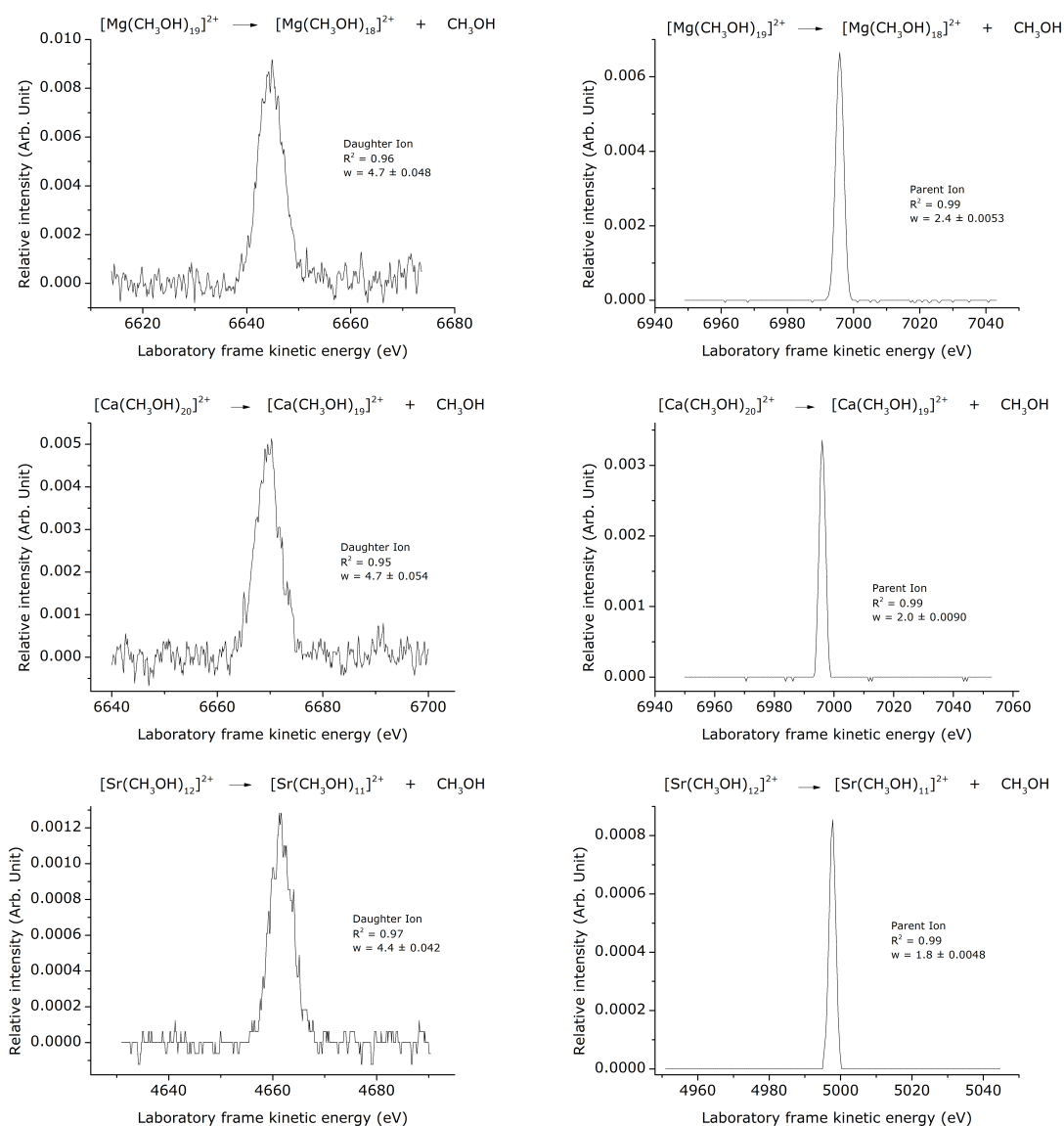


Figure 5.1.1: Examples of MIKE scan for for $[\text{Mg}(\text{CH}_3\text{OH})_n]^{2+}$, $[\text{Ca}(\text{CH}_3\text{OH})_n]^{2+}$ and $[\text{Sr}(\text{CH}_3\text{OH})_n]^{2+}$: daughter ions (left column) with $R^2 = 0.96, 0.95, 0.97$ and respective parent ions (right column) with $R^2 = 0.99$ and $w = 2.4 \text{ eV}, 2.0 \text{ eV}, 1.8 \text{ eV}$

We refer the reader to Chapter 9 for experimental values of w and R^2 and to Chapter 10 for more details on the experimental settings. A minimum of four measurements have been used to determine the kinetic energy release for the metastable neutral loss for each cluster size.

5.2 Binding Energies from Metastable KER Measurements

The studies of the neutral loss of a single methanol molecule of the cluster ions $[\text{Mg}(\text{CH}_3\text{OH})_n]^{2+}$, $[\text{Ca}(\text{CH}_3\text{OH})_n]^{2+}$, and $[\text{Sr}(\text{CH}_3\text{OH})_n]^{2+}$ for $4 \leq n \leq 20$ are discussed. The kinetic energy release from unimolecular (metastable) decay experiments of the cluster ions as a function of cluster size are reported in Table 5.2.1. They are experimental measurements of the average kinetic energy release, $\langle \varepsilon_\tau \rangle$, associated with the unimolecular (metastable) decay of cluster ions. Each value is the average of separates measurements and the error, $\pm \Delta \langle \varepsilon_\tau \rangle$, reflects the spread in uncertainty in the measurements.

n	$[\text{Mg}(\text{CH}_3\text{OH})_n]^{2+}$		$[\text{Ca}(\text{CH}_3\text{OH})_n]^{2+}$		$[\text{Sr}(\text{CH}_3\text{OH})_n]^{2+}$	
	$\langle \varepsilon_\tau \rangle$ (meV)	$\pm \Delta \langle \varepsilon_\tau \rangle$ (meV)	$\langle \varepsilon_\tau \rangle$ (meV)	$\pm \Delta \langle \varepsilon_\tau \rangle$ (meV)	$\langle \varepsilon_\tau \rangle$ (meV)	$\pm \Delta \langle \varepsilon_\tau \rangle$ (meV)
4	61	11	61	5.1	50	14
5	40	11	46	3.4	39	9.4
6	31	3.2	37	2.6	30	1.4
7	28	3.2	24	3.2	25	3.6
8	28	3.9	24	1.8	21	1.4
9	25	1.4	26	1.7	24	3.7
10	24	0.61	26	2.2	22	1.0
11	22	4.6	24	1.2	21	1.1
12	24	2.9	22	1.9	20	3.9
13	22	1.8	22	1.6	20	1.3
14	22	1.1	21	1.2	22	1.3
15	23	2.9	22	0.6	20	1.2
16	22	2.5	21	1.6	19	1.6
17	20	2.9	21	1.8	19	3.2
18	20	2.4	21	0.98	22	1.8
19	19	2.8	20	2.9	23	1.9
20	20	2.5	20	1.1	21	1.8

Table 5.2.1: Experimental measurements of the average kinetic energy release, $\langle \varepsilon_\tau \rangle$, associated with the unimolecular (metastable) decay of cluster ions. Each value is the average of at least four separates measurements and the error, $\pm \Delta \langle \varepsilon_\tau \rangle$, reflects the spread in uncertainty in the measurements

The binding energy of each of the ions as a function of the size of the corresponding cluster is given in Table 5.2.2. The data obtained in these experiments

were truncated after the second significant digit only once all the calculations had been processed.

n	$[\text{Mg}(\text{CH}_3\text{OH})_n]^{2+}$		$[\text{Ca}(\text{CH}_3\text{OH})_n]^{2+}$		$[\text{Sr}(\text{CH}_3\text{OH})_n]^{2+}$		$\text{H}^+(\text{CH}_3\text{OH})_n$
	E_b (kJ mol^{-1})	$\pm\Delta E_b$ (kJ mol^{-1})	E_b (kJ mol^{-1})	$\pm\Delta E_b$ (kJ mol^{-1})	E_b (kJ mol^{-1})	$\pm\Delta E_b$ (kJ mol^{-1})	$E_b \pm \Delta E_b$ (kJ mol^{-1})
4	199	38	200	16	164	47	50 ± 4.7
5	106	31	123	8.9	105	24	39 ± 1.0
6	73	7.5	87	6.0	71	3.3	34 ± 1.8
7	61	7.0	52	6.9	54	7.9	35 ± 1.0
8	58	8.1	50	3.8	44	3.0	31 ± 1.6
9	49	2.8	51	3.3	48	7.2	31 ± 1.3
10	45	1.1	50	4.2	42	1.9	30 ± 0.91
11	41	8.6	45	2.2	39	2.0	29 ± 1.8
12	44	5.4	41	3.5	37	7.2	27 ± 1.3
13	39	3.3	40	2.8	36	2.4	27 ± 0.98
14	40	1.9	38	2.1	39	2.4	26 ± 0.97
15	40	5.0	38	1.0	35	2.1	28 ± 1.8
16	38	4.4	36	2.8	33	2.9	28 ± 0.84
17	34	5.0	36	3.0	33	5.6	28 ± 0.66
18	34	4.1	36	1.6	37	3.1	28 ± 1.0
19	32	4.8	34	5.0	40	3.2	27 ± 1.4
20	34	4.2	35	1.8	36	3.1	29 ± 0.29

Table 5.2.2: Binding energies determined from the kinetic energy release data presented in Table 5.2.1. The binding energies of $\text{H}^+(\text{CH}_3\text{OH})_n$ are added for comparison

In addition, a plot of the binding energies as a function of n, the number of methanol molecules in each cluster, is shown in Figure 5.2.1, where error bars are an indication of the precision of the measurements.

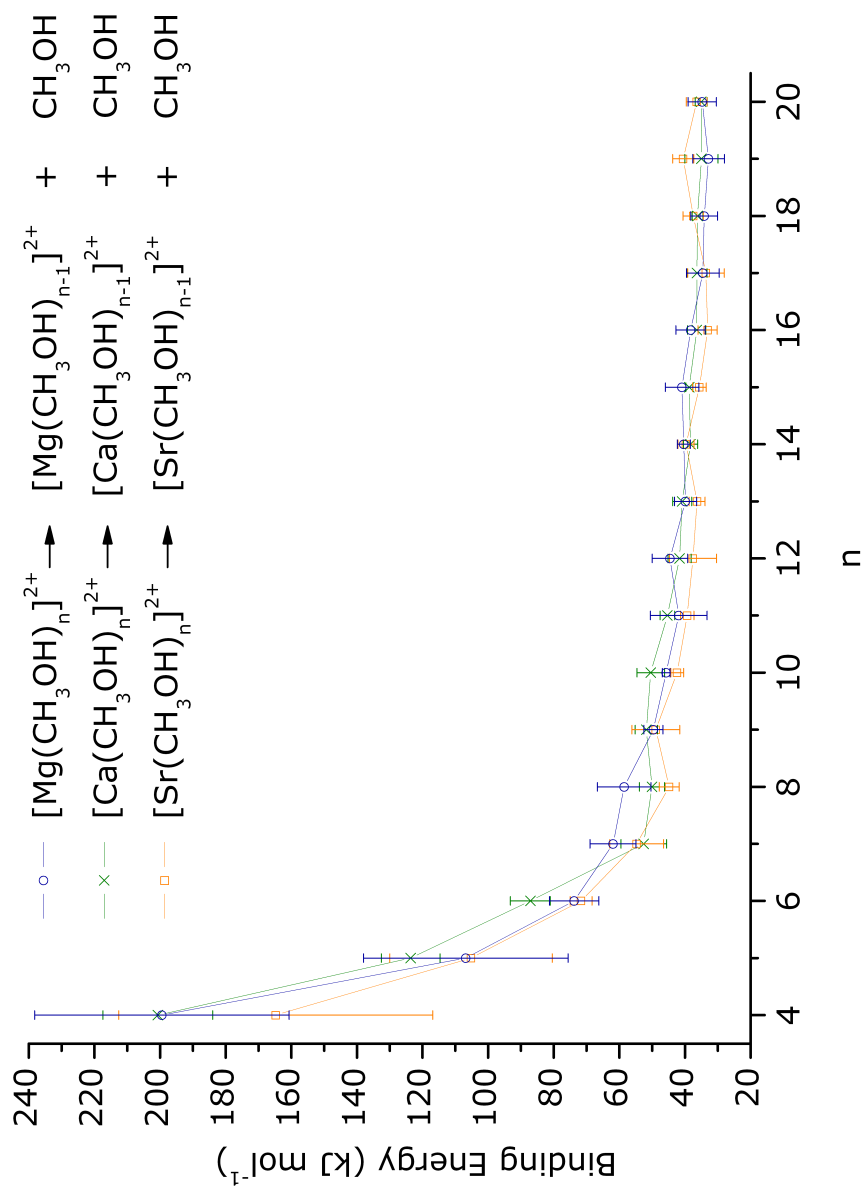


Figure 5.2.1: Plot of binding energies extracted from kinetic energy release measurements on $[\text{Mg}(\text{CH}_3\text{OH})_n]^{2+}$, $[\text{Ca}(\text{CH}_3\text{OH})_n]^{2+}$, and $[\text{Sr}(\text{CH}_3\text{OH})_n]^{2+}$ cluster ions. The binding energies are given in kJ mol^{-1} and are plotted as a function of n , the number of methanol molecules in each cluster

As shown in Figure 5.2.1, the change of the slope at $6 \leq n \leq 7$ of each binding energy versus cluster size plot suggests that, for $n \leq 6$, the metal directly binds to six methanol molecules; whereas, for $n \geq 7$, each of the methanol molecules added to the cluster binds to other methanol molecules. In other words, the steady decrease stops at a value of n that suggests the completion of the first solvent shell; this number n of methanol molecules coincides with the coordination number (CN) for a metal dication in these experiments. Therefore, these non equilibrium gas phase experiments on $[\text{Mg}(\text{CH}_3\text{OH})_n]^{2+}$, $[\text{Ca}(\text{CH}_3\text{OH})_n]^{2+}$, and $[\text{Sr}(\text{CH}_3\text{OH})_n]^{2+}$ clusters suggest that

- a) when coordinated with methanol the three alkaline earth metals have a coordination number of six in forming a complex in the gas phase under pressure conditions of 10^{-7} mbar;
- b) the seventh molecule just sits in a second shell attached to another methanol molecule instead of binding to the metal, and any other methanol molecule added binds to the cluster ion through hydrogen bonding (instead of binding to the metal);
- c) the weakest bond is broken in these experiments, which is one hydrogen bond between the metastable cluster ion and the most weakly bound molecule in the outer solvation shell;
- d) the detected kinetic energy releases are due to breaking a bond in geometrical structures which are not necessarily the most energetically stable;
- e) the charge on the metal is affecting the binding interactions at each n for all three cluster ions up to $n = 20$; and
- f) no magic numbers are observed (*cf.* Section 4.4 on page 83).

In particular, for d) the unimolecular (metastable) decay recorded by MIKE technique in these experiments is not necessarily of the most stable structure amongst the possible isomers for a particular cluster size, despite the fact that one of the foundations of the evaporative ensemble model by Klots is that evaporative cooling prior to the point of experimental observation establishes a temperature for an ion. In addition, it is possible to speculate that the experimental conditions increase the probability of the formation of a single preferred structure or of a series of isomers having similar energy of formation. Metastable decay processes in the field-free regions of a mass spectrometer are dominated by the lowest energy route to dissociation, described as competitive shift [1, 2, 3, 4] (*cf.* Section 4.3 on page 77). This is due to the fact that the investigated clusters

are metastable species with a lifetime of the duration of the flight time in the field-free region, which corresponds to the observation time range (also known as observation time window), around 5×10^{-4} s in this work, and they are in gas phase under high vacuum conditions (10^{-7} mbar). Therefore, the measured binding energy corresponds to the fragmentation of the most weakly bound molecule. In fact, the gas phase experiments reveal through the decay process the subtle difference for which a binding site may be preferred to other various sites available, even though the energy of a site may differ very slightly from the energy of another site [1]. Furthermore, the competition amongst dissociation paths may change with increasing clusters size and with the composition of the cluster [3, 4].

The electronic configuration of the ground state of each investigated metal is $[\text{Ne}]3s^0$ for Mg^{2+} , $[\text{Ar}]4s^0$ for Ca^{2+} , and $[\text{Kr}]5s^0$ for Sr^{2+} . Hence, as illustrated in Table 5.2.3, by going down the second group of the periodic table, the atomic and ionic radii of the alkaline earth metals increase [5, 6]; therefore, the charge density decreases [5, 6] since the double charge distributes over an increasing surface area.

Element	Electronic Configuration	Ionic Radius (Å)
Mg	$[\text{Ne}]3s^2$	0.78
Ca	$[\text{Ar}]4s^2$	1.06
Sr	$[\text{Kr}]5s^2$	1.27

Table 5.2.3: Some physical parameters of the alkaline earth metal ions under examination from reference [6]

The results presented in this work show that the charge on Mg^{2+} , Ca^{2+} , and Sr^{2+} has an effect on the binding energy at each value of n , in contrast to what expected from the charge density values. In other words, the double charge affects the binding interactions independently of the number of solvent molecules in the cluster, even after that the first solvation shell (also known as first coordination shell) has been filled and, therefore, regardless of the total radius of the cluster. Moreover, Mg^{2+} , Ca^{2+} , and Sr^{2+} have the ability to influence the binding interactions for clusters made up 20 molecules, even though it may be expected that each of the three alkaline earth metal ions would have behaved differently from the other two, owing to their different radius. Furthermore, as expected from the charge density values, the strength of the binding energy is higher for $[\text{Mg}(\text{CH}_3\text{OH})_n]^{2+}$ than for $[\text{Ca}(\text{CH}_3\text{OH})_n]^{2+}$ and, in turn, the binding energy for $[\text{Ca}(\text{CH}_3\text{OH})_n]^{2+}$ is higher than the one for $[\text{Sr}(\text{CH}_3\text{OH})_n]^{2+}$ at each n ; that is, the strength of the binding energies between the doubly charged metal and the ligands decreases at each n going down the second group of the periodic table.

The examination of the respective binding energy for $[\text{Mg}(\text{CH}_3\text{OH})_n]^{2+}$, $[\text{Ca}(\text{CH}_3\text{OH})_n]^{2+}$, $[\text{Sr}(\text{CH}_3\text{OH})_n]^{2+}$, and $\text{H}^+(\text{CH}_3\text{OH})_n$ – as shown in Table 5.2.2 and Figure 5.2.2 – does not help inferring the geometrical structure of the methanol molecules surrounding the central metal ion. This examination, however, proves that methanol molecules bind through one hydrogen bond, as it can be inferred by the fact that the binding energy of $[\text{Mg}(\text{CH}_3\text{OH})_n]^{2+}$, $[\text{Ca}(\text{CH}_3\text{OH})_n]^{2+}$, $[\text{Sr}(\text{CH}_3\text{OH})_n]^{2+}$ is higher than the one of $\text{H}^+(\text{CH}_3\text{OH})_n$, for a value that varies between 27 kJ mol^{-1} and 5 kJ mol^{-1} when $7 \leq n \leq 20$. In fact, the experimental results for $\text{H}^+(\text{CH}_3\text{OH})_n$ for each $3 \leq n \leq 30$ show a value of the binding energy that corresponds to a single hydrogen bonding; indeed, the considerations described in Section 4.3 (on page 77) explain that in these experimental conditions the route to dissociate one molecule from protonated cluster is via one hydrogen bond breaking. Moreover, the vaporization enthalpy for methanol at the condensed phase equilibrium is 37 kJ mol^{-1} [7, 8, 9, 10]; where the evaporation of one molecule in bulk phase implies breaking of two hydrogen bonds. As it can be seen in Table 5.2.2, the binding energies of the alkaline earth metals in association with methanol molecules (*a*) do differ consistently from the one of the protonated methanol and (*b*) are higher than the binding energy of $\text{H}^+(\text{CH}_3\text{OH})_n$ at each *n*, thus confirming that the charge affects the binding energy by increasing the strength of the bond.

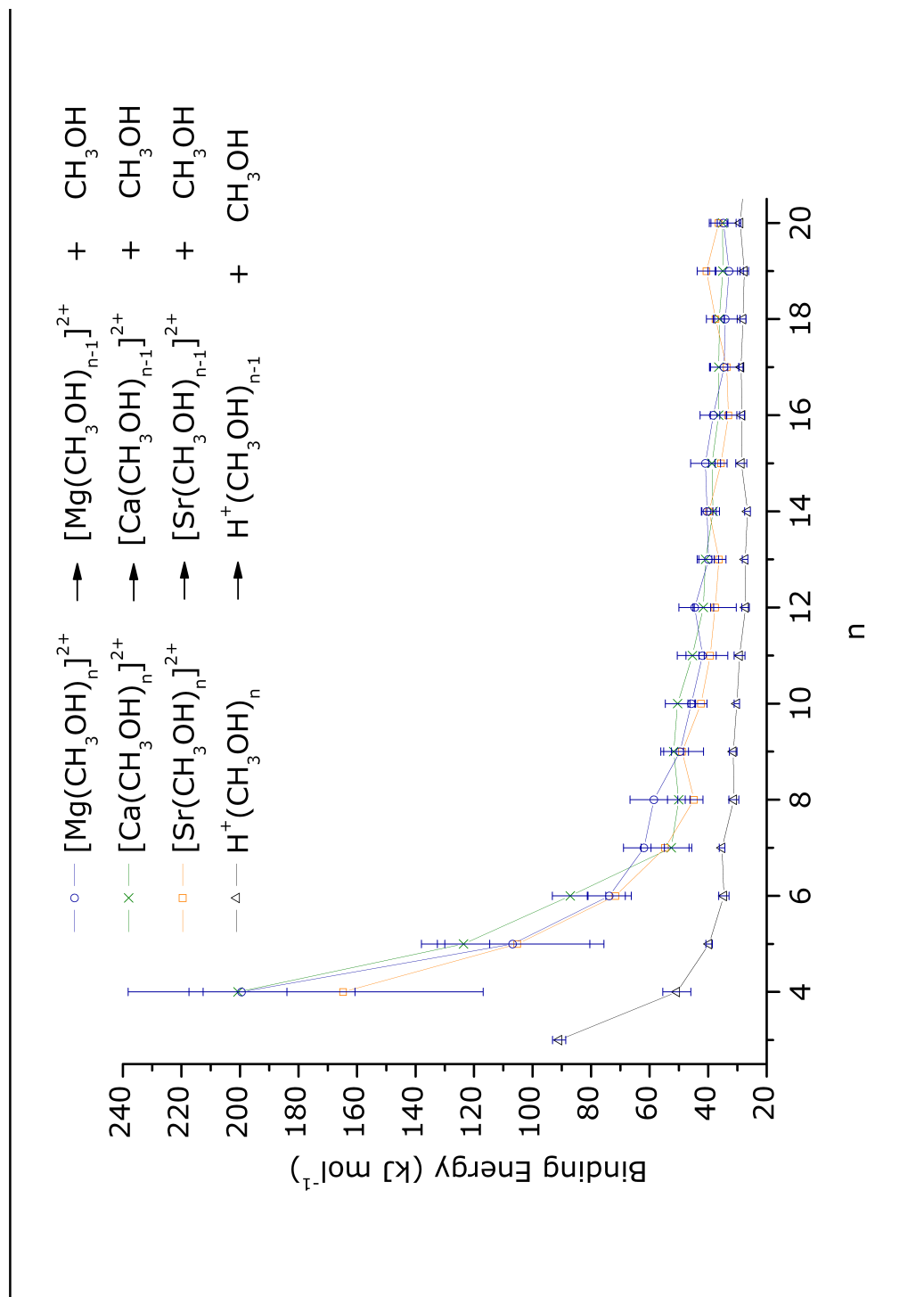


Figure 5.2.2: Binding energies (kJ mol⁻¹) extracted from kinetic energy release measurements on [Mg(CH₃OH)_n]²⁺, [Ca(CH₃OH)_n]²⁺, [Sr(CH₃OH)_n]²⁺ which are compared with H⁺(CH₃OH)_n as a function of n, the number of methanol molecules in each cluster.

The metal and solvent gaseous system may be compared with the liquid phase concentric shell model of solvation [11, 12]. The description of ion solvation in gas phase would imply three regions:

- (i) in a first region the solvent molecules are immobilized and orientated around the metal by the charge field of the metal ion;
- (ii) in a second region the solvent molecules are orientated to a varying degree depending on their distance from the ion charge field;
- (iii) in a third region the structure of the solvent molecules is not influenced by the ion.

According to the concentric solvation shell model, these experiments describe a doubly charged metal surrounded by a first shell completed with six methanol molecules; the second shell begins to form with the seventh methanol molecule. In these experiments for all three metal dications the 2+ charge influences the binding of molecules in clusters containing up to 20 solvent molecules, therefore the second solvation shell is established up to twenty solvent molecules, and the third region is still not initiated. It is plausible that there is no hydrogen bonding among methanol molecules in the first shell owing to the experimental binding energy data and geometric considerations on the possible orientations of the ligand in the space around the metal; yet, there is no evidence to support this conjecture. The effect of the double charge of the metal is to increase the strength of the binding energy amongst molecules in the cluster. In our observations, the methanol molecules that add up to the first shell are bonded through one hydrogen bond to another methanol molecule by using either their hydrogen acceptor site or their lone pair donor site.

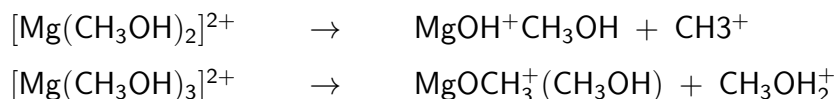
A conjecture on the binding dynamics is that the double charged metal is directly bonded to six methanol molecules through the interactions between the charge on the metal and both the permanent dipole and the induced dipole on each methanol molecule. Consequently, the molecules in the second shell are influenced by the dipole or induced dipole of other methanol molecules (either in the first or second shell), by hydrogen bonding, and by the charge of the metal. More precisely, being an electron acceptor, the metal binds to the molecules in the first shell; at the same time, the molecules directly coordinate to the metal to try to stabilize the charge. The molecules in the first shell cannot stabilise the double charge of the metal without interacting with molecules in the other solvation shells. The methanol molecules are orientated in the space to minimise steric hindrance and to reduce the total energy of the cluster as much as possible. The orientation of the molecules is influenced by the charge of the metal ion and

by the position they assume to form hydrogen bond networks. As the number of ligands increases, the overall number of hydrogen bonds increases until the charge on the metal does not affect anymore the bonding interactions. Twenty methanol molecules are not able to stabilize the double charge on Mg^{2+} , Ca^{2+} , and Sr^{2+} . Consequently, the bulk vaporization energy for the doubly charged metal solvent systems considered will be approached at $n > 20$.

The largest error bars in Tables 5.2.1 and 5.2.2 are at $n = 4, 5$ for all the clusters; remarkably, for $n = 4, 5$ the error bars are much larger than those for $6 \leq n \leq 20$. These results account for uncertainty in the instrumental measurements, because a weak fragment ion signal produces a MIKE scan with a poor Gaussian profile. As a result, the signal-to-noise ratio is low, and each performed MIKE scan for the same cluster provides laboratory frame FWHM of the daughter ion that largely differ from one another. Indeed, the pressure during all the experiments was $\sim 10^{-7}$ mbar, therefore the scans would reflect some characteristics of these clusters: the fragment ion signal is weak either because the number of small clusters that fragment is small or because of the presence of competing metastable decay channels; in fact, charge transfer and neutral loss would both be possible fragmentation reactions. Neutral loss was not observed for $[\text{Mg}(\text{CH}_3\text{OH})_n]^{2+}$ at $n = 3$, whereas was detected for $[\text{Ca}(\text{CH}_3\text{OH})_n]^{2+}$ and $[\text{Sr}(\text{CH}_3\text{OH})_n]^{2+}$ at $n = 3$, despite the goodness of fit to a Gaussian profile of the daughter ions at $n = 3$ was $R^2 < 0.4$ for the calcium clusters and $R^2 < 0.7$ for the strontium clusters. These experiments on complexes with $n = 3$ suggest that the dominant metastable dissociation process for $n \leq 3$ is not neutral loss. Nevertheless, if the R^2 values could account for the intensity signal of the corresponding ion, then it would be possible to suggest, by comparing the R^2 values at $n = 3$, that going from Ca^{2+} to Sr^{2+} the loss of one neutral methanol molecule becomes more prominent with respect to competing reactions. The observations obtained from metastable experiments of Mg^{2+} in association with methanol studies in [13, 14] complement and support this experimental work. As a matter of fact, the mass spectrometry measurements in [13] have provided the relative intensities of $[\text{Mg}(\text{CH}_3\text{OH})_n]^{2+}$ parent ion clusters for $2 \leq n \leq 40$ (plotted as a function of size cluster n). The study in [13] shows that (i) the cluster at $n = 1$ is not observed, (ii) the relative intensities for $n = 2, 3$ are much lower than those for $n = 4$, (iii) no magic numbers are observed for $1 \leq n \leq 40$, (iv) the first solvent shell is completed for $n = 5$ or $n = 6$, (v) the plateau region toward $n = 40$ would suggest a molecular arrangement that would approach bulk configuration, and (vi) neutral loss increases in relative intensity as n increases from 1 to 21. Furthermore, it has been found in [14] that the collisional activation of $[\text{Mg}(\text{CH}_3\text{OH})_n]^{2+}$ for $2 \leq n \leq 10$ has promoted electron capture induced decay

via charge reduction. More importantly,

- (i) charge separation via Coulomb explosion is the only metastable decay observable for $[\text{Mg}(\text{CH}_3\text{OH})_n]^{2+}$ at $n = 2, 3$; therefore, the metastable decay recorded by MIKE scan for $n = 2, 3$ in [14] was

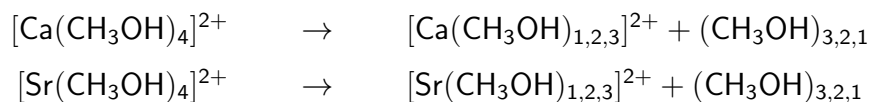


whereas

- (ii) at $n = 4, 5$ it was proved that clusters are stable with respect to charge separation.

Moreover, $[\text{Mg}(\text{CH}_3\text{OH})_n]^{2+}$ at $n = 1$ was also not observed in [14]. It is worthwhile to note that the results outlined from the work in [13, 14] have been performed with an experimental apparatus very similar to the one of this work. The comparison between [13, 14] and these experiments suggests that metastable neutral loss was not observed for $[\text{Mg}(\text{CH}_3\text{OH})_n]^{2+}$ with $n = 3$ because charge transfer occurred. For $[\text{Ca}(\text{CH}_3\text{OH})_n]^{2+}$ and $[\text{Sr}(\text{CH}_3\text{OH})_n]^{2+}$ neutral loss was observed at $n = 3$, but the goodness of the daughter ion to Gaussian profile was poor. It is possible to hypothesise that these cluster ions at $n = 3$ have similar reactivity and that charge transfer is the dominant dissociation path over the competing neutral loss. It is also possible to suggest that $[\text{Ca}(\text{CH}_3\text{OH})_n]^{2+}$ and $[\text{Sr}(\text{CH}_3\text{OH})_n]^{2+}$ for $n < 3$ may have a behaviour similar to $[\text{Mg}(\text{CH}_3\text{OH})_n]^{2+}$ clusters, and therefore fragmenting via charge separation.

In contrast, the analysis of the fragment ions recorded in the mass spectra of a collision induced dissociation (CID) experiment study [15] showed that the prominent dissociation products for Ca^{2+} and Sr^{2+} arise from neutral loss at $n = 4$, *viz.*



whereas the second most abundant fragments were due to proton transfer, owing to the presence of $[\text{CaCH}_3\text{O}]^+$, $[\text{SrCH}_3\text{O}]^+$, and CH_3OH_2^+ ions in the same mass spectrum.

The experimental measurements in [16] suggest that the minimum number of methanol molecules required to stabilize the dication complex in gas phase against metastable Coulomb fission is $n_s = 4$ for $[\text{Mg}(\text{CH}_3\text{OH})_n]^{2+}$ and $[\text{Ca}(\text{CH}_3\text{OH})_n]^{2+}$, and $n_s = 3$ for $[\text{Sr}(\text{CH}_3\text{OH})_n]^{2+}$; where $n_s = n_c + 1$ and n_c is

the critical size (the maximum value of n for which Coulomb fission is experimentally observable [17]).

To the best of our knowledge, there are no experimental studies reported in the literature which investigate the stepwise dissociation energy for metastable neutral ligand loss of Mg^{2+} , Ca^{2+} , and Sr^{2+} coordinated with methanol molecules.

5.3 A Note on Coordination Numbers

The coordination number (CN) for Mg^{2+} , Ca^{2+} , and Sr^{2+} has been investigated in several studies, as shown in Tables 5.3.1-5.3.3 below. The methods use in those studies are X-ray diffraction, Nuclear Magnetic Resonance (NMR), Extended X-ray Absorption Fine Structure (EXAFS), neutron diffraction, molecular dynamic (MD) simulations, *ab initio* Car-Parrinello Molecular Dynamics (CPMD), Monte-Carlo simulations (MCS), or Density Functional Theory (DFT).

	CN		
	[5]	[6]	[18]
Mg^{2+}	6	2, 3, 4, 5, 6, 7, 8	3, 4, 5, 6 , 7, 8
Ca^{2+}	6	3, 4, 5, 6, 7, 8, 9, 10	5, 6, 7, 8, 9, 10
Sr^{2+}	8	3, 4, 5, 6, 7, 8, 9, 10	

Table 5.3.1: Coordination numbers are from published inorganic chemistry books [5, 6]; literature search on Cambridge Structural Database (CSD) for crystal structures of purely inorganic materials [18]. In bold are the most frequent CN in [18]

CN	CN							
	This work	[13]	[19]	[20]	[21]	[22]	[24]	[25]
$[\text{Mg}(\text{CH}_3\text{OH})_n]^{2+}$	6	5, 6	6	6			5.7	6
$[\text{Ca}(\text{CH}_3\text{OH})_n]^{2+}$	6				6, 5	4, 5, 6		
$[\text{Sr}(\text{CH}_3\text{OH})_n]^{2+}$	6							

Table 5.3.2: Relative fragment ion intensity distribution for $2 \leq n \leq 20$ from mass spectroscopic measurements following unimolecular metastable loss of CH_3OH [13]; proton NMR of $[\text{Mg}(\text{ClO}_4)_2]$ in methanol solutions [19, 20, 24]; X-ray scattering and neutron diffraction of 1M and 2M solutions of CaCl_2 in methanol [21]; X-ray scattering of 1 – 6M solution of CaCl_2 in methanol [22]; kinetic solvation number by isotope dilution technique [25]. Values with explicit decimal digits indicate an average

The coordinative behaviour of the three metal ions varies depending on the method used to perform the investigation. In general, as shown in Table 5.3.1, the CN would depend solely on the size of the metal, magnesium would coordinate directly to a smaller number of molecules with respect to calcium and strontium, and calcium would coordinate directly to a smaller number of molecules

CN	CN					
	This work	[26]	[27]	[21] _a	[21] _b	[22]
$[\text{Mg}(\text{CH}_3\text{OH})_n]^{2+}$	6	6	6			
$[\text{Ca}(\text{CH}_3\text{OH})_n]^{2+}$	6	6	7	6.95	6.63	7
$[\text{Sr}(\text{CH}_3\text{OH})_n]^{2+}$	6					

Table 5.3.3: CPMD [26]; MCS of statistical perturbation theory [27]; MD, where the subscript a indicates 1M solution of CaCl_2 in methanol and the subscript b indicates 2M solution of CaCl_2 in methanol [21]; DFT / B3LYP [22]. Values with explicit decimal digits indicate an average

with respect to strontium. Indeed, Mg, Ca, and Sr show to have a preferred CN which is identified with the CN that a particular metal adopts most frequently, as shown in Table 5.3.1. Moreover, the analysis of Tables 5.3.2 and 5.3.3 suggests that a metal can acquire several coordination numbers; this effect depends on a number of factors such as the experimental conditions (sample concentration, presence of counter ion, temperature), instrumental apparatus, analysis methodology. For example, the CN in Table 5.3.2 are obtained in presence of a counter ion; therefore, the data reflect an average picture because

- (a) several geometric structures are present simultaneously the CN is individuated with more accuracy as the concentration of the solution increases,
- (b) that the CN decreases with an increase in concentration, and
- (c) the presence of the counter ion may affect the CN.

In these experiments, each of the metal ions adopts $\text{CN} = 6$ and is solvated in high vacuum conditions where collisions are absent and counter ions are not involved. These results show a CN that is independent by the size of the metal when we compare the radius of Mg^{2+} , Ca^{2+} , and Sr^{2+} . Moreover, it has been found that the metal affects the binding interaction at each cluster size for $3 \leq n \leq 20$. Intuitively, these results may be explained by the electronic charge transfer ability of Mg^{2+} and Ca^{2+} (as suggested in [26] by using Quantum Theory of Atoms in Molecules, QTAIM, by R. F. W. Bader) where the charge transfer from the methanol molecules in the second solvation shell to the first solvation shell is not sufficient to neutralise the doubly positive charge on the metal ion. The analysis in [26] also suggests that Ca^{2+} polarises the methanol molecules of the second solvation shell.

5.4 Related Theoretical Work

Theoretical data available from the literature is compared with these experimental data (*cf.* Section 4.5 on page 89)

Incremental bond energies of $[\text{Mg}(\text{CH}_3\text{OH})_n]^{2+}$ for $1 \leq n \leq 6$ computed by Density Functional Theory (DFT) [28] (*cf.* Table 5.4.1 below) show agreement with this experimental work in particular at $n = 4, 5$.

$[\text{Mg}(\text{CH}_3\text{OH})_n]^{2+} \rightarrow [\text{Mg}(\text{CH}_3\text{OH})_{n-1}]^{2+} + \text{CH}_3\text{OH}$			
n	E_b (kJ mol ⁻¹)	BE (kJ mol ⁻¹)	
	This work	[28] ^a	[28] ^b
		B3LYP	B3LYP
		6 – 31 + G*	6 – 31 + G*
1		396	403
2		327	341
3		242	258
4	199 ± 38	183	197
5	106 ± 31	106	118
6	73 ± 7.5	93.0	108

Table 5.4.1: Comparison between binding energies determined in these experiments for $[\text{Mg}(\text{CH}_3\text{OH})_n]^{2+}$ clusters ($4 \leq n \leq 6$) and those available from theoretical sources ($1 \leq n \leq 6$). Superscript a indicates enthalpy and superscript b indicates bond energy. Data of [28] are at 298.15 K

As shown in Table 5.4.2 below, there is also good agreement between the data in this work and [22] at $n = 5$. In [22] all the interactions energies were corrected for basis set superposition error (BSSE) by counterpoise (cp) method.

$[\text{Ca}(\text{CH}_3\text{OH})_n]^{2+} \rightarrow [\text{Ca}(\text{CH}_3\text{OH})_{n-1}]^{2+} + \text{CH}_3\text{OH}$			
n	E_b (kJ mol ⁻¹)	BE (kJ mol ⁻¹)	
	This work	[22] ^a	[22] ^b
		B3LYP	MP2
		6 – 311 + G**	6 – 311 + G**
1		284	257
2		232	221
3		196	198
4	200 ± 16	165	173
5	123 ± 8.9	123	118
6	87 ± 6.0	110	119
7	52 ± 6.9	29	

Table 5.4.2: Comparison between binding energies determined in these experiments for $[\text{Ca}(\text{CH}_3\text{OH})_n]^{2+}$ clusters ($4 \leq n \leq 7$) and those available from theoretical sources. The superscript a indicates DFT and b indicates *ab initio* calculations

The bond between the central metal and the ligands of the first solvation shell may imply also covalent interaction [23, 29]. In fact, the doubly charged alkaline earth metals have in their outer shell the s and p orbitals empty. Therefore, it would be also possible to consider Mg(II), Ca(II), and Sr(II) as Lewis [30] acids and methanol as Lewis base. The CPMD simulations in [26] have shown

that $[\text{Mg}(\text{CH}_3\text{OH})_n]^{2+}$ and $[\text{Ca}(\text{CH}_3\text{OH})_n]^{2+}$ for $1 \leq n \leq 40$ have no hydrogen bonding between the molecules directly bound to the metal ion.

5.5 Solvation of Monovalent Mg, Ca, and Sr ions in Methanol

Stepwise binding energy for neutral ligand loss reported in the literature are obtained with Threshold Collision Induced Dissociation (TCID) and *ab initio* calculations (bond energies were corrected for zero-point energies, ZPE, and basis set superposition error – BSSE – were subtracted in the full counterpoise approximation) for $[\text{Mg}(\text{CH}_3\text{OH})_n]^+$ with $1 \leq n \leq 3$ in [31]. In addition, ground state geometries with *ab initio* method were calculated: stable structures were fully optimized for $[\text{Mg}(\text{CH}_3\text{OH})_6]^+$ and for $[\text{Ca}(\text{CH}_3\text{OH})_6]^+$ in [32] (owing to the balance between solvent-metal interactions and solvent-solvent repulsion between the methyl group in methanol), and for $[\text{Mg}(\text{CH}_3\text{OH})_n]^+$ for $1 \leq n \leq 3$ in [31], for $1 \leq n \leq 5$ (unrestricted Hartree-Fock self-consistent field, UHF-SCF, method and 6-31G* basis set) in [33], and for $n = 6$ (B3LYP/6-311+G**) in [32]. Moreover, laser ablation beam method on $[\text{Mg}(\text{CH}_3\text{OH})_n]^+$ clusters have proposed that the first coordination shell is completed with two methanol ligands [34]; a similar result in [33] shows that the first coordination shell is completed with three methanol ligands. Furthermore, the reaction paths of $[\text{Mg}(\text{CH}_3\text{OH})_n]^+$ has been studied with various experimental techniques [13, 31, 33, 35].

It is not possible to provide a comprehensive comparison between the binding energy for the coordination of Mg^+ , Ca^+ , and Sr^+ and of Mg^{2+} , Ca^{2+} , and Sr^{2+} in methanol molecules. However, the bond energies provided in [33] for $[\text{Mg}(\text{CH}_3\text{OH})_n]^+$ for $1 \leq n \leq 5$ are given in Table 5.5.1.

The binding energy of $[\text{Mg}(\text{CH}_3\text{OH})_n]^+$ is higher than the binding energy of $[\text{Mg}(\text{CH}_3\text{OH})_n]^{2+}$ for $3 \leq n \leq 5$, therefore the consideration that can be drawn from the comparison is that the doubly positive charge affects the binding interactions.

n	$[\text{Mg}(\text{CH}_3\text{OH})_n]^{2+}$	$[\text{Mg}(\text{CH}_3\text{OH})_n]^+$		
	E_b (kJ mol ⁻¹) This work	BE (kJ mol ⁻¹) [31]	TCID experiment	MP2(full)/6-311G(2d,2p) MP2(full)/6-31G*
1		UHF-SCF 6-31G*	145	141
2		158	120	109
3		122	121	86
4	199 ± 38	91		
5	106 ± 31	72.9		
		56.7		

Table 5.5.1: Comparison between binding energies determined in these experiments for the cluster ions $[\text{Mg}(\text{CH}_3\text{OH})_n]^{2+} \rightarrow [\text{Mg}(\text{CH}_3\text{OH})_{n-1}]^{2+} + \text{CH}_3\text{OH}$ ($4 \leq n \leq 5$) and those available from the literature for $[\text{Mg}(\text{CH}_3\text{OH})_n]^+ \rightarrow [\text{Mg}(\text{CH}_3\text{OH})_{n-1}]^+ + \text{CH}_3\text{OH}$ ($1 \leq n \leq 5$). Data in [31] is at 0 K

Bibliography

- [1] A.J. Stace, C. Moore, *Journal of the American Chemical Society* 105 (1983) 1814.
- [2] C. Lifshitz, F.A. Long, *Journal of Chemical Physics* 41 (1964) 2468.
- [3] J.R. Gilbert, A.J. Stace, *International Journal of Mass Spectrometry and Ion Physics* 15 (1974) 311.
- [4] A.J. Stace, A.K. Shukla, *Journal of the American Chemical Society* 104 (1982) 5314.
- [5] C.E. Housecroft, A.G. Sharpe, *Inorganic Chemistry*, Pearson Education Limited 1st. edn., 2001, ch.11, 233-246.
- [6] F.A. Cotton, G.W. Wilkinson, C.A. Murillo, M. Bochmann, *Advanced Inorganic Chemistry*, John Wiley & Sons, Inc., London 6th edn., 1999, ch.2, 111-130.
- [7] K.N. Marsh Ed., *Recommended Reference Materials For The Realisation Of Physicochemical Properties*, Blackwell, Oxford, 1987, pp. 3-113.
- [8] P.W. Atkins, *Physical Chemistry*, Oxford University Press, 6th edn., 1999, pp.921.
- [9] D.R. Lide, *Handbook Of Chemistry And Physics*, CRC Press, 85th edn., 2004-2005, ch.6, 112-113.
- [10] I. Wadsö, *Acta Chemica Scandinavica* 20 (1966) 544.
- [11] H.S. Frank, M.W. Evans, *Journal of Chemical Physics* 13 (1945) 507.
- [12] H.S. Frank, W.-Y. Wen, *Discussions of the Faraday Society* 24 (1957) 133.
- [13] C.A. Woodward, M.P. Dobson, A.J. Stace, *Journal of Physical Chemistry A* 101 (1997) 2279.

- [14] B. Wu, B.J. Duncombe, A.J. Stace, *Journal of Physical Chemistry A* 112 (2008) 2182.
- [15] M. Kohler, J.A. Leary, *Journal of the American Chemical Society for Mass Spectrometry* 8 (1997) 1124.
- [16] X.J. Chen, A.J. Stace, *Journal of Physical Chemistry A* 117 (2013) 5015.
- [17] X. Chen, A.J. Stace, *Chemical Communications* 48 (2012) 10292.
- [18] O. Carugo, K. Djinović, M. Rizzi, *Journal of the Chemical Society, Dalton Transaction* (1993) 2127.
- [19] S. Nakamura, S. Meiboom, *Journal of the American Chemical Society* 89 (1967) 1765.
- [20] N.A. Matwiyoff, H. Taube, *Journal of the American Chemical Society* 90 (1968) 2796.
- [21] T. Megyes, S. Bálint, L. Bakó, T. Grósz, T. Radnai, G. Pálinkás, *Chemical Physics* 327 (2006) 415.
- [22] T. Megyes, T. Grósz, T. Radnai, L. Bakó, G. Pálinkás, *Journal of Physical Chemistry A* 108 (2004) 7261.
- [23] N. Walker, M.P. Dobson, R.R. Wright, P.E. Barran, J.N. Murrell, A.J. Stace, *Journal of the American Chemical Society* 122 (2000) 11138.
- [24] J.H. Swinehart, H. Taube, *Journal of Chemical Physics* 37 (1962) 1579.
- [25] J.H. Swinehart, T.E. Rogers, H. Taube, *Journal of Chemical Physics* 38 (1963) 398.
- [26] C. Faralli, M. Pagliai, G. Cardini, V. Schettino, *Journal of Chemical Theory and Computation* 4 (2008) 156.
- [27] H.-S. Kim, *Journal of Molecular Structure (Theochem)* 541 (2001) 59.
- [28] T. Dudev, C. Lim, *Journal of Physical Chemistry A* 103 (1999) 8093.
- [29] J.E. Huheey, E.A. Keiter, R.L. Keiter, *Inorganic Chemistry principle of Structure and Reactivity*, Harper Collins College Publishers, 4th edn., 1993, 129-134.
- [30] J.E. Huheey, E.A. Keiter, R.L. Keiter, *Inorganic Chemistry principle of Structure and Reactivity*, Harper Collins College Publishers, 4th edn., 1993, 324-325.

- [31] A. Andersen, F. Muntean, D. Walter, C. Due, P.B. Armentrout, *Journal of Physical Chemistry A* 104 (2000) 692.
- [32] K.W. Chan, Y. Wu, Z.-F. Liu, *Canadian Journal of Chemistry* 85 (2007) 873.
- [33] W. Lu, S. Yang, *Journal of Physical Chemistry A* 102 (1998) 825.
- [34] T. Kaya, Y. Horiki, M. Kobayashi, H. Shinohara, H. Sato, *Chemical Physics Letters* 200 (1992) 435.
- [35] M.R. France, S.H. Pullins, M.A. Duncan, *Chemical Physics* 239 (1998) 447.

Chapter 6

Binding Energy of $[\text{Mg}(\text{NH}_3)_n]^{2+}$, $[\text{Ca}(\text{NH}_3)_n]^{2+}$, and $[\text{Sr}(\text{NH}_3)_n]^{2+}$

In this chapter we discuss the experimental results of unimolecular (metastable) decay (neutral loss, in these experiments) of a single ammonia molecule from $[\text{Mg}(\text{NH}_3)_n]^{2+}$, $[\text{Ca}(\text{NH}_3)_n]^{2+}$, and $[\text{Sr}(\text{NH}_3)_n]^{2+}$ cluster ions for $4 \leq n \leq 20$.

6.1 Experimental Details

Artefact peaks were not detected in any of the recorded MIKE scans. The values, say w , of laboratory frame FWHM peak width of the precursor ions were

- $1.4 \text{ eV} < w < 2.4 \text{ eV}$ for $[\text{Mg}(\text{NH}_3)_n]^{2+}$,
- $1.6 \text{ eV} < w < 2.0 \text{ eV}$ for $[\text{Ca}(\text{NH}_3)_n]^{2+}$, and
- $1.7 \text{ eV} < w < 2.1 \text{ eV}$ for $[\text{Sr}(\text{NH}_3)_n]^{2+}$.

The goodness of fit to a Gaussian profile for all the precursor ions and the fragment ions was $R^2 > 0.9$ for all the measurements. The respective MIKE scans for the precursor ion of $[\text{Mg}(\text{NH}_3)_4]^{2+}$ and $[\text{Sr}(\text{NH}_3)_3]^{2+}$ were observed, but their respective daughter ions were not observed for the neutral loss process under examination. The MIKE scans for the precursor ions of $[\text{Ca}(\text{NH}_3)_3]^{2+}$ were observed, but they were not considered in the analysis because it was $R^2 < 0.4$ for the daughter ions.

We refer the reader to Chapter 9 for the experimental values of w and R^2 and to Chapter 10 for more details on the experimental settings. A minimum of four measurements were used to determine the kinetic energy release for the metastable neutral loss for each cluster size.

Figure 6.1.1 shows examples of MIKE scan profiles for a precursor ion and respective daughter ion for $[\text{Mg}(\text{NH}_3)_n]^{2+}$, $[\text{Ca}(\text{NH}_3)_n]^{2+}$, and $[\text{Sr}(\text{NH}_3)_n]^{2+}$ clusters.

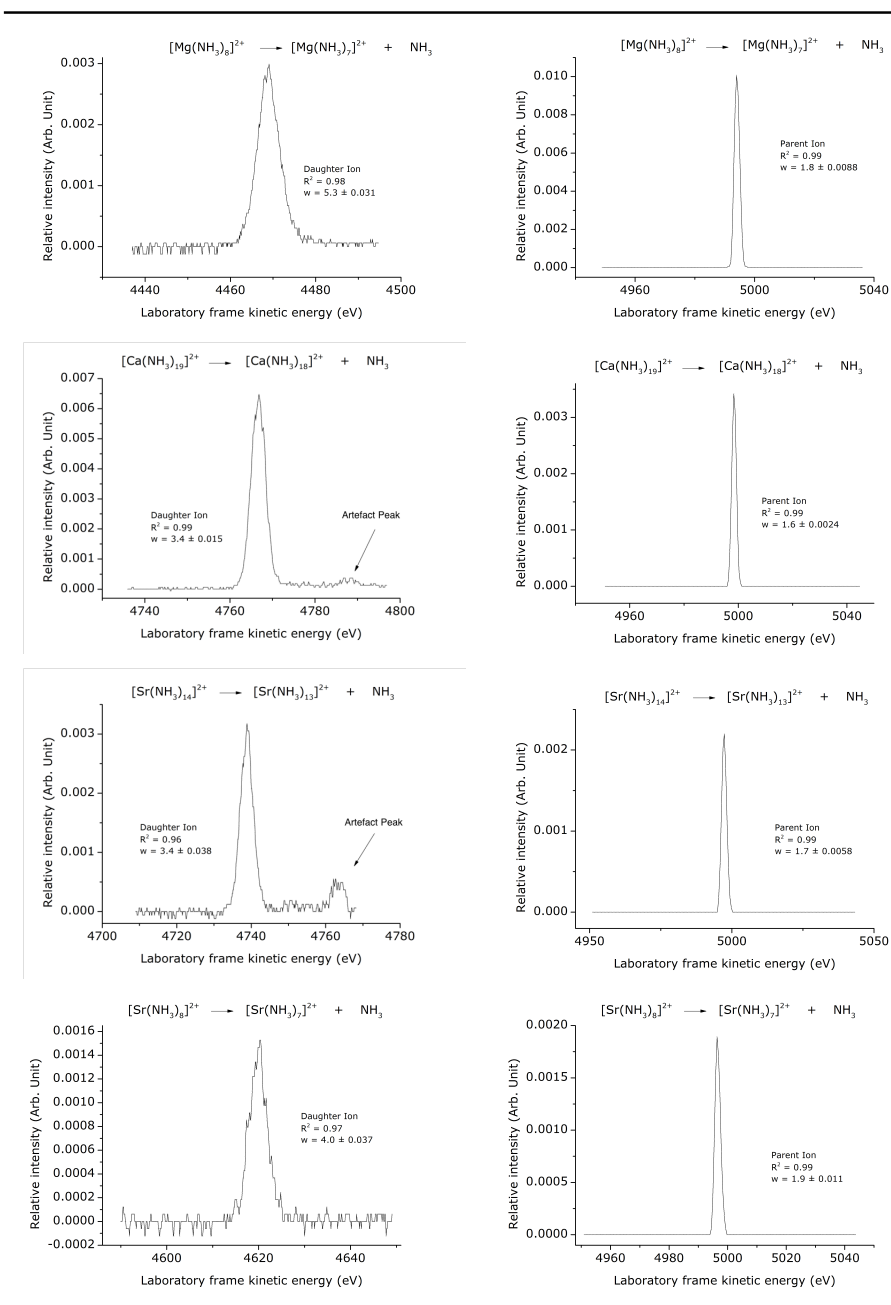


Figure 6.1.1: Examples of MIKE scans for $[\text{Mg}(\text{NH}_3)_n]^{2+}$, $[\text{Ca}(\text{NH}_3)_n]^{2+}$, and $[\text{Sr}(\text{NH}_3)_n]^{2+}$: daughter ions – in the left column of the first two rows – with $R^2 = 0.98, 0.99, 0.96, 0.97$; the respective parent ions (right column) have $R^2 = 0.99$ and $w = 1.8 \text{ eV}, 1.6 \text{ eV}, 1.7 \text{ eV}, 1.9 \text{ eV}$. As shown in the plots, the artefact peaks did not interfere with the acquisition of the data

6.2 Binding Energies from Metastable KER Measurements

The studies of the neutral loss of a single ammonia molecule of the clusters ions $[\text{Mg}(\text{NH}_3)_n]^{2+}$, $[\text{Ca}(\text{NH}_3)_n]^{2+}$, and $[\text{Sr}(\text{NH}_3)_n]^{2+}$ for $3 \leq n \leq 20$ are discussed. The kinetic energy release from unimolecular (metastable) decay experiments of the cluster ions as a function of cluster size are reported in Table 6.2.1. They are experimental measurements of the average kinetic energy release, $\langle \varepsilon_T \rangle$, associated with the unimolecular (metastable) decay of cluster ions. Each value is the average of at least four different measurements and the error, $\pm \Delta \langle \varepsilon_T \rangle$, reflects the spread in uncertainty in the measurements.

n	$[\text{Mg}(\text{NH}_3)_n]^{2+}$		$[\text{Ca}(\text{NH}_3)_n]^{2+}$		$[\text{Sr}(\text{NH}_3)_n]^{2+}$	
	$\langle \varepsilon_T \rangle$ (meV)	$\pm \Delta \langle \varepsilon_T \rangle$ (meV)	$\langle \varepsilon_T \rangle$ (meV)	$\pm \Delta \langle \varepsilon_T \rangle$ (meV)	$\langle \varepsilon_T \rangle$ (meV)	$\pm \Delta \langle \varepsilon_T \rangle$ (meV)
4			51	2.8	59	8.9
5	23	3.9	46	2.1	49	6.7
6	19	2.2	33	3.4	37	1.5
7	20	0.89	22	1.1	23	1.8
8	21	6.0	20	2.6	16	2.7
9	19	1.2	20	1.5	17	2.2
10	19	0.61	19	0.70	19	5.3
11	19	1.4	18	0.46	19	1.0
12	17	1.1	18	0.28	17	0.54
13	16	0.49	17	1.5	15	2.6
14	15	1.9	17	1.4	14	2.5
15	13	8.7	15	1.9	13	2.3
16	14	0.60	15	1.4	15	2.1
17	14	3.6	15	1.9	13	0.15
18	13	2.5	13	0.46	13	0.73
19	11	2.3	14	1.1	11	0.72
20	13	2.9	14	0.68	13	1.5

Table 6.2.1: Experimental measurements of the average kinetic energy release, $\langle \varepsilon_T \rangle$, associated with the unimolecular (metastable) decay of cluster ions. Each value is the average of separates measurements and the error, $\pm \Delta \langle \varepsilon_T \rangle$, reflects the spread in uncertainty in the measurements

The binding energy of each of the ions as a function of cluster size is given in Table 6.2.2. The data obtained in these experiments were truncated after the second significant digit only once all the calculations had been processed. In addition, a plot of the binding energies as a function of n , the number of ammonia molecules in each cluster, is shown in Figure 6.2.1.

n	$[\text{Mg}(\text{NH}_3)_n]^{2+}$		$[\text{Ca}(\text{NH}_3)_n]^{2+}$		$[\text{Sr}(\text{NH}_3)_n]^{2+}$		$\text{H}^+(\text{NH}_3)_n$
	E_b (kJ mol ⁻¹)	$\pm\Delta E_b$ (kJ mol ⁻¹)	E_b (kJ mol ⁻¹)	$\pm\Delta E_b$ (kJ mol ⁻¹)	E_b (kJ mol ⁻¹)	$\pm\Delta E_b$ (kJ mol ⁻¹)	$E_b \pm \Delta E_b$ (kJ mol ⁻¹)
4			169	9.4	193	29	85 ± 14
5	62	10	122	5.7	129	17	52 ± 3.7
6	45	5.2	77	7.9	86	3.6	29 ± 1.5
7	43	1.9	48	2.3	50	3.9	20 ± 1.4
8	44	12	41	5.4	34	5.5	19 ± 1.4
9	38	2.4	39	2.9	34	4.4	18 ± 1.9
10	37	1.1	36	1.3	36	10	17 ± 0.35
11	36	2.6	35	0.86	36	1.9	17 ± 0.85
12	32	2.0	33	0.51	31	0.98	17 ± 1.0
13	28	0.88	31	2.8	28	4.7	17 ± 0.67
14	27	3.3	30	2.5	26	4.5	16 ± 0.43
15	23	15	27	3.3	24	4.0	16 ± 0.32
16	24	1.0	27	2.5	26	3.6	16 ± 0.97
17	24	6.1	26	3.4	23	0.25	16 ± 0.73
18	22	4.3	23	0.79	23	1.2	16 ± 0.96
19	19	4.0	23	1.9	19	1.2	17 ± 0.19
20	22	5.0	23	1.1	21	2.5	17 ± 0.76

Table 6.2.2: Binding energies determined from the kinetic energy release data presented in Table 6.2.1. The binding energy of $\text{H}^+(\text{NH}_3)_n$ is added for comparison

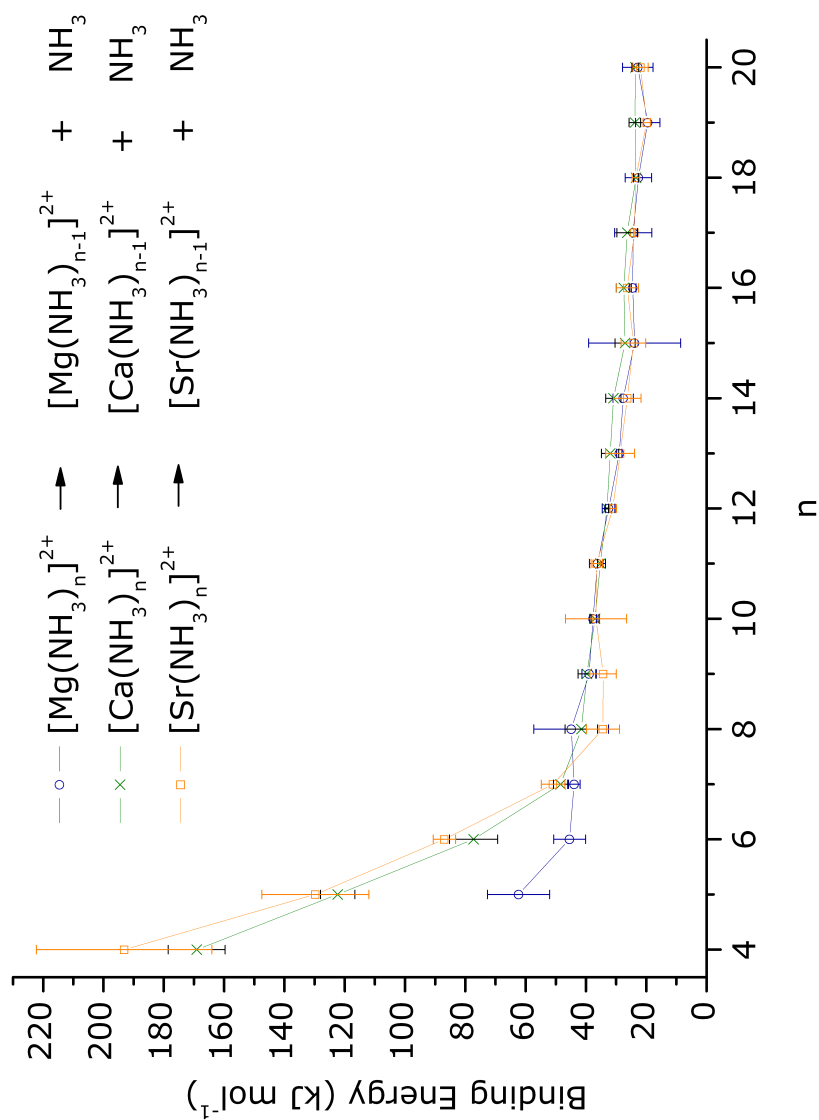


Figure 6.2.1: Plot of binding energies extracted from kinetic energy release measurements on $[\text{Mg}(\text{NH}_3)_n]^{2+}$, $[\text{Ca}(\text{NH}_3)_n]^{2+}$, $[\text{Sr}(\text{NH}_3)_n]^{2+}$ cluster ions. Binding energies are given in kJ mol^{-1} and are plotted as a function of n , the number of ammonia molecules in each cluster

Figure 6.2.1 shows the three sets of binding energies versus cluster size; the steady decrease stops at a value of n that suggests the completion of the first solvent shell, any other ammonia molecule added will bind to the first solvation shell. Moreover, the number of ammonia molecules completing the first solvation shell coincides with the coordination number (CN) for a metal dication in these experiments. Therefore, these non-equilibrium gas phase experiments suggest that

- a) the three alkaline earth metals differ in the coordination number in forming a complex in the gas phase under pressure condition of 10^{-7} mbar; the number of ammonia ligands coordinated directly to Mg^{2+} is four, whereas the number of ammonia molecules coordinated directly to Ca^{2+} and Sr^{2+} ions is six;
- b) any other ammonia molecule added to $[\text{Mg}(\text{NH}_3)_4]^{2+}$, to $[\text{Ca}(\text{NH}_3)_6]^{2+}$, or to $[\text{Sr}(\text{NH}_3)_6]^{2+}$ binds through hydrogen bonding to another ammonia molecule (instead of binding to the metal);
- c) the double positive charge of the metal has an effect on the energetics of the cluster bond interactions for each n in the series up to $n = 20$;
- d) The recorded MIKE scan of a unimolecular (metastable) dissociation is not necessarily of the most stable isomer in these experiments (*cf.* Section 5.2 on page 105);
- e) the weakest bond is broken in these experiments, which is one hydrogen bond between the most weakly bound molecule in the outer solvation shell and the metastable cluster ion;
- f) these results have shown that no magic numbers are observed (*cf.* Section 4.4 on page 83).

A justification for $[\text{Mg}(\text{NH}_3)_n]^{2+}$ completing the first solvation shell at $n = 4$ can be provided as follows: the experimental MIKE analysis did not detect the loss of one ammonia molecule from the metastable $[\text{Mg}(\text{NH}_3)_4]^{2+}$ in these experiments. As shown in Table 6.2.2 and Figure 6.2.1, there is a clear difference between the values of binding energies determined for $[\text{Ca}(\text{NH}_3)_n]^{2+}$ and $[\text{Sr}(\text{NH}_3)_n]^{2+}$ complexes for $4 \leq n \leq 6$, and the corresponding values determined for $[\text{Mg}(\text{NH}_3)_n]^{2+}$. This difference can find an explanation from the work in [1, 2] on alkaline earth metal dication complexes with water, $[\text{M}(\text{H}_2\text{O})_n]^{2+}$ where M is Mg, Ca, Sr, and Ba with $n = 6$. The blackbody infrared radiation dissociation (BIRD) experiments in [1, 2] identified a pattern of behaviour that

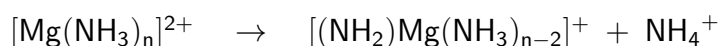
equated with the formation of a structure where one water in the magnesium complex occupies a site in a secondary solvation shell instead of a primary one. In [1, 2] it is argued that the structure of the magnesium complex evolves from $[\text{Mg}(\text{H}_2\text{O})_6]^{2+}$ where each water molecule binds to the central metal dication, to a structure of the form $[\text{Mg}(\text{H}_2\text{O})_5(\text{H}_2\text{O})]^{2+}$ in which a water molecule held in the second solvation shell is hydrogen bonded to molecules in the first shell. The promotion of the water molecule was observed in [1, 2] at temperatures > 350 K in conjunction with a drop in the binding energy. In the experiments of this work, the temperatures of the complexes are unknown, but with high probability they are higher than those used in the BIRD experiments. Indeed, (i) the only effective mechanism causing energy loss is molecular evaporation and (ii) only unimolecular (metastable) decay is observed in these experiments (*cf.* Section 3.5 on page 59). Moreover, Table 6.2.2 reports results following decay of complexes at $n = 4$, which in [1, 2] could only achieve using collisional activation. It can be therefore hypothesised that for $[\text{Mg}(\text{NH}_3)_n]^{2+}$ may start to form a secondary solvation shell before the primary shell is completed under certain conditions.

The type of experiment being undertaken is selective; many different geometries of the same cluster ion may be present in the ion signal. Nevertheless, their different contribution to unimolecular (metastable) decay is ruled by a competitive shift [3, 4, 5, 6] (*cf.* Section 4.3 on page 77 and Section 5.2 on page 105). In this way, metastable decay processes in the field-free regions are dominated by the fragmentation route with the lowest activation energy. Therefore, the measured binding energy corresponds to the fragmentation of the most weakly bound molecule. The error bars in Figure 6.2.1 are an indication of the precision of the measurements. The largest error bars are

- at $n = 5, 8, 15$ for $[\text{Mg}(\text{NH}_3)_n]^{2+}$,
- at $n = 4, 5, 6$ for $[\text{Ca}(\text{NH}_3)_n]^{2+}$, and
- at $n = 4, 5, 10$ for $[\text{Sr}(\text{NH}_3)_n]^{2+}$;

Remarkably, all the clusters have high error bars for all n of the inner shell. In particular, this uncertainty would account for the MIKE scans of a daughter ion (*cf.* Section 3.3 on page 56) with poor Gaussian profile. The uncertainty may be due to either instrumental measurements errors, or to weak signal of the daughter ion, or else to the presence of competing metastable decay channels, which causes a low signal of the daughter ion produced by neutral loss. For example, charge transfer and neutral loss would be both possible metastable fragmentation reactions. The experimental results of this work did not detect fragments

from neutral loss of $[\text{Mg}(\text{NH}_3)_4]^{2+}$ and $[\text{Sr}(\text{NH}_3)_3]^{2+}$, whereas the MIKE scan for $[\text{Ca}(\text{NH}_3)_3]^{2+}$ neutral loss provided daughter ion with poor Gaussian profile having $R^2 < 0.4$. Therefore, it can be argued that $[\text{Mg}(\text{NH}_3)_n]^{2+}$ with $n \leq 4$ and $[\text{Sr}(\text{NH}_3)_n]^{2+}$ with $n \leq 3$ preferably fragment by choosing a metastable route which is not neutral loss, besides $[\text{Ca}(\text{NH}_3)_n]^{2+}$ with $n \leq 3$ shows the competition between Coulomb fission and neutral loss. A study of the intensity distribution for $[\text{Mg}(\text{NH}_3)_n]^{2+}$ [12] derived $n = 4$ as the number for maximum intensity and $n = 3$ as the minimum number of ligand required to stabilise Mg^{2+} ; whereas the investigation of the relative abundance of the productions $[\text{Mg}(\text{NH}_3)_n]^{2+}$ in the photoionisation of neutral $\text{Mg}(\text{NH}_3)_n$ by femtosecond laser [13] yielded $n = 2$ as the minimum number of ammonia molecules to stabilise Mg^{2+} . The fragmentation pathway suggested for the smaller clusters of $[\text{Mg}(\text{NH}_3)_n]^{2+}$ for $n \leq 4$ was proton transfer, which was experimentally observed in [14]:



In addition, neutral loss (metastable) was not observed for $[\text{Mg}(\text{NH}_3)_n]^{2+}$ for $n \leq 4$. The fact that charge separation is the preferred route to fragmentation for $[\text{Mg}(\text{NH}_3)_n]^{2+}$ with $n \leq 4$ clusters may be due to an insufficient number of solvent molecules present in the complex to stabilize the doubly charged unit. The experimental investigations in [15] have indicated that $n = 5$ for $[\text{Mg}(\text{NH}_3)_n]^{2+}$ and $n = 4$ for both $[\text{Ca}(\text{NH}_3)_n]^{2+}$ and $[\text{Sr}(\text{NH}_3)_n]^{2+}$ as the minimum number of ammonia molecules necessary to stabilize the dication complex against metastable Coulomb fission.

It would be possible to suggest that $[\text{Ca}(\text{NH}_3)_n]^{2+}$ with $n \leq 3$ and $[\text{Sr}(\text{NH}_3)_n]^{2+}$ with $n \leq 3$ dissociate preferably via metastable charge transfer rather than via neutral loss, owing to an insufficient number of ligands which cannot stabilize the double charge.

The binding energy of the three metal complexes shown in Table 6.2.2 and in Figure 6.2.1 reveals that both the size and the charge of the metal affect the bonding interactions between the metal and the ligands at $n \leq 4$ for $[\text{Mg}(\text{NH}_3)_n]^{2+}$ and at $n \leq 6$ for $[\text{Ca}(\text{NH}_3)_n]^{2+}$ as well as for $[\text{Sr}(\text{NH}_3)_n]^{2+}$; in contrast, for $[\text{Mg}(\text{NH}_3)_n]^{2+}$ at $n \geq 5$ and for both $[\text{Ca}(\text{NH}_3)_n]^{2+}$ and $[\text{Sr}(\text{NH}_3)_n]^{2+}$ at $n \geq 7$, it is the charge to mostly have an effect on the strength of the bonds. According to these experimental results, it follows that the charge of the metal affects the binding interaction at each cluster size investigated, therefore, even in the complexes where the second solvation shell is firmly established. As it can be seen in Table 6.2.2 and in Figure 6.2.2 the binding energy of $[\text{Mg}(\text{NH}_3)_n]^{2+}$, $[\text{Ca}(\text{NH}_3)_n]^{2+}$, and $[\text{Sr}(\text{NH}_3)_n]^{2+}$ as a function of the number n of ammonia mol-

ecules in each cluster, differs consistently for each n when compared with the corresponding binding energy of $\text{H}^+(\text{NH}_3)_n$; more precisely, the binding energy of the alkaline earth metals in association with ammonia molecules is higher than the protonated ammonia molecular clusters at each n . This confirms that the charge affects the binding energy by increasing the strength of the bond, and that twenty ammonia molecules are not a sufficient number to stabilise the double charge on the metals under investigation. Consequently, the binding energy for these double charged clusters would equal the bulk vaporisation energy of ammonia for $n > 20$. The trend of the binding energies is not exactly what it would be expected from an analysis of the charge density of the three metal ions (*cf.* Table 5.2.3 and [7, 8]); since by going down the second group elements of the periodic table the double charge is distributed over an increasing surface area. In fact, the binding energies of $[\text{Sr}(\text{NH}_3)_n]^{2+}$ are higher than those of $[\text{Ca}(\text{NH}_3)_n]^{2+}$ for $4 \leq n \leq 7$, namely when the first coordination shell is not filled and until the first molecule is added in the second coordination shell. Moreover, the binding energies of $[\text{Mg}(\text{NH}_3)_n]^{2+}$ are lower than those of $[\text{Ca}(\text{NH}_3)_n]^{2+}$ at $4 \leq n \leq 7$, owing to Mg^{2+} having the first coordination shell filled at $n = 4$. Furthermore, it can be seen that $[\text{Mg}(\text{NH}_3)_n]^{2+}$ and $[\text{Ca}(\text{NH}_3)_n]^{2+}$ alternate in having the highest binding energy values for $8 \leq n \leq 11$, until $[\text{Ca}(\text{NH}_3)_n]^{2+}$ from $n \geq 11$ has the highest binding energy values with respect to $[\text{Mg}(\text{NH}_3)_n]^{2+}$ and $[\text{Sr}(\text{NH}_3)_n]^{2+}$, whereas the binding energy of $[\text{Mg}(\text{NH}_3)_n]^{2+}$ and $[\text{Sr}(\text{NH}_3)_n]^{2+}$ are similar but for small fluctuations in their values.

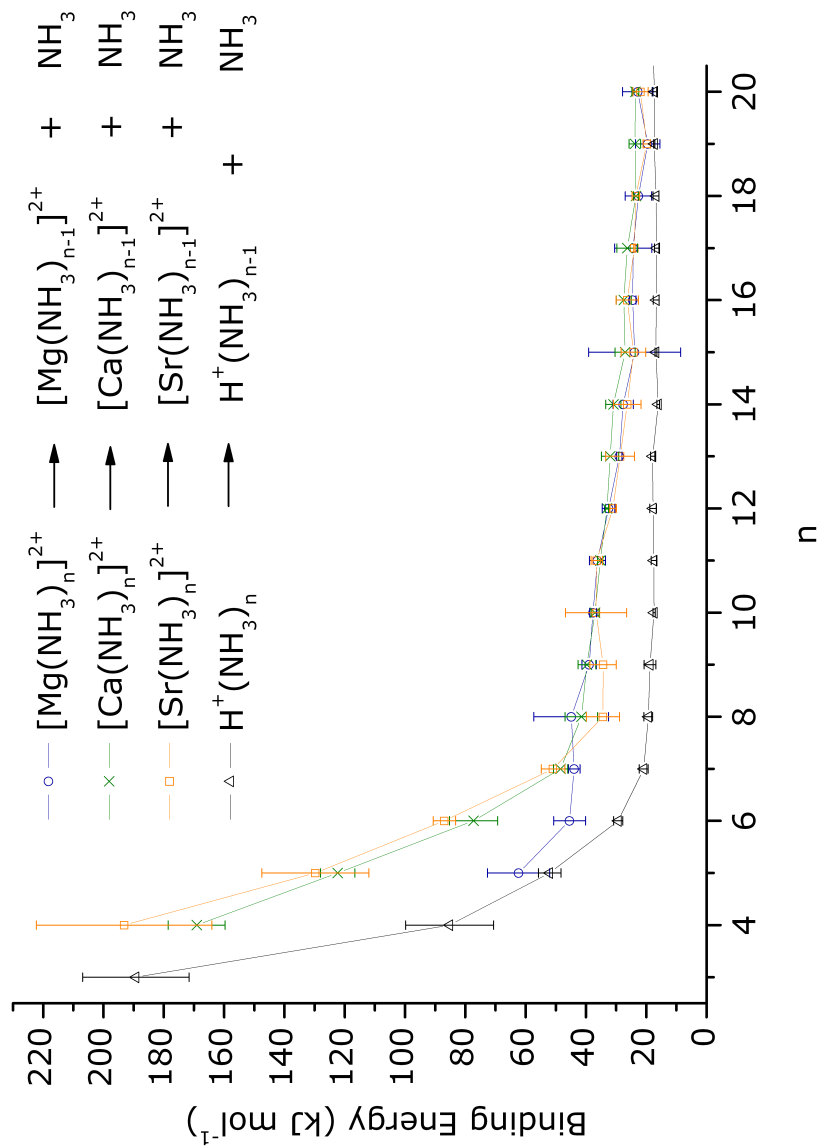


Figure 6.2.2: Binding energies (kJ mol⁻¹) extracted from kinetic energy release measurements on $[\text{Mg}(\text{NH}_3)_n]^{2+}$, $[\text{Ca}(\text{NH}_3)_n]^{2+}$, $[\text{Sr}(\text{NH}_3)_n]^{2+}$, which are compared with $\text{H}^+(\text{NH}_3)_n$ as a function of n , the number of ammonia molecules in each cluster

These experiments cannot give any information about the geometrical structure with the corresponding symmetry adopted neither by the inner shell nor by the entire cluster at a particular value of n . The experimental studies for $\text{H}^+(\text{NH}_3)_n$ at each $3 \leq n \leq 30$ show a value of the binding energy due to breaking one hydrogen bond during (metastable) neutral loss (*cf.* Section 4.3 on page 77). When compared with the corresponding binding energy of the protonated ammonia clusters, the binding energy of the alkaline earth metals in association with ammonia molecules is higher for each n , but they are not high enough to justify that two hydrogen bonds are involved in the dissociation. In fact, the vaporization enthalpy for the ammonia condensed phase equilibrium is 23 kJ mol^{-1} [9, 10, 11], which implies the breaking of two hydrogen bonds. Since the charge is affecting the binding interactions, and by the considerations in Section 4.3 (page 77), the route to dissociate one molecule from the $[\text{Mg}(\text{NH}_3)_n]^{2+}$, $[\text{Ca}(\text{NH}_3)_n]^{2+}$, and $[\text{Sr}(\text{NH}_3)_n]^{2+}$ clusters is via breaking one hydrogen bond in these experiments.

According to this model (*cf.* Section 5.3), these experiments describe a doubly charged metal surrounded by a first shell completed with four or six ammonia molecules, where a second shell begins to form with the fifth or seventh ammonia molecule respectively for Mg^{2+} , Ca^{2+} , and Sr^{2+} .

6.3 A Note on Coordination Numbers

The coordination numbers available from the literature for Mg^{2+} , Ca^{2+} , and Sr^{2+} are listed in Tables 6.3.1-6.3.3 below. The general result in Table 6.3.1 is that the coordination number ranges from two to eight for divalent magnesium, and from three to ten for both divalent calcium and strontium. It is worth noting that the analyses in [16, 17, 18] are based on the analysis of the available data on crystal structures from the Cambridge Structural Database (CSD) and Protein Databank (PDB). These studies have searched in CSD and PDB databases for crystal structures containing divalent magnesium, calcium, and strontium ions; the investigations were limited to the metal ion bound to oxygen, nitrogen, chlorine, bromine, and sulphur elements. The numbers of crystal structures found in the databases have revealed that Mg^{2+} prefers six ligands bound directly to the central metal ion, whereas Ca^{2+} favours either six, seven, or eight ligands bound directly to the central metal ion; while Sr^{2+} favours eight ligands bound directly to the central metal ion. Furthermore, the investigation in [17, 18] shows that Mg^{2+} and Ca^{2+} prefer ligands that are oxygen donors rather than either nitrogen or sulphur donors. Consequently, the analysis of Table 6.3.1 suggests that magnesium would form a stronger bond and would coordinate to a smaller number

	CN					
	[17]	[18] _(a)	[18] _(b)	[16]	[7]	[8]
Mg ²⁺	3, 4, 5, 6 , 7			4, 6 , (6)	6	2, 3, 4, 5, 6, 7, 8
Ca ²⁺	3, 4, 6 , 7, 8, 9, 10	3, 4, 5, 6 , 7, 8, 9, 10	3, 4, 6, 7, 8, 9	6 , 7, (7)	6	3, 4, 5, 6, 7, 8, 9, 10
Sr ²⁺				6, 8	8	3, 4, 5, 6, 7, 8, 9, 10

Table 6.3.1: Comparison between coordination numbers for Mg²⁺, Ca²⁺, and Sr²⁺ mono-atomic ions available from literature. [7, 8] are from published inorganic chemistry books; [17] CSD entries for metal ion binding to elements O, N, S. [18]_(a) CSD entries for metal ion binding to elements O, N, S, Cl and/or Br. [18]_(b) CSD entries for metal ion binding to element nitrogen. [17, 18] Binding to oxygen is preferred. [16] CSD entries; PBN entries are between parentheses. In bold are the predominant coordination numbers in [16, 17, 18]

of molecules than calcium and strontium.

It has been noted in [14, 19, 20] that the experimental conditions may also vary the coordination number; in fact, gas phase complexes have lower coordination numbers than their corresponding condensed phase complexes, and favour hydrogen bond networks. The studies in [14] and in [21] are noteworthy since they explain that the solvation of a multiply charged metal by hydrogen bonded solvents in the gas phase is different from the solvation in the condensed phase. In fact, in gas phase experiments the capability of a ligand to form hydrogen bonds influences the chemistry of the multiply charged ion in a cluster. For example, if a solvent is capable of forming strong hydrogen bond networks, it will coordinate a smaller number of ligands to a central atom than a solvent forming weaker hydrogen bonds [14, 21]. Moreover, bulky ligands may have a lower ability to participate in hydrogen bonding and they therefore influence the formation of a gas phase cluster through steric factors. Another aspect of the process of multiply charged metal solvation in gas phase stressed in [21] is the formation of charged enhanced hydrogen bonds; in other words, the multiply charged ion affects the hydrogen bond network by increasing the magnitude of the strength between the bonding interactions amongst the molecules involved.

The experimental coordination numbers of this work are compared in Tables 6.3.2 and 6.3.3 with the results found in the literature.

The coordination number is determined in presence of a counter ion with proton magnetic resonance (NMR) in [22] and with neutron diffraction studies in [23]. Whereas, the results from [24, 5] are from photodissociation spectra; the results from [25] are obtained by density functional calculations at B3LYP, and the data from [26] and from [27, 28] are achieved respectively with molecular dynamics and Metropolis Monte-Carlo simulations. There is agreement on the number at which the first solvation shell is completed for [Mg(NH₃)_n]²⁺

	CN					
	Experimental					
	This work	[12]	[24]	[5]	[22]	[23]
$[\text{Mg}(\text{NH}_3)_n]^{2+}$	4	4	4		5.0	
$[\text{Ca}(\text{NH}_3)_n]^{2+}$	6					6.5, 7.0
$[\text{Sr}(\text{NH}_3)_n]^{2+}$	6			6		

Table 6.3.2: Comparison between coordination numbers determined in these experiments for $[\text{Mg}(\text{NH}_3)_n]^{2+}$, $[\text{Ca}(\text{NH}_3)_n]^{2+}$, and $[\text{Sr}(\text{NH}_3)_n]^{2+}$ clusters and those in experimental studies available from the literature. Values with decimal digits are average

	CN					
	Theoretical					
	This work	[27]	[28]	[26]	[29]	[25]
$[\text{Mg}(\text{NH}_3)_n]^{2+}$	4	8	6, 8			6
$[\text{Ca}(\text{NH}_3)_n]^{2+}$	6			9, 8	6	
$[\text{Sr}(\text{NH}_3)_n]^{2+}$	6					

Table 6.3.3: Comparison between coordination numbers determined in these experiments for $[\text{Mg}(\text{NH}_3)_n]^{2+}$, $[\text{Ca}(\text{NH}_3)_n]^{2+}$ and $[\text{Sr}(\text{NH}_3)_n]^{2+}$ clusters and those in theoretical studies available from the literature

clusters with a previous investigation of this laboratory in [12], where an instrumentation very similar to the equipment of this work was used to derive the coordination number from intensity distribution of fragments arising from collision induced dissociation (CID) experiments. Moreover, the coordination number of $[\text{Ca}(\text{NH}_3)_n]^{2+}$ was found to be six in [23], and by ONIOM-XS (our own-layered integrated molecular orbital and molecular mechanics with extension to solvation) simulation method in [29], which concurs with the result of this work.

6.4 Related Work on Monovalent Mg, Ca, and Sr

Experimental studies have focused the attention on the coordination number for metal ion either in liquid ammonia or in the gas phase with one to six ammonia ligands. Theoretical studies have focused on the calculations of the lowest energy geometries with one to six ammonia molecules. Nonetheless, few studies have determined binding energies for $[\text{Mg}(\text{NH}_3)_n]^+$ for $5 \leq n \leq 8$ that can be compared with $[\text{Mg}(\text{NH}_3)_n]^{2+}$: threshold collision induced dissociation (TCID) experiments [30], and theoretical calculations [30, 31, 25]. The computations in [30] are performed with full second-order Møller-Plesset perturbation (MP2) method, equilibrium bond energies where corrected for zero-point energies (ZPE) and basis set superposition error (BSSE) were subtracted in the

full counterpoise approximation. In [31] the computations applied density functional theory hybrid method at B3LYP.

$[\text{Mg}(\text{NH}_3)_n]^{2+}$		$[\text{Mg}(\text{NH}_3)_n]^+$			
n	E_b (kJ mol ⁻¹)	BE (kJ mol ⁻¹)			
	This work	[25]		B3LYP	
		6-31+G(d)		DZVP	
		uncorr	uncorr	corr	uncorr
1		169		159	168
2		123	<u>64</u>	111	121
3		97	<u>54</u>	88	95
4		69	<u>35</u>	57	<u>30</u>
5	62 ± 10	64		50	52
6	45 ± 5.2	59		47	47
7	43 ± 1.9		35		
8	44 ± 12		72		

Table 6.4.1: Comparison between binding energies determined in these experiments for $[\text{Mg}(\text{NH}_3)_n]^{2+} \rightarrow [\text{Mg}(\text{NH}_3)_{n-1}]^{2+} + \text{NH}_3$ ($5 \leq n \leq 8$) and those for $[\text{Mg}(\text{NH}_3)_n]^+ \rightarrow [\text{Mg}(\text{NH}_3)_{n-1}]^+ + \text{NH}_3$ available in [25]. The data in [25] are calculated at 298 K. The underlined data are for detachment of a molecule not directly bound to the metal ion; 'corr' indicates corrections for BSSE error, whereas 'uncorr' indicates that the data were not corrected for BSSE error

$[\text{Mg}(\text{NH}_3)_n]^{2+}$		$[\text{Mg}(\text{NH}_3)_n]^+$			
n	E_b (kJ mol ⁻¹)	BE (kJ mol ⁻¹)			
	This work	$[30]_{(a)}^{0\text{ K}}$	$[30]_{(b)}^{0\text{ K}}$	$[30]_{(a)}^{298\text{ K}}$	$[31]_{(b)}^{0\text{ K}}$
		MP2 (full)/6-311+G(2d,2p)//		MP2	
		MP2 (full)6-31+G*		6-31++G(d,p)	
1		154	148	158.9	149
2		122	110	123.9	112
3		95	88	97.8	89.6
4		43	46	45.4	45.6
5	62 ± 10	55	42	57.0	43.5
6	45 ± 5.2				56.9
7	43 ± 1.9				
8	44 ± 12				

Table 6.4.2: Comparison between binding energies determined in these experiments for $[\text{Mg}(\text{NH}_3)_n]^{2+} \rightarrow [\text{Mg}(\text{NH}_3)_{n-1}]^{2+} + \text{NH}_3$ ($5 \leq n \leq 8$) and those for $[\text{Mg}(\text{NH}_3)_n]^+ \rightarrow [\text{Mg}(\text{NH}_3)_{n-1}]^+ + \text{NH}_3$ available from literature. (The superscript next to a citation indicates the temperature; the subscript (a) indicates experimental data; the subscript (b) refers to theoretical data)

In [25] the computations were conducted using MP2 with froze core approximation. The data in [25] are reported in Table 6.4.1 and correspond to the bond energy for breaking one hydrogen bond for $1 \leq n \leq 6$ and two hydrogen bonds for $7 \leq n \leq 8$; moreover, the coordination number for all the structures in [25]

is six. The bond energies from [30] and [31], in Table 6.4.2 are equilibrium geometries that have all ammonia ligands attached directly to the magnesium ion.

It is worthwhile mentioning that fully optimized minimum energy geometries and isomeric structures have been calculated by theoretical methods [32, 30, 31, 25, 33, 34, 35] for $[\text{Mg}(\text{NH}_3)_n]^+$ with $1 \leq n \leq 8$. Also, minimum energy equilibrium structures for $[\text{Mg}(\text{NH}_3)_n]^+$ with coordination number from one to six has been theoretically found. Moreover, spectroscopic investigation in gas phase have ascertained the existence of monovalent magnesium with a maximum coordination number of three [32] or four [24], which only partially confirm theoretical calculations. Despite the limited literature, it is possible to argue that the difference in energy between the monovalent and the divalent clusters in Table 6.4.2 confirms that the double charge affects the binding energy.

Bibliography

- [1] S.E. Rodriguez-Cruz, R.A. Jockusch, E.R. Williams, *Journal of the American Chemical Society* 120 (1998) 5842.
- [2] S.E. Rodriguez-Cruz, R.A. Jockusch, E.R. Williams, *Journal of the American Chemical Society* 121 (1999) 8898.
- [3] A.J. Stace, A.K. Shukla, *Journal of the American Chemical Society* 104 (1982) 5314.
- [4] J.R. Gilbert, A.J. Stace, *International Journal of Mass Spectrometry and Ion Physics* 15 (1974) 311.
- [5] C. Lifshitz, F.A. Long, *Journal of Chemical Physics* 41 (1964) 2468.
- [6] A.J. Stace, C. Moore, *Journal of the American Chemical Society* 105 (1983) 1814.
- [7] C.E. Housecroft, A.G. Sharpe, *Inorganic Chemistry*, Pearson Education Limited, Harlow, 2001, pp. 744.
- [8] F. A. Cotton, G. Wilkinson, C. A. Murillo, M. Bochmann, *Advanced Inorganic Chemistry*, John Wiley & Sons Inc., New York, 6th edn., 1996, pp. 111-130.
- [9] K.N. Marsh Ed., *Recommended Reference Materials For The Realisation Of Physicochemical Properties*, Blackwell, Oxford, 1987, pp. 3-113.
- [10] P.W. Atkins, *Physical Chemistry*, Oxford University Press, 6th edn., 1999, pp.921.
- [11] D.R. Lide, *Handbook Of Chemistry And Physics*, CRC Press, 85th edn., (2004-2005), ch.6, 112-113.
- [12] N. Walker, M.P. Dobson, R.R. Wright, P.E. Barran, J.N. Murrell, A.J. Stace, *Journal of the American Chemical Society* 122 (2000) 11138.

- [13] N. Okai, S. Yoshida, K. Aranishi, A. Takahata, K. Fuke, *Physical Chemistry Chemical Physics* 7 (2005) 921.
- [14] B. Wu, B.J. Duncombe, A.J. Stace, *Journal of Physical Chemistry A* 110 (2006) 8423.
- [15] X.J. Chen, A.J. Stace, *Journal of Physical Chemistry A* 117 (2013) 5015.
- [16] M. Dudev, J. Wang, T. Dudev, C. Lim, *Journal of Physical Chemistry B* 110 (2006) 1889.
- [17] C.W. Bock, A.K. Katz, G. D. Markham, J.P. Glusker, *Journal of the American Chemical Society* 121 (1999) 7360.
- [18] A.K. Katz, J.P. Glusker, S.A. Beebe, C.W. Bock, *Journal of the American Chemical Society* 118 (1996) 5752.
- [19] G.N Patawari, J.M. Lisy, *Journal of Chemical Physics* 118 (2003) 8555.
- [20] A.J. Stace, N.R. Walker, S. Firth, *Journal of the American Chemical Society* 119 (1997) 10239.
- [21] A.J. Stace, *Physical Chemistry Chemical Physics* 3 (2001) 1935.
- [22] T.J. Swift, H.H. Lo, *Journal of the American Chemical Society* 89 (1967) 3988.
- [23] J.C. Wasse, C.A. Howard, H. Thompson, N.T. Skipper, R.G. Delaplane, A. Wannberg, *Journal of Chemical Physics* 121 (2004) 996.
- [24] J.I. Lee, D.C. Sperry, J.M. Farrar, *Journal of Chemical Physics* 121 (2004) 8375.
- [25] T. Shoeib, R.K. Milburn, G.K. Koyanagi, V.V. Lavrov, D.K. Bohme, K.W.M. Siu, A.C. Hopkinson, *International Journal of Mass Spectrometry* 201 (2000) 87.
- [26] W. Sidhisoradej, S. Hannongbua, D. Ruffolo, *Zeitschrift fur Naturforschung Section A. Journal of Physical Science* 53 (1998) 208.
- [27] S. Hannongbua, B.M. Rode, *Chemical Physics* 162 (1992) 257.
- [28] S. Hannongbua, *Journal of Chemical Physics*, 106 (1997) 6076.
- [29] T. Kerdcharoen, K. Morokuma, *Journal of Chemical Physics* 118 (2003) 8856.

- [30] A. Andersen, F. Muntean, D. Walter, C. Rue, P.B. Armentrout, *Journal of Physical Chemistry A* 104 (2000) 692.
- [31] K. Daigoku, K. Hashimoto, *Journal of Chemical Physics* 121 (2004) 3569.
- [32] R.K. Milburn, V.I. Baranov, A.C. Hopkinson, D.K. Bohme, *Journal of Physical Chemistry A* 102 (1998) 9803.
- [33] S. Yoshida, K. Daigoku, N. Okai, A. Takahata, A. Sabu, K. Hashimotoa, K. Fuke, *Journal of Chemical Physics* 117 (2002) 8657.
- [34] K. W. Chan, Y. Wu, Z.-F. Liu, *Canadian Journal of Chemistry* 85 (2007) 873.
- [35] M. Elhanine, L. Dukan, P. Maître, W.H. Breckenridge, S. Massick, B. Soep, *Journal of Chemical Physics* 112 (2000) 10912.

Chapter 7

Binding Energy of $[\text{Mg}(\text{H}_2\text{O})_n]^{2+}$, $[\text{Ca}(\text{H}_2\text{O})_n]^{2+}$, and $[\text{Sr}(\text{H}_2\text{O})_n]^{2+}$

We now discuss the experimental results for unimolecular (metastable) decay (neutral loss in these experiments) of a single water molecule from $[\text{Ca}(\text{H}_2\text{O})_n]^{2+}$ for $4 \leq n \leq 20$ and $[\text{Sr}(\text{H}_2\text{O})_n]^{2+}$ for $7 \leq n \leq 20$. We also present preliminary studies on $[\text{Mg}(\text{H}_2\text{O})_n]^{2+}$ cluster ions for $8 \leq n \leq 13$. The $[\text{Mg}(\text{H}_2\text{O})_n]^{2+}$ for $n \leq 7$ and $n \geq 14$ were not investigated in these experiments due to time constraints.

7.1 Experimental Details

Artefact peaks have not been observed in the recorded scans. The value of laboratory frame FWHM peak widths (w) of the precursor ions were ranging as follows

- between 2.2 eV and 2.8 eV for $[\text{Mg}(\text{H}_2\text{O})_n]^{2+}$ at $8 \leq n \leq 13$;
- between 6.1 eV and 9.4 eV for $[\text{Ca}(\text{H}_2\text{O})_n]^{2+}$ at $n = 4$;
- between 5.6 eV and 6.0 eV for $[\text{Ca}(\text{H}_2\text{O})_n]^{2+}$ at $5 \leq n \leq 6$;
- between 1.5 eV and 2.7 eV for $[\text{Ca}(\text{H}_2\text{O})_n]^{2+}$ at $7 \leq n \leq 20$;
- between 2.2 eV and 3.9 eV for $[\text{Sr}(\text{H}_2\text{O})_n]^{2+}$ at $12 \leq n \leq 13$;
- between 1.5 eV and 2.8 eV for $[\text{Sr}(\text{H}_2\text{O})_n]^{2+}$ at $7 \leq n \leq 11$ and $14 \leq n \leq 20$.

The goodness of fit to a Gaussian profile of precursor ions was $R^2 > 0.9$ for all the measurements. The goodness of fit to a Gaussian profile of daughter ions was as follows

- $0.6 < R^2 < 0.8$ for $[\text{Mg}(\text{H}_2\text{O})_n]^{2+}$;
- $R^2 > 0.9$ for $[\text{Ca}(\text{H}_2\text{O})_n]^{2+}$;
- $0.6 < R^2 < 0.7$ for $[\text{Sr}(\text{H}_2\text{O})_n]^{2+}$ at $7 \leq n \leq 8$;
- $0.7 < R^2 < 0.8$ for $[\text{Sr}(\text{H}_2\text{O})_n]^{2+}$ at $9 \leq n \leq 11$ and $n = 19$;
- $0.8 < R^2 < 0.9$ for $[\text{Sr}(\text{H}_2\text{O})_n]^{2+}$ at $15 \leq n \leq 18$ and $n = 20$;
- $R^2 > 0.9$ for $[\text{Sr}(\text{H}_2\text{O})_n]^{2+}$ at $12 \leq n \leq 14$.

The MIKE scans for the precursor ion and the daughter ion of $[\text{Ca}(\text{H}_2\text{O})_3]^{2+}$, $[\text{Sr}(\text{H}_2\text{O})_6]^{2+}$, and $[\text{Sr}(\text{H}_2\text{O})_5]^{2+}$ were observed, but these data were not considered in the analysis because the Gaussian profiles of the daughter ions were respectively $R^2 < 0.6$, $R^2 < 0.5$, and $R^2 < 0.2$.

We refer the reader to Chapter 9 for the experimental values of w and R^2 , and to Chapter 10 for more details about the experimental settings. A minimum of four measurements have been used to determine the kinetic energy release for the metastable neutral loss for each cluster size.

The background noise affected the signal of the daughter ions (*i.e.* the signal of the daughter ion was weak); consequently only the profiles which retained a Gaussian shape were considered in the analysis. Moreover, it has been necessary to slightly compromise the accuracy of MIKE scans for both the parent and the daughter ions. In order to improve on the R^2 value of the daughter ion MIKE scan, the w value of the MIKE scan of a particular parent ion was adjusted depending on the signal-to-noise ratio of the corresponding daughter ion under investigation.

Examples of MIKE scan profiles of the $[\text{Mg}(\text{H}_2\text{O})_n]^{2+}$, $[\text{Ca}(\text{H}_2\text{O})_n]^{2+}$, and $[\text{Sr}(\text{H}_2\text{O})_n]^{2+}$ cluster ions with different values of w and R^2 are shown in Figures 7.1.1 and 7.1.2 below. It can be seen that MIKE scans of daughter ions having $R^2 < 0.9$ are characterized by a noisy signal with respect to those having $R^2 > 0.9$, owing to the interference of the signal of the background with the signal of a daughter ion. The effect of the noise in the scans is to lower the goodness of fit to a Gaussian profile, R^2 , this is reflected in the oscillations in the graphs of the Gaussian profiles. Nonetheless, the peak profile retains a good Gaussian shape despite the fact that the noise is affecting the shape of the peak. However, such noise increases the error in the measurement of the peak width from a MIKE scan, due to the increased error in the determination of the value of w from the oscillating curve (with respect to a curve without oscillations). In Figures 7.1.1 and 7.1.2 are presented various parent ions with different laboratory frame FWHM peak widths in these experiments. Ideally, the width of a

parent ion scan should be as narrow as possible so to obtain as much as possible accuracy.

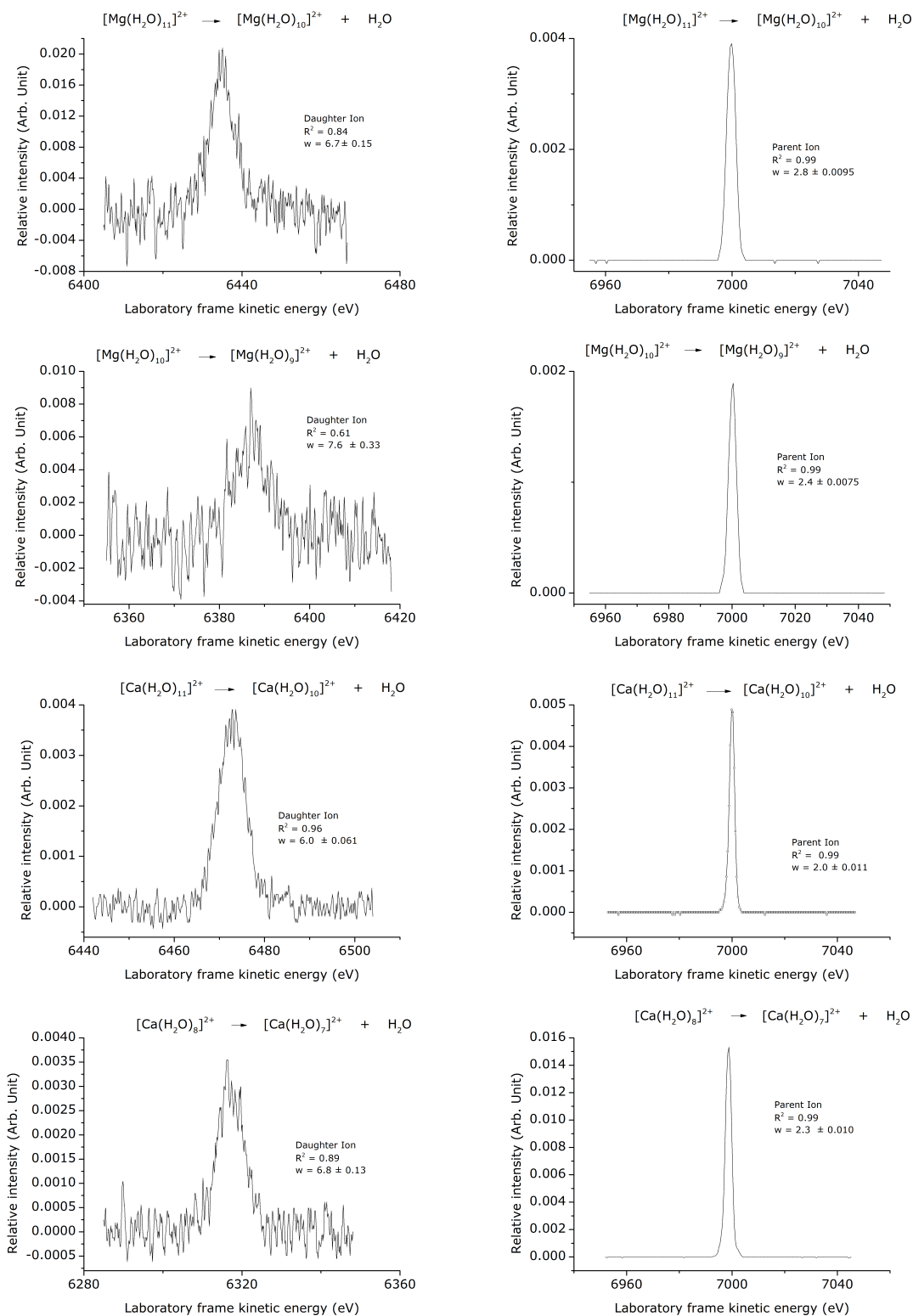


Figure 7.1: Examples of MIKE scans for $[\text{Mg}(\text{H}_2\text{O})_n]^{2+}$ (daughter ions scans are in the left column of the first two rows) with $R^2 = 0.84, 0.61$ and for $[\text{Ca}(\text{H}_2\text{O})_n]^{2+}$ (daughter ions scans are in the left column of the last two rows – with $R^2 = 0.96, 0.89$). The respective parent ions (right column) have $R^2 = 0.99$ and $w = 2.8 \text{ eV}, 2.4 \text{ eV}, 2.0 \text{ eV}, 2.3 \text{ eV}$

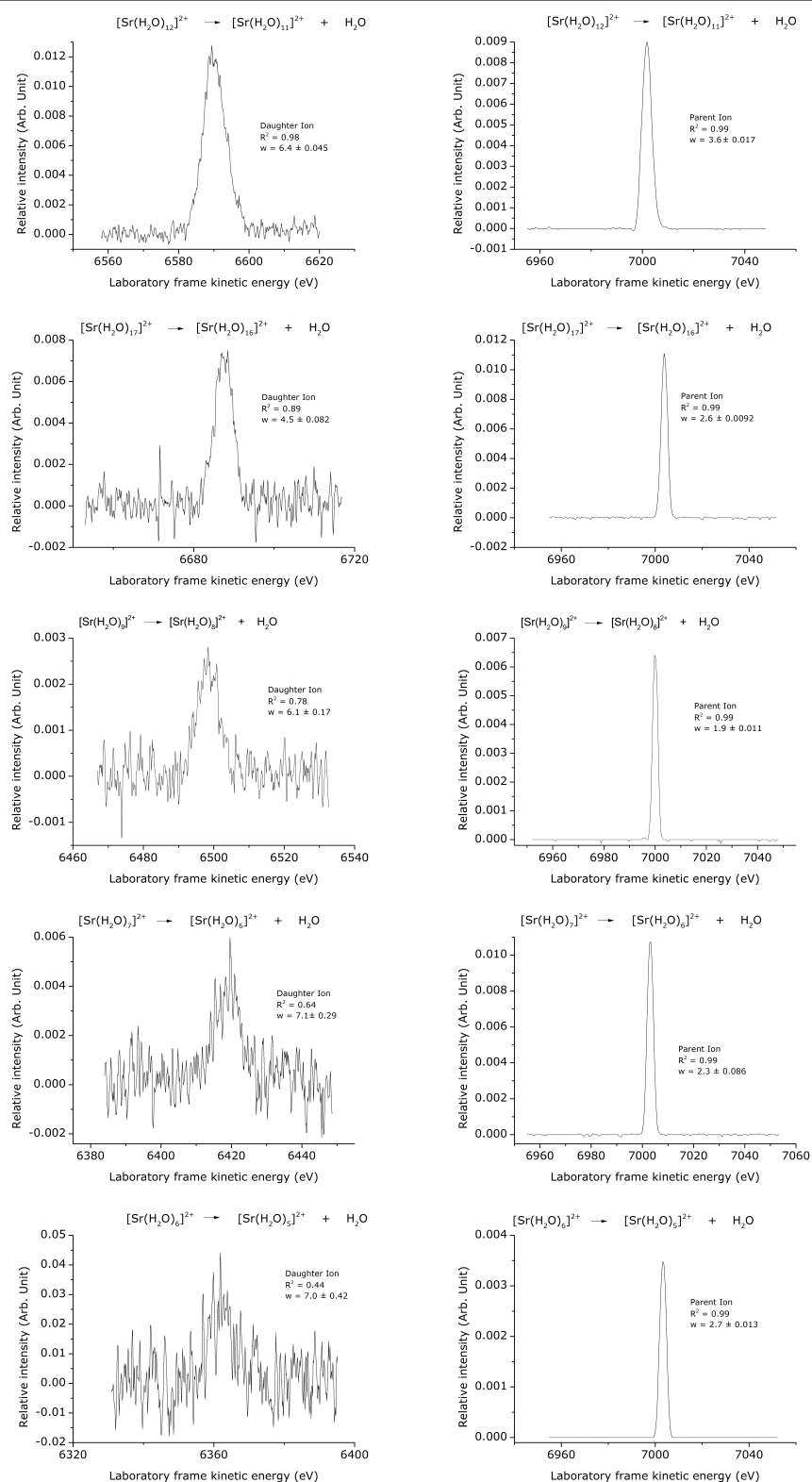


Figure 7.1.2: Examples of MIKE scan for $[\text{Sr}(\text{H}_2\text{O})_n]^{2+}$: daughter ions (left column) with $R^2 = 0.98, 0.89, 0.78, 0.64, 0.44$ and respective parent ions (right column) with $R^2 = 0.99$ and $w = 3.6 \text{ eV}, 2.6 \text{ eV}, 1.9 \text{ eV}, 1.3 \text{ eV}, 2.7 \text{ eV}$. MIKE scans for $[\text{Sr}(\text{H}_2\text{O})_6]^{2+}$ were not accepted

7.2 Binding Energies of KER Measurements

We now discuss the studies of the neutral loss of a single water molecule of the clusters ions $[\text{Ca}(\text{H}_2\text{O})_n]^{2+}$ for $4 \leq n \leq 20$ and $[\text{Sr}(\text{H}_2\text{O})_n]^{2+}$ for $7 \leq n \leq 20$, as well as the preliminary investigations on neutral loss for the cluster ions $[\text{Mg}(\text{H}_2\text{O})_n]^{2+}$ for $8 \leq n \leq 13$. The kinetic energy release from unimolecular (metastable) decay experiments of the cluster ions as a function of cluster size are reported in Table 7.2.1. They are experimental measurements of the average kinetic energy release, $\langle \varepsilon_\tau \rangle$, associated with the unimolecular (metastable) decay of cluster ions. Each value is the average of separate measurements and the error, $\pm \Delta \langle \varepsilon_\tau \rangle$, reflects the spread in uncertainty in the measurements.

n	$[\text{Mg}(\text{H}_2\text{O})_n]^{2+}$		$[\text{Ca}(\text{H}_2\text{O})_n]^{2+}$		$[\text{Sr}(\text{H}_2\text{O})_n]^{2+}$	
	$\langle \varepsilon_\tau \rangle$ (meV)	$\pm \Delta \langle \varepsilon_\tau \rangle$ (meV)	$\langle \varepsilon_\tau \rangle$ (meV)	$\langle \varepsilon_\tau \rangle$ (meV)	$\langle \varepsilon_\tau \rangle$ (meV)	$\pm \Delta \langle \varepsilon_\tau \rangle$ (meV)
4			38	5.3		
5			37	5.1		
6			30	5.0		
7			30	7.4	25	3.1
8	21	7.8	30	2.9	19	6.2
9	26	7.7	28	2.6	21	2.4
10	25	8.6	25	3.8	19	2.2
11	24	2.5	26	3.8	18	6.7
12	25	4.1	24	3.5	24	1.3
13	24	8.6	24	1.3	20	0.53
14			26	2.4	18	2.1
15			23	3.4	17	2.0
16			22	1.8	15	1.0
17			24	3.4	16	2.3
18			28	2.4	17	4.4
19			23	2.7	16	5.1
20			22	1.2	18	2.4

Table 7.2.1: Experimental measurements of $\langle \varepsilon_\tau \rangle$ (average kinetic energy release) associated with the unimolecular (metastable) decay of cluster ions. Each value is the average of at least four separate measurements, and the error, $\langle \varepsilon_\tau \rangle$, reflects the spread in uncertainty in the measurements

The binding energy of each of the ion as a function of cluster size is given in Table 7.2.2. The data obtained in these experiments were truncated after the second significant digit only once all the calculations had been processed.

n	$[\text{Mg}(\text{H}_2\text{O})_n]^{2+}$		$[\text{Ca}(\text{H}_2\text{O})_n]^{2+}$		$[\text{Sr}(\text{H}_2\text{O})_n]^{2+}$		$\text{H}^+(\text{H}_2\text{O})_n$
	E_b (kJ mol ⁻¹)	$\pm\Delta E_b$ (kJ mol ⁻¹)	E_b (kJ mol ⁻¹)	$\pm\Delta E_b$ (kJ mol ⁻¹)	E_b (kJ mol ⁻¹)	$\pm\Delta E_b$ (kJ mol ⁻¹)	$E_b \pm \Delta E_b$ (kJ mol ⁻¹)
4			125	17			52 ± 14
5			98	13			39 ± 4.7
6			70	11			35 ± 0.43
7			65	16	54	6.8	32 ± 2.9
8	54	18	62	6.0	39	12	31 ± 2.8
9	52	15	55	5.1	41	4.7	32 ± 1.3
10	48	16	49	7.2	36	4.2	32 ± 0.77
11	45	4.6	48	7.0	35	12	27 ± 2.0
12	46	7.5	44	6.4	45	2.4	30 ± 0.80
13	44	15	43	2.4	37	0.95	28 ± 1.7
14			46	4.3	33	3.7	28 ± 0.40
15			40	5.9	30	3.5	29 ± 1.1
16			38	3.2	27	1.8	27 ± 1.3
17			41	5.9	27	4.1	29 ± 2.7
18			48	4.1	30	7.5	28 ± 2.5
19			40	4.5	27	8.7	27 ± 0.61
20			38	2.1	31	4.1	27 ± 2.8

Table 7.2.2: Binding energies determined from the kinetic energy release data presented in Table 7.2.1. The binding energy of $\text{H}^+(\text{H}_2\text{O})_n$ is added for comparison

In addition, a plot of the binding energy as a function of the number n of water molecules in each cluster is shown in Figure 7.2.1 below, where the error bars are an indication of the accuracy of the measurements.

The change in slope of the binding energies of $[\text{Mg}(\text{H}_2\text{O})_n]^{2+}$, $[\text{Ca}(\text{H}_2\text{O})_n]^{2+}$, and $[\text{Mg}(\text{H}_2\text{O})_n]^{2+}$ versus cluster size is shown in Figure 7.2.1. The steady decrease stops at a value of n that suggests the completion of the first solvent shell, any other water molecule added will bind to the first solvation shell forming a successive solvation shell. As a matter of fact, the metal and ligands gaseous system may be compared with the liquid phase concentric shell model of solvation [1, 2]. Moreover, the number of water molecules completing the first solvation shell coincides with the coordination number (CN) for a metal dication in these experiments. Therefore, these non-equilibrium gas phase experiments performed at a pressure $< 10^{-7}$ mbar suggest that

- even though it is not known from these investigations the number of water molecules coordinated directly to Mg^{2+} , it is possible to suggest that the number of water molecules required to complete the first solvation shell of Mg^{2+} are $n \leq 6$, owing to the binding energy values of $[\text{Mg}(\text{H}_2\text{O})_n]^{2+}$ at $n \geq 8$ with respect to $\text{H}^+(\text{H}_2\text{O})_n$;
- when coordinated with water, Ca^{2+} and Sr^{2+} ions complete the first solvation

shell with six water molecules;

- c) any other water molecule added to $[\text{Ca}(\text{H}_2\text{O})_6]^{2+}$ or $[\text{Sr}(\text{H}_2\text{O})_6]^{2+}$ binds to metastable cluster ion through hydrogen bonding (instead of binding to the metal);
- d) the charge on the metal is affecting the binding interactions for $[\text{Mg}(\text{H}_2\text{O})_n]^{2+}$ at each n , for $[\text{Ca}(\text{H}_2\text{O})_n]^{2+}$ up to $n = 20$, and for $[\text{Sr}(\text{H}_2\text{O})_n]^{2+}$ up to $n = 14$;
- e) the recorded MIKE scan for a unimolecular (metastable) decay in these experiments is not necessarily of the most stable structure (*cf.* Section 5.2 on page 105);
- f) the weakest bond (the hydrogen bond between the most weakly bound molecule in the outer solvation shell and the metastable cluster ion) is broken in these metastable decay experiments;
- g) these results have shown that no magic numbers [3, 4] are observed (*cf.* Section 4.4 on page 83);

As shown in Figure 7.2.1, the uncertainty in the measurements of $[\text{Mg}(\text{H}_2\text{O})_n]^{2+}$ is high at each n . Each error bar is so large that it overlaps with the value of the binding energies for $[\text{Ca}(\text{H}_2\text{O})_n]^{2+}$ and $[\text{Sr}(\text{H}_2\text{O})_n]^{2+}$, so that it would be hard to infer a comparison of the binding energy trends amongst the three systems at each n . The main cause of the high uncertainty for $[\text{Mg}(\text{H}_2\text{O})_n]^{2+}$ is a poor Gaussian profile of the daughter ions; in fact, the background noise signal was too high to allow a good peak shape, as shown in Figure 7.1.1; and it was not possible to improve the signal-to-noise ratio due to time constraints. A study on the relative parent ion intensities of $[^{25}\text{Mg}(\text{H}_2\text{O})_n]^{2+}$ as a function of n for $2 \leq n \leq 24$ [5] determined by collision induced dissociation reported a drop in intensity after $n = 6$. This drop has been connected with the completion of the first solvation shell of $[\text{Mg}(\text{H}_2\text{O})_n]^{2+}$ at $n = 6$ [5]. Unimolecular metastable decay processes in the field-free regions of a mass spectrometer are dominated by the lowest energy route to dissociation, described as competitive shift [6, 7, 8, 9]. Furthermore, the competition amongst dissociation paths may change with increasing clusters size [7, 8]. Therefore, the measured binding energy corresponds to the fragmentation of the most weakly bound molecule (*cf.* Section 4.3 on page 77).

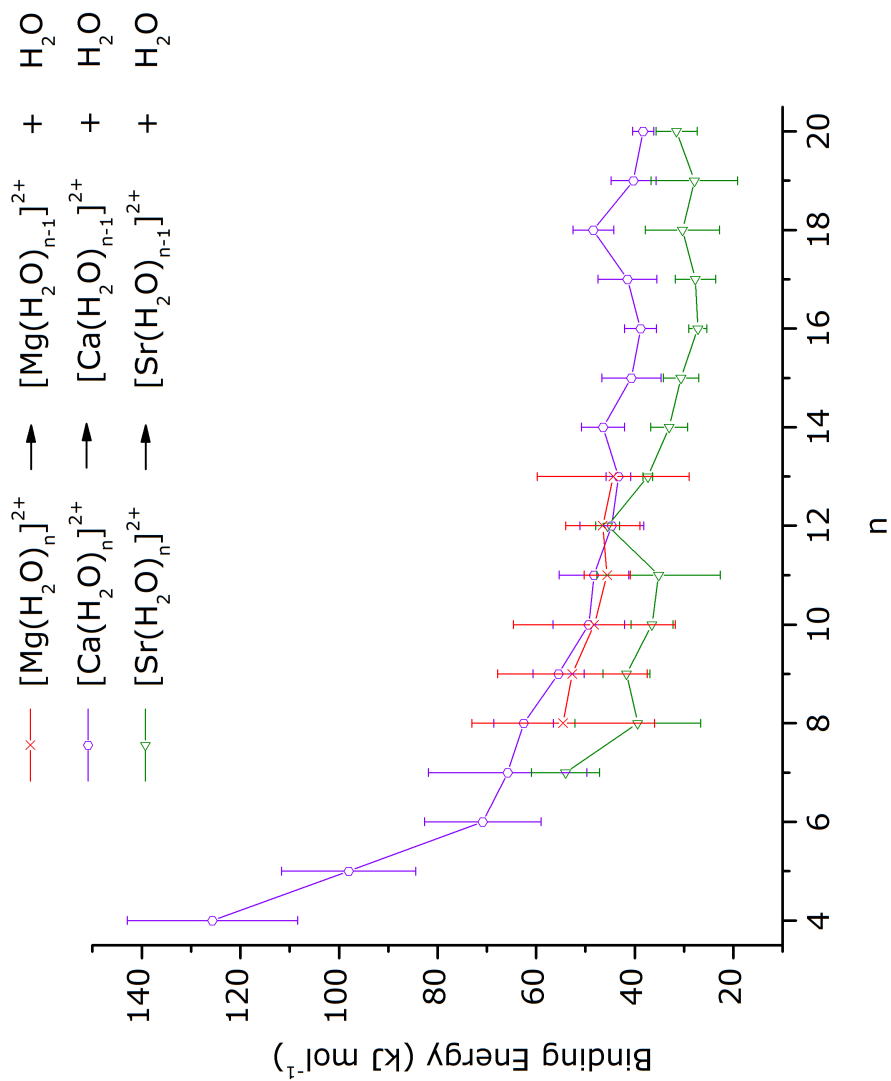


Figure 7.2.1: Plot of binding energies extracted from kinetic energy release measurements on $[Mg(H_2O)_n]^{2+}$, $[Ca(H_2O)_n]^{2+}$, and $[Sr(H_2O)_n]^{2+}$ cluster ions. Binding energy is given in kJ mol^{-1} and plotted as a function of n

It has been determined that unimolecular (metastable) decay for $\text{H}^+(\text{H}_2\text{O})_n$ in these experiments is caused by breaking one hydrogen bond of the mostly weak bound molecule in the cluster (*cf.* Section 4.3 on page 77). The comparison of the binding energies of $[\text{Mg}(\text{H}_2\text{O})_n]^{2+}$ for $8 \leq n \leq 13$, $[\text{Ca}(\text{H}_2\text{O})_n]^{2+}$ for $7 \leq n \leq 20$, and $[\text{Sr}(\text{H}_2\text{O})_n]^{2+}$ for $7 \leq n \leq 14$ with $\text{H}^+(\text{H}_2\text{O})_n$ for $7 \leq n \leq 20$ (as shown in Table 7.2.2 and Figure 7.2.2) ascertains that binding energy value is higher than the value of one hydrogen bond at each n , but it is not high enough to justify the presence of two hydrogen bonds. This confirms that the dissociation occurs by breaking one hydrogen bond and it is mostly the charge to affect the binding energy. In fact, the binding energy of a molecule held in position by a single hydrogen bond should be approximately 22 kJ mol^{-1} , whereas the enthalpy of vaporization of water at approximately 44 kJ mol^{-1} would equate with the breaking of two hydrogen bonds [10, 11, 12, 13, 14]. The binding energy of $\text{H}^+(\text{H}_2\text{O})_n$ and $[\text{Sr}(\text{H}_2\text{O})_n]^{2+}$ is approximately the same for each $n \geq 15$; this reflects an arrest of the effect on the strength of the bonding interactions by the double charge of the metal. Therefore, the energy for the loss of one water molecule for $n \geq 15$ equals the energy of one hydrogen bonding interaction. This observation implies that water acts as a poor electron donor once strontium dication is coordinated by 15 water molecules. Consequently, the bulk vaporization energy for the doubly charged metal-solvent systems considered will be approached at $n > 20$ for $[\text{Ca}(\text{H}_2\text{O})_n]^{2+}$ and at $n > 14$ for $[\text{Sr}(\text{H}_2\text{O})_n]^{2+}$. Furthermore, the binding energy values for $[\text{Ca}(\text{H}_2\text{O})_n]^{2+}$ and $[\text{Sr}(\text{H}_2\text{O})_n]^{2+}$ with $n \leq 6$ are much higher than the corresponding values for $\text{H}^+(\text{H}_2\text{O})_n$, indicating that both the size and the charge of the metal affect the strength of the bond between the metal and the ligand in the first coordination shell. Also, once the first coordination shell is completed, each water molecule is bound through one hydrogen bond, but it is the charge that mostly has an effect on the strength of the bond because the binding energy values of $[\text{Ca}(\text{H}_2\text{O})_n]^{2+}$ at $7 \leq n \leq 20$ and $[\text{Sr}(\text{H}_2\text{O})_n]^{2+}$ at $7 \leq n \leq 14$, are higher than the corresponding values for $\text{H}^+(\text{H}_2\text{O})_n$ for each n , even for the values of n at which the first coordination shell is completed. Moreover, the binding energy values of $[\text{Mg}(\text{H}_2\text{O})_n]^{2+}$ are higher than those of $\text{H}^+(\text{H}_2\text{O})_n$ at each n for $8 \leq n \leq 13$. Therefore, it is experimentally observed that the unimolecular (metastable) dissociation is due to breaking a hydrogen bonding for $[\text{Mg}(\text{H}_2\text{O})_n]^{2+}$ as well.

These gas phase experiments show that Ca^{2+} and Sr^{2+} have the same CN, but a different behaviour for $n \geq 15$ because the charge on Sr^{2+} stops to have an effect on the binding interactions. These ions, Ca^{2+} and Sr^{2+} , have both the characteristic of “structure making” [15], and in these experiments it is evident that they have different behaviours when solvated in water. Few theoretical cal-

culations (density functional theory [16] and *ab initio* [18, 19]) for $[\text{Ca}(\text{H}_2\text{O})_2]^{2+}$ and for $[\text{Sr}(\text{H}_2\text{O})_2]^{2+}$ found that the binding interactions are enhanced due to the core polarization (*i.e.* hybridisation and role of d orbitals of the metal), which in turn compensates for ligand repulsion in forming a stable bent structure (where the bent geometry was found to be more stable than the linear geometry by 1.2 kJ mol^{-1}) [18]. Conversely, a linear structure is favoured for $[\text{Mg}(\text{H}_2\text{O})_2]^{2+}$ as reported in [16]. Moreover, *ab initio* calculations have found that the Sr–O distance increases as more water molecules bind to Sr^{2+} in $[\text{Sr}(\text{H}_2\text{O})_n]^{2+}$ for $1 \leq n \leq 6$, and that the water molecules form weak hydrogen bonding while water-water repulsion is minimised due to the orientation position of ligands. Furthermore, the *ab initio* calculations on $[\text{Ca}(\text{H}_2\text{O})_n]^{2+}$ for $1 \leq n \leq 8$ in [20] suggested that the Ca–O bond increases and charge transfer decreases as the number of water molecules added directly to the metal centre increases from $n = 1$ to $n = 8$. Again in [20], the same trend was found for $[\text{Mg}(\text{H}_2\text{O})_n]^{2+}$ for $1 \leq n \leq 7$, but with an Mg–O bond shorter than the Ca–O one at each n , while an higher degree of charge transfer occurs. In addition, an investigation on the factors governing CN in gas phase suggested that the interactions between the metal ion, the first solvent shell, and the second solvent shell are determining the coordination of the metal [21]. The analysis on the hydration of Li^+ , Na^+ , K^+ , Mg^{2+} , and Ca^{2+} performed by first principles Car-Parrinello molecular dynamics simulations [22] found that the water-water interactions affect solvation even in the first solvation shell for all the examined ions.

The results provided in [16, 20, 18, 19, 22] suggest the hypothesis that the polarizability of water has a greater effect on the binding interactions with Sr^{2+} than with Ca^{2+} . More precisely, as the number of water molecules solvating Sr^{2+} goes from $n = 1$ to $n = 14$, charge transfer from the water molecule to the metal ion compensates the presence of the double charge. This condition may be due to the difference in polarizability-volume of Sr^{2+} with respect to the one of H_2O (according to [23] such polarizability-volumes are $5.8 \times 10^{-30} \text{ m}^3$ and $1.48 \times 10^{-30} \text{ m}^3$ respectively). The different behaviour of Ca^{2+} with respect to Sr^{2+} is therefore due to Ca^{2+} having polarizability volume $3.2 \times 10^{-30} \text{ m}^3$. In other words, the charge on Sr^{2+} does not compensate for the polarizability of H_2O as efficiently as Ca^{2+} .

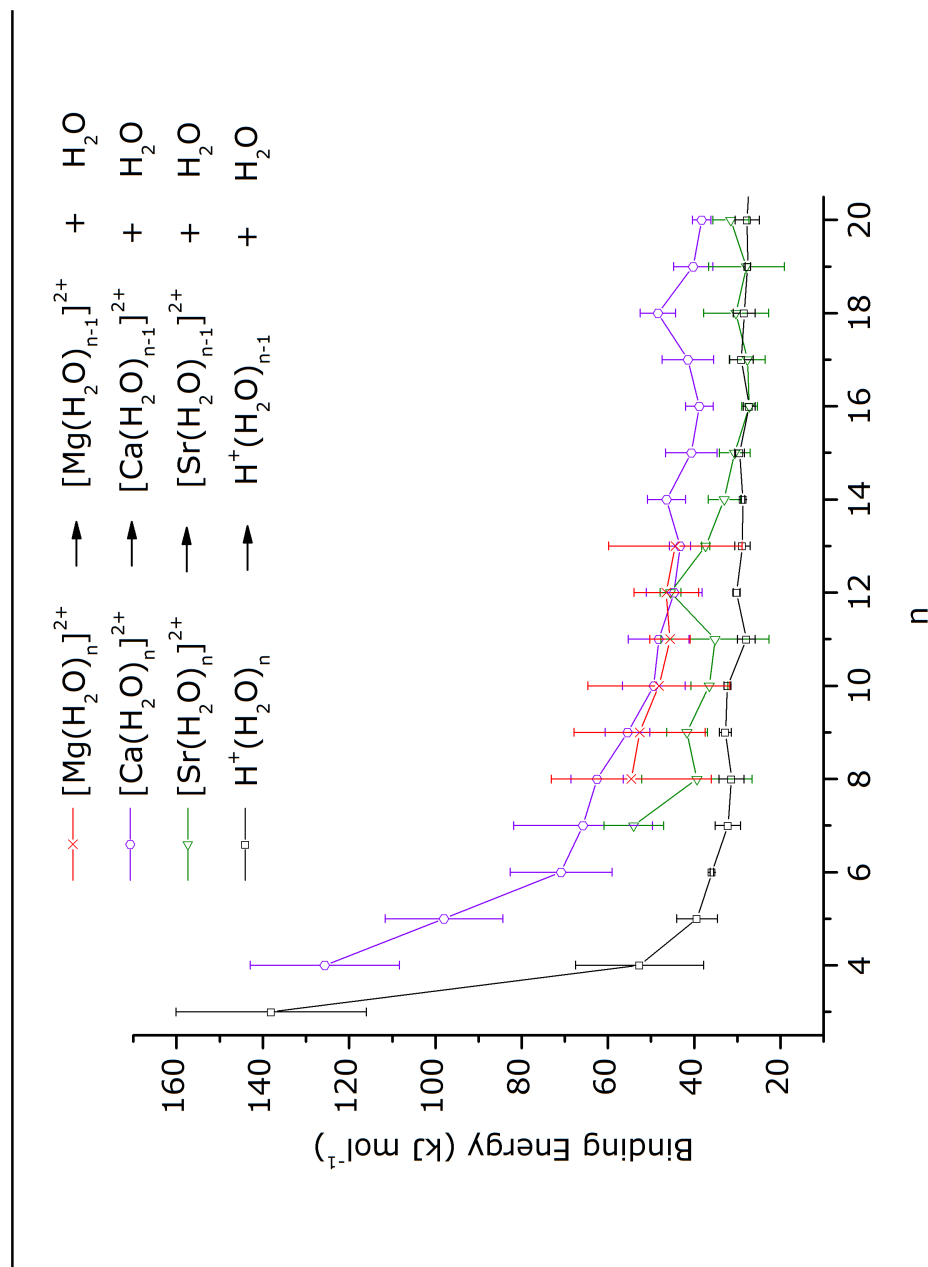


Figure 7.2.2: Plot of binding energies extracted from kinetic energy release measurements on $[\text{Ca}(\text{H}_2\text{O})_n]^{2+}$, $[\text{Sr}(\text{H}_2\text{O})_n]^{2+}$, $\text{H}^+(\text{H}_2\text{O})_n$ cluster ions. The binding energy is given in kJ mol^{-1} and plotted as a function of n .

One of the main difficulties in experimentally measuring the binding energy of ion clusters in the gas phase arises when charge reduction becomes competitive with neutral loss [24, 25]; in fact, the investigations performed in [26, 16, 27] were not able to provide binding energies at the cluster size where Coulomb fission and neutral loss were both present. In addition, the high exothermic reactions at low cluster sizes, $1 \leq n \leq 5$, prevent the determination of hydration energies from equilibrium experiments [28]. The critical size (n_c) of various systems has been investigated in [29, 24, 25, 30, 31, 32] and it has been defined as the maximum value of n for which Coulomb fission (charge reduction in [29], charge transfer in [30]) is competitive with ligand loss, which corresponds to the maximum value of n for which Coulomb fission is experimentally observable [33]. The relationship $n_s = n_c + 1$ has been formulated in [33, 34] as well, where n_s is the minimum number of water molecules required to stabilize a dication complex in the gas phase against spontaneous Coulomb fission. The experimental n_c found in the selected literature are listed in Table 7.2.3.

	n_c										
	[26]	[24]	[25]	[33]	[35]	[36]	[16]	[37]	[30]	[27]	[31]
$[\text{Mg}(\text{H}_2\text{O})_n]^{2+}$	3, 4	3	2, 3	3	0				4		
$[\text{Ca}(\text{H}_2\text{O})_n]^{2+}$		2	2	0, 2	0	2		2	0	2, 3	2
$[\text{Sr}(\text{H}_2\text{O})_n]^{2+}$		2	2	0, 2	0		0, 2		2		

Table 7.2.3: Critical size (n_c) of $[\text{Mg}(\text{H}_2\text{O})_n]^{2+}$, $[\text{Ca}(\text{H}_2\text{O})_n]^{2+}$, and $[\text{Sr}(\text{H}_2\text{O})_n]^{2+}$ from selected literature determined experimentally; values in bold identifies n_c derived by *ab initio* calculations

The accuracy of the measurements of $[\text{Ca}(\text{H}_2\text{O})_n]^{2+}$ when $n = 3$ and of $[\text{Sr}(\text{H}_2\text{O})_n]^{2+}$ when $n = 6$ would have been too low with respect to the other values of n for the respective clusters, owing to the MIKE scan with $R^2 < 0.6$ for calcium and $R^2 < 0.4$ for strontium daughter ions (*cf.* Section 3.3, page 56). Therefore, no experiments have been conducted for $n \leq 2$ for calcium and $n \leq 4$ for strontium due to our requirements on data quality to minimise the error of the measurements. The daughter ion MIKE scans with poor Gaussian profile in these experiments would reflect the difficulty in obtaining a good signal-to-noise ratio for the neutral loss metastable decay. In particular, the observations would suggest that Coulomb fission may possibly be the preferred dissociation route, so that the experimental signal from the neutral loss fragments may be lower when compared to the Coulomb fission fragments. On the contrary, it is not possible to conjecture the presence of the competition between neutral loss and Coulomb fission from the n_c data shown in Table 7.2.3. In addition, it is worth considering previous unimolecular metastable decay experiments per-

formed in this laboratory [33], which have shown that $n_s = 4$ for $[\text{Mg}(\text{H}_2\text{O})_n]^{2+}$, and $n_s = 0$ or possibly 3 for both $[\text{Ca}(\text{H}_2\text{O})_n]^{2+}$ and $[\text{Sr}(\text{H}_2\text{O})_n]^{2+}$. As a result, the comparison of the results of this work and the ones in [33] would suggest that the signal-to-noise ratio has limited the experimental measurements. We have not investigated if neutral loss could be observed for $n \leq 2$ for calcium and for $n \leq 4$ for strontium, therefore it is not possible to confirm $n_s = n_c = 0$ for $[\text{Ca}(\text{H}_2\text{O})_n]^{2+}$ and $[\text{Sr}(\text{H}_2\text{O})_n]^{2+}$. The requirements to accept a measurement were that

- the goodness of fit to a Gaussian profile, R^2 , for a fragment ion has to be as close as possible to the best value, which is 1, and
- the laboratory frame FWHM peak width (w) has to be as narrower as possible.

These conditions have been satisfied; however, MIKE scans with $R^2 < 0.9$ have been considered in the analysis if the profile of the daughter peak had a Gaussian shape, despite the uncertainty being higher with respect to those with $R^2 > 0.9$. Furthermore, the value of the laboratory frame FWHM peak width of the precursor ion has to be widened in order to obtain a satisfactory Gaussian profile for $[\text{Ca}(\text{H}_2\text{O})_n]^{2+}$ with $4 \leq n \leq 6$ and for $[\text{Sr}(\text{H}_2\text{O})_n]^{2+}$ with $12 \leq n \leq 13$ with respect to the other cluster ions. Our studies on $[\text{Ca}(\text{H}_2\text{O})_n]^{2+}$ and $[\text{Sr}(\text{H}_2\text{O})_n]^{2+}$ suggest the presence of a competition between neutral loss and Coulomb fission at $[\text{Ca}(\text{H}_2\text{O})_3]^{2+}$, $[\text{Sr}(\text{H}_2\text{O})_5]^{2+}$, and $[\text{Sr}(\text{H}_2\text{O})_6]^{2+}$ (owing to values of $R^2 < 0.6$, $R^2 < 0.2$ and $R^2 < 0.5$ respectively for the MIKE profile of the daughter ion). The experimental studies described in [27] for $[\text{Ca}(\text{H}_2\text{O})_n]^{2+}$ and in [16] for $[\text{Sr}(\text{H}_2\text{O})_n]^{2+}$ have reported the reactions observed from collision induced dissociation studies: the only reactions observed of $[\text{M}(\text{H}_2\text{O})_n]^{2+}$ for $n \leq 10$ where $\text{M} = \text{Ca}^{2+}, \text{Sr}^{2+}$

- $\text{M}^{2+}(\text{H}_2\text{O})_n \rightarrow \text{M}^{2+}(\text{H}_2\text{O})_{n-1} + \text{H}_2\text{O}$
loss of a single water molecule is the primary dissociation channel of $[\text{Ca}(\text{H}_2\text{O})_n]^{2+}$ for $2 \leq n \leq 10$ in [27] and $[\text{Sr}(\text{H}_2\text{O})_n]^{2+}$ for $1 \leq n \leq 6$ in [16], and that sequential water loss until the bare metal ion is formed was detected for each n , and
- $\text{M}^{2+}(\text{H}_2\text{O})_n \rightarrow \text{MOH}^+(\text{H}_2\text{O})_{n-2} + \text{H}_3\text{O}^+$
proton transfer/charge separation process was observed from the complexes $[\text{Ca}(\text{H}_2\text{O})_n]^{2+}$ for $n = 2, 3, 4$ in [27] and $[\text{Sr}(\text{H}_2\text{O})_n]^{2+}$ for $n = 2, 3$ in [16].

For completeness, we observe that the dominant collision induced fragmentation channels observed in [26] for the analysis on $[\text{Mg}(\text{H}_2\text{O})_n]^{2+}$ were

- for $3 \leq n \leq 10$



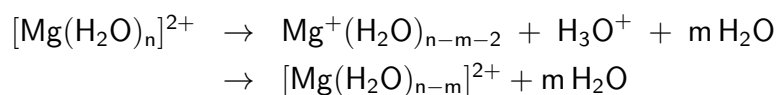
where single water loss and sequential water loss has been observed until the reactant ion was completely dehydrated,

- for $n = 3, 4, 5$

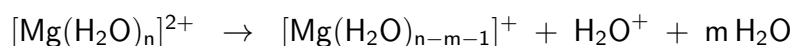


whereas the pathways in [5] were

- for $3 \leq n \leq 12$



- for $n = 3$ and $m = 0, 1$; for $n = 4$ and $m = 1, 2, 3$; and for $n = 5$ and $m = 2, 3$



Our investigations on $[\text{Mg}(\text{H}_2\text{O})_n]^{2+}$ can neither confirm the results in [33] nor compare with the experimental finding from the literature in Table 7.2.3, because the experimental investigations on $[\text{Mg}(\text{H}_2\text{O})_n]^{2+}$ are still in progress.

7.3 Related Experimental Work

The literature on experimental investigation shows that researchers have preferentially focused on the studies of the small clusters such as $[\text{Mg}(\text{H}_2\text{O})_n]^{2+}$, $[\text{Ca}(\text{H}_2\text{O})_n]^{2+}$, and $[\text{Sr}(\text{H}_2\text{O})_n]^{2+}$ with $n \leq 10$, although some investigations on $n \leq 18$ cluster ions have also been conducted. A comparison between the binding energy of $[\text{Mg}(\text{H}_2\text{O})_n]^{2+}$, $[\text{Ca}(\text{H}_2\text{O})_n]^{2+}$, and $[\text{Sr}(\text{H}_2\text{O})_n]^{2+}$ determined in this experimental work and the energy measured experimentally in the literature are reported in Tables 7.3.1-7.3.3. The data in [26, 16, 37, 27] are binding enthalpies calculated by using the experimental results and parameters (vibrational frequencies and rotational constants) derived by quantum mechanical calculations. The experimental results consist of threshold cross section measurements from an experiment involving three steps: electrospray ionisation (ESI),

threshold collision induced dissociation (TCID) using xenon as collision gas, and guided ion beam mass spectrometry (GIBMS). The data in [38, 39, 40, 41] are binding enthalpies; the methodology implies an experiment to determine the threshold dissociation energy and then the derivation of the dissociation enthalpy by using some parameters (vibrational frequencies and transition dipole moments) obtained by theoretical calculations. The experiment consists in using ESI and a Fourier transform mass spectrometer, and by performing blackbody infrared radiation dissociation (BIRD) in order to acquire the threshold dissociation energies from the Arrhenius parameters within a temperature range. The data in [24, 28] are binding enthalpies, the thermochemical data was obtained from van't Hoff plots of the data derived by equilibrium experiments using high pressure mass spectrometry techniques (HPMS). More precisely, the experiment consists in preparing the sample with ESI, in performing an equilibrium experiment in a reaction chamber, and in measuring both the production and the reactant ion intensity signal at a particular temperature by using a triple quadrupole mass spectrometer. The comparison between $[\text{Mg}(\text{H}_2\text{O})_n]^{2+}$ cluster ions data in Table 7.3.1 suggests that there is agreement with the data of [26] at $9 \leq n \leq 10$, whereas the other results in [40, 24, 28] are higher. The comparison between $[\text{Ca}(\text{H}_2\text{O})_n]^{2+}$ cluster ions data in Table 7.3.2 shows that there is not agreement with the literature data at $n \leq 17$, whereas there is agreement for $n = 8$ with [37, 27], for $n = 9$ with [37], for $n = 10$ with [40], and for $n = 14$ with [28]. The comparison of $[\text{Sr}(\text{H}_2\text{O})_n]^{2+}$ cluster ions data in Table 7.3.3 shows that there is not agreement with the literature data in [38, 39, 24, 28, 16] because such data are all higher than the results of this work. The discordant experimental results may be the consequence of the observations of different isomers and that the data in the literature measured binding energies for breaking two hydrogen bonds. The experimental studies in [42, 29] provide some evidence that Mg^{2+} and Ca^{2+} solvated in water favor one hydrogen bonding when forming small cluster ions. These findings were attributed to the effects of Mg^{2+} in disrupting the hydrogen bond networks of the water up to $n = 32$, whereas Ca^{2+} and Sr^{2+} do not manifest these characteristic [42]. In fact, the effect of the metal ion size on the hydration is investigated by infrared multiple photon dissociation (IRMPD) action spectra, where the clusters $[\text{Mg}(\text{H}_2\text{O})_n]^{2+}$ and $[\text{Ca}(\text{H}_2\text{O})_n]^{2+}$ for $n \leq 32$ [42], and $[\text{Ca}(\text{H}_2\text{O})_n]^{2+}$ for $11 \leq n \leq 69$ [29] were formed by ESI and isolated by a Fourier transform ion cyclotron resonance mass spectrometer. The results in [29] suggest that one hydrogen bond is preferred for $[\text{Ca}(\text{H}_2\text{O})_n]^{2+}$ until $n \sim 18$, although two hydrogen bonds may be accepted by the outermost molecules in the solvation shells [42], and that from $n \sim 30$ the water molecules would only accept two hydrogen bonds. Moreover, the experi-

mental observations [42] indicate that for large clusters from $n \sim 32$, the water molecules have the majority of the outer molecules binding with one hydrogen bond in Mg^{2+} , and two hydrogen bonds in Ca^{2+} and in Sr^{2+} [42]. A density functional theory (B3LYP) [20] has investigated the number of hydrogen bonds involved when adding the first ligand to the first coordination shell. The results have shown that the first water molecule will add by forming two hydrogen bonds with the first solvent shell for $[\text{Mg}(\text{H}_2\text{O})_n]^{2+}$ $n = 4, 6$ and $\text{CN} = 4, 5, 6$; or by coordinating with one hydrogen bond for $[\text{Mg}(\text{H}_2\text{O})_n]^{2+}$ at $n = 5$. Moreover, when the first solvation shell of $[\text{Mg}(\text{H}_2\text{O})_n]^{2+}$ is completed at $n = 6$, two or three water molecules will add two hydrogen bonds [20]. A further study on $[\text{Mg}(\text{H}_2\text{O})_n]^{2+}$ structures (quantum chemical calculations) [26] has shown structures for $7 \leq n \leq 10$, where the molecules in the second solvation shell bind through two hydrogen bonds; the few exceptions are two isomers where one or two water molecules add to $[\text{Mg}(\text{H}_2\text{O})_6]^{2+}$ with one hydrogen bond. A full comparison of our results with the findings in [26, 42, 29, 20] is not possible, owing to different cluster sizes investigated in the various works and different experimental or theoretical conditions; nevertheless, the literature does not rule out the possibility of structures formed by molecules binding through one hydrogen bond, which is in agreement with the findings of this work.

$[\text{Mg}(\text{H}_2\text{O})_n]^{2+} \rightarrow [\text{Mg}(\text{H}_2\text{O})_{n-1}]^{2+} + \text{H}_2\text{O}$										
n	E_b (kJ mol ⁻¹)	E (kJ mol ⁻¹)								
	This work	[26] ^a	[26] ^b	[38] ^a	[39] ^a	[39] ^b	[40] ^a	[40] ^b	[24] ^c	[28] ^b
3		226.2	229.4							
4		178.3	180.7							
5		116.1	119.5		106	110				
6		97.4	100.1	98.4, 88.4	98.4, 88.4	101, 98.0				103
7		70.3	73.3		73.3	78.3				85.0
8	54 ± 18	67.4	71.2				76	79	64	75.4
9	52 ± 15	59.0	63.3				67	71	63	71.2
10	48 ± 16	44.1	44.6				52	53	63	65.7
11	45 ± 4.6								59	59.9
12	46 ± 7.5								59	54.0
13	44 ± 15									51.5
14										50.6

Table 7.3.1: Binding energies determined in these experiments for $[\text{Mg}(\text{H}_2\text{O})_n]^{2+}$ clusters and those experimental available from literature ($1 \leq n \leq 14$). Superscripts indicate the temperature at which the binding energy has been determined: at 0 K for a, at 298 K for b, and at 300 K for c

$[\text{Ca}(\text{H}_2\text{O})_n]^{2+} \rightarrow [\text{Ca}(\text{H}_2\text{O})_{n-1}]^{2+} + \text{H}_2\text{O}$		E (kJ mol ⁻¹)											
n	E_b (kJ mol ⁻¹)	[38] ^a	[39] ^a	[39] ^b	[40] ^a	[40] ^b	[24] ^c	[28] ^b	[37] ^a	[37] ^b	[27] ^a	[27] ^b	[41] ^a
	This work												
1											242.7	247.3	
2											197.4	199.0	
3											169.7	171.0	
4	125 ± 17										140.6	142.4	
5	98 ± 13		110	111				112.8	115.0	111.8	114.0	110	110
6	70 ± 11	90.5	90.5	92.1			106	88.9	90.7	98.8	100.3	91.7	91.7
7	65 ± 16		68.7	70.3, 74.1			70.8	60.0	63.7	59.3	63.0	68.7	68.7
8	62 ± 6.0				70	73	67.4	58.9	63.3	57.0	61.4		
9	55 ± 5.1				60	64	64.1	57.8	62.1		62		
10	49 ± 7.2				49	49	60.7						
11	48 ± 7.0						59	55.7					
12	44 ± 6.4						58	54.4					
13	43 ± 2.4						51.9						
14	46 ± 4.3						49.8						

Table 7.3.2: Binding energies determined in these experiments for $[\text{Ca}(\text{H}_2\text{O})_n]^{2+}$ clusters and those experimental ones from literature ($1 \leq n \leq 14$). Superscripts indicate the temperature at which the binding energy has been determined: at 0 K for a, at 298 K for b, and at 300 K for c

$[\text{Sr}(\text{H}_2\text{O})_n]^{2+} \rightarrow [\text{Sr}(\text{H}_2\text{O})_{n-1}]^{2+} + \text{H}_2\text{O}$								
n	E_b (kJ mol ⁻¹)	E (kJ mol ⁻¹)						
		This work	[38] ^a	[39] ^a	[39] ^b	[24] ^c	[28] ^b	[16] ^a
1							201.3	205.6
2							172.1	173.1
3							144.2	145.7
4							124.2	125.2
5			99.7	100			102.6	104.4
6		86.3	86.3	87.5		95.1	93.6	94.7
7	54 ± 6.8		70.3	71.6		71.2		
8	39 ± 12					67.4		
9	41 ± 4.7				62	64.9		
10	36 ± 4.2				59	62.4		
11	35 ± 12				59	59.4		
12	45 ± 2.4				57	57.4		
13	37 ± 0.95					54.4		

Table 7.3.3: Binding energies determined in these experiments for $[\text{Sr}(\text{H}_2\text{O})_n]^{2+}$ clusters and those experimental ones from literature ($1 \leq n \leq 13$). Superscripts indicate the temperature at which the binding energy has been determined: at 0 K for a, at 298 K for b, and at 300 K for c

7.4 Related Theoretical Work

In this section, theoretical data available from the literature is compared with the experimental data of this work (*cf.* Section 4.5 on page 89).

The binding energies are shown in Table 7.4.1 for $[\text{Sr}(\text{H}_2\text{O})_n]^{2+}$, in Tables 7.4.2, 7.4.3, and 7.4.4 for $[\text{Ca}(\text{H}_2\text{O})_n]^{2+}$, and in Tables 7.4.4 and 7.4.5 for $[\text{Mg}(\text{H}_2\text{O})_n]^{2+}$.

The theoretical investigations were performed on small clusters:

- $[\text{Mg}(\text{H}_2\text{O})_n]^{2+}$ for $1 \leq n \leq 10$ and $n = 18$ [26, 43, 20, 44, 45, 46, 47, 17, 18, 19, 48, 49, 50, 51, 52],
- $[\text{Ca}(\text{H}_2\text{O})_n]^{2+}$ for $1 \leq n \leq 9$ and $n = 18$ [43, 37, 20, 44, 18, 19, 53, 49, 50, 27, 54, 55], and
- $[\text{Sr}(\text{H}_2\text{O})_n]^{2+}$ for $1 \leq n \leq 6$ [16, 18, 19, 53, 50, 27, 56].

The theoretical data shown in Tables 7.4.1-7.4.4 were calculated by using [16] *ab initio* method and density functional theory (DFT), where it were included zero-point energy (ZPE) corrections with full counterpoise (cp) method; [19] *ab initio* method, BSSE was approximately treated with cp method of Boys and Bernardi, ZPE, and enthalpy corrections were evaluated using standard

statistical mechanical expression; [50] *ab initio* method with either valence-electron calculations with single polarisation function – TZ1P – basis (VE1P) or all-electron calculations with TZ1P basis (AE1P); [18] self consistent field (SCF) bond energies were confirmed using the modified coupled-pair functional (MCPF) approach; [53] *ab initio* uncontracted correlated calculations; [37] *ab initio* and DFT, by including ZPE and thermal corrections to 298 K both with and without BSSE corrections iwth cp method; [20] DFT method; [49] *ab initio* method where ZPE and finite temperature corrections to 298.15 K and 1 atm were included; [43] *ab initio* molecular orbital studies; [27] *ab initio* and DFT, with thermal corrections to 298 K with BSSE corrections; [54] *ab initio* and DFT methods where BSSE was corrected with cp method; [55] *ab initio* and DFT methods where BSSE was corrected with cp method; [44] *ab initio* and DFT methods with BSSE included; [26] *ab initio* and DFT methods, with and without BSSE corrections with cp method.

The theoretical bond energies for $[\text{Mg}(\text{H}_2\text{O})_n]^{2+}$ and $[\text{Sr}(\text{H}_2\text{O})_n]^{2+}$ are all higher for each n than the binding energies determined in these experiments. The theoretical bond energies for $[\text{Ca}(\text{H}_2\text{O})_n]^{2+}$ are all higher than the binding energies obtained in these experiments except for few data in which an agreement is found; the theoretical data similar to the data in this experimental work are at $n = 5, 6, 7$ in [20], $n = 8$ in [54], and $n = 9$ in [43].

		$n = 1$					
		2	3	4	5	6	
$[\text{Sr}(\text{H}_2\text{O})_n]^{2+} \rightarrow [\text{Sr}(\text{H}_2\text{O})_{n-1}]^{2+} + \text{H}_2\text{O}$							
This work							57 ± 3.0
[16]	M06	195, (196)	167, (169)	148, (150)	131, (133)	111, (113)	100, (102)
	B3LYP	191, (192)	165, (166)	146, (148)	130, (131)	104, (106)	93, (95)
	B3P86	194, (195)	166, (167)	147, (149)	130, (132)	104, (106)	93, (95)
	MP2(full)	180, (186)	158, (163)	142, (148)	127, (134)	108, (116)	98, (109)
[16]	M06	195, (196)	167, (169)	148, (150)	130, (132)	111, (113)	101, (103)
	B3LYP	193, (193)	166, (167)	147, (149)	130, (132)	104, (106)	93, (95)
	B3P86	194, (195)	167, (168)	148, (150)	130, (132)	104, (106)	93, (95)
	MP2(full)	183, (188)	160, (166)	144, (151)	130, (137)	109, (117)	101, (110)
[16]	M06	195, (198)	169, (172)	148, (151)	130, (133)	111, (114)	101, (105)
	B3LYP	197, (200)	171, (175)	150, (154)	132, (136)	105, (110)	94, (99)
	B3P86	197, (200)	171, (174)	149, (153)	131, (135)	105, (109)	93, (97)
	MP2(full)	188, (194)	166, (172)	147, (154)	132, (139)	110, (118)	100, (110)
[16]	BH&HLYP	199, (202)	166, (166)	151, (151)	132, (132)	105, (106)	95, (95)
[19]	MP2/6-31 + G*	198 ^a , 198	174 ^a , 173	(156) ^a , 156	141 ^a , 141	116 ^a , 117	106 ^a , 107
[50]	SCF/VE1P	(181) ^a , 190	(166) ^a , 173	(154) ^a , 161	(137) ^a , 144		116
[18]	SCF/TZP	(187) ^a , 195	(168) ^a , 175	(152) ^a , 159			
[53]	MP2/656p5dIf	(198) ^a , 208	(179) ^a , 186				
[53]	MP4SDTQ/656p5dIf	206 ^a					

Table 7.4.1: Binding energies determined in this experiment for $[\text{Sr}(\text{H}_2\text{O})_n]^{2+}$ clusters and theoretical ones available from the literature ($1 \leq n \leq 6$) in kJ mol^{-1} . [16], [19] at 298 K and [18], [53], [50] at 0 K. In parenthesis are single point energies that do not include cp corrections. Superscript a indicates that the values have been corrected to the 298 K by the authors of [16]. The basis sets for the MP2 in [53] is uncontracted group two augmented by one f-function. The basis sets for single point energies in [16] are HW*/6-311 + G(2d, 2p), SD/6-311 + G(2d, 2p), or Def2TZVPP

	n = 1	2	3	4	5	6	7	8	9	
	$[\text{Ca}(\text{H}_2\text{O})_n]^{2+} \rightarrow [\text{Ca}(\text{H}_2\text{O})_{n-1}]^{2+} + \text{H}_2\text{O}$									
This work										
[37]	228, (229)	197, (199)	172, (174)	125 ± 17	98 ± 13	70 ± 11	65 ± 16	62 ± 6.0	55 ± 5.1	
[37]	229, (230)	197, (199)	172, (174)	148, (149)	114, (115)	102, (104)	74, (77)	77, (80)	73, (76)	
[37]	228, (230)	196, (198)	171, (173)	147, (149)	113, (116)	101, (104)	74, (77)	77, (80)	73, (76)	
[37]	212, (216)	188, (194)	168, (174)	146, (148)	114, (116)	101, (104)	77, (80)	79, (82)	75, (78)	
[37]	234, (234)	200, (200)	173, (173)	147, (152)	120, (127)	108, (117)	73, (82)	76, (85)	72, (81)	
[37]	234, (235)	199, (200)	172, (173)	147, (148)	113, (113)	101, (102)	74, (75)	77, (78)	73, (74)	
[37]	220, (224)	193, (198)	171, (175)	147, (147)	113, (113)	101, (102)	77, (78)	78, (80)	75, (76)	
[37]	219, (222)	193, (196)	171, (173)	149, (155)	120, (126)	109, (117)	77, (86)	79, (88)	75, (84)	
[20]*	(236)	(200)	(177)	151	(118)	(105)	(77)	(39)		
[19]*	224	198	179	157	126	114				
[49]*	(220)	(196)	(177)	(157)	(129)	(117)				
[43]*	(235)	(216)	(200)	(170)	(143)	(133)	(90)	(85)	(57)	
[27]	242	201	174	148	113	102	76	77	74	
[27]	243	201	173	147	113	102	77	80	81	
[27]	230	196	173	152	120	109	74	76	77	
[27]	241	204	178	153	119	108				

Table 7.4.2: Binding energies in kJ mol^{-1} determined in these experiments for $[\text{Ca}(\text{H}_2\text{O})_n]^{2+}$ clusters and those theoretical available from literature ($1 \leq n \leq 9$). The theoretical data are at 298 K. Values in parenthesis do not include BSSE corrections. In [37] either 6-311+G(2d,2p) or aug-cc-pVTZ basis sets are used. The data reported for the references with superscript * are those computed in [37] by adjusting the original data to 298 K

		$[\text{Ca}(\text{H}_2\text{O})_n]^{2+} \rightarrow [\text{Ca}(\text{H}_2\text{O})_{n-1}]^{2+} + \text{H}_2\text{O}$										
		n = 1	2	3	4	5	6	7	8	18		
This work					125 ± 17	98 ± 13	70 ± 11	65 ± 16	62 ± 6.0	40 ± 5.9		
[49]	EFP/6-31+G*	220	196	177	156	129	116					
[49]	RHF/6-31+G*	230	201	180	157	126	113					
[49]	MP2/6-31+G*	243	214	187	166	137	128					
[50]	SCF/AEIP	216	198	181	161		128					
[54]	MP2/6-311+G**	237	211	185	165	120	117	52	55			
[54]	B3LYP/6-311+G**	247	200	179	159	128	114	74	68			
[55]	BLYP/6-311+G**	236	199	186	149	108	101	53	52			
[20]	B3LYP/6-311+G(2d,2p)	238	199	175	149	86.7, 92.5, 116	90.5, 77.5, 78.7, 103	68.2, 73, 7, 57.8	36.8	54.0		
[44]*	CCSD(T)/6-31+G(d)	217	189	169	148	119	108					
[44]*	G3	228	199	176	156	130	120					

Table 7.4.3: Binding energies determined in these experiments for $[\text{Ca}(\text{H}_2\text{O})_n]^{2+}$ clusters and those theoretical available from literature ($1 \leq n \leq 18$). Data are in kJ mol^{-1} . The data in [20] are at 0 K and for [44]* are data from [44] taken from [27]. Data in [44, 54, 55] include cp corrections for BSSE

$[M(H_2O)_n]^{2+} \rightarrow [M(H_2O)_{n-1}]^{2+} + H_2O$		where		M = Mg or M = Ca								
[44]												
M^{2+}	n	This work	B3LYP			MP2(full)			CCSD(T)		G3	
			6-31+G(d)	6-31++G(d,p)	6-31++G(2d,2p)	6-31++G(3d,3p)	6-31+G(d)	6-31++G(d,p)	6-31++G(2d,2p)	6-31++G(3d,3p)		6-31+G(d)
Mg ²⁺	1	343.26	339.92	342.09	345.10	326.92	317.51	322.70	327.59	321.86	313.79	335.95
	2	302.51	302.59	301.88	302.59	291.72	286.71	288.46	290.59	287.54	283.45	297.28
	3	243.61	240.02	240.31	241.40	241.23	233.54	235.92	238.22	236.63	232.28	237.22
	4	193.37	191.24	190.11	190.69	195.54	190.02	191.61	193.24	190.73	189.40	196.13
	5	126.49	127.16	124.48	125.36	131.54	130.79	131.50	132.26	129.58	130.08	134.51
	6	105.21	96.73	97.23	98.69	101.66	103.08	102.74	104.33	100.95	102.91	111.40
Ca ²⁺	1	223.09	242.27	238.30	241.14	212.64	223.38	221.50	225.51	211.22	220.12	224.13
	2	202.40	206.99	201.02	202.14	198.55	198.34	194.58	196.92	197.71	195.92	197.67
	3	180.20	186.64	182.54	184.42	176.48	179.28	177.69	179.95	175.85	177.27	176.02
	4	157.38	158.80	154.91	154.74	157.84	156.71	154.79	156.04	157.75	155.45	155.08
	5	125.36	124.19	120.05	120.34	130.21	127.28	126.49	128.03	130.96	126.74	128.45
	6	101.45	98.56	96.31	96.68	107.59	104.50	104.58	105.84	108.43	104.42	110.14

Table 7.4.4: Sequential binding energies values in kJ mol^{-1} determined in these experiments for $[Ca(H_2O)_n]^{2+}$ clusters and those theoretical available for $[M(H_2O)_n]^{2+}$ where $M = \text{Mg}$ and $M = \text{Ca}$ calculated at various level of theory in [44]. BSSE corrections for CCSD(T) calculations are taken from MP2 method

		$[\text{Mg}(\text{H}_2\text{O})_n]^{2+} \rightarrow [\text{Mg}(\text{H}_2\text{O})_{n-1}]^{2+} + \text{H}_2\text{O}$							
This work		[26]						[20]	[44]*
n		B3LYP/6-311+G(2d,2p)		B3LYP/pCVTZ		MP2/6-311+G(2d,2p)		B3LYP/6-311+G(2d,2p)	G3
1		339	(341)	348	(348)	319	(325)	341	337
2		293	(297)	298	(297)	280	(289)	297	299
3		231	(234)	235	(236)	225	(234)	230	240
4		182	(185)	184	(185)	183	(192)	183	198
5		117	(120)	115	(116)	122	(133)	99.3, 102, 117	138
6		105	(109)	105	(106)	113	(125)	99.3, 87.1, 82.1, 102	131
7		76	(79)	79	82	75	(84)	75.4, 79.6, 16.3	
8	54 ± 18	81	(84)	84	86	81	(90)	64.1	
9	52 ± 15	78	(81)	81	83	78	(86)		
10	48 ± 16	55	(58)	57	60	54	(63)		
18								54.8	

Table 7.4.5: Binding energies determined in these experiments for $[\text{Mg}(\text{H}_2\text{O})_n]^{2+}$ clusters and those theoretical available from literature ($1 \leq n \leq 18$) in kJ mol^{-1} . Values in parenthesis do not include cp corrections. Data for [26] and [44]* are at 298 K. Superscript indicates that data from [44] adjusted for ZPE and thermal effects by [26]

Interestingly, it has been suggested that more than eight water molecules would be required to approach the experimental value of the free energy of hydration in $[\text{Mg}(\text{H}_2\text{O})_n]^{2+}$ [47], which is probably in accordance with what it is expected from the suggested trend of the investigations of this work on $[\text{Mg}(\text{H}_2\text{O})_n]^{2+}$. Furthermore, the studies of $[\text{Mg}(\text{H}_2\text{O})_n]^{2+}$ in [45, 19, 49, 50], of $[\text{Ca}(\text{H}_2\text{O})_n]^{2+}$ in [19, 53, 49, 50], and of $[\text{Sr}(\text{H}_2\text{O})_n]^{2+}$ in [19, 53, 50] for $1 \leq n \leq 8$ have stressed the difficulties that *ab initio* theoretical procedures have in investigating the interactions amongst the ion and the molecules in the solvation shells, on one hand, and amongst the molecules in the different solvent shells, on the other hand.

7.5 A Note on Coordination Numbers

This work does not produce any evidence about possible geometrical structures of cluster ions (Section 4.5 on page 89); nonetheless, some examples of the lowest energy isomers calculated by theoretical methods are presented in order to have an overview of the theoretical CN for $[\text{Mg}(\text{H}_2\text{O})_n]^{2+}$, $[\text{Ca}(\text{H}_2\text{O})_n]^{2+}$, and $[\text{Sr}(\text{H}_2\text{O})_n]^{2+}$. The geometries of several isomers have been computed with *ab initio* or DFT methods for Mg^{2+} , Ca^{2+} , and Sr^{2+} solvated by a number of water molecules in the range $1 \leq n \leq 10$ in [26, 38, 39, 43, 16, 37, 20, 57, 58, 47, 51, 18, 53, 50, 21, 27, 54] and for $n = 18$ in [20, 58, 48]. Tables 7.5.1-7.5.5 below (where decimal data are the result on an average) summarise some data from the literature.

CN	[26]	[38]	[43]	[37]	[20]	[44]	[47]	[50]	[21]	[27]	[59]	[60]
$[\text{Mg}(\text{H}_2\text{O})_n]^{2+}$	5, 6				6	6	6	6	6			
$[\text{Ca}(\text{H}_2\text{O})_n]^{2+}$		6	6-8	6-8	6-7	6	6	6	6-8	6	8.3, 9.2, 10	8, 9.1
$[\text{Sr}(\text{H}_2\text{O})_n]^{2+}$								6	7-8			

Table 7.5.1: Examples of coordination numbers for $[\text{Mg}(\text{H}_2\text{O})_n]^{2+}$, $[\text{Ca}(\text{H}_2\text{O})_n]^{2+}$, and $[\text{Sr}(\text{H}_2\text{O})_n]^{2+}$ from theoretical literature

CN	This work	[26]	[39]	[42]	[29]	[57]	[28]	[5]	[37]	[45]
$[\text{Mg}(\text{H}_2\text{O})_n]^{2+}$		6	6	6-7			6	6	6	6
$[\text{Ca}(\text{H}_2\text{O})_n]^{2+}$			6	6-7	8	6	6		6	
$[\text{Sr}(\text{H}_2\text{O})_n]^{2+}$			6				6-7			

Table 7.5.2: Examples of coordination numbers for $[\text{Mg}(\text{H}_2\text{O})_n]^{2+}$, $[\text{Ca}(\text{H}_2\text{O})_n]^{2+}$, and $[\text{Sr}(\text{H}_2\text{O})_n]^{2+}$ from experimental literature

CN	[61]	[62]	[63]	[64]	[65]	[66]	[67]	[68]	[69]	[70]	[54]	[71]	[72]	[73]	[74]	[75]	[76]
Mg^{2+}					6			6.8						6		6	6
Ca^{2+}	5.5	6.4, 7.2, 10.0	6	8.0, 8.2	6.9		6	6	7	7	5-10	6, 8	8	6	6	7	
Sr^{2+}							8	8									8

Table 7.5.3: Examples of coordination numbers for Mg^{2+} , Ca^{2+} , and Sr^{2+} from literature on crystal structure from aqueous solution measurements with spectroscopic methods

CN	[56]	[65]	[18]	[77]	[59]	[78]	[79]	[80]	[81]	[82]	[72]	[83]	[84]	[55]	[85]	[86]
Mg ²⁺	5.1, 6		6	6.2								6			6	6.0
Ca ²⁺	6, 7	9.0		8.0	8.3, 9.2	8	7, 8	7, 8, 9	7.1, 7.6, 8.1	7.9	8		6, 7, 8	8	9, 10	8.0
Sr ²⁺				9.1												

Table 7.5.4: Examples of coordination numbers for Mg²⁺, Ca²⁺, and Sr²⁺ from literature on simulations of condensed phase metal ions solvated in water

More precisely, Tables 7.5.1-7.5.5 consider results from the literature on coordination numbers for divalent magnesium, calcium, and strontium ions solvated in water is given in In particular,

- Table 7.5.1 shows a few examples from the analysis on the coordination of the inner shell of the lowest energy isomers from *ab initio* theoretical computations;
- Table 7.5.2 presents a series of CN from gas phase experimental investigations;
- Table 7.5.3 lists results from the spectroscopic studies on concentrated aqueous solution by several different techniques (in particular, extended X-ray absorption fine structure spectrometry [69, 72, 74], X-ray diffraction [62, 65, 66, 67, 68, 54, 71, 73], large angle X-ray scattering [72], neutron diffraction studies [61, 70, 54], and proton NMR [76]);
- finally, Table 7.5.4 illustrates CN values from simulations (in particular, molecular dynamic simulations [65, 77, 78, 82, 72, 85], Car-Parrinello molecular dynamics simulations [56, 78, 79, 83, 84, 55], quantum mechanics/molecular mechanics molecular dynamics simulations [59, 80, 81], and Monte-Carlo simulations of statistical perturbation theory [86]).

The overall result is that there is a good agreement between CN determined with gas phase experiments, and that the common CN is 6 for all the dications. Theoretical results agree on the CN of gas phase experiments; in contrast, CN determined with spectroscopic methods on crystal structures and with molecular dynamics simulations disagree and are generally higher than the CN of gas phase experiments. *Ab initio* studies on $[\text{Ca}(\text{H}_2\text{O})_n]^{2+}$ with $1 \leq n \leq 9$ [43] have provided a series of isomers where Ca^{2+} can accommodate nine water molecules in the first solvation shell, even though coordination number six is the energetically preferred complex. In addition, *ab initio* calculations suggest that (6, 0) isomer is the lowest energy geometry for $[\text{Ca}(\text{H}_2\text{O})_n]^{2+}$ with $1 \leq n \leq 9$ [37, 27] where the notation (x, y) stands for describing a cluster geometry in which x molecules are in the first solvation shell and y molecules are in the second solvation shell. Furthermore, it has also been found that the energy difference among isomers (6, 1) and (7, 0), and among (6, 2), (7, 1), and (8, 0) are small [43]. Few studies have been reported for $[\text{Mg}(\text{H}_2\text{O})_n]^{2+}$ with $1 \leq n \leq 18$. Noticeably, a model has been proposed for $n = 18$ by density functional theory (DFT) [20] and *ab initio* analysis in [48] (and references therein) in which $[\text{Mg}(\text{H}_2\text{O})_6(\text{H}_2\text{O})_{12}]^{2+}$ has an inner shell completed with six water molecules,

and the second solvent shell filled with twelve water molecules. Moreover, the structure of $[\text{Mg}(\text{H}_2\text{O})_6]^{2+}$ has been investigated. Two isomers were observed experimentally from blackbody infrared radiative dissociation [38] and collisional induced dissociation [39] for $[\text{Mg}(\text{H}_2\text{O})_6]^{2+}$: (4, 2) and (6, 0). In addition, the authors of [39] have indicated that it is probable that the structure of $[\text{Mg}(\text{H}_2\text{O})_5]^{2+}$ is (4, 1). Other geometries for $[\text{Mg}(\text{H}_2\text{O})_6]^{2+}$ have been proposed: (4, 2) [39, 44, 47, 17, 50], (6, 0) [44, 47, 17], and (5, 1) [38, 39, 47, 17, 44]; whereas the lowest energy structure was suggested to be (6, 0) [38, 39, 47, 17, 44]. The experimental results in [26] (threshold collision induced dissociation method) have provided $\text{CN} = 6$, although DFT [38, 46] and quantum mechanical calculations [39] suggest CN to be either 5 or 6. Furthermore, it was not possible to optimize a configuration neither with eight water molecules directly bound to Mg^{2+} [47] nor with seven [17]. The infrared laser action spectrometry experiments in [29] on $\text{Ca}^{2+}(\text{H}_2\text{O})_n$ with $11 \leq n \leq 69$ had the aim to provide an insight into Ca^{2+} solvation in the bulk environment. The results suggest that if the number of water molecules is $n \leq 11$ then Ca^{2+} acquires $\text{CN} = 6$, whereas if Ca^{2+} is solvated by $n \geq 12$ water molecules then $\text{CN} = 8$. Although the study performed in [29] is for Ca^{2+} in the presence of a large number of water molecules $11 \leq n \leq 69$, and the investigation has been conducted in the gas phase, the results contrast with those presented in our gas phase experiments. In fact, in [29] it is stated that $[\text{Ca}(\text{H}_2\text{O})_n]^{2+}$ for $12 \leq n \leq 69$ has the predominant geometry with $\text{CN} = 8$, whereas in this work it has been observed that $[\text{Ca}(\text{H}_2\text{O})_n]^{2+}$ for $4 \leq n \leq 20$ has the preferred geometry with $\text{CN} = 6$. Nonetheless, Tables 7.5.3 and 7.5.4 show that $[\text{Ca}(\text{H}_2\text{O})_n]^{2+}$ may adopt $6 \leq \text{CN} \leq 10$. It is also worth mentioning that in a molecular dynamics simulation study [85] it has been observed that, when comparing Li^+ , Cs^+ , Mg^{2+} , and Ca^{2+} , the change in the hydration shell structure with increasing ion size depends on the charge on the ion.

The coordination numbers observed in the solid state for Mg^{2+} , Ca^{2+} , and Sr^{2+} based on the analysis of the available data on crystal structures from the Cambridge Structural Database (CSD) [43, 17, 48, 87, 51] and Protein Databank (PDB) [43, 17, 87] are listed in Table 7.5.5.

More precisely, Table 7.5.5 reports

- the highest number of entries on CSD and PDB for structures containing a bond between the metal ion and O, N, S, Cl and/or Br for Ca^{2+} [43] and Mg^{2+} [17];
- CSD entries for metal ion binding to elements O, N, S for Mg^{2+} and Ca^{2+} [51];

CN								
	[43] ^a	[43] ^b	[17]	[48]	[87] ^c	[87] ^d	[87] ^e	[51]
Mg ²⁺			3, 4, 5, 6, 7, 8	6	6, 4	6	6	3, 4, 5, 6, 7
Ca ²⁺	4, 5, 6, 7, 8, 9, 10	3, 4, 5, 6, 7, 8, 9, 10			6, 7	7	7, 6, 8	3, 4, 6, 7, 8, 9, 10
Sr ²⁺					8, 6		8	

Table 7.5.5: Highest number of entries on CSD and PDB for structures containing: bond between the metal ion and oxygen [43]^a and bond between the metal ion and O, N, S, Cl and/or Br ([43]^b, [17]). Highest number of entries on CSD [87]^c and PDB [87]^d. Highest number of entries on CSD for water complexes [87]^e. Entries on CSD containing metal ion bond to element O, N, S [51]. In bold are the predominant coordination numbers in [43, 17, 87, 51]. Entries on CSD of Mg²⁺ octahedral coordinated with water [48]

- the highest number of entries on CSD and PDB for structures containing a bond between the metal ion and oxygen [43];
- the highest number of entries on CSD, on PDB, and for water complexes for Mg²⁺, Ca²⁺ and Sr²⁺ [87].

The general result from the analysis of the databases have revealed that Mg²⁺ has a preference to directly bind to six ligands, Ca²⁺ favours either six, seven, or eight ligand, and Sr²⁺ favours eight ligands. In addition, the results show that calcium can have up to ten molecules directly coordinated, but that CN = 6, 7, 8 result to be the predominant coordination numbers from CSD, whereas CN = 7 is the preferred from PDB structures. Moreover, it has been found [43, 51] that divalent calcium ion prefers to bind to the oxygen atom of a ligand rather than to nitrogen, chlorine, or bromine, and that rarely binds to sulphur. The investigations on divalent magnesium on the CSD for crystal structures [17, 48] have found that in an aqueous environment this ion prefers to coordinate with six groups and preferably to oxygen containing ligands. Furthermore, the investigations on the crystal structure in which magnesium dication binds solely with water [17, 48] suggest that the ion acquires CN = 6 [17], and no geometries have been found with CN = 4 [17]. Noticeably, the coordination number of metal ion complexes is an important property in the understanding of the characteristics of the metal ion; but the preferred coordination for several metal cation appears to change depending on the environment, so that the CN of a metal ion and the factors determining the CN still remains ambiguous [87, 62].

7.6 Hydration of Monovalent Mg, Ca, and Sr Ions

To the best of our knowledge, no comprehensive information on the stepwise dissociation energy for (metastable) neutral ligand loss has been reported in

the literature for the hydrated Mg^+ , Ca^+ , and Sr^+ cations in the gas phase. As a result, it is not possible to provide a detailed comparison between the binding energy for the unimolecular metastable decay of divalent alkaline earth metals of this work and other experimental or theoretical sources investigating the respective monovalent metal ions. However, a few examples on binding energy may be found in the literature [18, 88, 89, 90, 91] for $[\text{Mg}(\text{H}_2\text{O})_n]^+$ for $n \leq 6$, [18, 91, 93] $[\text{Ca}(\text{H}_2\text{O})_n]^+$ for $1 \leq n \leq 3$ and [18, 92, 91, 52] for $[\text{Sr}(\text{H}_2\text{O})_n]^+$ for $1 \leq n \leq 11$. Experimental studies have determined the bond energy for $[\text{Sr}(\text{H}_2\text{O})_n]^+$ for $1 \leq n \leq 11$ and they are illustrated in Table 7.6.1, where the investigation in [92] proposes binding energies measured as enthalpies, which were derived from van't Hoff plots in high pressure mass spectrometry (HPMS) equilibrium experiments. In [52] DFT calculations at the B3LYP level were used to calculate D_e (dissociation energy measured from the bottom of the potential well) and D_0 (dissociation energy measured from the zero point level) by applying zero-point vibrational energy (ZPVE) corrections, whereas the B3LYP vibrational energies were used to correct D_e and D_0 values of the *ab initio* calculations at the RCCSDI(T) and UCCSD(T) levels of theory.

n	$[\text{Sr}(\text{H}_2\text{O})_n]^{2+}$	$[\text{Sr}(\text{H}_2\text{O})_n]^+$						
	This work	[92]	[18]		[52]			
			SCF/TZP	MCPF/ANO	B3LYP 6-311+G(2d,p)	CBS-Q	UCCSD(T)	RCCSD(T) aug-cc-pCVQZ
1		144	97.2	103	131(137)	127	127	131(137)
2		127	88.8	93.0				105(114)
3		107	71.2					
4		93						
5		86						
6		76						
7	54 ± 6.8	72						
8	39 ± 12	68						
9	41 ± 4.7	56						
10	36 ± 4.2	49						
11	35 ± 12	41						

Table 7.6.1: Comparison between experimentally determined binding energies in this work for $[\text{Sr}(\text{H}_2\text{O})_n]^{2+} \rightarrow [\text{Sr}(\text{H}_2\text{O})_{n-1}]^{2+} + \text{H}_2\text{O}$ and those available from the literature for $[\text{Sr}(\text{H}_2\text{O})_n]^+ \rightarrow [\text{Sr}(\text{H}_2\text{O})_{n-1}]^+ + \text{H}_2\text{O}$ ($1 \leq n \leq 11$). Data in [92] are determined at 300 K; for [52], data in parenthesis are D_e binding energies while the others are D_0 . [18] and [52] are examples chosen amongst theoretical studies.

The study on $[\text{Sr}(\text{H}_2\text{O})_n]^+$ has stressed that the stability of these clusters represent the importance of the valence electron of the central ion ($5s^1$) to promote chemical bonding with the water molecules. However, it is not possible to make a precise comparison between $[\text{Sr}(\text{H}_2\text{O})_n]^{2+}$ and $[\text{Sr}(\text{H}_2\text{O})_n]^+$ because the number of hydrogen bonds involved in the fragmentation of $[\text{Sr}(\text{H}_2\text{O})_n]^+$ is not

known from the discussion in [92]. In addition, the values at $n = 10$ and $n = 11$ have been extrapolated by the authors of [92]. Nevertheless, it is possible to conjecture that if the water molecules in $[\text{Sr}(\text{H}_2\text{O})_n]^+$ binds through one hydrogen bond then the comparison suggests that the bond between a water molecule and the cluster ion is stronger in the mono-charged than in the doubly charged clusters, which in turn would mean that (i) the presence of the double charge does not have a great effect on the binding energy for $7 \leq n \leq 11$, and that (ii) the presence of a single charge on the metal has a greater impact on the binding energy than a double charge owing to the presence of the valence electron. Moreover, it is possible to conjecture that if water molecules in $[\text{Sr}(\text{H}_2\text{O})_n]^+$ binds through two hydrogen bonds then the comparison indicates that the double charge in $[\text{Sr}(\text{H}_2\text{O})_n]^{2+}$ is having an effect on the binding interactions for $7 \leq n \leq 10$.

Bibliography

- [1] H.S. Frank, M.W. Evans, *Journal of Chemical Physics* 13 (1945) 507.
- [2] H.S. Frank, W.-Y. Wen, *Discussions of the Faraday Society* 24 (1957) 133.
- [3] A.W. Castleman Jr., R.G. Keesee, *Chemical Reviews* 86 (1986) 589.
- [4] S. Wei, Z. Shi, A.W. Castleman Jr., *Journal of Chemical Physics* 94 (1991) 8604.
- [5] P.E. Barran, N.R. Walker, A.J. Stace, *Journal of Chemical Physics* 112 (2000) 6173.
- [6] C. Lifshitz, F.A. Long, *Journal of Chemical Physics* 41 (1964) 2468.
- [7] J.R. Gilbert, A.J. Stace, *International Journal of Mass Spectrometry and Ion Physics* 15 (1974) 311.
- [8] A.J. Stace, A.K. Shukla, *Journal of the American Chemical Society* 104 (1982) 5314.
- [9] A.J. Stace, C. Moore, *Journal of the American Chemical Society* 105 (1983) 1814.
- [10] I. Wadsö, *Acta Chemica Scandinavica* 20 (1966) 536.
- [11] K.N. Marsh Ed., *Recommended Reference Materials For The Realisation Of Physicochemical Properties*, Blackwell, Oxford, 1987, pp. 3-113.
- [12] P.W. Atkins, *Physical Chemistry*, Oxford University Press, 6th edn., 1999, pp.921.
- [13] D.R. Lide, *Handbook Of Chemistry And Physics*, CRC Press, 85th edn., (2004-2005), ch.6, 112-113.

- [14] David R. Lide, ed., *CRC Handbook of Chemistry and Physics*, Internet Version 2005, <http://www.hbcpnetbase.com>, CRC Press, Boca Raton, FL, 2005. If a specific table is cited, use the format: "Physical Constants of Organic Compounds", in *CRC Handbook of Chemistry and Physics*, Internet Version 2005, David R. Lide, ed., <http://www.hbcpnetbase.com>, CRC Press, Boca Raton, FL, 2005.
- [15] Y. Marcus, *Chemical Reviews* 109 (2009) 1346.
- [16] D.R. Carl, B.K. Chatterjee, P.B. Armentrout, *Journal of Chemical Physics* 132 (2010) 044303.
- [17] C.W. Bock, A. Kaufman, J.P. Glusker, *Inorganic Chemistry* 33 (1994) 419.
- [18] C.W. Bauschlicher Jr., M. Sodupe, H. Partridge, *Journal of Chemical Physics* 96 (1992) 4453.
- [19] E.D. Glendening, D. Feller, *Journal of Physical Chemistry* 100 (1996) 4790.
- [20] M. Pavlov, P.E.M. Siegbahn, M. Sandström, *Journal of Physical Chemistry A* 102 (1998) 219.
- [21] I. Tunell, C. Lim, *Inorganic Chemistry*, 45 (2006) 4811.
- [22] C. Krekeler, L. Delle Site, *Journal of Physics: Condensed Matter* 19 (2007) 192101.
- [23] P.W. Atkins, *Physical Chemistry*, Oxford University Press, Oxford, 1999, 6th Ed., p. 945.
- [24] A.T. Blades, P. Jayaweera, M.G. Ikononou, P. Kebarle, *Journal of Chemical Physics* 92 (1990) 5900.
- [25] M. Peschke, A.T. Blades, P. Kebarle, *International Journal of Mass Spectrometry* 185/186/187 (1999) 685.
- [26] D.R. Carl, P.B. Armentrout, *ChemPhysChem: A European Journal of Chemical Physics and Physical Chemistry* 14 (2013) 681.
- [27] D.R. Carl, P.B. Armentrout, *Journal of Physical Chemistry A* 116 (2012) 3802.
- [28] M. Peschke, A.T. Blades, P. Kebarle, *Journal of Physical Chemistry A* 102 (1998) 9978.

- [29] M.F. Bush, R.J. Saykally, E.R. Williams, *Journal of the American Chemical Society* 130 (2008) 15842.
- [30] A.A. Shvartsburg, K.W.M. Siu, *Journal of the American Chemical Society* 123 (2001) 10071.
- [31] D.R. Carl, R.M. Moision, P. B. Armentrout, *International Journal of Mass Spectrometry* 20 (2009) 2312.
- [32] T.E. Cooper, P.B. Armentrout, *Journal of Physical Chemistry A* 113 (2009) 13742.
- [33] X. Chen, A.J. Stace, *Chemical Communications* 48 (2012) 10292.
- [34] X. Chen, A.J. Stace, *Journal of Physical Chemistry A* 117 (2013) 5015.
- [35] M. Beyer, E.R. Williams, V.E. Bondybey, *Journal of the American Chemical Society* 121 (1999) 1565.
- [36] K.G. Spears and F.C. Fehsenfeld, *Journal of Chemical Physics* 56 (1972) 5698.
- [37] D.R. Carl, R.M. Moision and P.B. Armentrout, *International Journal of Mass Spectrometry* 265 (2007) 308.
- [38] S.E. Rodriguez-Cruz, R.A. Jockusch, E.R. Williams, *Journal of the American Chemical Society* 121 (1999) 1986.
- [39] S.E. Rodriguez-Cruz, R.A. Jockusch, E.R. Williams, *Journal of the American Chemical Society* 121 (1999) 8898.
- [40] R.L. Wong, K. Paech, E.R. Williams, *International Journal of Mass Spectrometry* 232 (2004) 59.
- [41] S.E. Rodriguez-Cruz, R.A. Jockusch, E.R. Williams, *Journal of the American Chemical Society* 120 (1998) 5842.
- [42] M.F. Bush, J.T. O'Brien, J.S. Prell, C.-C. Wu, R.J. Saykally, E.R. Williams, *Journal of the American Chemical Society* 131 (2009) 13270.
- [43] A.K. Katz, J.P. Glusker, S.A. Beebe, C.W. Bock, *Journal of the American Chemical Society* 118 (1996) 5752.
- [44] J.S. Rao, T.C. Dinadayalane, J. Leszczynski, G.N. Sastry, *Journal of Physical Chemistry A* 112 (2008) 12944.

- [45] J.M. Martínez, R.R. Pappalardo, E.S. Marcos, *Journal of American Chemical Society* 121 (1999) 3175.
- [46] T. Dudev, C. Lim, *Journal of Physical Chemistry A* 103 (1999) 8093.
- [47] G.D. Markham, J.P. Glusker, C.L. Bock, M. Trachtman, C.W. Bock, *Journal of Physical Chemistry* 100 (1996) 3488.
- [48] G.D. Markham, J.P. Glusker, C.L. Bock, M. Trachtman, C.W. Bock, *Journal of Physical Chemistry* 106 (2002) 5118.
- [49] G.N. Merrill, S.P. Webb, D.B. Bivin, *Journal of Physical Chemistry A* 107 (2003) 386.
- [50] M. Klobukowski, *Canadian Journal of Chemistry* 70 (1992) 589.
- [51] C.W. Bock, A.K. Katz, G. D. Markham, J.P. Glusker, *Journal of the American Chemical Society* 121 (1999) 7360.
- [52] R.J. Plowright, T.J. McDonnell, T.G. Wright, J.M.C. Plane, *Journal of Physical Chemistry A* 113 (2009) 9354.
- [53] M. Kaupp, P.v.R. Schleyer, *Journal of Physical Chemistry* 96 (1992) 7316.
- [54] T. Megyes, T. Grósz, T. Radnai, I. Bakó, G. Pálinkás, *Journal of Physical Chemistry A* 108 (2004) 7261.
- [55] I. Bakó, J. Hutter, G. Pálinkás, *Journal of Chemical Physics* 117 (2002) 9838.
- [56] T. Ikeda, M. Boero, K. Terakura, *Journal of Chemical Physics* 127 (2007) 074503-1.
- [57] M.F. Bush, R.J. Saykally, E.R. Williams, *ChemPhysChem: A European Journal of Chemical Physics and Physical Chemistry* 8 (2007) 2245.
- [58] C.C. Pye, W.W. Rudolph, *Journal of Physical Chemistry A* 102 (1998) 9933.
- [59] A. Tongraar, K.R. Liedl, B.M. Rode, *Journal of Physical Chemistry A* 101 (1997) 6299.
- [60] F.M. Floris, M. Persico, A. Tani, J. Tomasi, *Chemical Physics Letters* 227 (1994) 126.

- [61] S. Cummings, J.E. Enderby, R.A. Howe, *Journal of Physics C: Solid State Physics* 13 (1980) 1.
- [62] N.A. Hewish, G.W. Neilson, J.E. Enderby, *Nature* 297 (1982) 138.
- [63] G. Licheri, G. Piccaluga, G. Pinna, *Journal of Chemical Physics* 64 (1976) 2437.
- [64] J.N. Albright, *Journal of Chemical Physics* 56 (1972) 3783.
- [65] M.M. Probst, T. Radnai, K. Heinzinger, P. Bopp, B.M. Rode, *Journal of Physical Chemistry* 89 (1985) 753.
- [66] N.T. Skipper, G.W. Neilson, S.C. Cummings, *Journal of Physics: Condensed Matter* 1 (1989) 3489.
- [67] R. Caminiti, A. Musinu, G. Paschina, G. Pinna, *Journal of Applied Crystallography* 15 (1982) 482.
- [68] J.A. Albright, *Journal of Chemical Physics* 56 (1972) 3783.
- [69] J.L. Fulton, S.M. Heald, Y.S. Badyal, J.M. Simonson, *Journal of Physical Chemistry A* 107 (2003) 4688.
- [70] Y.S. Badyal, A.C. Barnes, G.J. Cuello, J.M. Simonson, *Journal of Physical Chemistry A* 108 (2004) 11819.
- [71] G. Licheri, G. Piccaluga, G. Pinna, *Journal of Chemical Physics* 63 (1975) 4412.
- [72] F. Jalilehvand, D. Spångberg, P. Lindqvist-Reis, K. Hermansson, I. Persson, M. Sandström, *Journal of American Chemical Society* 123 (2001) 431.
- [73] R. Caminiti, G. Licheri, Piccaluga, G. Pinna, *Chemical Physics Letters* 47 (1977) 275.
- [74] T.M. Seward, C.M.B. Henderson, J.M. Charnock, T. Driesner, *Geochimica et Cosmochimica Acta* 63 (1999) 2409.
- [75] M.I. Bernal-Uruchurtu, I. Ortega-Blake, *Journal of Chemical Physics* 103 (1995) 1588.
- [76] N.A. Matwiyoff, H. Taube, *Journal of the American Chemical Society* 90 (1968) 2796.

- [77] S. Obst, H. Bradaczek, *Journal of Physical Chemistry* 100 (1996) 15677.
- [78] F.M. Floris, J.M. Martínez, J. Tomasi, *Journal of Chemical Physics* 116 (2002) 5460.
- [79] M.M. Naor, K. Van Nostrand, C. Dellago, *Chemical Physical Letters* 369 (2003) 159.
- [80] C.F. Schwenk, H.H. Loeffler, B.M. Rode, *Chemical Physics Letters* 349 (2001) 99.
- [81] C.F. Schwenk, H.H. Loeffler, B.M. Rode, *Chemical Physics Letters* 115 (2001) 10808.
- [82] S.G. Kalko, G. Sesé, J.A. Padró, *Journal Chemical Physics* 104 (1996) 9578.
- [83] F.C. Lightstone, E. Schwegler, R.Q. Hood, F. Gygi, G. Galli, *Chemical Physics Letters* 343 (2001) 549.
- [84] F.C. Lightstone, E. Schwegler, M. Allesch, F. Gygi, G. Galli, *ChemPhysChem: A European Journal of Chemical Physics and Physical Chemistry* 6 (2005) 1745.
- [85] G. Pálinkás, K. Heinzinger, *Chemical Physics Letters* 126 (1986) 251.
- [86] H.-S. Kim, *Journal of Molecular Structure (Theochem)* 541 (2001) 59.
- [87] M. Dudev, J. Wang, T. Dudev, C. Lim, *Journal of Physical Chemistry B* 110 (2006) 1889.
- [88] N.F. Dalleska, B.L. Tjelta, P.B. Armentrout, *Journal of Physical Chemistry* 98 (1994) 4191.
- [89] C. W. Bauschlicher, Jr., H. Partridge, *Journal of Physical Chemistry* 95 (1991) 3946.
- [90] K. Daigoku, K. Hashimoto, *Journal of Chemical Physics* 121 (2004) 3569.
- [91] K. W. Chan, Y. Wu, Z.-F. Liu, *Canadian Journal of Chemistry* 85 (2007) 873.
- [92] I.N. Tang, M.S. Lian, A.W. Castleman, *Journal of Chemical Physics* 65 (1976) 4022.

- [93] R.J. Plowright, T.G. Wright, J.M.C. Plane, *The Journal of Physical Chemistry A* 112 (2008) 6550.

Chapter 8

Conclusion

The experimental technique used in this work has been designed in Stace's group to measure the binding energy for the attachment of a single molecule to large cluster ions from unimolecular (metastable) decomposition in the gas phase. The proposed technique is a method to progress the gas phase experimentation on ion solvation and metal-ion solvation, in order to investigate the properties of cluster ions. The necessity to develop a new experimental procedure arose from the limitations of the available experimental methods in measuring binding energies of large cluster ions (such as the experimental methodologies developed by the groups of Armentrout, of Castleman, of Kebarle, and of Williams). The experimental apparatus is equipped with a high resolution double-focusing mass spectrometer having reversed sector geometry, a pick-up chamber, and a supersonic nozzle. The experimental method consists of measuring the kinetic energy release (KER) that accompanies fragmentation of cluster ions with mass-analysed ion kinetic energy (MIKE) method. Moreover, these data are analysed in order to determine binding energies using evaporative ensemble statistical model by Klots. The experimental procedure is used to generate and investigate molecular cluster ions containing up to thirty molecules and, doubly charged metal ions coordinated in a variety of ligands containing up to twenty molecules.

The study on $\text{H}^+(\text{H}_2\text{O})_n$, $\text{H}^+(\text{NH}_3)_n$, and $\text{H}^+(\text{CH}_3\text{OH})_n$ for $3 \leq n \leq 30$ has been used as calibration method to prove the reliability of the experimental procedure. In addition, our experiments indicate that only a metastable peak, and hence a binding energy, is recorded for the mostly weak bound molecule present in a given cluster. From the analysis of the binding energies, we can determine that the weakest bound molecule of large clusters with ammonia, methanol, and water solvents studied in our experiments corresponds to the one bound with a single hydrogen bonding. The justification for this conclusion is given by considering that unimolecular (metastable) decay in these experiments is ruled by

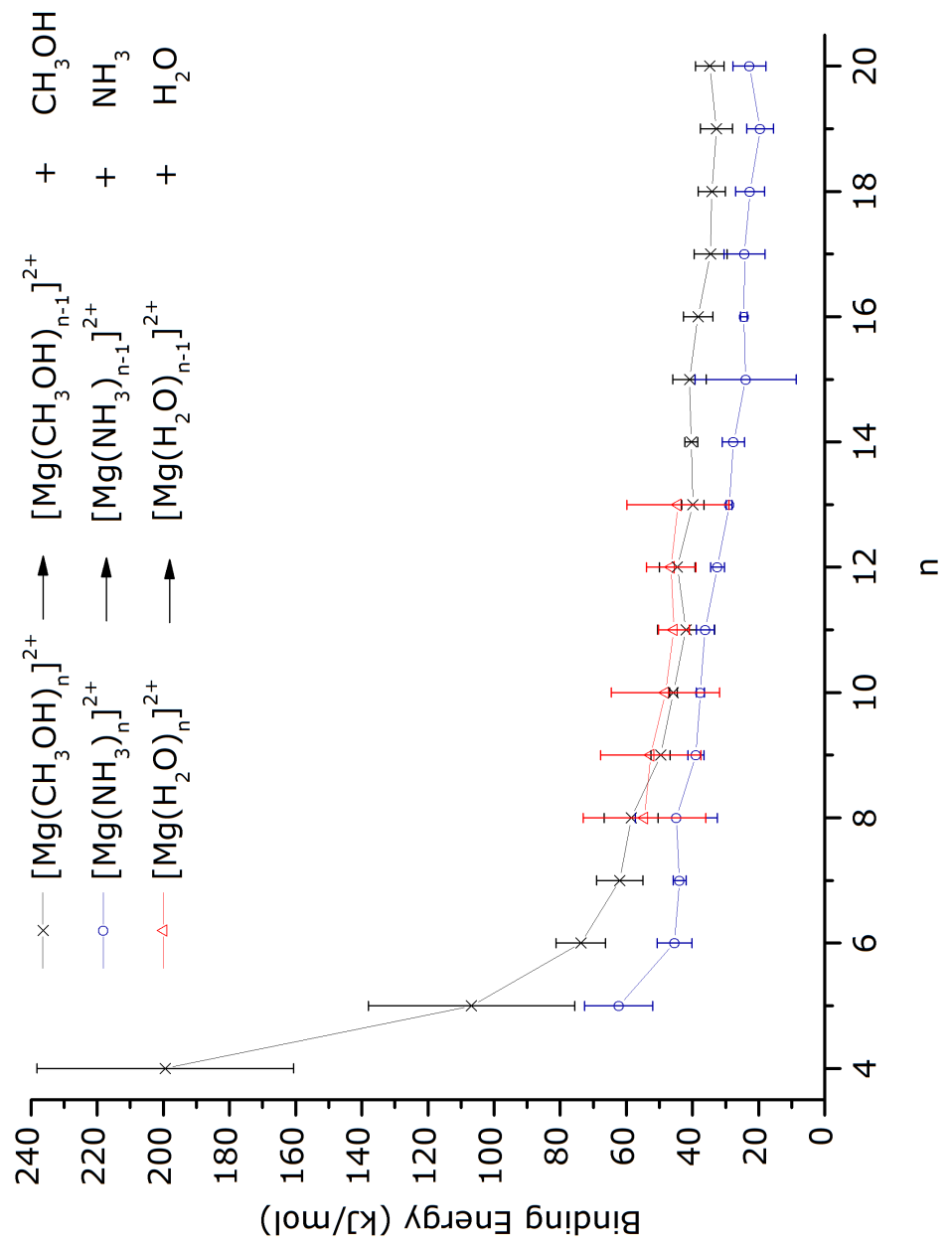
a competitive shift, so that the decay with the lowest activation energy is detected. Moreover, the only possible decay mechanism in these experiments is evaporative cooling, owing to the lifetime of the metastable ions $\sim 10^{-4}$ s and to the high vacuum pressure 1×10^{-7} mbar at which the experiments are performed. The method has been used to study how each of Mg^{2+} , Ca^{2+} , and Sr^{2+} coordinates with each of H_2O , NH_3 , and CH_3OH . The main result of our study is the identification of the influence of the double charge of the earth alkaline metal on the binding interactions, even once the first coordination shell is completed. This result is understood by comparing the binding energy of $[\text{M}(\text{L})_n]^{2+}$ with H^+L_n at each n , where $\text{M} = \text{Mg}, \text{Ca}, \text{Sr}$ and $\text{L} = \text{H}_2\text{O}, \text{NH}_3, \text{CH}_3\text{OH}$. In fact, when the solvation shell of $[\text{M}(\text{L})_n]^{2+}$ is completed, the binding energy at each n is higher than the expected value, *i.e.*, it is higher than one hydrogen bonding value. This implies that the size of the metal does not diminish the effect of the positive charge on the binding energy for all the clusters with up to twenty solvent molecules, and for $[\text{Sr}(\text{H}_2\text{O})_n]^{2+}$, for which only fourteen water ligands stabilise the charge of the metal. Another important application of this experimental technique is for the determination of the number of solvent molecules required to completely fill the first solvation shell of a cluster ion in the gas phase.

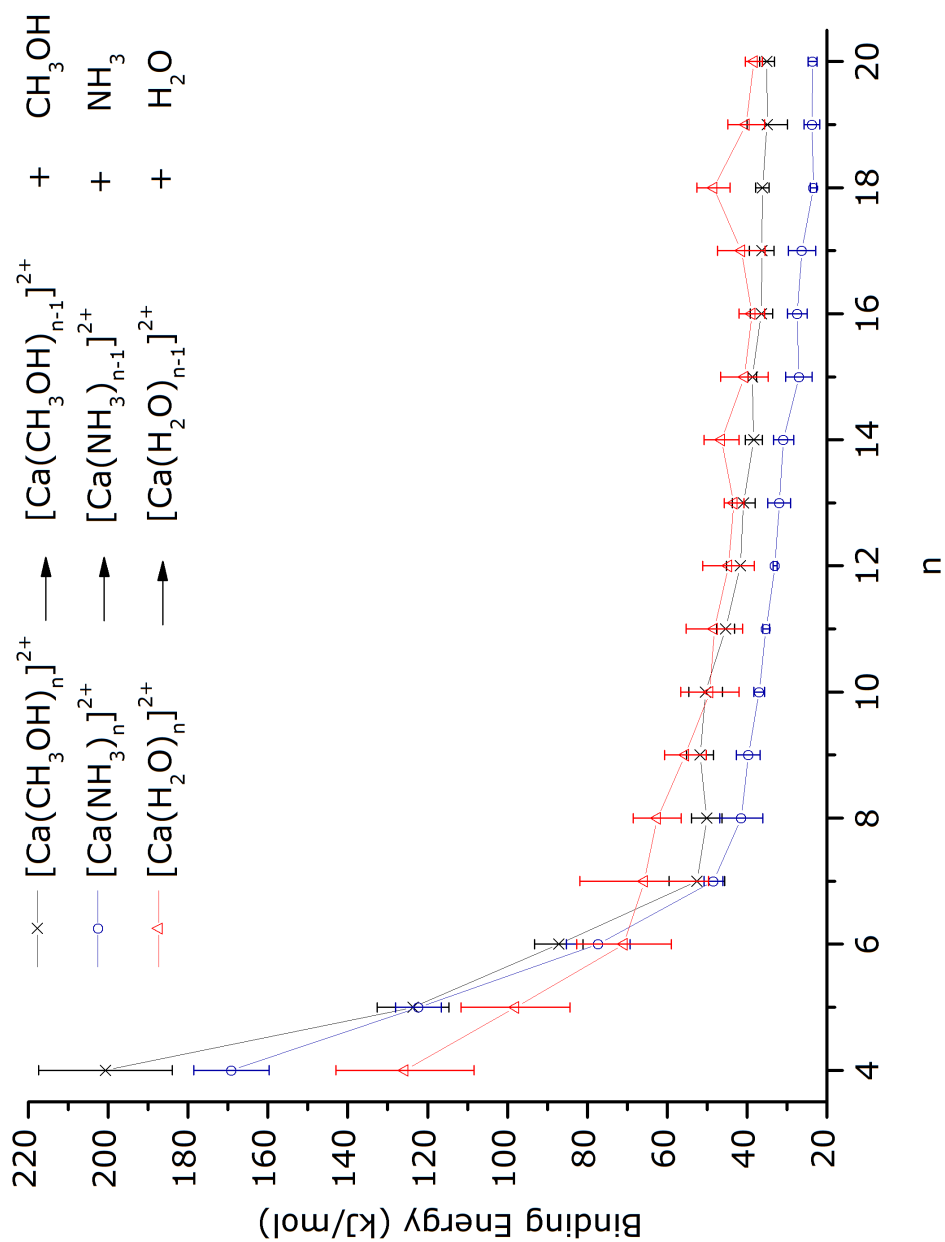
This study has shown that all but one of the considered metal-solvent systems close their first solvent shell with six solvent molecules; the only exception being $[\text{Mg}(\text{NH}_3)_n]^{2+}$ for which the coordination number is four. Moreover, these metal-solvent cluster ions bind through one hydrogen bond once the first solvation shell is completed.

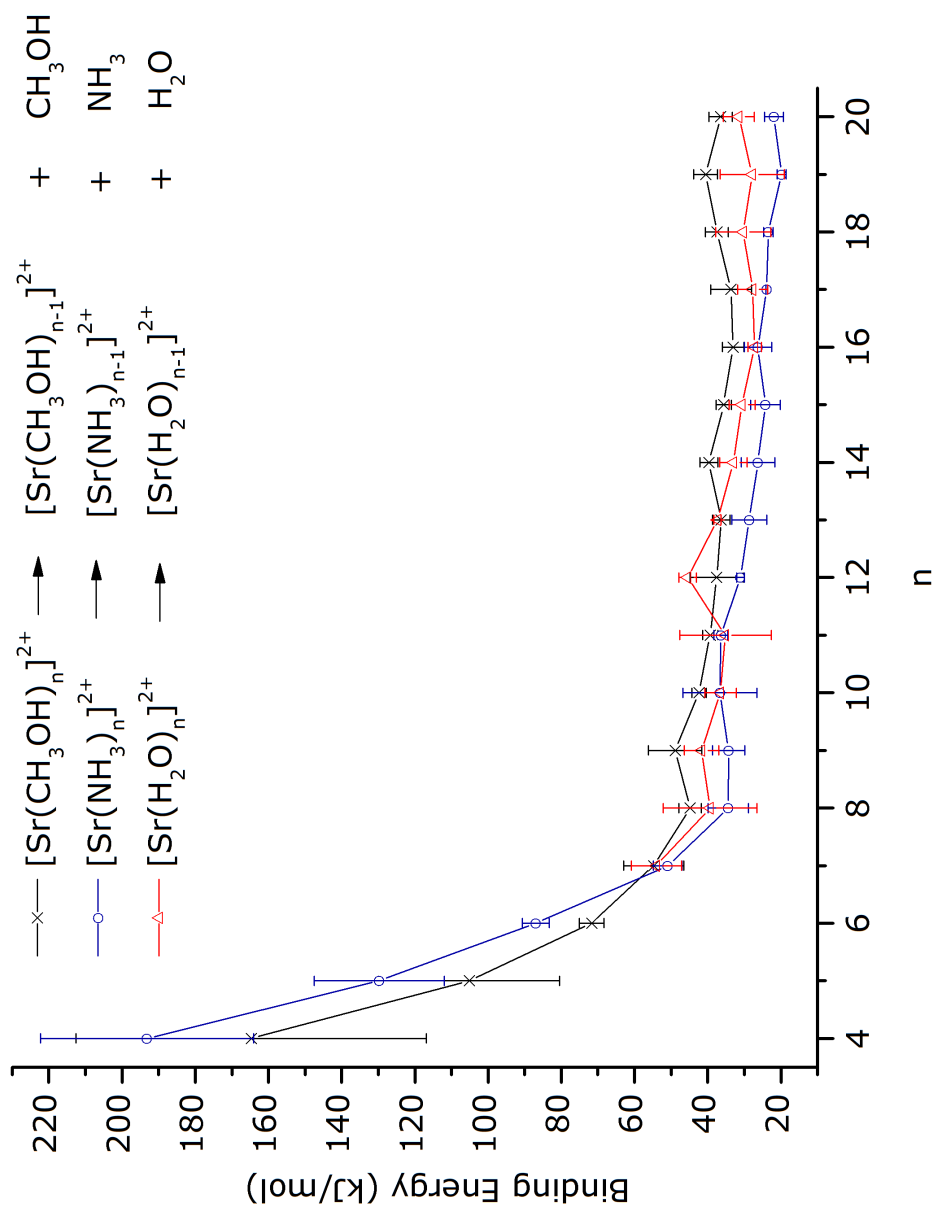
The comparison of the binding energy of a metal in a solvent with the one of the other solvent molecules suggests that the charge of the metal affects the binding energy. After the completion of the first solvation shell, the binding energies decrease:

- (i) from water to methanol, to ammonia for Mg^{2+} ,
- (ii) from water to methanol, to ammonia for Ca^{2+} , and
- (iii) from methanol to water, to ammonia for Sr^{2+} .

This trend is shown in the graphs below where the binding energies in Table 5.2.2, Table 6.2.2, and Table 7.2.2 are plotted versus the number n of solvent molecules in each cluster:







Here, the metals form the lowest energy bonds with ammonia. This suggests that ammonia is the poorest electron donor in these experiments. Interestingly, $\text{H}^+(\text{NH}_3)_n$ has the lowest binding energy with respect to $\text{H}^+(\text{H}_2\text{O})_n$ and $\text{H}^+(\text{CH}_3\text{OH})_n$; hence, the trend observed in the molecular clusters is maintained in the metal-solvent clusters.

The essential requirement to ensure precise measurements is that the laboratory frame full width half maximum (FWHM) peak widths of the precursor ions are as narrow as possible. This requires that the mass spectrometer has high energy resolving capabilities because, as the resolution increases by narrowing the width of the parent ion, the sensitivity decreases so that the signal-to-noise ratio of the corresponding daughter ion increases.

This experimental procedure can be applied to measure the binding energy of singly- and doubly-charged cluster ions. The requirements are that the solvent or the ligand has sufficient vapour pressure to generate gas phase clusters, and that the metal can be placed in a Knudsen effusion cell. As observed in this study, our technique does not allow the measurement of small clusters with sufficient precision. The smaller clusters showed MIKE scans with poor Gaussian profile owing to low signal-to-noise ratio; in other words, weak fragment ion signals. A main justification for the weak signal from metastable neutral loss is the presence of competing fragmentation channels. It would be therefore ideal to pinpoint a method to ameliorate the experimental conditions for these small cluster ions.

In order to improve the method in measuring binding energies for unimolecular (metastable) decay, it is worthwhile to consider how to improve the evaporative ensemble statistical method by C. E. Klots. Namely, to consider the possibility to find the value of Gspann parameter ℓ and, more importantly, of the heat capacity that uniquely describes an investigated system.

In this study, the dimensionless Gspann parameter was set to $\gamma = 23.5 \pm 1.5$, the heat capacity was $C = 6(n - 1)$ in units of Boltzmann constant minus 1 (where n was the number of molecules in the cluster ion), and the dimensionless ℓ parameter was set to 1.5.

Ideally, the choice of γ , ℓ , and C characteristics of an individual cluster system would give binding energy values which are close to the true value. However, the use of the same γ , ℓ , and C for all the systems, as done in these experiments, allows easily to compare the data of various systems.

Another aspect that it is worthwhile is to consider how to improve the experimental technique; more precisely, it would be helpful to find a more selective method for generating clusters having a narrow mass and energy distribution.

The binding energy for neutral loss via unimolecular (metastable) decay

could be investigated for Mg^{2+} , Ca^{2+} , and Sr^{2+} coordinated with solvents that do not have protic hydrogen (such as COS, CO_2 , SCN, etc.), or organic molecules (such as methyl fluoride, pyridine, aromatic compounds, alcohols, or biomolecules). The measurements of the binding energy for the same metals in several solvents would give information for example on the acidic and basic properties of the systems. Moreover, such measurements could prove how ligands coordinate in the first solvation shell; in other words, it could be possible to suggest which atom(s) in the ligand directly binds to the metal ion, *e.g.*, to individuate if COS binds to magnesium by using either its S or O atom. The investigation may elucidate how the charge affects the binding interactions, or how the coordination varies for the same metal ion in various solvents. We believe that this experimental procedure can be applied to study the loss of one molecule from any cluster ions (any multiply charged metal – and in general any molecule – solvated by any ligand). A better understanding of the properties of clusters in the gas phase is of support to the modelling of bio-inorganic systems (where the metals are in high oxidation states, *e.g.*, Zn(II) and Cu(II)), and to the possible development of clusters in electronic, optical, and magnetic devices. In fact, cluster studies offer the opportunity to relate the properties of gas phase molecules with the behaviour of condensed phase molecules. It would be interesting to apply this experimental method to study unimolecular (metastable) decay of negative ions, even though it is known that negative ions are formed in low abundance in mass spectrometers (about 0.1 – 1.0% of the abundance of positive ions). Finally, it would be worth continuing the investigations on $[\text{Mg}(\text{H}_2\text{O})_n]^{2+}$ that are incomplete in this study.

Chapter 9

Supporting Information

In this section are indicated the data obtained from the Gaussian normal distribution function fit of the experimental MIKE scans. More precisely, the tables show the collected points which have been analysed by using Origin 7.0 (Origin-Lab, Northampton, MA); where R^2 is the correlation coefficient of the fitting, and w (eV) is the value provided by the software which allows to calculate the standard deviation of a Gaussian profile $\frac{w}{2}$. The following equation between relates the laboratory frame FWHM w with the centre of mass-frame FWHM:

$$\text{FWHM} = w\sqrt{2\ln(2)}$$

The names of the files occurring in the following tables correspond to the files containing the electronic version of the experimental data.

9.1 $\text{H}^+(\text{H}_2\text{O})_n$

Artefact peaks from $n \geq 23$ (N.C. stands for 'not considered').

n	Name of the file		w (eV) daughter	R^2 daughter	w (eV) parent	R^2 parent
2	02032011_2930	N.C.	12.77851	0.71462	2.34869	0.99905
2	02032011_313233	N.C.	18.32387	0.64574	2.2851	0.99948
2	02032011_3435	N.C.	14.96256	0.47022	2.28545	0.99928
2	02032011_3637	N.C.	17.27532	0.71014	2.35673	0.99915
2	02032011_3839	N.C.	14.71009	0.60431	2.36922	0.99899
2	02032011_4041	N.C.	16.62364	0.68623	2.46792	0.99933
2	02032011_4243	N.C.	18.08449	0.62061	2.32138	0.99898
2	02032011_4445	N.C.	16.72558	0.74655	2.38903	0.99959

2	02032011_4647	N.C.	18.99307	0.63663	2.42124	0.99963
3	01032011_01bis02		13.45725	0.93691	2.48303	0.99908
3	01032011_03bis04		12.46168	0.91847	2.44653	0.99913
3	01032011_0506		11.67578	0.89718	2.56869	0.99916
3	01032011_0708		12.44958	0.90848	2.43086	0.99952
4	01032011_1314		10.29138	0.95469	2.39096	0.99945
4	02032011_0405		8.78218	0.94411	2.36006	0.99755
4	02032011_0607		8.03318	0.95473	2.34643	0.99782
4	02032011_0809		9.40421	0.95775	2.39339	0.99828
5	02032011_1011		7.87037	0.97905	2.36615	0.99943
5	02032011_1314		7.91505	0.97931	2.46482	0.99822
5	02032011_1516		8.63834	0.9784	2.36509	0.99919
5	02032011_1718		8.34868	0.97953	2.40189	0.99908
6	02032011_1920		7.75708	0.98114	2.45324	0.99947
6	02032011_2122		7.79996	0.9841	2.44126	0.99895
6	02032011_2324		7.87041	0.98725	2.53826	0.99862
6	02032011_2526		7.80901	0.98287	2.39602	0.99922
7	03032011_0506		7.18111	0.98789	2.47184	0.99917
7	03032011_0708		7.57431	0.9852	2.4385	0.99952
7	03032011_0910		7.34998	0.98471	2.47697	0.99948
7	03032011_1112		7.01791	0.98123	2.45471	0.99959
8	03032011_1314		6.71574	0.98296	2.52979	0.99881
8	03032011_1516		6.95857	0.986	2.52907	0.99908
8	03032011_1718		7.31506	0.9856	2.49579	0.99933
8	03032011_1920		7.16237	0.9852	2.54799	0.99855
9	03032011_2122		6.9019	0.98971	2.52728	0.9992
9	03032011_2324		6.90846	0.99177	2.56993	0.99841
9	03032011_2526		7.04892	0.99193	2.49449	0.99838
9	03032011_2728		7.11935	0.99144	2.502	0.99904
10	04032011_0102		6.8231	0.99426	2.5427	0.99911
10	04032011_0304		6.69441	0.99579	2.55581	0.99927
10	04032011_0506		6.8423	0.99587	2.53279	0.99942
10	04032011_0708		6.72039	0.99472	2.49664	0.99872

11	04032011_0910	6.39737	0.99509	2.55798	0.99941
11	04032011_1112	6.05714	0.99441	2.48407	0.99911
11	04032011_1314	6.12613	0.99558	2.53821	0.99917
11	04032011_1516	6.17249	0.9951	2.48143	0.99945
12	04032011_1718	6.23728	0.99561	2.4871	0.99803
12	04032011_1920	6.29766	0.99507	2.96163	0.99839
12	04032011_2122	6.29788	0.99474	2.55574	0.99905
12	04032011_2324	6.31867	0.99534	2.52061	0.99949
13	04032011_2526	5.86954	0.99477	2.52187	0.9992
13	04032011_2728	5.79963	0.99355	2.5065	0.99884
13	04032011_2930	6.1577	0.9941	2.58871	0.99896
13	04032011_3132	6.16535	0.99362	2.58256	0.99897
14	07032011_0102	5.79368	0.99186	2.34844	0.99921
14	07032011_030405	5.80593	0.99189	2.32007	0.99907
14	07032011_0607	5.81989	0.99254	2.35671	0.9987
14	07032011_0809	5.72953	0.9928	2.42525	0.99882
15	07032011_1011	5.71276	0.99157	2.43243	0.99877
15	07032011_1213	5.82758	0.98988	2.38822	0.99937
15	07032011_1415	5.7237	0.99175	2.43002	0.99915
15	07032011_1617	5.69449	0.99122	2.32495	0.99914
16	07032011_1819	5.41472	0.98873	2.34126	0.99861
16	07032011_2021	5.32997	0.98964	2.39144	0.99821
16	07032011_2223	5.43514	0.99236	2.34389	0.99929
16	07032011_2425	5.5543	0.99279	2.38983	0.99929
17	07032011_2627	5.18831	0.97983	2.32537	0.99896
17	08032011_0102	5.53023	0.98835	2.28191	0.9984
17	08032011_0304	5.42988	0.98295	2.31266	0.99814
17	08032011_0506	5.65646	0.989	2.28378	0.99913
18	08032011_0708	5.30521	0.98761	2.28641	0.99864
18	08032011_0910	5.48115	0.98841	2.28051	0.99907
18	08032011_1112	5.22567	0.98999	2.3648	0.99891
18	08032011_1314	5.21228	0.99129	2.36339	0.9985
19	08032011_1516	5.27626	0.98522	2.51166	0.99898

19	08032011_1718	5.19857	0.98798	2.36006	0.99837
19	08032011_1920	5.11641	0.9869	2.3612	0.99875
19	08032011_2122	5.15365	0.98862	2.39448	0.99925
20	09032011_0102	5.05455	0.98932	2.36863	0.99837
20	09032011_0304	5.07961	0.99212	2.26605	0.99875
20	09032011_0506	5.00134	0.99203	2.3308	0.99886
20	09032011_0708	5.30021	0.99131	2.37425	0.99895
21	09032011_0910	4.88414	0.99381	2.45957	0.99907
21	09032011_1112	5.28366	0.99126	2.49175	0.99886
21	09032011_1314	5.02258	0.9894	2.48098	0.99908
21	09032011_1516	4.88986	0.99322	2.45847	0.99892
22	09032011_1718	5.09655	0.99478	2.39973	0.99893
22	09032011_1920	4.89472	0.99399	2.42733	0.99897
22	09032011_2122	5.26162	0.99628	2.50099	0.99842
22	09032011_2324	5.00443	0.99431	2.49646	0.99882
23	09032011_2526_doubly	5.05489	0.99443	2.32383	0.99891
23	10032011_0102_doubly	5.31884	0.99215	2.4278	0.99864
23	10032011_0304_doubly	4.91947	0.99262	2.43486	0.9974
23	10032011_0506_doubly	5.00419	0.99365	2.33393	0.99707
24	10032011_0708_doubly	4.75776	0.99547	2.45515	0.99824
24	10032011_0910_doubly	4.89944	0.99425	2.54151	0.99882
24	10032011_1112_doubly	4.82401	0.98743	2.37359	0.99799
24	10032011_1314_doubly	4.89184	0.99093	2.28603	0.99864
25	10032011_1516_doubly	4.87415	0.98999	2.4278	0.99556
25	10032011_1718_doubly	4.82728	0.98946	2.41222	0.99698
25	10032011_1920_doubly	4.91396	0.98989	2.33405	0.99581
25	10032011_2122_doubly	4.68947	0.98783	2.37503	0.99498
26	11032011_0102_doubly	4.61846	0.98121	2.39833	0.9987
26	11032011_0304_doubly	5.2385	0.98949	2.35637	0.99849
26	11032011_0506_doubly	4.69192	0.98671	2.42792	0.99734
26	11032011_0708_doubly	4.95407	0.98437	2.49006	0.99612
27	11032011_0910_doubly	4.90583	0.9912	2.36094	0.99814
27	11032011_1112_doubly	4.72763	0.99282	2.45379	0.99776

27	11032011_1314_doubly	4.61083	0.99167	2.43113	0.99814
27	11032011_1516_doubly	4.75818	0.99084	2.19658	0.99822
28	11032011_1718_doubly	4.64107	0.99198	2.2925	0.99739
28	11032011_1920_doubly	4.69073	0.99257	2.31766	0.99858
28	11032011_2122_doubly	4.56821	0.99285	2.2718	0.99835
28	11032011_2324_doubly	4.46741	0.9934	2.3298	0.99791
29	11032011_2526_doubly	4.38722	0.99503	2.43179	0.99707
29	11032011_2728_doubly	4.65553	0.99395	2.35618	0.99846
29	11032011_2930_doubly	4.46618	0.992	2.26952	0.99738
29	11032011_3132_doubly	4.66268	0.99253	2.4212	0.99757
30	11032011_3334_doubly	4.74269	0.98629	2.25514	0.99782
30	11032011_3536_doubly	4.50258	0.98856	2.32017	0.99725
30	11032011_3738_doubly	4.54681	0.98859	2.36731	0.99793
30	11032011_3940_doubly	4.47365	0.98814	2.2867	0.99849

9.2 $H^+(NH_3)_n$

Artefact peaks from $n \geq 24$ (N.C. stands for 'not considered').

n	Name of the file		w (eV)	R ²	w (eV)	R ²
			daughter	daughter	parent	Parent
2	14072011_0102	N.C.	21.06784	0.71558	1.8397	0.99976
2	14072011_0506	N.C.	19.5911	0.78454	1.8182	0.99927
2	14072011_0708	N.C.	19.27556	0.78541	1.8872	0.99945
2	14072011_0910	N.C.	20.13831	0.79939	1.8838	0.99949
2	19082011_1516	N.C.	19.943	0.52914	2.5873	0.9983
2	19082011_1718	N.C.	-	-	2.5202	0.9983
2	19082011_1920	N.C.	17.03585	0.43347	2.368	0.99862
3	31062011_0102	N.C.	12.9985	0.88805	2.0023	0.99804
3	31062011_0304	N.C.	12.64577	0.7643	2.0169	0.9988
3	31062011_0506	N.C.	12.54772	0.75784	1.9694	0.99804
3	31062011_0708	N.C.	15.43279	0.85406	2.1227	0.99921
3	31062011_0910	N.C.	12.69524	0.58042	2.0431	0.99736
3	31062011_1314	N.C.	11.99195	0.75866	2.1273	0.99839
3	19082011_0102		14.6977	0.9599	2.553	0.99806
3	19082011_0304		14.01142	0.94879	2.5672	0.99862

3	19082011_0506		14.94956	0.94156	2.5169	0.99864
3	19082011_0708		14.68177	0.90343	2.6018	0.99875
3	19082011_0910		14.41498	0.94717	2.5679	0.99832
3	19082011_1112		15.26912	0.94521	2.509	0.99844
3	19082011_1314		14.28043	0.94302	2.5406	0.99839
4	31062011_1920		11.59653	0.94426	1.73	0.99974
4	31062011_2122		11.87029	0.93687	1.7499	0.9999
4	31062011_2324		12.40816	0.95679	1.9733	0.99935
4	31062011_2526		10.49421	0.95004	1.9839	0.99945
4	31062011_2728		10.98273	0.94961	1.9568	0.99929
4	01072011_0102	N.C.	10.94615	0.82011	2.0622	0.99681
5	31062011_2930		9.10577	0.9705	1.9152	0.99917
5	31062011_3132		9.59606	0.96971	1.8596	0.99928
5	31062011_3334		9.06323	0.96484	1.8691	0.99925
5	31062011_3536		9.12563	0.97234	1.783	0.9992
5	31062011_3738		9.48336	0.9709	1.7602	0.99928
6	01072011_0304		6.77322	0.97097	1.9157	0.99997
6	01072011_0506		7.13967	0.9716	1.7901	0.99989
6	01072011_0708		6.89141	0.96718	1.7597	0.99989
6	01072011_0910		7.09309	0.97066	1.8281	0.99998
7	01072011_1112		6.03412	0.98585	1.935	0.99964
7	01072011_1314		5.65032	0.98205	1.9433	0.99987
7	01072011_1516		5.8686	0.98475	1.8946	0.9999
7	01072011_1718		5.80708	0.98359	1.8385	0.99992
8	01072011_1920		5.42637	0.98775	1.8161	0.99989
8	01072011_2122		5.6775	0.98751	1.866	0.99983
8	01072011_2324		5.39365	0.98768	1.8707	0.99983
8	01072011_2526		5.48431	0.99069	1.9242	0.99983
9	01072011_2728		5.50087	0.98106	1.8048	0.99985
9	01072011_2930		5.20679	0.99236	1.8344	0.99983
9	01072011_3132		5.10854	0.9901	1.8572	0.99974
9	01072011_3334		5.42418	0.99059	1.7902	0.99966
9	01072011_3536		5.09178	0.98976	1.8279	0.99961
10	04072011_0102		5.0442	0.99305	1.9621	0.99937

10	04072011_0304	4.97659	0.99384	1.9887	0.99939
10	04072011_0506	5.03789	0.99434	1.9913	0.99965
10	04072011_0708	4.98393	0.99373	2.0291	0.99977
10	04072011_0910	5.02066	0.9937	2.0447	0.99985
11	04072011_1112	4.77414	0.99462	1.8204	0.99975
11	04072011_1314	4.91761	0.99579	1.734	0.99984
11	04072011_1516	4.78818	0.99586	1.762	0.99984
11	04072011_1718	4.79808	0.99669	1.6977	0.99986
12	04072011_1920	4.76364	0.99737	1.9612	0.9997
12	04072011_2122	4.75401	0.99742	1.9899	0.99967
12	04072011_2324	4.90596	0.99771	1.9037	0.99993
12	04072011_2526	4.71742	0.99752	1.8239	0.99986
13	04072011_2728	4.61315	0.99762	1.8842	0.99961
13	04072011_2930	4.76917	0.99803	1.9364	0.99993
13	04072011_3132	4.7739	0.99817	1.9511	0.99987
13	04072011_3334	4.6121	0.99826	1.9532	0.9998
14	04072011_3536	4.35728	0.99783	1.9101	0.99984
14	04072011_3738	4.3878	0.99807	1.9077	0.99989
14	04072011_3940	4.31023	0.99798	1.8458	0.99992
14	04072011_4142	4.40385	0.9981	1.8507	0.99997
15	04072011_4344	4.34496	0.99809	1.8223	0.99973
15	04072011_4546	4.38699	0.99787	1.8622	0.99952
15	04072011_4748	4.33021	0.99767	1.8705	0.9997
15	04072011_4950	4.35564	0.99811	1.9206	0.99985
16	05072011_0102	4.20043	0.99802	1.9766	0.99983
16	05072011_0304	4.41364	0.99803	2.005	0.99994
16	05072011_0506	4.27073	0.99871	1.9696	0.99987
16	05072011_0708	4.3291	0.99819	1.9794	0.99979
17	05072011_0910	4.16217	0.99713	1.9695	0.99995
17	05072011_1112	4.17871	0.99645	1.9979	0.99995
17	05072011_1314	4.21888	0.99513	1.9936	0.99991
17	05072011_1516	4.28379	0.99642	1.9824	0.99989
18	05072011_1718	4.24065	0.98996	1.9567	0.99984

18	05072011_1920	4.0678	0.9906	1.993	0.9999
18	05072011_2122	4.23172	0.98964	1.9625	0.99992
18	05072011_2324	4.10613	0.98974	1.9787	0.99994
18	05072011_2526	4.15221	0.98907	2.0456	0.99996
19	07072011_0102	4.19595	0.99197	2.0631	0.99961
19	07072011_0304	4.16759	0.99185	2.0105	0.99973
19	07072011_0506	4.11596	0.99238	1.9612	0.99972
19	07072011_0708	4.13202	0.99367	1.9948	0.99982
20	07072011_0910	4.10195	0.99491	1.8899	0.99976
20	07072011_1112	4.00697	0.99344	1.957	0.99974
20	07072011_1314	4.10311	0.99214	1.9653	0.99972
20	07072011_1516	4.00781	0.99262	1.9682	0.99962
21	07072011_1718	3.99074	0.99521	1.8552	0.99993
21	07072011_1920	4.0883	0.99541	1.8969	0.99991
21	07072011_2122	3.92363	0.99619	1.9266	0.99986
21	07072011_2324	4.1052	0.99622	1.9105	0.99988
22	07072011_2526	3.88277	0.99364	1.8508	0.9995
22	07072011_2728	3.99359	0.99407	1.8876	0.99951
22	07072011_2930	3.83326	0.99195	1.8596	0.99986
22	07072011_3132	3.90555	0.99363	1.8606	0.99973
23	07072011_3334	3.80505	0.99274	1.9342	0.99974
23	07072011_3536	3.97421	0.99279	1.9484	0.99964
23	07072011_3738	3.90444	0.99372	1.983	0.99961
23	07072011_3940	3.84938	0.99364	1.9122	0.99972
23	07072011_4142	3.8196	0.99291	1.9182	0.99981
23	07072011_4344	3.83758	0.99302	1.9705	0.99987
24	08072011_0102	3.80791	0.98956	1.833	0.99919
24	08072011_0304	3.65617	0.99038	1.8419	0.99884
24	08072011_0506	3.80479	0.99726	1.736	0.99922
24	09072011_0102	4.00738	0.99797	1.7213	0.99956
24	09072011_0304	3.85897	0.99747	1.7295	0.99883
24	09072011_0506	3.92684	0.99829	1.7553	0.99973
24	09072011_0708	3.91394	0.99739	1.7417	0.99984
24	09072011_0910	3.86827	0.99707	1.7562	0.99968

24	09072011_1112		3.91104	0.99769	1.7527	0.99967
25	10072011_0102		3.9401	0.99735	1.6904	0.99945
25	10072011_0304		3.67517	0.99779	1.7293	0.99972
25	10072011_0506		3.72251	0.9975	1.7214	0.99985
25	10072011_0708		3.81972	0.99699	1.7023	0.99983
26	10072011_0910		3.65858	0.99605	1.6709	0.99957
26	10072011_1112		3.61208	0.99394	1.7147	0.9996
26	10072011_1314		3.80428	0.99597	1.7547	0.99962
26	10072011_1516		3.65546	0.99584	1.7302	0.99926
27	10072011_1718		3.64859	0.98854	1.6469	0.99961
27	10072011_1920		3.6605	0.99015	1.5838	0.99896
27	10072011_2122		3.5241	0.99037	1.5747	0.99918
27	10072011_2324		3.55918	0.98886	1.589	0.9994
28	11072011_0102		3.70101	0.99327	1.7228	0.99938
28	11072011_0304		3.43422	0.99174	1.6959	0.99925
28	11072011_0506		3.66012	0.99119	1.7305	0.99953
28	11072011_0708		3.55589	0.99223	1.7348	0.99935
29	11072011_1314		3.61429	0.99102	1.7073	0.99875
29	11072011_1516		3.6923	0.98742	1.6832	0.99882
29	11072011_1718		3.6541	0.98846	1.677	0.99888
29	11072011_1920		3.64299	0.99192	1.6637	0.99915
30	11072011_2728		3.70436	0.99081	1.4668	0.99861
30	11072011_2930		3.52374	0.99007	1.4668	0.99924
30	11072011_3132		3.68359	0.99223	1.4384	0.99836
30	11072011_3334		3.53417	0.99098	1.4552	0.99822

9.3 $H^+(CH_3OH)_n$

Artefact peaks from $n \geq 26$ (N.C. stands for 'not considered').

n	Name of the file		w (eV) daughter	R ² daughter	w (eV) parent	R ² parent
2	21092011_0102	N.C.	23.7088	0.3821	2.31203	0.97732
2	21092011_0304	N.C.	24.83433	0.36071	2.19665	0.99867
2	21092011_0506	N.C.	17.92181	0.85096	2.1438	0.99823

2	21092011_0708	N.C.	18.55125	0.86063	2.15013	0.99774
2	21092011_0910	N.C.	17.71088	0.79414	2.20352	0.98692
2	21092011_1112	N.C.	19.20667	0.74535	2.21226	0.9994
2	21092011_1314	N.C.	18.13542	0.83375	2.14709	0.9989
2	21092011_1516	N.C.	15.19413	0.82696	2.13014	0.99838
2	21092011_1718	N.C.	18.31479	0.83777	2.14668	0.99786
2	21092011_1920	N.C.	17.93394	0.80842	2.18686	0.99911
3	20092011_3536		10.30057	0.98314	2.17133	0.99357
3	20092011_3738		10.121	0.98454	2.24362	0.98828
3	20092011_3940		10.02858	0.98121	2.23567	0.98919
3	20092011_4142		10.32016	0.97593	2.27961	0.98661
4	20092011_2526		8.97098	0.98989	2.22828	0.99547
4	20092011_2728		8.28774	0.98953	2.19375	0.99464
4	20092011_2930		9.31474	0.99091	2.21948	0.99453
4	20092011_3132		8.85568	0.98944	2.22342	0.99497
4	20092011_3334		9.35651	0.99151	2.22447	0.99539
5	20092011_1718		8.31955	0.99319	2.23729	0.99651
5	20092011_1920		8.24413	0.99515	2.33153	0.9966
5	20092011_2122		8.28553	0.99446	2.2971	0.99661
5	20092011_2324		8.03077	0.99495	2.24405	0.99742
6	20092011_0910		7.47354	0.99547	2.13723	0.99819
6	20092011_1112		7.7236	0.99588	2.14246	0.99874
6	20092011_1314		7.49486	0.99488	2.15243	0.99839
6	20092011_1516		7.81072	0.99627	2.13495	0.9983
7	20092011_0102		7.38818	0.99724	2.04299	0.99998
7	20092011_0304		7.62583	0.99734	2.17914	0.9991
7	20092011_0506		7.50409	0.99757	2.11173	0.99936
7	20092011_0708		7.63213	0.9981	2.14069	0.99936
7	19092011_0102		7.43289	0.99747	2.11006	0.99921
7	19092011_0304		7.57541	0.99803	2.11627	0.99936
8	21092011_2122		6.99393	0.99631	2.23026	0.99738
8	21092011_2324		7.10683	0.99755	2.15204	0.9989
8	21092011_2526		6.6596	0.99737	2.10846	0.99948
8	21092011_2728		6.97773	0.99659	2.08678	0.9994

9	21092011_2930	6.69498	0.99813	2.22867	0.99879
9	21092011_3132	6.85564	0.99742	2.19289	0.99968
9	21092011_3334	6.67681	0.99761	2.20126	0.99868
9	21092011_3536	6.91561	0.99737	2.21881	0.99892
10	21092011_3738	6.5672	0.99715	2.19465	0.99918
10	21092011_3940	6.54935	0.99802	2.22436	0.99955
10	21092011_4142	6.47869	0.99809	2.23858	0.99963
10	21092011_4344	6.3754	0.99741	2.31045	0.99901
11	22092011_0102	6.25915	0.99557	2.33345	0.99707
11	22092011_0304	6.17829	0.99814	2.29766	0.99794
11	22092011_0506	6.14371	0.99618	2.2477	0.99985
11	22092011_0708	6.42225	0.99751	2.29236	0.99987
12	22092011_0910	5.92354	0.99779	2.24863	0.99958
12	22092011_1112	5.80546	0.99637	2.21519	0.99978
12	22092011_1314	5.82711	0.99691	2.29563	0.9998
12	22092011_1516	6.01477	0.9981	2.24774	0.99977
13	22092011_1718	5.80349	0.99721	2.31346	0.99974
13	22092011_1920	5.83818	0.99792	2.37719	0.99981
13	22092011_2122	5.63439	0.99663	2.25896	0.99995
13	22092011_2324	5.87162	0.99807	2.2991	0.99896
14	22092011_2526	5.50979	0.99717	2.24451	0.99984
14	22092011_2728	5.65866	0.99723	2.27762	0.99983
14	22092011_2930	5.48108	0.99751	2.30621	0.99973
14	22092011_3132	5.64719	0.9978	2.31271	0.99969
15	23092011_0102	5.56268	0.9965	2.30632	0.99971
15	23092011_0304	5.56787	0.99669	2.26202	0.99982
15	23092011_0506	5.78656	0.99658	2.26699	0.99983
15	23092011_0708	5.61645	0.99536	2.26147	0.99993
16	23092011_0910	5.49664	0.9963	2.27742	0.99993
16	23092011_1112	5.58041	0.99683	2.31199	0.9999
16	23092011_1314	5.40888	0.9961	2.24873	0.99983
16	23092011_1516	5.50843	0.99675	2.26785	0.99974
17	23092011_1718	5.34824	0.99574	2.2696	0.9999

17	23092011_1920	5.43165	0.99552	2.28277	0.99986
17	23092011_2122	5.42729	0.99493	2.28833	0.99984
17	23092011_2324	5.47213	0.99539	2.27894	0.99981
18	23092011_2526	5.28849	0.99567	2.17993	0.99946
18	23092011_2728	5.33636	0.99425	2.2533	0.99929
18	23092011_2930	5.26394	0.99345	2.27903	0.99947
18	23092011_3132	5.12196	0.99456	2.26543	0.9995
19	23092011_3334	5.2267	0.99003	2.31959	0.99958
19	23092011_3536	5.11196	0.99164	2.31064	0.99956
19	23092011_3738	5.27428	0.99141	2.34018	0.99981
19	23092011_3940	5.01296	0.99123	2.31934	0.99986
20	23092011_4142	5.20293	0.98841	2.32962	0.99979
20	23092011_4344	5.22408	0.98801	2.38587	0.99956
20	23092011_4546	5.2044	0.98727	2.34943	0.99968
20	23092011_4748	5.15429	0.98756	2.39658	0.99945
21	23092011_4950	5.04509	0.98405	2.28255	0.99937
21	23092011_5152	4.87868	0.98492	2.32369	0.99878
21	23092011_5354	5.08166	0.98525	2.33964	0.99967
21	23092011_5556	4.91515	0.98603	2.40257	0.99962
22	26092011_0102	5.17454	0.96989	2.30176	0.99931
22	26092011_0304	4.91323	0.96387	2.25716	0.99964
22	26092011_0506	5.09265	0.97277	2.3221	0.99927
22	26092011_0708	4.87383	0.97755	2.36003	0.99946
23	26092011_0910	4.35635	0.62913	2.43541	0.98837
23	26092011_1112	4.54201	0.71146	2.23125	0.99561
23	26092011_1314	5.01489	0.95212	2.32958	0.99966
23	26092011_1516	4.68175	0.96025	2.32877	0.99937
23	26092011_1718	4.82385	0.9591	2.37136	0.9993
23	26092011_1920	4.92694	0.96297	2.45184	0.96297
24	26092011_2122	4.87954	0.95536	2.25136	0.99856
24	26092011_2324	4.67795	0.96382	2.17918	0.99958
24	26092011_2526	4.74351	0.96584	2.25202	0.99849
24	26092011_2728	4.7653	0.95433	2.34996	0.99811

25	27092011_0304	4.72773	0.95207	2.20913	0.99924
25	27092011_0506	4.81613	0.95974	2.23626	0.99769
25	27092011_0708	4.50884	0.95689	2.19121	0.99891
25	27092011_0910	4.62309	0.95079	2.23258	0.99836
26	27092011_1112	4.63662	0.92285	2.14649	0.99881
26	27092011_1314	4.80144	0.91657	2.1441	0.99799
26	27092011_1516	4.78027	0.99357	2.39476	0.99767
26	27092011_1718	5.01324	0.99428	2.17047	0.99848
27	27092011_1920	4.68936	0.99434	2.21537	0.99765
27	27092011_2122	4.93272	0.99432	2.17716	0.9983
27	27092011_2324	4.83916	0.99476	2.18319	0.99691
27	27092011_2526	4.85454	0.9943	2.18707	0.99844
28	27092011_2728	4.66644	0.99168	1.88448	0.99831
28	27092011_2930	4.58526	0.99131	2.02308	0.99588
28	27092011_3132	4.7066	0.99298	2.07452	0.99723
28	27092011_3334	4.60105	0.99207	1.94693	0.99702
29	28092011_0102	4.29341	0.99144	2.01062	0.99701
29	28092011_0304	4.56036	0.99412	2.10125	0.99697
29	28092011_0506	4.59922	0.98998	2.03564	0.99638
29	28092011_0708	4.34801	0.99061	2.02618	0.99763
30	28092011_0910	4.2378	0.9905	1.87754	0.99684
30	28092011_1112	4.52551	0.99238	1.95516	0.99635
30	28092011_1314	4.59663	0.99215	1.89479	0.99785
30	28092011_1516	4.53971	0.99139	1.97322	0.99469

9.4 $[\text{Mg}(\text{NH}_3)_n]^{2+}$

N.C. stands for 'not considered'.

n	Name of the file	w (eV) daughter	R ² daughter	w (eV) parent	R ² parent
4	01122010_0910_Gaussian	-	-	1.88539	0.999
4	02122010_0102_Gaussian	-	-	1.94327	0.99782
4	02122010_0304_Gaussian	-	-	1.87717	0.99489
4	02122010_0506_Gaussian	-	-	1.91952	0.99667

5	29112010_1314_Gaussian		6.37507	0.97479	2.4362	0.99308
5	29112010_1516_Gaussian		6.34151	0.9764	2.37395	0.99337
5	29112010_1718_Gaussian		6.71666	0.96539	2.36579	0.99295
5	29112010_1920_Gaussian		6.30731	0.96772	2.44957	0.99317
5	31012011_0102_Gaussian		6.95689	0.99504	2.02223	0.99839
5	31012011_0304_Gaussian		7.1628	0.99444	1.95447	0.99805
5	31012011_0506_Gaussian		6.92728	0.99697	1.89953	0.99829
5	31012011_0708_Gaussian		6.99603	0.99574	2.03093	0.99939
5	29072011_1516	N.C.	8.49871	0.84453	2.05728	0.9972
5	29072011_1718	N.C.	8.4115	0.82008	1.93442	0.99694
5	29072011_192	N.C.	7.92897	0.86592	1.96565	0.99782
5	29072011_2122	N.C.	7.73152	0.87369	2.07116	0.99846
6	29112010_0102_Gaussian		5.66046	0.95594	2.48641	0.99465
6	29112010_0304_Gaussian		5.8695	0.92999	2.40376	0.99436
6	29112010_0506_Gaussian		5.81345	0.98577	2.32619	0.99474
6	29112010_0708_Gaussian		5.67019	0.95644	2.35429	0.9926
6	29112010_0910_Gaussian		6.16275	0.98619	2.31203	0.99396
6	01122010_0506_Gaussian		5.91947	0.98476	2.16802	0.99543
6	01122010_0708_Gaussian		5.92559	0.97264	1.85205	0.99898
7	30112010_0102_Gaussian		5.53601	0.99504	2.09011	0.99839
7	30112010_0304_Gaussian		5.77107	0.99444	2.13127	0.99805
7	30112010_0506_Gaussian		5.70506	0.99697	2.11868	0.99829
7	30112010_0708_Gaussian		5.52098	0.99574	1.93513	0.99939
7	30112010_0910_Gaussian		5.6379	0.9959	1.88595	0.99933
8	30112010_1213_Gaussian	N.C.	4.8742	0.81553	2.06602	0.99517
8	30112010_1415_Gaussian	N.C.	4.57037	0.77587	2.13027	0.99578
8	30112010_1617_Gaussian		4.91093	0.901	2.07758	0.99499
8	31012011_0910_Gaussian		5.33162	0.98977	1.80768	0.99784
8	31012011_1112_Gaussian		6.20188	0.9886	1.8793	0.99769
8	31012011_1314_Gaussian		5.65566	0.9907	1.85167	0.99761
8	28072011_0102		6.0499	0.96367	1.99986	0.99727
8	28072011_0304		5.71173	0.94798	2.07255	0.99856
8	29072011_0102		5.51293	0.90416	2.08585	0.99944
8	29072011_0304		5.68249	0.93683	2.13603	0.99833
8	29072011_0506		5.61312	0.95604	2.16591	0.99939
8	29072011_0708		5.68917	0.95171	2.08703	0.9988
8	29072011_0910		5.98154	0.94233	2.06742	0.999

8	29072011_1112		5.10603	0.93886	2.10576	0.99896
8	29072011_1314		5.73631	0.95691	2.11055	0.99916
8	03082011_1920		5.09082	0.93267	2.05238	0.99908
8	03082011_2122		5.55547	0.92658	2.11261	0.9992
8	03082011_2324		5.85712	0.91522	2.13936	0.99896
8	03082011_2526		5.4877	0.91359	2.09382	0.9988
8	03082011_2728		5.91835	0.90907	2.06854	0.99908
8	03082011_2930		5.20173	0.93413	2.04008	0.99924
8	03082011_3132	N.C.	5.53806	0.8887	2.21937	0.99672
8	03082011_3334		6.20982	0.90183	2.1585	0.99809
8	03082011_3536		5.0384	0.90866	2.1183	0.99837
9	02122010_0708_Gaussian		5.08162	0.9966	2.03799	0.99728
9	02122010_0910_Gaussian		5.05023	0.99616	1.9888	0.99837
9	02122010_1112_Gaussian		5.27222	0.99713	2.02177	0.99798
9	02122010_1314_Gaussian		5.13762	0.9963	2.04733	0.99794
10	02122010_1516_Gaussian	N.C.	4.8075	0.79541	2.07012	0.99757
10	02122010_1718_Gaussian		5.01382	0.99311	2.05215	0.99764
10	02122010_1920_Gaussian		4.96296	0.99666	2.06681	0.99754
10	02122010_212223_Gaussian		4.97396	0.99735	2.36014	0.99757
10	03122010_0102_Gaussian		5.05421	0.99718	2.11848	0.99725
11	31012011_1516_Gaussian		4.73481	0.99485	1.88646	0.99764
11	31012011_1718_Gaussian		4.49599	0.99294	1.91815	0.99854
11	31012011_1920_Gaussian		4.88761	0.99559	1.93631	0.99787
11	31012011_2122_Gaussian		4.80849	0.99544	1.92589	0.99856
12	31012011_2324_Gaussian		4.36964	0.99541	1.89217	0.99802
12	31012011_2526_Gaussian		4.41754	0.99594	1.90208	0.99838
12	31012011_2728_Gaussian		4.54278	0.99483	1.91165	0.99832
12	31012011_2930_Gaussian		4.46684	0.99567	2.18505	0.99836
13	1022011_0102_Gaussian		4.12791	0.99307	1.92427	0.99902
13	1022011_0304_Gaussian		4.17429	0.99263	1.88396	0.9992
13	1022011_0506_Gaussian		4.05425	0.99297	1.86965	0.99942
13	1022011_0708_Gaussian		4.16157	0.99344	1.92632	0.99913
14	1022011_0910_Gaussian		3.91086	0.99466	1.86886	0.99927
14	1022011_1112_Gaussian		3.86438	0.99482	1.93863	0.99866
14	02062011_1718		3.83512	0.9742	1.51979	0.9995

14	02062011_1920	4.04467	0.97817	1.55945	0.99951
15	29072011_2324	4.04999	0.96961	2.03938	0.99754
15	29072011_2526	3.69945	0.96733	2.04833	0.99679
15	29072011_2728	3.54239	0.96827	2.00693	0.99756
15	29072011_2930	3.83234	0.97271	1.99006	0.9981
15	29072011_3132	3.50174	0.96969	2.01364	0.99843
15	03082011_0910	4.54295	0.96379	1.99044	0.99753
15	03082011_1112	3.66689	0.94217	1.96461	0.99783
15	03082011_1314	3.33698	0.95731	1.94812	0.99671
15	03082011_1516	3.86321	0.9481	1.95581	0.99788
15	03082011_1718	3.34371	0.94913	1.92504	0.99661
16	01082011_0102	3.64064	0.94081	2.05901	0.99902
16	01082011_0304	3.66648	0.93855	1.99863	0.99864
16	01082011_0506	3.62823	0.95418	1.6755	0.99885
16	01082011_0708	3.60301	0.9503	1.61708	0.99885
16	01082011_0910	3.6076	0.95013	1.6925	0.99866
17	01082011_1112	3.40169	0.97371	1.68396	0.99884
17	01082011_1314	3.35992	0.96724	1.73643	0.99891
17	01082011_1516	3.53594	0.96668	1.75162	0.99896
17	01082011_1718	3.76999	0.96757	1.49767	0.99905
17	01082011_1920	3.3436	0.95503	1.45854	0.99938
18	01082011_2122	3.51112	0.96465	1.48673	0.99882
18	01082011_2324	3.35424	0.96261	1.63965	0.99898
18	01082011_2526	3.12995	0.96898	1.58271	0.99889
18	01082011_2728	3.31462	0.96883	1.57038	0.99935
18	01082011_2930	3.21474	0.96917	1.61009	0.99933
19	02082011_0102	3.10717	0.95676	1.55232	0.99862
19	02082011_0304	3.31725	0.95387	1.60558	0.99907
19	02082011_0506	3.22444	0.95788	1.6755	0.99885
19	02082011_0708	2.96333	0.9515	1.59146	0.99865
19	02082011_0910	2.8537	0.95931	1.65907	0.99785
20	02082011_1112	3.29857	0.9543	1.7888	0.99775
20	02082011_1314	3.40038	0.96189	1.83701	0.99541
20	02082011_1516	3.68283	0.94448	2.02179	0.99772
20	02082011_1718	3.3229	0.96851	2.19118	0.99884

20	02082011_1920	3.50321	0.96797	2.1687	0.99884
20	01082011_0102	3.20467	0.9191	1.80562	0.99826
20	01082011_0304	3.23578	0.95524	1.84739	0.9977
20	01082011_0506	3.38239	0.93861	1.84646	0.9978
20	01082011_0708	3.46575	0.93382	1.86416	0.99807

9.5 $[\text{Ca}(\text{NH}_3)_n]^{2+}$

N.C. stands for 'not considered'.

n	Name of the file		w (eV)	R ²	w (eV)	R ²
			daughter	daughter	parent	parent
3	14072011_1112	N.C.	14.20734	0.34023	1.67666	0.99983
3	14072011_1314	N.C.	24.10576	0.28419	1.59364	0.99983
3	14072011_1516	N.C.	16.48988	0.43422	1.65608	0.99986
3	14072011_1718	N.C.	15.45829	0.35677	1.63259	0.99979
4	13072011_2930		9.73627	0.96806	1.9285	0.99944
4	13072011_3132		9.63103	0.95761	1.98284	0.99854
4	13072011_3334		9.94113	0.96749	2.02552	0.99874
4	13072011_3536		9.69441	0.95952	2.05069	0.9985
4	13072011_3738		9.47906	0.95534	2.00737	0.99875
4	13072011_3940		9.6408	0.96207	2.04852	0.99855
4	13072011_4142		9.76502	0.95327	2.02621	0.99845
4	13072011_4344		9.99196	0.95914	1.98667	0.99883
5	13072011_2122		8.81795	0.973	1.96942	0.99988
5	13072011_2324		8.90629	0.97482	1.94953	0.99988
5	13072011_2526		8.5998	0.97231	1.90914	0.99987
5	13072011_2728		8.51328	0.97764	1.90103	0.99987
6	13072011_1314		6.48657	0.96905	1.93715	0.99939
6	13072011_1516		7.18956	0.9837	2.05366	0.99913
6	13072011_1718		7.17541	0.97639	2.02212	0.99818
6	13072011_1920		7.394	0.98419	1.99922	0.99906
7	13072011_0102		5.57828	0.98422	2.08115	0.99886
7	13072011_0304		5.53752	0.98718	1.93659	0.99842
7	13072011_0506		5.7504	0.98772	1.94423	0.99893
7	13072011_0708		5.74159	0.98621	2.00723	0.99941

7	13072011_0910	5.76838	0.98673	1.99406	0.99938
7	13072011_1112	5.49599	0.98583	2.00566	0.99944
8	14072011_1920	5.29767	0.98994	1.67136	0.99945
8	14072011_2122	4.88662	0.98359	1.70923	0.99949
8	14072011_2324	5.15721	0.98678	1.67163	0.99927
8	14072011_2526	4.82029	0.98401	1.64126	0.9985
8	14072011_3738	5.27198	0.98958	1.92016	0.99951
8	14072011_3940	5.46432	0.98775	1.93069	0.99924
8	14072011_4142	5.09484	0.98737	1.92327	0.9994
8	14072011_4344	5.09484	0.98737	1.92327	0.9994
9	14072011_2728	4.85612	0.98935	1.85497	0.99968
9	14072011_2930	5.03881	0.99275	1.91271	0.99963
9	14072011_3132	5.13982	0.99032	1.91809	0.99941
9	14072011_3334	4.95838	0.9921	1.92158	0.99937
9	14072011_3536	4.86444	0.99202	1.86155	0.99956
10	15072011_0102	4.86198	0.98863	2.06637	0.99968
10	15072011_0304	4.65342	0.99353	2.00899	0.99968
10	15072011_0506	4.84788	0.99184	1.96699	0.99982
10	15072011_0708	4.6185	0.99236	1.98904	0.99982
10	15072011_1920	4.83501	0.99352	1.93905	0.9996
11	15072011_0910	4.59817	0.99109	1.91946	0.99955
11	15072011_1112	4.56214	0.99237	1.9244	0.99995
11	15072011_1314	4.50284	0.99364	1.89184	0.99986
11	15072011_1516	4.49092	0.98926	1.9004	0.99987
11	15072011_1718	4.59262	0.99411	1.89618	0.99993
12	15072011_2122	4.36245	0.99465	1.89952	0.99984
12	15072011_2324	4.32637	0.99429	1.91706	0.99968
12	15072011_2526	4.37041	0.9946	1.9059	0.9998
12	15072011_2728	4.31019	0.99288	1.90445	0.99982
13	18072011_0102	4.27031	0.99141	1.91406	0.99994
13	18072011_0304	4.10543	0.99189	1.8837	0.99974
13	18072011_0506	4.17814	0.99079	1.86151	0.99996
13	18072011_0708	4.09201	0.98928	1.84718	0.99991

13	18072011_0910	4.20514	0.98941	1.93201	0.99996
13	18072011_1112	4.36847	0.99285	1.9342	0.99997
14	18072011_1314	3.9812	0.99071	1.93047	0.99993
14	18072011_1516	4.04003	0.99047	1.89822	0.99989
14	18072011_1718	4.12469	0.99357	1.87554	0.99997
14	18072011_1920	4.06619	0.99252	1.93177	0.99989
14	18072011_2122	4.03975	0.99435	1.90931	0.99989
14	18072011_2324	4.21767	0.99388	1.93175	0.99995
15	18072011_2526	3.61986	0.99119	1.83845	0.99988
15	18072011_2728	3.86241	0.99116	1.85322	0.9999
15	18072011_2930	3.6477	0.98763	1.87197	0.99984
15	18072011_3132	3.83939	0.98949	1.85246	0.99987
15	18072011_3334	3.96087	0.99101	1.86046	0.99986
15	18072011_3536	3.76112	0.99049	1.87573	0.9999
16	18072011_3738	3.65754	0.98489	1.89097	0.99959
16	18072011_3940	3.66177	0.98544	1.87541	0.99989
16	18072011_4142	3.63851	0.98547	1.84505	0.9993
16	19072011_0102	3.53758	0.98547	1.69248	0.99971
16	19072011_0304	3.7524	0.98664	1.83647	0.99947
16	19072011_0506	3.79787	0.97764	1.9756	0.99972
16	19072011_0708	3.4788	0.98362	1.88993	0.99972
16	20072011_3738	3.59707	0.98495	1.8482	0.99956
16	20072011_3944	3.45085	0.98173	1.82709	0.99989
16	20072011_4041	3.63846	0.98522	1.81553	0.99993
16	20072011_4243	3.61114	0.98517	1.80976	0.99992
16	18072011_3738	3.76349	0.99318	1.89097	0.99959
16	18072011_3940	3.76784	0.99363	1.87541	0.99989
16	18072011_4142	3.86913	0.99411	1.84505	0.9993
16	19072011_0102	3.6265	0.99085	1.69248	0.99971
16	19072011_0304	3.86382	0.99081	1.83647	0.99947
16	19072011_0506	3.91652	0.98723	1.9756	0.99972
16	19072011_0708	3.57681	0.98673	1.88993	0.99972
16	20072011_3738	3.71872	0.99291	1.8482	0.99956
16	20072011_3944	3.55966	0.99215	1.82709	0.99989
16	20072011_4041	3.74415	0.99233	1.81553	0.99993

16	20072011_4243	3.71979	0.99317	1.80976	0.99992
17	20072011_0102	3.69688	0.98813	1.85428	0.9998
17	20072011_0102	3.79941	0.99206	1.85428	0.9998
17	20072011_0304	3.43343	0.99151	1.79511	0.99984
17	20072011_0506	3.49851	0.98988	1.85185	0.99983
17	20072011_0506	3.59653	0.99365	1.85185	0.99983
17	20072011_0708	3.61389	0.99148	1.81465	0.99919
17	20072011_0910	3.64592	0.99077	1.7753	0.99921
17	20072011_1112	3.51805	0.9904	1.7403	0.99929
18	20072011_1314	3.43889	0.99264	1.80643	0.99967
18	20072011_1516	3.35548	0.99279	1.77545	0.99969
18	20072011_1718	3.41687	0.99145	1.76593	0.99935
18	20072011_1920	3.32054	0.99188	1.76843	0.99942
19	20072011_2122	3.40621	0.99384	1.66861	0.99979
19	20072011_2324	3.26563	0.99095	1.67218	0.99951
19	20072011_2526	3.28347	0.99289	1.67566	0.99983
19	20072011_2728	3.24279	0.99192	1.61366	0.9996
20	20072011_2930	3.21889	0.99277	1.76025	0.99968
20	20072011_3132	3.26383	0.99325	1.77362	0.99985
20	20072011_3334	3.37178	0.99366	1.7981	0.99987
20	20072011_3536	3.33312	0.99332	1.72238	0.99986

9.6 $[\text{Sr}(\text{NH}_3)_n]^{2+}$

N.C. stands for 'not considered'.

n	Name of the file		w (eV) daughter	R ² daughter	w (eV) parent	R ² parent
3	16092011_4142	N.C.	-	-	1.99465	0.99819
3	16092011_4344	N.C.	-	-	2.14494	0.99846
3	16092011_4546	N.C.	-	-	2.20492	0.99951
3	24082011_0102	N.C.	-	-	2.03531	0.99979
3	24082011_0304	N.C.	-	-	1.68915	0.99954
3	23082011_0102	N.C.	-	-	2.19377	0.99944
4	09082011_0102		8.91799	0.92941	2.14025	0.99952

4	09082011_0304		8.70627	0.92408	2.17977	0.99937
4	09082011_0506		9.6007	0.91919	2.15142	0.99956
4	09082011_0708	N.C.	4.53179	0.92757	2.17168	0.99955
4	09082011_0910		8.68032	0.91544	2.11113	0.99933
4	09082011_1112	N.C.	8.65656	0.86795	2.12826	0.9988
4	09082011_1314	N.C.	9.7053	0.80183	2.10205	0.99848
5	08082011_3132		7.66719	0.95236	1.89981	0.99946
5	08082011_3334		8.34536	0.9487	1.97285	0.99956
5	08082011_3536		7.59253	0.95293	2.03336	0.99935
5	08082011_3738		7.79894	0.9593	1.97886	0.99929
6	08082011_2122		6.68743	0.94832	2.0088	0.99958
6	08082011_2324		6.55915	0.95672	2.11472	0.99858
6	08082011_2526		6.50818	0.95384	2.01432	0.99938
6	08082011_2728		6.76224	0.96665	1.99654	0.99914
6	08082011_2930		6.68959	0.95807	2.00771	0.99918
7	08082011_1314		4.95199	0.95006	1.91226	0.99964
7	08082011_1516		5.3421	0.95798	1.84883	0.99958
7	08082011_1718		5.14343	0.95224	1.86614	0.99942
7	08082011_1920		5.26364	0.95529	1.85845	0.99945
8	24082011_1617	N.C.	4.94711	0.84181	1.66712	0.9901
8	24082011_1819	N.C.	4.27805	0.82599	1.83405	0.99365
8	24082011_2021	N.C.	4.57856	0.7333	1.97897	0.99678
8	24082011_2223	N.C.	3.95674	0.78177	1.83201	0.99622
8	26082011_0102		4.67225	0.93359	2.02413	0.99807
8	26082011_0304	N.C.	5.02954	0.78407	2.08715	0.99694
8	26082011_0506	N.C.	4.84696	0.88827	1.74772	0.99938
8	26082011_0708	N.C.	4.18689	0.76967	1.98509	0.99629
8	16092011_3334		4.31532	0.97089	1.87913	0.99806
8	16092011_3536		4.48812	0.96928	1.90319	0.9983
8	16092011_3738		4.01905	0.97355	1.92873	0.99679
8	16092011_3940		4.29888	0.96963	1.93467	0.99666
9	24082011_0607		4.19876	0.90873	1.91617	0.9995
9	24082011_0809		4.25268	0.94189	1.86675	0.99973
9	24082011_1011		4.44414	0.93684	1.93673	0.99926
9	24082011_1213		4.53535	0.94463	1.93732	0.99916

9	24082011_1415		4.07533	0.9466	1.89055	0.99932
10	24082011_2425		4.85106	0.94935	1.93858	0.99756
10	24082011_2627		4.36966	0.93078	2.02461	0.99907
10	24082011_2829		4.3061	0.96187	2.03425	0.99925
10	24082011_3031		4.25707	0.96949	2.09321	0.99957
10	24082011_3233		4.19306	0.92714	1.82661	0.99914
11	24082011_3435		4.37633	0.96434	1.97568	0.99891
11	24082011_3637		4.38765	0.96654	1.94499	0.99868
11	24082011_3839		4.06954	0.97046	1.92958	0.99835
11	24082011_4041		4.39144	0.96269	1.92879	0.99835
12	05092011_0102	N.C.	3.44577	0.45766	1.63658	0.99749
12	15092011_0102		4.01131	0.98329	1.89715	0.9958
12	15092011_0304		4.01848	0.96581	2.0026	0.9961
12	15092011_0506		3.88459	0.98134	1.88985	0.99925
12	15092011_0708		4.01523	0.97802	1.97073	0.99957
12	15092011_0910		3.99467	0.97578	1.99551	0.99966
13	02092011_0506	N.C.	2.89628	0.79452	1.70887	0.99811
13	05092011_0304	N.C.	3.73132	0.722	1.63658	0.99749
13	07092011_0304	N.C.	3.51195	0.88713	1.95141	0.99777
13	07092011_0506	N.C.	4.00957	0.89938	1.86354	0.99901
13	07092011_0708	N.C.	3.61987	0.8919	1.7972	0.99909
13	07092011_0910	N.C.	3.48437	0.86955	1.745	0.99853
13	07092011_1112	N.C.	3.84761	0.86675	1.73707	0.99906
13	15092011_1112		3.8066	0.96009	2.01891	0.99967
13	15092011_1314		3.77243	0.95591	2.02924	0.99933
13	15092011_1516		3.68631	0.95646	2.02996	0.99933
13	15092011_1718		3.85692	0.95781	1.96839	0.99957
14	15092011_1920		3.50508	0.96859	1.94482	0.99921
14	15092011_2122		3.62567	0.96456	2.04486	0.99717
14	15092011_2324		3.8898	0.94657	2.00129	0.99508
14	15092011_2526		3.44443	0.96234	1.77106	0.99899
14	15092011_2728		3.7053	0.96295	1.9334	0.99749
15	15092011_2930		3.451	0.97393	2.138	0.99955
15	15092011_3132		3.43777	0.97427	2.10812	0.99914
15	15092011_3334		3.43445	0.97874	2.07869	0.99938

15	15092011_3536	3.70609	0.97594	1.97533	0.99901
15	15092011_3738	3.71	0.97258	1.99008	0.99928
16	15092011_3940	3.435	0.97905	1.86091	0.99839
16	15092011_4142	3.60087	0.9807	1.89822	0.99924
16	15092011_4344	3.48906	0.93022	1.88533	0.99898
16	15092011_4546	3.72361	0.98282	1.94619	0.99944
16	15092011_4748	3.41363	0.96885	1.98692	0.9988
17	16092011_0102	3.42124	0.98045	2.00093	0.9996
17	16092011_0304	3.48753	0.98085	2.10701	0.99902
17	16092011_0506	3.41605	0.98768	2.02809	0.99912
17	16092011_0708	3.40434	0.98718	1.97732	0.99877
18	16092011_0910	3.21135	0.98079	1.76241	0.99743
18	16092011_1112	3.24282	0.98619	1.94814	0.9989
18	16092011_1314	3.41868	0.98762	2.00268	0.99963
18	16092011_1516	3.44194	0.98753	2.06998	0.9998
19	16092011_1718	3.23895	0.98355	2.05672	0.99845
19	16092011_1920	3.12451	0.98533	2.1652	0.9982
19	16092011_2122	3.2245	0.9824	1.92003	0.99687
19	16092011_2324	3.01018	0.98018	1.8614	0.99887
20	16092011_2526	3.31581	0.98312	1.97057	0.99684
20	16092011_2728	3.12857	0.98475	1.95344	0.99842
20	16092011_2930	3.11514	0.98371	1.95689	0.99796
20	16092011_3132	3.20624	0.98514	1.95014	0.99817

9.7 $[\text{Mg}(\text{CH}_3\text{OH})_n]^{2+}$

N.C. stands for 'not considered'.

n	Name of the file	w (eV) daughter	R ² daughter	w (eV) parent	R ² parent	
3	18042011_2324	-	-	2.31066	0.99889	
3	18042011_2526	-	-	1.97534	0.96743	
3	18042011_2728	-	-	2.45879	0.99925	
3	18042011_2930	-	-	2.20068	0.99916	
4	16042012_1314	N.C.	19.58756	0.52765	2.21155	0.99946

4	16042012_1516	N.C.	17.47838	0.21227	2.2215	0.99926
4	16042012_1718		14.39946	0.74156	2.20226	0.99969
4	16042012_1920	N.C.	14.38276	0.61696	2.23625	0.9991
4	17042012_0102	N.C.	13.24819	0.61305	2.40648	0.99875
4	17042012_0304	N.C.	14.98624	0.56126	2.48294	0.99875
4	17042012_0506	N.C.	13.96345	0.57087	2.43645	0.99859
4	18042012_0102	N.C.	13.22005	0.64652	2.34223	0.99937
4	18042012_0304	N.C.	16.60711	0.38831	2.36597	0.99899
4	18042012_0506		12.96247	0.76167	2.37054	0.99938
4	18042012_0708	N.C.	0.32593	0.11218	2.38413	0.99943
4	18042012_0910	N.C.	11.92865	0.66097	2.45772	0.9989
4	18042012_1112		12.79826	0.74833	2.41597	0.9986
4	18042012_1314		13.12211	0.71832	2.42646	0.99836
4	18042012_1516	N.C.	14.42511	0.65411	2.43991	0.99863
4	18042012_1718		14.44982	0.73901	2.35164	0.99858
4	18042012_1920		14.44982	0.73901	2.33911	0.99882
4	18042012_2122		15.18331	0.75705	2.40938	0.99897
5	28032012_0506	N.C.	8.74426	0.7733	2.18317	0.99893
5	28032012_0708		11.58726	0.80236	2.18317	0.99893
5	28032012_0910		8.4279	0.83169	2.11348	0.9992
5	28032012_1112	N.C.	11.33986	0.77225	2.13726	0.99916
5	28032012_1314		12.00316	0.80828	2.14185	0.99938
5	16042012_0102		9.87439	0.85847	2.18882	0.99926
5	16042012_0304		10.74188	0.87548	2.22946	0.99948
5	16042012_0506		10.34929	0.89569	2.19492	0.99959
5	16042012_0708		11.20184	0.87376	2.25707	0.99956
5	16042012_0910		11.11307	0.86754	2.2591	0.99937
5	16042012_1112		10.1298	0.8742	2.21484	0.99969
6	02042012_0102	N.C.	10.18743	0.77831	2.14359	0.99911
6	02042012_0304	N.C.	9.02367	0.75194	2.07744	0.9987
6	02042012_0506	N.C.	13.68195	0.11125	2.11124	0.99916
6	11042012_0910	N.C.	9.68043	0.78753	2.25516	0.99969
6	11042012_1112	N.C.	9.18069	0.81982	2.20004	0.99596
6	11042012_1314	N.C.	9.32393	0.83354	2.27846	0.99966
6	11042012_1516	N.C.	8.88144	0.87711	2.24752	0.99982
6	11042012_1718	N.C.	8.54789	0.85555	2.26341	0.99951
6	11042012_1920	N.C.	8.62666	0.82292	2.25503	0.99981

6	11042012.2122	N.C.	8.83472	0.86295	2.2048	0.99945
6	11042012.2324	N.C.	9.47872	0.86232	2.16487	0.99934
6	11042012.2526		8.20208	0.91268	2.17747	0.99919
6	11042012.2728		9.16202	0.90395	2.21215	0.99914
6	11042012.2930	N.C.	8.98351	0.86086	2.17174	0.99921
6	11042012.3132	N.C.	9.1641	0.76559	2.13339	0.99894
6	11042012.3334	N.C.	13.56247	0.10642	2.13734	0.99933
6	11042012.3536	N.C.	7.32085	0.71634	2.13029	0.99921
6	11042012.3738	N.C.	7.72807	0.76752	2.08997	0.99924
6	11042012.3940	N.C.	9.05492	0.64272	2.10608	0.99924
6	11042012.4142	N.C.	9.8968	0.78507	2.04962	0.99942
6	11042012.4344	N.C.	9.78728	0.70784	2.14634	0.99851
6	12042012.0102	N.C.	9.56011	0.85498	2.30343	0.99955
6	12042012.0304	N.C.	9.60951	0.8393	2.29879	0.99954
6	12042012.0506		6.1859	0.93171	2.31017	0.99958
6	12042012.0708	N.C.	7.95661	0.8435	2.28304	0.99968
6	12042012.0910	N.C.	12.30766	0.07895	2.30931	0.9997
6	12042012.1112	N.C.	9.26602	0.53933	2.20403	0.99931
6	12042012.1314	N.C.	9.68258	0.78458	2.17633	0.99916
6	12042012.1516	N.C.	8.35361	0.79204	2.1212	0.99877
6	12042012.1718	N.C.	8.88929	0.7574	2.12529	0.99869
6	12042012.2122	N.C.	9.5857	0.79079	2.15419	0.99951
6	13042012.0102	N.C.	8.33088	0.81592	2.25055	0.99945
6	13042012.0304	N.C.	9.97358	0.88593	2.26918	0.99946
6	13042012.0506	N.C.	8.81097	0.88565	2.27758	0.99949
6	13042012.0708	N.C.	9.41473	0.88422	2.29306	0.99944
6	13042012.0910	N.C.	12.30766	0.07895	2.30931	0.9997
6	13042012.1112	N.C.	9.26602	0.53933	2.20403	0.99931
6	13042012.1314	N.C.	9.68258	0.78458	2.17633	0.99916
6	13042012.1516	N.C.	8.35361	0.79204	2.1212	0.99877
6	13042012.1718		9.27872	0.9107	2.25871	0.99938
6	13042012.1920		8.76678	0.89612	2.28835	0.99938
6	13042012.2122		8.88156	0.89839	2.32786	0.99913
6	13042012.2324		9.38397	0.88267	2.3282	0.99908
6	13042012.2526		8.25193	0.88978	2.3081	0.99917
7	05042012.1112		7.73326	0.92282	2.27133	0.99964
7	05042012.1314		7.83884	0.90373	2.2926	0.99984
7	02042012.0708	N.C.	7.12827	0.7943	2.11805	0.99956

7	02042012_0910	N.C.	8.21034	0.84182	2.18656	0.9993
7	02042012_1112	N.C.	7.49794	0.8515	2.09218	0.99941
7	11042012_0102		8.45815	0.93925	2.37251	0.99982
7	11042012_0304		7.86459	0.92491	2.33438	0.99981
7	11042012_0506		8.27465	0.90163	2.36283	0.99962
7	11042012_0708	N.C.	8.82934	0.89525	2.40953	0.99971
8	05042012_0102		7.56532	0.90783	2.31256	0.99953
8	05042012_0304		8.00148	0.94719	2.32525	0.99971
8	05042012_0506		7.07829	0.94433	2.33834	0.99972
8	05042012_0708		8.13383	0.93688	2.34397	0.99982
8	05042012_0910		7.47928	0.94432	2.32808	0.99968
9	19042012_0102		6.82941	0.95158	2.37287	0.99976
9	19042012_0304		6.92922	0.95044	2.39538	0.99964
9	19042012_0506		6.88532	0.96204	2.39902	0.99969
9	19042012_0708		7.12023	0.95131	2.38064	0.99952
10	19042012_0910		6.54987	0.96581	2.33826	0.99964
10	19042012_1112		6.58879	0.96517	2.3299	0.99972
10	19042012_1314		6.42015	0.9607	2.16897	0.99978
10	19042012_1516		6.47603	0.94847	2.39755	0.99958
11	19042012_1718		6.16252	0.94179	2.40019	0.99965
11	19042012_1920		5.78932	0.90515	2.47578	0.99802
11	19042012_2122		6.11656	0.95152	2.37718	0.9995
11	19042012_2324		6.01416	0.92833	2.47279	0.99927
11	19042012_2526		6.66751	0.9229	2.38997	0.99954
12	19042012_2728		6.341	0.93172	2.44821	0.99973
12	19042012_2930		5.97202	0.92728	2.459	0.99974
12	19042012_3132		6.49049	0.91941	2.42696	0.99964
12	19042012_3132		14.16597	0.0911	2.42696	0.99964
12	19042012_3334		6.06318	0.90273	2.42057	0.99923
12	19042012_3536		6.04092	0.94909	2.49555	0.99858
13	20042012_0102		5.70788	0.94916	2.11401	0.99924
13	20042012_0304		5.73663	0.9198	2.11712	0.99894
13	20042012_0506		5.31497	0.93133	2.1577	0.99873
13	20042012_0708		5.85916	0.92829	2.12835	0.99921

14	20042012.0910		5.56211	0.9423	2.26322	0.99909
14	20042012.1112		5.72966	0.93647	2.29212	0.99947
14	20042012.1314		5.7407	0.93138	2.30867	0.99904
14	20042012.1516		5.44578	0.92667	2.31572	0.99916
15	20042012.1718		5.80892	0.91424	2.26011	0.99899
15	20042012.1920	N.C.	5.19424	0.87485	2.24844	0.99921
15	20042012.2122	N.C.	5.60386	0.84503	2.47458	0.9987
15	24042012.0102	N.C.	5.36114	0.88498	2.34439	0.99958
15	24042012.0304	N.C.	5.55826	0.86773	2.39669	0.99965
15	24042012.0506		5.30148	0.90494	2.37857	0.99953
15	24042012.0708		5.38817	0.91458	2.47382	0.99924
15	24042012.0910		5.12615	0.89703	2.46259	0.99975
15	24042012.1112		5.80737	0.90915	2.47539	0.99968
15	24042012.1314	N.C.	5.98939	0.88716	2.51551	0.99973
16	25042012.0102		5.12393	0.90473	2.64047	0.99958
16	25042012.0304		5.6625	0.96243	2.62829	0.99887
16	25042012.0506		5.62897	0.96087	2.67619	0.99929
16	25042012.0708		5.37801	0.96112	2.56165	0.99938
16	25042012.0910		5.19302	0.94622	2.38269	0.99984
17	25042012.1112		5.03986	0.95592	2.48247	0.99924
17	25042012.1314		5.32101	0.94107	2.45663	0.99879
17	25042012.1516		5.06547	0.94644	2.39862	0.99957
17	25042012.1718		4.69454	0.91019	2.38444	0.99844
18	25042012.1920		4.70616	0.91924	2.42925	0.99929
18	25042012.2122	N.C.	12.23185	0.3137	2.46443	0.99745
18	25042012.2324		4.84299	0.90494	2.40922	0.99964
18	25042012.2526		5.1523	0.90579	2.43789	0.99963
18	25042012.2728	N.C.	5.67574	0.68856	2.43693	0.99911
18	26042012.0102		5.13982	0.97534	2.48418	0.99967
18	26042012.0304		4.92277	0.97236	2.5005	0.99974
18	26042012.0506		4.90945	0.96311	2.49338	0.99979
18	26042012.0708		4.89984	0.96262	2.50029	0.99968
19	26042012.0910		4.75566	0.96708	2.41946	0.99952
19	26042012.1112		5.06331	0.9588	2.49216	0.99937
19	26042012.1314		4.60758	0.96647	2.51858	0.99953

19	26042012_1516	4.76258	0.95493	2.49143	0.99957
20	26042012_1718	5.01904	0.94269	2.4082	0.99904
20	26042012_1920	4.74607	0.93485	2.46508	0.99948
20	26042012_2122	4.69429	0.92275	2.42957	0.9993
20	26042012_2324	4.87436	0.87232	2.47909	0.99921
20	26042012_2526	4.71569	0.94038	2.40785	0.9991

9.8 $[\text{Ca}(\text{CH}_3\text{OH})_n]^{2+}$

N.C. stands for 'not considered'.

n	Name of the file		w (eV)	R ²	w (eV)	R ²
			daughter	daughter	parent	parent
3	08032012_1314	N.C.	20.1079	0.32293	2.16178	0.99168
3	08032012_1516	N.C.	9.72472	0.48743	2.16178	0.99168
3	08032012_1718	N.C.	8.63178	0.13007	2.12799	0.99537
4	08032012_0102	N.C.	13.45563	0.79379	2.25901	0.99641
4	08032012_0304	N.C.	12.86519	0.82903	2.16189	0.99601
4	08032012_0506	N.C.	14.1895	0.67997	2.15474	0.99744
4	08032012_0708	N.C.	14.30946	0.81085	2.20258	0.99613
4	08032012_0910	N.C.	15.33158	0.85557	1.91057	0.99662
4	08032012_1112	N.C.	12.52004	0.83384	2.2673	0.99567
4	08032012_1920	N.C.	3.50164	0.88754	2.28077	0.99813
4	08032012_2122		12.71238	0.9249	2.31942	0.99791
4	08032012_2324		13.13521	0.9282	2.28155	0.9987
4	08032012_2526		13.96073	0.9138	2.31937	0.99874
4	08032012_2728		13.98796	0.93229	2.30603	0.9983
5	07032012_2526		11.35125	0.93849	2.29395	0.99846
5	07032012_2728		11.42246	0.92684	2.2988	0.99756
5	07032012_2930		10.23715	0.93765	2.03066	0.99688
5	07032012_3132		11.112	0.92989	2.29622	0.99828
6	07032012_1718		9.26541	0.96529	2.2164	0.99766
6	07032012_1920		9.63485	0.97288	2.25756	0.99812
6	07032012_2122		8.81543	0.973	2.32267	0.99812
6	07032012_2324		9.60755	0.97168	2.28149	0.99758

7	07032012.0910	7.21672	0.98587	2.15556	0.99893
7	07032012.1112	6.70749	0.98167	2.28063	0.9979
7	07032012.1314	7.37266	0.98346	2.22254	0.99896
7	07032012.1516	7.66826	0.97481	2.1965	0.99908
8	07032012.0102	7.08999	0.98742	2.12499	0.99418
8	07032012.0304	7.15924	0.98467	2.12998	0.9963
8	07032012.0506	6.72179	0.9887	2.13733	0.99867
8	07032012.0708	6.71424	0.99035	2.1636	0.99632
9	06092012.1112	6.9879	0.98882	2.29318	0.99874
9	06092012.1314	6.85518	0.99118	2.24324	0.99854
9	06092012.1516	6.6575	0.98808	2.30013	0.99838
9	06092012.1718	6.91281	0.99094	2.21612	0.99687
9	06092012.1920	7.11006	0.98361	2.27225	0.99606
10	09032012.0102	6.63568	0.99495	2.15195	0.99575
10	09032012.0304	6.88417	0.9931	2.1577	0.99794
10	09032012.0506	6.3565	0.99413	2.18022	0.99628
10	09032012.0708	6.68884	0.99384	2.21741	0.99745
11	09032012.0910	6.16312	0.99483	2.21613	0.99894
11	09032012.1112	6.35099	0.99454	2.27458	0.99731
11	09032012.1314	6.02748	0.99434	2.15536	0.99539
11	09032012.1516	6.24925	0.99456	2.21211	0.99767
12	22032012.0102	5.96962	0.99422	2.12812	0.99536
12	22032012.0304	5.80348	0.99449	2.07436	0.99684
12	22032012.0506	5.98968	0.9946	2.02286	0.99657
12	22032012.0708	5.41835	0.98448	2.10681	0.99656
13	22032012.0910	5.44181	0.99537	1.99942	0.99562
13	22032012.1112	5.50952	0.99493	2.06084	0.99371
13	22032012.1213	5.82942	0.99421	2.19626	0.99928
13	22032012.1415	5.74635	0.99146	2.21038	0.99912
14	23032012.0102	5.24952	0.98915	2.19011	0.9994
14	23032012.0304	5.40149	0.91309	2.28441	0.99913
14	23032012.0506	5.3929	0.99171	2.09385	0.9993
14	23032012.0708	5.50438	0.99056	2.15485	0.99894

15	23032012_0910	5.2751	0.99177	2.15979	0.99872
15	23032012_1112	5.28453	0.99186	2.1985	0.9993
15	23032012_1314	5.35526	0.99268	2.15635	0.99934
15	23032012_1516	5.28495	0.99214	2.1817	0.9993
16	23032012_1718	5.19987	0.99156	2.15866	0.9993
16	23032012_1920	4.84397	0.991	2.16095	0.999
16	23032012_2122	4.997	0.99207	2.16275	0.99939
16	23032012_2324	5.23372	0.99001	2.17747	0.99878
17	23032012_2526	5.12429	0.99093	2.10977	0.99929
17	23032012_2728	5.03841	0.99107	2.13358	0.99874
17	23032012_2930	4.84054	0.9921	2.1408	0.99921
17	23032012_3132	4.83399	0.98995	2.14016	0.9994
18	26032012_0708	4.91601	0.99365	2.13311	0.99885
18	26032012_0910	4.98413	0.99321	2.19896	0.99917
18	26032012_1112	4.77761	0.99418	2.15608	0.99903
18	26032012_1314	4.84549	0.99215	2.19367	0.99896
19	26032012_1516	4.68106	0.99093	2.09998	0.99928
19	26032012_1718	4.74757	0.98976	2.16807	0.99913
19	26032012_1920	4.51159	0.98638	2.23124	0.99888
19	26032012_2122	4.997	0.99207	2.14699	0.99885
20	26032012_2324	4.67154	0.94788	2.10162	0.9984
20	26032012_2526	4.61948	0.96145	2.10762	0.99818
20	26032012_2728	4.7318	0.95915	2.08867	0.99803
20	26032012_2930	4.51543	0.95735	2.07138	0.99887

9.9 $[\text{Sr}(\text{CH}_3\text{OH})_n]^{2+}$

Artefact peaks from $n \geq 18$ (N.C. stands for 'not considered').

n	Name of the file		w (eV) daughter	R ² daughter	w (eV) parent	R ² parent
3	01052012_1112	N.C.	95.11431	0.08961	2.54781	0.99973
3	01052012_1314	N.C.	15.02435	0.76677	2.43194	0.99892
4	30042012_4142	N.C.	9.7907	0.51026	2.04211	0.99847
4	01052012_0102		10.46505	0.85956	2.53049	0.99886

4	01052012_0304		10.82097	0.83477	2.66364	0.99951
4	01052012_0506		11.18776	0.84255	2.64708	0.9997
4	01052012_0708		10.66791	0.85197	2.72903	0.99937
5	30042012_3334		10.35232	0.85971	2.07588	0.99878
5	30042012_3536		9.2599	0.83004	2.10654	0.99883
5	30042012_3738		9.52394	0.86298	2.10602	0.99861
5	30042012_3940		8.26247	0.84596	2.04614	0.99868
6	30042012_1920	N.C.	8.38339	0.88186	2.10288	0.99911
6	30042012_2122		7.06331	0.88591	2.05849	0.99877
6	30042012_2324		7.43247	0.92601	2.11143	0.99891
6	30042012_2526		8.32614	0.89706	2.12438	0.99885
6	30042012_2728		8.213	0.90815	2.13668	0.99892
6	30042012_2930	N.C.	5.89239	0.96023	2.10491	0.99929
6	30042012_3132	N.C.	8.77911	0.92193	2.12269	0.99885
7	30042012_0102	N.C.	6.78097	0.8885	2.09899	0.99859
7	30042012_0304		5.83234	0.93123	2.07813	0.99893
7	30042012_0506		7.30324	0.92699	2.12091	0.99898
7	30042012_0708		7.12339	0.92674	2.09461	0.99866
7	30042012_0910		6.73865	0.9326	2.05712	0.99877
7	30042012_1112		6.68501	0.93626	2.07729	0.99892
7	30042012_1314		7.19658	0.91648	2.10661	0.99875
7	30042012_1516		6.8951	0.92019	2.07124	0.99865
7	30042012_1718		7.32947	0.92039	2.06016	0.99858
8	13102011_1718		5.17134	0.94769	1.81387	0.99941
8	13102011_1920		5.44866	0.94948	1.98346	0.99791
8	13102011_2122		5.27516	0.92958	1.89886	0.99862
8	13102011_2324		5.18382	0.94643	1.92696	0.99901
9	14102011_0102		5.1318	0.95343	2.02277	0.99884
9	14102011_0304		5.44473	0.94881	2.06835	0.99788
9	14102011_0506		5.34697	0.95637	1.98764	0.99953
9	14102011_0708		5.76587	0.96427	2.0221	0.99869
10	14102011_0910		4.90495	0.97337	1.97924	0.99735
10	14102011_1112		5.15251	0.97077	2.17659	0.99743

10	14102011_1314	4.99715	0.96325	2.03339	0.99782
10	14102011_1516	4.99715	0.96325	2.03339	0.99782
11	14102011_1718	4.50505	0.95177	2.03299	0.99496
11	14102011_1920	4.86207	0.96047	2.0738	0.9976
11	14102011_2122	4.84253	0.96639	1.97897	0.99722
11	14102011_2324	4.82448	0.96325	2.04501	0.99513
12	14102011_2526	4.3277	0.95438	1.88422	0.99723
12	14102011_2728	4.45895	0.97127	1.84112	0.99934
12	14102011_2930	4.88462	0.96981	1.88448	0.99831
12	14102011_3132	4.43447	0.97405	1.88503	0.9981
13	14102011_3334	4.29011	0.9733	1.85665	0.99796
13	14102011_3536	4.51573	0.96611	1.9107	0.99862
13	14102011_3738	4.42231	0.96964	1.92599	0.99861
13	14102011_3940	4.32322	0.96771	1.87333	0.99863
14	17102011_0102	4.56487	0.95931	2.00946	0.99415
14	17102011_0304	4.61534	0.95935	1.96119	0.99826
14	17102011_0506	4.37542	0.95757	1.90277	0.99746
14	17102011_0708	4.41869	0.95372	1.88557	0.99646
15	17102011_0910	4.20362	0.93603	1.74174	0.99747
15	17102011_1112	4.09688	0.94355	1.86087	0.99334
15	17102011_1314	4.33351	0.93995	1.9618	0.99174
15	17102011_1516	4.19793	0.95047	2.01973	0.99384
16	17102011_1718	4.10136	0.96654	1.92807	0.99553
16	17102011_1920	3.97437	0.96254	2.05105	0.99524
16	17102011_2122	3.97437	0.96254	2.02	0.99448
16	17102011_2324	4.23028	0.97492	2.06878	0.9923
17	17102011_2526	4.21912	0.96498	1.85552	0.99369
17	17102011_2728	4.04062	0.96465	2.02175	0.99772
17	17102011_2930	4.02996	0.97377	1.95601	0.99452
17	17102011_3132	3.72409	0.9726	1.95117	0.9961
18	18102011_0102	3.96987	0.97813	1.82688	0.99385
18	18102011_0304	4.13718	0.9851	1.99141	0.99741
18	18102011_0506	4.09415	0.98284	1.98701	0.99678

18	18102011_0708	4.26935	0.98056	1.99142	0.99741
19	18102011_0910	4.29839	0.97981	1.96431	0.99512
19	18102011_1112	4.29839	0.97981	2.12702	0.99321
19	19102011_0102	3.88517	0.97425	1.87336	0.99862
19	19102011_0304	4.29859	0.96977	1.90133	0.99365
20	19102011_0506	4.03045	0.97722	1.80951	0.99429
20	19102011_0708	3.98648	0.98663	1.90671	0.99067
20	19102011_0910	3.92344	0.97714	1.97174	0.99478
20	19102011_1112	3.76922	0.97484	1.83407	0.99039

9.10 $[\text{Mg}(\text{H}_2\text{O})_n]^{2+}$

N.C. stands for 'not considered'.

n	Name of the file			w (eV)	R ²	w (eV)	R ²
				daughter	daughter	parent	parent
7	18092012_1718	N.C.		8.00665	0.6206	2.44275	0.99878
7	18092012_2526	N.C.		8.13183	0.46255	2.51434	0.99841
7	18092012_2930	N.C.		5.09628	0.38759	2.64108	0.99875
8	18092012_0506			8.3259	0.53988	2.54683	0.9982
8	18092012_0708			7.61999	0.62489	2.53659	0.99865
8	18092012_0910			7.61999	0.62489	2.53659	0.99865
8	18092012_1112			8.54492	0.65393	2.53099	0.99837
8	18092012_1314			6.49184	0.71006	2.4801	0.99873
8	18092012_1516			7.20844	0.57479	2.50745	0.99833
9	17092012_5253			6.94956	0.68885	2.80859	0.99897
9	17092012_5455			7.18905	0.63514	2.86683	0.99902
9	17092012_6162			8.14077	0.67888	2.85888	0.9991
9	18092012_0102			7.6408	0.79171	2.54542	0.99882
9	18092012_0304			6.27034	0.74051	2.57374	0.99871
10	16092012_0304			6.71836	0.66925	2.51921	0.99519
10	16092012_0708			6.4646	0.7248	2.41237	0.99924
10	16092012_0910			6.15498	0.67439	2.47316	0.99887
10	16092012_1112			7.66001	0.61351	2.45304	0.99909
10	17092012_4243			6.49525	0.79496	2.64172	0.99906

10	17092012_4445	6.77088	0.68615	2.73717	0.99918
10	17092012_4647	6.76813	0.79198	2.80836	0.99916
10	17092012_4849	6.8754	0.7669	2.84331	0.99903
10	17092012_5051	7.02475	0.75561	2.85926	0.99916
11	17092012_3435	6.79315	0.84913	2.81581	0.9989
11	17092012_3637	6.4525	0.80005	2.79999	0.99862
11	17092012_3839	6.40629	0.81648	2.80272	0.99914
11	17092012_4041	6.39616	0.82049	2.7804	0.99916
12	17092012_2627	6.77565	0.84078	2.60136	0.99923
12	17092012_2829	6.32513	0.82342	2.74193	0.99931
12	17092012_3031	6.49069	0.78312	2.72535	0.99951
12	17092012_3233	5.9499	0.84731	2.70716	0.99898
13	17092012_0608	6.59789	0.631	2.26251	0.99701
13	17092012_0911	7.74993	0.49237	2.44614	0.9956
13	17092012_1213	6.24452	0.70667	2.89765	0.99929
13	17092012_1415	7.05644	0.64394	2.97614	0.99928
13	17092012_1617	5.62854	0.6649	3.19413	0.99924
13	17092012_2425	5.38109	0.70973	2.6297	0.99883
13	17092012_1820	6.87236	0.59586	3.08742	0.99691
13	17092012_1921	5.42645	0.55279	3.04012	0.99851

9.11 $[\text{Ca}(\text{H}_2\text{O})_n]^{2+}$

N.C. stands for 'not considered'.

	Name of the file		w (eV)	R ²	w (eV)	R ²
n			daughter	daughter	parent	parent
3	22082012_3435	N.C.	12.56141	0.69885	9.2418	0.92019
4	21082012_4445	N.C.	11.01662	0.7757	5.54001	0.96081
4	21082012_4647	N.C.	10.95671	0.8364	5.7051	0.96191
4	21082012_4849	N.C.	10.92871	0.80864	5.75272	0.96056
4	22082012_0607	N.C.	11.01752	0.8867	5.69666	0.9626
4	22082012_0809	N.C.	11.41022	0.8276	5.93179	0.95868
4	22082012_1011	N.C.	11.41022	0.8276	6.18616	0.95011
4	22082012_1213		11.55322	0.89459	6.17409	0.95155
4	22082012_1415	N.C.	10.79229	0.86953	7.11823	0.94738

4	22082012_1617		12.09424	0.9022	7.11455	0.93992
4	22082012_1819	N.C.	10.52043	0.87087	7.15479	0.93892
4	22082012_2021	N.C.	11.18407	0.83015	7.2108	0.93902
4	22082012_2223	N.C.	10.67229	0.811	7.57467	0.93962
4	22082012_2425	N.C.	12.52578	0.75875	7.23079	0.94028
4	22082012_2627		11.37067	0.89829	7.71178	0.93738
4	22082012_2829		11.76538	0.90907	7.64009	0.93865
4	22082012_3031		11.2306	0.89699	7.92877	0.92431
4	22082012_3233		12.80577	0.93011	9.43844	0.9214
5	21082012_2627	N.C.	12.21319	0.8565	5.12081	0.96484
5	21082012_2829	N.C.	10.16512	0.89547	5.26243	0.9711
5	21082012_3031		10.88257	0.90014	5.6429	0.96834
5	21082012_3233	N.C.	6.52416	0.90628	5.64842	0.96532
5	21082012_3435		10.41931	0.90519	5.79904	0.96757
5	21082012_3637	N.C.	10.51215	0.88596	5.79721	0.97035
5	21082012_3839	N.C.	10.31203	0.89696	5.79721	0.97035
5	21082012_4041		10.3248	0.90751	5.66214	0.96122
5	21082012_4243		9.82671	0.91166	5.70054	0.96105
6	17082012_1516	N.C.	9.05184	0.78201	2.41624	0.98006
6	18082012_0607	N.C.	9.05184	0.78201	2.35895	0.99388
6	20082012_1314	N.C.	9.62288	0.87966	4.7557	0.99353
6	20082012_1617	N.C.	9.10458	0.86348	5.64023	0.99761
6	20082012_1819	N.C.	9.41091	0.89534	4.89483	0.99753
6	20082012_2021	N.C.	9.41091	0.89534	3.74694	0.99659
6	21082012_1415		9.49729	0.9227	5.74954	0.9702
6	21082012_1617		8.85257	0.92488	5.69948	0.96791
6	21082012_1819		9.11036	0.94556	6.05355	0.96749
6	21082012_2021		9.45053	0.94761	5.90831	0.96927
6	21082012_2223		9.80649	0.94292	5.71447	0.96768
6	21082012_2425		9.05527	0.93483	5.37603	0.97003
7	13082012_0405	N.C.	6.86016	0.78312	2.3006	0.99876
7	13082012_0607	N.C.	7.62837	0.83377	2.26806	0.99807
7	13082012_0809	N.C.	7.08799	0.888	2.27553	0.99815
7	13082012_1012	N.C.	7.37393	0.85721	2.28461	0.99841
7	13082012_0102	N.C.	7.49674	0.81623	2.36017	0.99823
7	13082012_1314	N.C.	7.22466	0.85613	2.30113	0.99839
7	15082012_0910		6.99428	0.93697	2.63423	0.99905

7	17082012_0708		7.46722	0.90427	2.25666	0.9926
7	17082012_0910		8.53878	0.90992	2.28924	0.99348
7	17082012_1112		8.36635	0.91851	2.4584	0.9935
7	17082012_1314		7.30346	0.92554	2.27656	0.99353
8	12082012_4849		7.39536	0.93433	2.32769	0.99822
8	12082012_5051		6.84777	0.89122	2.35009	0.99798
8	12082012_5253		7.31459	0.89237	2.32381	0.99781
8	12082012_5455	N.C.	6.66207	0.85717	2.40755	0.99822
8	16082012_1718		7.72878	0.94744	2.47557	0.98275
8	16082012_1920		7.80009	0.9326	2.56446	0.98185
8	17082012_0506		7.51177	0.93792	2.28265	0.98627
9	12082012_3031	N.C.	7.16807	0.83819	2.43564	0.99733
9	12082012_3233		7.17946	0.91563	2.43032	0.99894
9	12082012_3435		7.20644	0.91488	2.44263	0.99826
9	12082012_3637		6.74916	0.92753	2.47266	0.99807
9	12082012_3839		6.56205	0.92886	2.44777	0.99846
9	12082012_4445	N.C.	7.26052	0.89149	2.34781	0.9979
9	12082012_4647	N.C.	6.96323	0.89713	2.33313	0.99784
10	10072012_0102	N.C.	6.80032	0.84122	1.94512	0.99694
10	11082012_0304	N.C.	6.53639	0.79697	2.06399	0.98797
10	11082012_0506	N.C.	6.13442	0.88917	1.98665	0.99342
10	11082012_0708		5.84325	0.93004	1.96331	0.99297
10	11082012_0910		6.34127	0.92317	1.9702	0.99384
10	11082012_1112		6.31487	0.92564	1.97629	0.99424
10	11082012_1314		6.71226	0.91756	1.9552	0.99474
10	11082012_1516	N.C.	6.86013	0.83136	1.56678	0.99487
10	12082012_0102	N.C.	6.01776	0.77484	2.1853	0.99135
10	12082012_0304	N.C.	6.457	0.69881	2.23226	0.99446
10	12082012_0708	N.C.	6.7086	0.79203	1.77135	0.9903
10	12082012_0910	N.C.	6.66514	0.85442	1.83383	0.99425
10	12082012_1112	N.C.	6.47759	0.80852	1.87386	0.99436
10	12082012_1314	N.C.	6.75014	0.78766	1.78482	0.99499
10	12082012_1718	N.C.	5.81794	0.741	2.42302	0.9983
10	12082012_1920	N.C.	6.26631	0.70219	2.08891	0.99762
10	12082012_2123	N.C.	7.18613	0.79972	2.4582	0.99831
10	12082012_2829	N.C.	7.12999	0.87024	2.48309	0.99821

11	24072012_010203	N.C.	6.1151	0.85953	1.72723	0.99005
11	24072012_0607	N.C.	6.06808	0.70453	1.96118	0.99263
11	27072012_0102	N.C.	5.59489	0.74992	1.956	0.99434
11	27072012_0304	N.C.	5.81408	0.72132	2.02202	0.99295
11	27072012_0506	N.C.	6.40632	0.86837	2.08722	0.99632
11	27072012_0708		5.6387	0.9137	2.19825	0.99841
11	30072012_0304	N.C.	6.44112	0.89712	2.08168	0.99761
11	30072012_0506		6.41892	0.90482	2.05145	0.99771
11	30072012_0708	N.C.	5.12034	0.86917	2.15199	0.99722
11	30072012_0910	N.C.	6.26738	0.89923	2.17781	0.99771
11	01082012_0102		6.12798	0.94628	2.09977	0.99444
11	01082012_0304	N.C.	5.89212	0.85716	2.16699	0.99036
11	01082012_0506		6.24798	0.91521	2.02211	0.99471
11	01082012_0708		6.09728	0.95143	2.05727	0.99588
11	01082012_0910		5.98177	0.96652	1.9992	0.99498
11	01082012_1112		6.51845	0.9693	2.03377	0.99632
11	01082012_1314		6.04418	0.96701	2.01848	0.99661
12	01082012_1515b16m		5.93285	0.92978	2.76971	0.99417
12	01082012_1718m		6.00022	0.96695	2.05509	0.99589
12	01082012_1920m		5.57313	0.94787	2.21097	0.99583
12	01082012_2122m		6.20077	0.92906	2.18168	0.99556
12	01082012_2324m		5.69619	0.93267	2.20966	0.99609
13	02082012_0506		5.54504	0.93755	1.57273	0.99817
13	02082012_0708		5.41444	0.92073	1.58603	0.99811
13	02082012_0910		5.63047	0.91279	1.64217	0.99642
13	02082012_1112	N.C.	5.98387	0.87539	1.64765	0.99665
13	02082012_1314	N.C.	5.41865	0.85523	1.58922	0.99439
13	02082012_1516		5.32441	0.92648	1.61759	0.99757
14	03082012_0506		5.82417	0.92805	1.78357	0.99582
14	03082012_0708		5.58569	0.92479	1.89291	0.99628
14	03082012_0910		5.5348	0.93761	1.92644	0.99527
14	03082012_1112		5.50633	0.92363	1.85624	0.99532
15	03082012_1314		4.88197	0.94395	1.77025	0.99816
15	03082012_1516	N.C.	5.18106	0.89393	1.79559	0.99673
15	03082012_1718		5.48511	0.93457	1.76207	0.99811

15	03082012_1920		4.93298	0.92921	1.79937	0.9981
15	03082012_2122	N.C.	5.23669	0.79559	1.82663	0.99821
15	03082012_232425	N.C.	5.13963	0.81901	1.733	0.99762
15	03082012_2627		5.3081	0.90986	1.64872	0.998
16	03082012_3233		4.99865	0.93216	1.93541	0.99336
16	03082012_3435		5.22327	0.93531	2.03046	0.99398
16	03082012_3637		4.99747	0.95136	2.05762	0.99356
16	03082012_3839		4.94869	0.94953	2.04239	0.99565
17	03082012_4041		5.31979	0.9115	1.75889	0.99674
17	03082012_4243		5.02029	0.94186	1.77265	0.99676
17	03082012_4445		4.93607	0.93698	1.75013	0.99741
17	03082012_4647		4.73808	0.9385	1.67649	0.99688
18	06082012_0506		5.41214	0.91006	2.20191	0.99643
18	06082012_070809	N.C.	5.1123	0.88262	2.19076	0.99646
18	07082012_0506		5.41214	0.91006	1.5362	0.99269
18	08082012_0708		5.53052	0.92037	2.29918	0.99761
18	08082012_0910		5.23873	0.93224	2.37548	0.99703
19	09082012_0102		4.84322	0.90823	2.15026	0.99329
19	09082012_0304	N.C.	5.34581	0.86023	2.31699	0.99617
19	09082012_0506		4.84691	0.92202	2.11397	0.99479
19	09082012_0708		4.77872	0.91824	2.01986	0.99267
19	09082012_0910		5.13487	0.90643	2.1221	0.99617
20	10082012_0607		4.61097	0.964	2.34433	0.99541
20	10082012_0809		4.90652	0.94694	2.38058	0.99088
20	10082012_101112		4.91072	0.95728	2.39375	0.98847
20	10082012_131415		4.95111	0.95252	2.37864	0.98903

9.12 $[\text{Sr}(\text{H}_2\text{O})_n]^{2+}$

N.C. stands for 'not considered'.

n	Name of the file		w (eV) daughter	R ² daughter	w (eV) parent	R ² parent
5	14092012_0105	N.C.	5.81283	0.21013	2.69655	0.9982
6	13092012_3536	N.C.	9.09778	0.41913	2.38639	0.99925

6	13092012.5462	N.C.	6.88415	0.355	2.93656	0.99678
6	13092012.5560	N.C.	6.12522	0.27907	3.021	0.99357
6	13092012.5763	N.C.	7.77745	0.47572	2.96067	0.99601
6	13092012.5864	N.C.	4.37138	0.64451	2.88356	0.9958
6	13092012.8889	N.C.	7.42345	0.551	2.70297	0.99734
6	13092012.9095	N.C.	10.15298	0.53819	2.87525	0.99826
6	13092012.9196	N.C.	7.30579	0.44442	2.65844	0.99817
6	13092012.9297	N.C.	7.03776	0.44152	2.75179	0.99779
6	13092012.9398	N.C.	9.47612	0.26041	2.71883	0.99748
7	13092012.1920		6.6687	0.7437	2.34567	0.99886
7	13092012.2122		6.29975	0.71965	2.37452	0.99925
7	13092012.2324		7.21174	0.67738	2.24159	0.99937
7	13092012.2526		7.31321	0.68155	2.33684	0.99832
7	13092012.2728		7.1215	0.64013	2.35299	0.99867
8	12092012.708		6.27978	0.76999	2.64578	0.99941
8	12092012.0910		6.07905	0.72983	2.64416	0.99923
8	12092012.1213		5.24351	0.68546	2.64304	0.99941
8	12092012.1415		6.04677	0.69668	2.62841	0.99948
8	12092012.1617		6.36708	0.62194	2.63892	0.99915
8	12092012.1819		6.81954	0.67801	2.66957	0.99937
8	12092012.2021		6.01554	0.67088	2.69045	0.99933
8	12092012.2223		5.44823	0.65584	2.53798	0.9978
8	12092012.2425		-	-	2.62591	0.99919
9	26082012.0506		5.29127	0.70399	1.5852	0.99773
9	26082012.0708		5.7207	0.78228	1.55597	0.99847
9	26082012.1112		6.12592	0.84249	1.99103	0.9967
9	27082012.1415		6.15859	0.78983	1.95714	0.99691
9	27082012.1617		5.82815	0.82847	1.94944	0.99721
9	27082012.1819		6.17289	0.87836	2.34868	0.99341
9	27082012.2021		5.84862	0.90428	2.37343	0.99251
9	27082012.2223		6.27009	0.90273	2.41352	0.99214
9	27082012.242526		5.97207	0.88815	2.40676	0.99308
9	27082012.2728		5.87011	0.8333	2.35879	0.99496
9	27082012.2930		5.82581	0.83685	2.39085	0.9954
10	27082012.3132		5.34587	0.76453	2.40738	0.99339

10	11092012_1415		5.84877	0.74717	2.5103	0.99747
10	11092012_1617		5.45912	0.74536	2.42892	0.99661
10	11092012_1819		5.43895	0.77499	2.41611	0.99726
10	11092012_2021		5.87106	0.77555	2.49572	0.99801
10	11092012_2223		5.59862	0.78165	2.53798	0.9978
11	11092012_0405		6.25521	0.77015	2.75498	0.99783
11	11092012_0607		4.71311	0.75724	2.82228	0.99714
11	11092012_0809		5.52867	0.81443	2.50342	0.99653
11	11092012_1011		5.22686	0.74713	2.60075	0.99553
11	11092012_1213		5.71911	0.78687	2.48979	0.99488
12	01092012_1112		6.45047	0.98355	3.69416	0.9979
12	01092012_1314		6.53823	0.98201	3.90185	0.9987
12	01092012_1617		5.90722	0.95128	2.41684	0.99915
12	01092012_1819		5.96317	0.96008	2.21992	0.9989
12	01092012_2021		5.75284	0.96673	2.30762	0.99882
12	01092012_2223		5.76159	0.96591		0.96591
12	01092012_2425		5.94717	0.96856	2.33308	0.99856
13	01092012_2728		5.65352	0.97073	3.03186	0.99789
13	01092012_2930		5.50718	0.9634	3.00549	0.99758
13	01092012_4546	N.C.	5.68132	0.80606	2.78811	0.97728
13	01092012_4748		5.28352	0.91292	2.78605	0.98078
13	01092012_5051		5.36291	0.91975	2.51443	0.98415
13	01092012_5253		5.69784	0.93126	2.70598	0.97812
13	01092012_5455		5.84323	0.89295	2.72475	0.97799
14	01092012_5657	N.C.	5.23032	0.89257	1.77882	0.99799
14	01092012_5859	N.C.	4.80949	0.87105	1.77756	0.99844
14	03092012_1213	N.C.	5.37597	0.74079	2.56531	0.99803
14	03092012_1415	N.C.	4.64971	0.80205	3.14099	0.99624
14	03092012_1617	N.C.	4.85046	0.82209	2.60252	0.99592
14	03092012_1819	N.C.	4.82967	0.76574	2.64555	0.99586
14	03092012_2728	N.C.	5.41717	0.8824	2.32136	0.99685
14	03092012_2930	N.C.	4.8782	0.87307	2.25018	0.99598
14	03092012_3132		5.2178	0.90114	2.44473	0.99772
14	03092012_3334		4.90187	0.9431	2.34377	0.99799
14	03092012_3536		4.87154	0.93713	2.37876	0.99826

14	03092012_3738		4.91859	0.93239	2.39535	0.99745
15	03092012_3940		5.09137	0.8508	2.67146	0.99838
15	03092012_4143		4.94893	0.8262	2.74207	0.99829
15	06092012_0102		4.53212	0.80378	2.63527	0.99918
15	06092012_0304		4.84124	0.83899	2.58202	0.99917
15	06092012_0506		4.96208	0.82466	2.59896	0.99949
15	06092012_0708	N.C.	4.34126	0.79165	2.57851	0.99923
15	06092012_0910	N.C.	4.40445	0.79835	2.53886	0.9994
15	06092012_1112	N.C.	4.98534	0.79009	2.51069	0.99904
16	06092012_1415		4.45398	0.89526	2.42065	0.99811
16	06092012_1617		4.59022	0.90371	2.40616	0.99903
16	06092012_1819		4.59815	0.90337	2.41332	0.99868
16	06092012_2021		4.32308	0.90559	2.43401	0.99831
16	06092012_2223		5.01461	0.86927	2.45852	0.99882
17	06092012_2425		4.19204	0.89098	2.59357	0.99912
17	06092012_2627		4.79599	0.89356	2.63424	0.99842
17	06092012_2829		4.53504	0.89034	2.59448	0.99873
17	06092012_3031		4.74442	0.9034	2.8163	0.99902
17	06092012_3233		4.66243	0.91505	2.59838	0.99908
17	06092012_3435	N.C.	5.05122	0.76591	2.56105	0.99865
17	06092012_3637		4.51421	0.8958	2.65991	0.99879
18	06092012_3839		4.39546	0.91021	2.30018	0.99839
18	06092012_4041		4.36689	0.89534	2.31483	0.9975
18	06092012_4243		4.45847	0.84296	2.31856	0.9972
18	06092012_4445		4.55713	0.81689	2.32538	0.99684
18	07092012_0102		4.88437	0.81097	2.27401	0.99815
18	07092012_0304	N.C.	4.95126	0.77218	2.31868	0.99764
18	07092012_0506	N.C.	3.91353	0.68878	2.35519	0.9976
18	07092012_0708		4.30404	0.82287	2.31111	0.99649
18	07092012_0910	N.C.	4.37418	0.63717	2.47323	0.99669
19	13092012_6667		4.35429	0.72703	2.58291	0.99914
19	13092012_6869		3.98458	0.75961	2.67197	0.99946
19	13092012_7071		4.16496	0.78612	2.60454	0.99912
19	13092012_7273		4.90898	0.83977	2.61536	0.99887
19	13092012_7475		4.90366	0.81921	2.62819	0.99888

20	13092012_7677	4.39544	0.87121	2.46747	0.99867
20	13092012_7879	4.65261	0.93773	2.43017	0.99876
20	13092012_8081	4.25446	0.93838	2.44245	0.99878
20	13092012_8283	4.71284	0.95737	2.4382	0.99894

9.13 Conversion Units

- Electron volt - joule relationship

$$1 \text{ eV} = 1.602176487 \times 10^{-19} \text{ J}$$

http://physics.nist.gov/cgi-bin/cuu/Value?evj|search_for=electronvolt

$$1 \text{ J} = 6.24150965 \times 10^{18} \text{ eV}$$

http://physics.nist.gov/cgi-bin/cuu/Value?jev|search_for=electronvolt

- Calorie mean - joule relationship

$$1 \text{ cal} = 4.19002 \text{ J}$$

Handbook of chemistry and physics 85th edition, a ready reference book of chemical and physical data, CRC press, 2004-2005, editor in chief David R. Lide, PhD, ch.1, pp.34.

- Boltzmann constant

$$k_B = 1.3806504 \times 10^{-23} \text{ J K}^{-1} = 8.617343 \times 10^{-5} \text{ eV K}^{-1}$$

<http://physics.nist.gov/cgi-bin/cuu/Value?k>

- Avogadro constant

$$6.02214179 \times 10^{23} \text{ mol}^{-1}$$

http://physics.nist.gov/cgibin/cuu/Value?na|search_for=physchem_in!

9.14 Atomic Weights and Isotopic Compositions of Elements

The relative atomic mass for an atom used in this work corresponds to the relative atomic mass of the isotope with the highest isotopic composition.

The relative atomic mass used are from:

The atomic weights are available for elements 1 through 118 and isotopic compositions or abundances are given when appropriate. The atomic weights data were published by M.E. Weiser and M. Berglund in Atomic Weights of the Elements 2007, and the isotopic compositions data were published by J.K. Böhlke, J.R. de Laeter, P. De Bièvre, H. Hidaka, H.S. Peiser, K.J.R. Rosman, and P.D.P. Taylor in Isotopic Compositions of the Elements, 2001. The relative atomic masses of the isotopes data were published by G. Audi, A.H. Wapstra, and C. Thibault in The 2003 Atomic Mass Evaluation. Developers and Contributors: J.S. Coursey, D.J. Schwab, J.J. Tsai, and R.A. Dragoset, NIST Physical Measurement Laboratory.

(i) <http://www.nist.gov/pml/data/comp.cfm>

(ii) http://physics.nist.gov/cgi-bin/Compositions/stand_alone.pl?ele=&ascii=html&isotype=some

9.15 Some Physical Parameters of the Atoms and Molecules Under Examination

The Table 9.15.1 and Table 9.15.2 are borrowed from:

David R. Lide, ed., CRC Handbook of Chemistry and Physics, Internet Version 2005, <http://www.hbcpnetbase.com>, CRC Press, Boca Raton, FL, 2005. If a specific table is cited, use the format: "Physical Constants of Organic Compounds", in CRC Handbook of Chemistry and Physics, Internet Version 2005, David R. Lide, ed., <http://www.hbcpnetbase.com>, CRC Press, Boca Raton, FL, 2005.

Molecule	H ₂ O		NH ₃		CH ₃ OH	
Temperature (° C)	25	100.0	25	-33.33	25	64.6
Enthalpy of Vaporization (kJ mol ⁻¹)	43.98	40.65	19.86	23.33	37.43	35.21

Table 9.15.1: Enthalpy of vaporization at boiling temperature and at 25° C of H₂O, CH₃OH, and NH₃

The Tables 9.15.2 and 9.15.3 below are borrowed from:

Atom or molecule in gas phase	Ionisation Potential (eV)	
	1st	2nd
Mg	15.03528	80.1437
Ca	11.87172	50.9131
Sr	11.03013	42.89
H ₂ O	12.6206 ± 0.0020	
NH ₃	10.070 ± 0.020	
CH ₃ OH	10.85 ± 0.01	

Table 9.15.2: Ionisation potential of atoms and molecules in gas phase investigated in this work

F.A. Cotton, G. Wilkinson, C.A. Murillo, M. Bochmann, *Advanced Inorganic Chemistry*, John Wiley & Sons Inc., New York, 6th Edition, 1996, pp. 112, pp.1297, pp.1302.

Element	Z	Ionisation Enthalpy (kJ mol ⁻¹)				CN	Ionic Radius (Å)
		1st	2nd	3rd	4th		
Mg	12	737.5	1450	7731	10540	4	0.71
						6	0.86
						8	1.03
Ca	20	589.6	1146	4942	6500	6	1.14
						8	1.26
						10	1.37
						12	1.48
Sr	38	549.3	1064		5500	6	1.32
						8	1.40
						10	1.50
						12	1.58

Table 9.15.3: Ionisation enthalpies and ionic radii of the Mg, Ca, and Sr atoms (Z is the atomic number, and CN is the coordination number)

Chapter 10

Experimental Details

10.1 Details on the Reagents

Argon cylinder: compressed gas, filled to 230 bar, max at 15° C, UN 1006, CLASS 2.2, BOC PURESIELD ARGON

Argon and ammonia mixture cylinder: compressed gas, N.O.S., 5% Ammonia/Argon, 5% balance, UN 1956, Material 162803-L, BOC

Methanol: boiling point 64.6° C, MW 32.06, Code M/4000/17, UN 1230, CAS 67-56-1, Lot 1151813, Fisher Chemical

Water: deionised water

Magnesium: chips, 4-30 mesh, 99.98% trace metals basis, Pcode 101044917, CAS 7439-95-4, Lot # 59796JKV, Aldrich 254118-250G

Calcium: particle size < 1 cm, 99%, CAS 7440-70-2, FW 40.08, mp 845° C, d 1.54, Aldrich 327387-500G Batch # 05211TB

Strontium: random pieces, 99%, packaged under mineral oil (the metal was washed with toluene), CAS 7440-24-6, FW 87.62, Sigma Aldrich 343730-10G Batch # MKAA2530.

Neutral molecular clusters were provided to the cluster chamber in two ways. Water and methanol were placed in a reservoir cooled in an ice bath and gaseous argon was passed through the liquid. Gaseous ammonia was extracted from premixed cylinder consisting of 5% ammonia in argon.

Neutral clusters of methanol were generated by passing gaseous argon through liquid methanol placed in a reservoir cooled in an ice bath.

Neutral clusters of ammonia were generated using a premixed cylinder consisting of 5% ammonia in argon.

Neutral clusters of water were generated by passing gaseous argon through liquid water placed in a reservoir cooled in an ice bath.

10.2 Experimental Metal Vaporization or Sublimation Temperature

The temperature inside the Knudsen effusion cell is optimised in order to both atomize the metal and form a high intensity metal cluster beam. Table 10.2.1 reports the temperatures used in these experiments, which have been measured by a thermocouple, and the respective settings of the power supply to maintain a particular temperature inside the furnace.

Metal Cluster	Temperature (° C)	Current (A)	Voltage (V)
$[\text{Mg}(\text{CH}_3\text{OH})_n]^{2+}$	540	4.7	9.70
$[\text{Ca}(\text{CH}_3\text{OH})_n]^{2+}$	720	5.7	14.0
$[\text{Sr}(\text{CH}_3\text{OH})_n]^{2+}$	610	4.7	10.4
$[\text{Mg}(\text{NH}_3)_n]^{2+}$	450	3.6	7.00
$[\text{Ca}(\text{NH}_3)_n]^{2+}$	630	4.8	10.8
$[\text{Sr}(\text{NH}_3)_n]^{2+}$	560	4.3	9.20
$[\text{Mg}(\text{H}_2\text{O})_n]^{2+}$	560	5.5	10.7
$[\text{Ca}(\text{H}_2\text{O})_n]^{2+}$	650	6.2	13.5
$[\text{Sr}(\text{H}_2\text{O})_n]^{2+}$	588	5.7	11.5

Table 10.2.1: Temperature of vaporization of the metals in these experiments

10.3 Experimental Extracting Potential At The Ion Source

It can be seen in Table 10.3.1, the accelerating potential corresponding to the initial kinetic energy of a precursor molecular cluster ion which leaves the ionisation chamber and enters in the flight tube of the mass spectrometer.

10.4 Energy of Bombarding Electrons

Neutral clusters were ionised by electron impact (also known as electron bombardment) in the electron impact ion source. The energy of the electrons was 70 eV.

10.5 Experimental Pressure

The pressure during experimental analysis was $\sim 10^{-5} - 10^{-6}$ mbar in the cluster chamber, $\sim 10^{-5}$ mbar in the source chamber, and $< 1 \times 10^{-7}$ mbar in the 1st ffr and 2nd ffr.

Cluster	Potential (eV)	
$[\text{Mg}(\text{CH}_3\text{OH})_n]^{2+}$	7000	
$[\text{Ca}(\text{CH}_3\text{OH})_n]^{2+}$	7000	
$[\text{Sr}(\text{CH}_3\text{OH})_n]^{2+}$	5000	(for $n = 6$ and $n \geq 8$)
$[\text{Sr}(\text{CH}_3\text{OH})_n]^{2+}$	5000	(for $n = 4, 5, 7$)
$[\text{Mg}(\text{NH}_3)_n]^{2+}$	5000	
$[\text{Ca}(\text{NH}_3)_n]^{2+}$	5000	
$[\text{Sr}(\text{NH}_3)_n]^{2+}$	5000	
$[\text{Mg}(\text{H}_2\text{O})_n]^{2+}$	7000	
$[\text{Ca}(\text{H}_2\text{O})_n]^{2+}$	7000	
$[\text{Sr}(\text{H}_2\text{O})_n]^{2+}$	7000	
$\text{H}^+(\text{CH}_3\text{OH})_n$	5000	
$\text{H}^+(\text{NH}_3)_n$	5000	
$\text{H}^+(\text{H}_2\text{O})_n$	5000	

Table 10.3.1: Accelerating voltage on the Ion Source for each cluster ion in these experiments

10.6 Reference to Digitizing Software Employed to Derive the Data from Images Found in the Literature

Engauge Digitizer 4.1; <http://digitizer.sourceforge.net> (Engauge Digitizer is free software; redistribute it and/or modify it under the terms of the GNU General Public License (version 2) as published by the Free Software Foundation <http://www.gnu.org/copyleft/gpl.html>).